



GABAergic cell types and modulation of GABAergic synaptic transmission by group III metabotropic glutamate receptors in the human neocortex

Doctor of Philosophy (D. Phil.) Thesis
Michaelmas Term, 2021

István Paul Lukács
Brasenose College

Supervisors:
Prof. Péter Pál Somogyi
Prof. R. Angus Silver
Prof. Colin J. Akerman

Department of Pharmacology
University of Oxford
Oxford, UK

Abstract

The neocortex is a layered, modular structure on the surface of the mammalian brain, which together with other brain structures supports behavioural adaptation to the changing environment. It is greatly expanded in humans and is thought to be necessary for unique human behaviours such as abstraction and language, functions which contribute to the high flexibility of human behaviour and underlie the adaptability of the species.

In the neocortex, the activity of spiny pyramidal neurons correlates with behaviourally relevant information processing and is governed by multiple types of GABAergic interneuron, which show great diversity and specialisation in the distribution of their dendrites and axon, molecular composition, electrical behaviour and synaptic connections. Although some GABAergic neuron types have been extensively studied in non-human animals, other cell types, such as the double bouquet cell (DBC) have been less frequently reported. Double bouquet cells are abundant in humans in layer II and upper layer III with a radial 'horsetail' axon descending through multiple layers in a narrow cortical column, yet details of their molecular content, electrical behaviour and synaptic targets in humans are not known.

The synaptic signalling of different types of GABAergic interneuron is regulated by presynaptic receptors, including group III metabotropic glutamate receptors (mGluR). In rodents, group III mGluRs show a cell type-specific expression in the neocortex and inhibit neurotransmitter release presynaptically, including that of GABA. However, their distribution and effects in human neocortex are not known. Although, drugs acting on presynaptic group III mGluRs have been proposed and investigated for treatment of various mental and neurodegenerative disorders in humans, none have been introduced into clinical practice so far. A direct investigation of group III mGluR function in human neocortex may help explain their

effects, or the lack thereof, in health and disease and could facilitate development of more efficacious drugs.

The aims of my studies have been twofold: **i**, to explore the diversity of GABAergic interneuron types in the human neocortex by anatomical, molecular and electrophysiological methods, and **ii**, to test if GABAergic synaptic transmission is suppressed by group III mGluR activation in the human neocortex.

I recorded and labelled single and pairs of GABAergic interneuron, using the whole-cell patch clamp technique *in vitro* in acute neocortical slices prepared from samples obtained from tumour and epilepsy patients undergoing neurosurgery. I tested the effects of group III mGluR activation on spontaneous GABAergic synaptic transmission in two distinct GABAergic cell types, DBCs and parvalbumin-expressing multipolar cells (PMCs) by bath application of the orthosteric group III mGluR agonist, L-amino-phosphonobutyric-acid (L-AP4). I studied and compared the molecular expression and synaptic targets of DBCs and PMCs using immunohistochemistry and electron microscopy.

My main results are the following: **1**. I identified 5 different GABAergic interneuron types based on the distribution of their dendrites and axon, including DBCs, PMCs, axo-axonic cells (AACs), neurogliaform cells (NGCs) and rosehip cells (RHCs). **2**. The calcium-binding proteins calbindin (CB), calretinin (CR) and parvalbumin (PV) were differentially expressed among DBCs, and PMCs, such that the majority of DBCs were immunoreactive for CB and a small proportion were immunoreactive for CR, whereas the majority of PMCs were immunoreactive only for PV. **3.** Voltage responses of DBCs were characterised by a large voltage sag potential and strong adaptation, whereas those of PMCs showed small or no voltage sag potential and weak or no adaptation. **4**. Evoked firing patterns of DBCs exhibited bursting or non-bursting phenotypes. **5**. Evoked firing patterns of DBCs and PMCs did not depend on

medical history and did not vary with cortical area. **6.** Half of the synaptic targets of the 'horsetail' axon of CB+ DBCs in layer III were dendritic spines, the remainder were dendritic shafts. In the neuropil of layer III, on average, 15% of GABAergic synapses innervated dendritic spines, the rest dendritic shafts; therefore, targeting of dendritic spines by DBCs is selective. 7. The majority (83%) of the synaptic targets of the CR+ DBC were dendritic shafts, the remainder dendritic spines. Two thirds of the synaptic targets of PMCs were dendritic shafts, the remainder dendritic spines and to a smaller extent somata. **8**. Postsynaptic effects of DBCs were outward currents and showed short-term depression on their synaptic targets, which included pyramidal cells, DBCs, bipolar and bi-tufted smooth-dendritic neurons. **9**. Activation of group III mGluRs paradoxically increased the frequency of spontaneous inhibitory postsynaptic currents (sIPSCs) in DBCs, but decreased sIPSC frequency in PMCs; there was no effect on the amplitude of sIPSCs in either cell type.

My results reveal the differences in the molecular content, electrical behaviour and synaptic targets of DBCs and PMCs, and the cell type-specific effects of group III mGluR activation on GABAergic synaptic transmission onto these two distinct cell types in humans. I demonstrate a paradoxical enhancement of spontaneous GABAergic synaptic input to DBCs, which has not been observed in any species and is most likely due to a network effect. These results could provide experimental basis for the interpretation of drug action in the human cerebral cortex and for the development of novel treatments. Furthermore, I provide an integrated anatomical, molecular and electrophysiological characterisation of human DBCs, as an example of how to distinguish different cell types in the neocortex of humans and other species.

Acknowledgments

This thesis is the result of my scientific research in neuroscience, specifically in the investigation of human neuronal circuits of the neocortex, as part of my studies for the D. Phil degree in the Neuroscience programme at the university of Oxford. I wish to express my gratitude to my supervisors, Professor Péter Somogyi, Professor Angus Silver and Professor Colin Akerman, who guided and supported me through this challenge. In particular, I would like to thank Professor Somogyi, who was not only my supervisor, but also a mentor inside and outside the lab, inspiring my curiosity in biology through dedicated and enthusiastic teaching and standing as an example of critical thinking.

This work would not have been possible without the contributions and the support of many excellent scientists and physicians, colleagues and friends. I thank the neurosurgeons at the John Radcliffe Hospital, Mr Richard Stacey, Mr Puneet Plaha, Mr James Livermore, Mr Mouness Obeidat, Ms Roisin Finn, Ms Joy Roach and Ms Jane Halliday, who kindly allowed me into the operating theatres and provided the samples and the clinical information for my research. I also thank Professor Olaf Ansorge, Carolyn Sloan and Hannah Brooks at the Oxford Brain Bank, Department of Neuropathology, who provided advice and the ethical approval and assisted with the administration of the samples, and Dr Martin Gillies, who provided clinical information. I am forever grateful for Dr Marco Bocchio and Dr Gáspár Oláh, who taught me *in vitro* patch clamp electrophysiology, pharmacology and signal analysis, and Dr József Somogyi for his teaching and technical support in fluorescent and transmitted light microscopy. I would also like to thank Ms Emily Hunter and Mr Michael Howarth for their excellent assistance in human sample collection, immunohistochemical experiments, microscopy and documentation and stimulating discussions. I am thankful to Dr Martin Field, Dr Ruggiero

Francavilla, Dr Sawa Horie, Dr Qianru Zhao, Mr Puneet Pareek, Ms Rhukshanda Habib and Zalán Ilyés for their contribution to experiments presented in this thesis and helpful discussions. I thank Professor Gábor Tamás and members of his lab, Dr Gábor Molnár, Dr Márton Rózsa, Ms Nelli Tóth and Ms Éva Tóth, at the University of Szeged, who kindly provided samples for my research and accepted me as a visiting student to learn human sample collection and processing as well as in vitro electrophysiology. I thank Professor Zoltán Nusser, Dr. Andrea Lőrincz and Professor Gábor Nyíri, at the Institute of Experimental Medicine in Hungary, who provided their lab space, electron-microscope and Neurolucida setup during the 2020 Covid-19 lockdown, where I could continue my research. I thank Professor Zameel Cader and Dr Tatjana Lalic at the MRC Weatherall Institute of Molecular Medicine in Oxford for providing their equipment to us for electrophysiological recordings. I also thank Professor Andrew King at the Department of Physiology, Anatomy and Genetics for giving access to their Neurolucida equipment, and Errin Johnson at the Sir William Dunn School of Pathology for support in electron-microscopy. I am grateful to Professor Marco Capogna, Dr Linda Katona, Professor Limei Zhang and Professor Lisa Topolnik for their critical comments, feedback and advice on my work, and current and past members of our lab, Dr Tim Viney, Dr Tugrul Özdemir, Ms Barbara Sárkány and Dr Abhilasha Joshi for inspiring scientific discussions and their friendly support. I thank the Medical Research Council and the Dulverton Trust for funding my studies in Oxford. Last but not least I am thankful to Dr Deborah Clarke and Mrs Mary Gilgunn-Jones for their administrative support, all members of the Department of Pharmacology providing a supportive environment and Mrs Klara Somogyi for her friendly support of living in Oxford as a student.

Finally, I wish to dedicate this thesis to my parents and wife, who continuously believed in me, and without the love and support of whom I could not have completed this work.

Contribution of others

I, Istvan-Paul Lukacs, DPhil student at the University of Oxford, Department of Pharmacology, hereby declare that parts of the data presented in this thesis, submitted for the degree of Doctor of Philosophy at the university of Oxford, are the work of other people.

I recorded and labelled a total of 499 neurons and 9 glial cells. In addition to these, 12 neurons (PMCs 1-7, 9-11 and 13) were recorded and labelled by Dr. Ruggiero Francavilla, former postdoctoral scientist in the lab. On 7 of these 12 PMCs pharmacological experiments with L-AP4 were performed and analysed by Dr. Francavilla; I carried out the final comparison of the cells with the 32 double bouquet cells recorded by me. Further three pyramidal cells, used for electron-microscopic study of their synaptic targets, were recorded and labelled in Prof. Gabor Tamas's laboratory at the University of Szeged, Hungary by Mr. Márton Rózsa. Of the 24 reconstructed neurons, 10 were reconstructed by me, 2 (PMC 1 and 5) were reconstructed by Dr. Sawa Horie, current postdoctoral scientist in the lab, 2 by Miss Rhukshanda Habib, visiting student, 3 by Mr. Ilyés Zalán, visiting student, 2 by Mr. Puneet Pareek, visiting student, 2 by Mr. Michael Howarth, former research assistant, 1 by Mrs. Qianru Zhao, former postdoctoral scientist, 1 by Miss Emily Hunter, current research assistant, and 1 was reconstructed in Prof. Gabor Tamas' lab. Of the 372 boutons examined using electron-microscopy, 87 (all from PMCs) were examined and photographed by Dr. Sawa Horie, who also performed all necessary tissue processing in preparation for electron-microscopic examination of these boutons; the rest were processed and imaged by me. Dr. Horie also jointly prepared figures 3.4 and 3.7 with me and Ms Emily Hunter (chapters 3.1.5 and 3.2.1 respectively). Figure 3.5 (chapter 3.1.6) was prepared by Dr. Martin Field, current postdoctoral scientist in the lab, from data measured and analysed by me. Figure 3.1 was prepared by Ms

Emily Hunter under my coordination (chapter 3.1.1), and tables 2.1, 2.2 and 3.1 were jointly prepared by me and Ms Emily Hunter. Approximately 50 % of pre-embedding immunohistochemical experiments were performed by Miss Emily Hunter and Mr. Michael Howarth, the rest by me. All experiments, analysis and figures contributed by others were planned by me, and were produced under my supervision.

Contents

ABSTRACT **2**

ACKNOWLEDGMENTS **5**

CONTRIBUTION OF OTHERS **7**

1 INTRODUCTION **15**

1.1 THE NEOCORTEX 15
1.1.1 Structural subdivision *16*
1.1.2 Functional subdivision *17*
1.1.3 Neuronal elements *19*
1.1.4 Definition of double bouquet cells *24*
1.1.5 The columnar organisation of the neocortex *26*
1.1.6 Comparative aspects of neocortical structure and function with special focus on humans *28*

1.2 GROUP III METABOTROPIC GLUTAMATE RECEPTORS (MGLUR) 31
1.2.1 General aspects and differentiation from group I and group II mGluRs *31*
1.2.2 Pharmacology *33*
1.2.3 Expression pattern and subcellular location in the cerebral cortex *34*
1.2.4 Synaptic effects *37*
1.2.5 Roles in behaviour *39*
1.2.6 Related pathological processes and therapeutic potential *39*

1.3 RATIONALE AND AIMS 42

2 EXPERIMENTAL PROCEDURES **44**

2.1 ETHICAL APPROVAL AND PATIENT CONSENT 44

2.2 SAMPLE COLLECTION AND SLICE PREPARATION 50

2.3 ELECTROPHYSIOLOGY 51
2.3.1 Whole-cell patch-clamp recordings *51*
2.3.2 Drugs and compounds *54*
2.3.3 Data analysis and inclusion criteria *54*
2.3.4 Statistics *58*

2.4 ANATOMICAL ANALYSIS 59
2.4.1 Streptavidin visualisation and immunohistochemistry *59*
2.4.2 Wide field epifluorescence and confocal laser scanning microscopy. *61*
2.4.3 Peroxidase reactions *65*
2.4.4 Light microscopy and reconstruction of labelled cells *66*
2.5.5 Serial section electron microscopy of labelled cells and reconstruction of target dendrites *67*
2.5.6 Post-embedding immunohistochemistry for GABA *68*

3 RESULTS **70**

3.1 GABAERGIC CELL TYPES IN THE HUMAN NEOCORTEX 70
3.1.1 Recorded cells and samples *70*
3.1.2 Interneuron types identified based on the spatial distribution of their axons *73*
3.1.3 Anatomical and molecular characterization of DBCs and the relationship of their 'horsetail' axons to calbindin immunoreactive radial bundles *75*
3.1.4 Electrophysiological characterization of DBCs *85*
3.1.5 Anatomical and molecular characterization of PMCs *87*
3.1.6 Electrophysiological characterization of PMCs *90*

3.2 CELL TYPE-SPECIFIC SYNAPTIC TARGETING IN THE HUMAN NEOCORTEX 94
3.2.1 Synaptic targets of DBCs and PMCs 94
3.2.2 Unitary postsynaptic currents evoked by DBCs 102
3.2.3 Local synaptic targets of pyramidal cells 108
3.2.4 Targets of GABAergic and non-GABAergic synapses in the neuropil of layer III 114
3.2.5 Evoked and spontaneous (IPSCs) are mediated by $GABA_A$ receptors 119
3.3 DIFFERENTIAL REGULATION OF GABAERGIC INPUTS TO DBCS AND PMCS BY GROUP III MGLURS IN THE HUMAN NEOCORTEX 121
3.4 EFFECTS OF PATIENT- AND SAMPLE-RELATED FACTORS ON THE CHANGE IN SIPSC FREQUENCY IN RESPONSES TO GROUP III MGLUR ACTIVATION 128
4 DISCUSSION 137
4.1 IDENTIFICATION OF GABAERGIC CELL TYPES 139
4.2 COMPARISON OF DBCS AND PMCS ACROSS DIFFERENT SPECIES 142
4.2.1 Molecular expression 142
4.2.2 Intrinsic membrane properties 146
4.2.3 Synaptic targets 148
4.2.4 Postsynaptic effects of DBCs 153
4.2.5 Unique effects of group III mGluR activation on GABAergic inputs to DBCs 156
4.3 LOCAL SYNAPTIC TARGETS OF PYRAMIDAL CELLS 162
4.4 NEOCORTICAL DENDRITIC SPINES ARE SELECTIVELY TARGETED BY GABAERGIC DBCS 165
5 CONCLUSIONS 169
REFERENCES 172

List of figures

Figure 3.1: Identification of neocortical layers and the location of recorded neurons 72

Figure 3.2. In vitro recorded and biocytin labelled double bouquet cell in the human inferotemporal neocortex 79

Figure 3.3. Examples of recorded and labelled DBCs 81

Figure 3.4. Diversity of double bouquet cells with 'horsetail' axons 83

Figure 3.5. In vitro recorded and biocytin labelled basket cell in the human temporal neocortex .. 89

Figure 3.6. Comparison of membrane properties of DBCs and PMCs 92

Figure 3.6. Comparison of membrane properties of DBCs and PMCs 93

Figure 3.7. Synaptic targets of double bouquet cells in layer III of the human neocortex 99

Figure 3.7. Synaptic targets of double bouquet cells in layer III of the human neocortex 100

Figure 3.8. Synaptic targets of Parvalbumin-positive multipolar cells in layer III of the human neocortex 101

Figure 3.9. Unitary eIPSCs evoked by DBCs 106

Figure 3.10. Spatial distribution of the dendrites and axons of three pyramidal cells 111

Figure 3.11. Local synaptic targets of pyramidal cells 113

Figure 3.12. Synaptic targets of GABAergic synapses in the neuropil of layer III 117

Figure 3.13. Spontaneous and evoked outward currents are IPSCs are mediated by GABAA receptors 120

Figure 3.14. Effects of group III mGluR activation on sIPSCs in DBCs and PMCs. 126

Figure 3.15. Effects of sample- and patient-related parameters on L-AP4 induced changes in sIPSC frequency 133

List of tables

Table 2.1 Patient information.....45

Table 2.2 Primary antibody information..... 63

Table 3.1 Information on recorded and labelled DBCs, PMCs, pyramidal cells, and cells used for pharmacological control measurements..... 134

Table 3.2 Multiple linear regression models for the effect of group III mGluR activation on sIPSC frequency..... 136

Abbreviations

AAC, axo-axonic cell
ab, antibody
ACSF, artificial cerebrospinal fluid
AHP, afterhyperpolarisation
AP, action potential
CB, calbindin
CB1, cannabinoid type 1 receptor
CCK, cholecystokinin
CR, calretinin
CTR, pharmacological control
DBC, double bouquet cell
DAB, 3,3’-diaminobenzidine
EM, electron microscopy
EPSC, excitatory postsynaptic current
F, frontal
FR, failure rate
GABA, gamma aminobutyric acid
$GABA_A$, gamma-aminobutyric acid type A receptor
GA, glutaraldehyde
HW, half-width
HRP, horseradish peroxidase enzyme
HTN, hypertension
IDH1, isocitrate dehydrogenase 1
IHC, immunohistochemistry
IPL, inferior parietal lobule
IPSC, inhibitory postsynaptic current
ISI CV, coefficient of variation of the inter-spike interval
ITG, inferior temporal gyrus
I-V, current-voltage traces
L-AP4, L-(+)-2-Amino-4-phosphonobutyric acid
MFG, middle frontal gyrus

MIT, mitochondrion

mt, microtubule

MTG, middle temporal gyrus;

NAM, negative allosteric modulator

NeuN, hexaribonucleotide binding protein-3

NGC, neurogliaform cell

NHS, hormal horse serum

P, parietal

PAM, positive allosteric modulator

PB, phosphate buffer

PFA, paraformaldehyde

PMC, parvalbumin-expressing multipolar cell

POL, parieto-occipital lobe

PPR, paired-pulse ratio

PV, parvalbumin

PYR, pyramidal cell

RB, rheobase

RHC, rosehip cell

SA, spine apparatus

SD, standard deviation

SE, standard error

SFG, superior frontal gyrus

SM, somatostatin

SPL, superior parietal lobule

STG, superior temporal gyrus

sv, synaptic vesicles

T, temporal

TBS-Tx, tris buffered saline with Triton x-100®

TLE, temporal lobe epilepsy

VIP, vasoactive intestinal polypeptide

VGAT, vesicular GABA transporter

WT, wild type

1 Introduction

1.1 The neocortex

The cortex is a laminated collection of nerve cells at the surface of the forebrain, which is present in reptiles, birds and mammals. The most recently evolved form of cortex, the neocortex, is only present in mammals and occupies proportionally the largest volume in humans (Clark et al., 2001; DeFelipe, 2011; de Winter & Oxnard, 2001; Nieuwenhuys, 1994; Nieuwenhuys et al., 2008). The large expansion of the neocortex in humans is thought to underlie unique human capabilities, such as language (Binder et al., 1997; Broca, 1861; Wernicke, 1874) , but also behaviours which are not unique, but are greatly advanced in humans compared to other mammals, such as abstraction, tool use and planning (Wallis et al., 2001). The neocortex represents the highest hierarchical stage of sensory information processing (Belin et al., 2000; Disbrow et al., 2000; Hubel & Wiesel, 1962, 1968; Penfield & Boldrey, 1937; Tootell et al., 1997, 2003, 2004; Tootell & Hamilton, 1989) and is the source of voluntary motor control (Fink et al., 1997; Georgopoulos et al., 1982; Geyer et al., 2000; Graziano et al., 2005; Kwan et al., 1978; Lillicrap & Scott, 2013; Penfield & Boldrey, 1937). It is also the brain region where long-term episodic memories are stored in the synaptic connections of spiny pyramidal cells (Bero et al., 2014; Insel & Takehara-Nishiuchi, 2013). Furthermore, the neocortex contributes to functions such as attention (Pessoa et al., 2003; Petersen & Posner, 2012; Zhang et al., 2014), working memory (Constantinidis et al., 2018; Fuster & Alexander, 1971; Kubota & Niki, 1971) and decision making (Platt & Glimcher, 1999). In order to explain how the neocortex supports these functions, and how they are impaired in mental disorders, it is necessary to understand the organising principles of the underlying neocortical neuronal networks.

1.1.1 Structural subdivision

In the neocortex, neuronal cell bodies have been allocated traditionally into six main layers based on the density, size and shape of neuronal cell bodies, as evidenced by Nissl staining: (I) *lamina molecularis,* is a layer of few cell bodies and is composed mainly of nerve fibres of subcortical and intracortical origin and apical dendritic tufts of pyramidal neurons; *(II) lamina granularis externa,* contains densely packed round and triangular shaped cell bodies; *(III) lamina pyramidalis externa,* contains mostly triangular cell bodies of larger size and of lower density than those in layer II; *(IV) lamina granularis interna,* contains small, densely packed round cell bodies; *(V) lamina pyramidalis interna,* contains large triangular cell bodies of moderate density; *(VI) lamina multiformis,* contains cell bodies of round, triangular and fusiform shape of different sizes. These layers are not uniformly represented throughout the entire extent of the neocortex and are also divided into sublayers. The relative thickness and the cell density of the layers varies across different areas and this has been used to divide the neocortex into cytoarchitectural areas with sharp or less sharp boundaries (Brodmann, 1909; Sarkissov et al., 1955; von Economo & Koskinas, 1925). Others divided the neocortex based on the laminar and radial distribution patterns of myelinated axons, which often coincided with the cytoarchitectural areas of Brodmann (Vogt & Vogt, 1954; Vogt, 1910). These structural differences reflect the functional specialization of neocortical areas, and correlate with their afferent and efferent connectivity with specific thalamic nuclei (Jones & Burton, 1976; Leonard, 1969; Rose & Woolsey, 1948, 1949; Steriade et al., 1997). For example, von Economo defined 5 fundamental types of neocortex (von Economo & Koskinas, 1925): three types of homotypical cortices (2,3,4), and two types of heterotypical cortices (1, 5). Type 1 is the agranular heterotypical cortex, in which the pyramidal layers (III and V) are well developed, but the granule layers (II and IV) are not. This type of cortex is present in the primary motor cortex and the premotor area (Brodmann's 4 and 6), which receive input from the motor relay

nuclei of the thalamus, i.e. the anterior and posterior divisions of the ventral lateral nucleus. Type 5 is the granular heterotypical cortex, in which the pyramidal layers are poorly developed, and is present in the primary somatosensory (Brodmann's 1, 2 and 3), visual (Brodmann's 17) and auditory (Brodmann's 41 and 42) areas. These receive direct input from the specific thalamic sensory nuclei, the lateral posterior nucleus, the lateral and medial geniculate bodies respectively. Types 2, 3 and 4 are homotypical cortices of the frontal, parietal and polar type respectively, which are present in association areas, and receive input from the thalamic association nuclei. These thalamic nuclei in turn are mainly driven by neocortical inputs and together with reciprocal connection they form the cortico-thalamo-cortical circuit. By immunohistochemical labelling of various glycoproteins and calcium-binding proteins, such as calbindin and parvalbumin, some areas, such as the orbitofrontal and medial prefrontal cortex, have been subdivided into even smaller cytoarchitectonic units (Carmichael & Price, 1994; Öngür et al., 2003; Uylings et al., 1999) with specific cortico-cortical connectivity (Carmichael & Price, 1996), reflecting further functional specialization within the neocortex. Such fine parcellation based on structural specialization and specific afferent and efferent connections lead to the conclusion that the neocortex consists of discrete modules, each with a specific role in information processing (Öngür et al., 2003).

1.1.2 Functional subdivision

The first evidence for localization of function in the neocortex came well before the structural parcellation, from observations of patients with circumscribed lesions of different neocortical areas. For example, Paul Broca described that lesions of the posterior part of the inferior frontal gyrus in patients lead to motor aphasia, i.e. the inability to produce articulated speech, while speech comprehension was unaffected (Broca, 1861). Conversely, Carl Wernicke reported that patients with sensory aphasia, i.e. the inability to comprehend speech, while the production of speech is relatively unaffected, had lesions to the area where the occipital, parietal

and temporal lobes meet in the left hemisphere (Wernicke, 1874). Subsequently, the neocortical areas specialised for processing somatic (Penfield & Boldrey, 1937; Starr, 1884; C. N. Woolsey et al., 1943), auditory (Ferrier & Yeo, 1884; Mills, 1891), and visual (Henschen, 1893) sensation, and those responsible for motor control (Ferrier & Yeo, 1884; Fritsch & Hitzig, 1870; Penfield & Boldrey, 1937), as well as cortical areas involved in personality traits and cognitive functions (Harlow, 1868) were identified in different species, including humans, by observation of patients, experimental lesions or electrical stimulation (Finger, 1994; Foerster, 1936; Vogt & Vogt, 1919, 1926; von Monakow, 1914). Others suggested that functions were distributed across the neocortex (Brown-Séquard, 1877; Lashley, 1933). However, such conclusions may be partly due inter-individual variability in localisation of function, or partly because of interactions between different cortical areas observed in certain behaviours. Indeed, disconnection syndromes in humans, characterised by deficits in some high order cognitive functions, are caused by lesions which disrupt connections between distinct sensory and motor areas (Geschwind, 1965). More recently, electrophysiological recordings of neuronal activity in different cortical areas, such as those in the visual cortex pioneered by Hubel and Wiesel (Hubel & Wiesel, 1962, 1968), revealed in more detail the functional specialisation of sensory (Belin et al., 2000; Disbrow et al., 2000; Tootell et al., 2004) and motor (Lillicrap & Scott, 2013) areas. Furthermore, cognitive processes, such as working memory, decision-making and speech have been localized to various association areas in the frontal, parietal and temporal cortices by functional imaging (Brett et al., 2002; Ferstl & von Cramon, 2002; Haller et al., 2017; Laurienti et al., 2003; Menon et al., 2002; Osaka et al., 2004; Riley & Constantinidis, 2016; Simon et al., 2004). Modern theory proposes that interconnected networks of multiple cortical areas form the substrate of higher order cognitive functions (Catani & Ffytche, 2005; Mesulam, 1998). Recently, a detailed parcellation of the entire human neocortex has been

achieved, also taking into account inter-individual variability, by combination of functional and structural imaging (Glasser et al., 2016).

1.1.3 Neuronal elements

Projection neurons

The Principal projection neurons in the neocortex are the spiny pyramidal cells, which constitute approximately 70 % of all neocortical neurons (DeFelipe, 2011; Nieuwenhuys, 1994; Winfield et al., 1980). Their cell bodies are located in layers II – VI, but mainly II-III and V-VI across all neocortical areas and species. Typical pyramidal cells have a prominent radially oriented apical dendrite which ascends towards the pial surface and reaches layer I where it forms an apical tuft, although there are exceptions which terminate in deeper layers (Koester & O'Leary, 1992; Lund, 1988; Peters & Sethares, 1991). The apical dendrite on its way towards the pia emits layer specific side branches. Several shorter and thinner basal dendrites radiate from the cell body in the lateral direction and towards the white matter. Dendrites of pyramidal cells are densely covered with spines, where they receive the majority of their synaptic input (Nieuwenhuys, 1994). Spines compartmentalise postsynaptic responses (Bloodgood & Sabatini, 2005; Matsuzaki et al., 2001; Noguchi et al., 2005) and allow isolated changes in the efficacy of synaptic transmission (Koester & Sakmann, 1998; Yuste & Denk, 1995), which contribute to the expression of long-term synaptic plasticity (Bliss & Collingridge, 1993; Matsuzaki et al., 2004; Padamsey & Emptage, 2011; Trachtenberg et al., 2002). Spine density varies across different layers along the same dendrite (Lund, 1973; Valverde, 1986).

The main axon of pyramidal cells descends radially to the white matter and projects to distant cortical areas or to subcortical regions. Typically, pyramidal cells located in the supra-granular layers II and III project to other cortical areas either ipsilaterally, or contralaterally via the corpus callosum, where they terminate in layers II and III. Conversely, pyramidal cells projecting subcortically to the thalamus, striatum, pons, spinal cord etc. are located in the

infragranular layers V and VI (Isseroff et al., 1984; Jones & Wise, 1977; Nieuwenhuys, 1994). On its course towards the white matter collateral branches are emitted from the descending main axon at different depths, which provide innervation to the local cortical area surrounding the cell body, including layer I, while some may travel laterally over several millimetres innervating distinct patches of the neuropil (Kisvárday & Eysel, 1992; Winfield et al., 1981). The majority of the local and distant synaptic targets of pyramidal cells are dendritic spines of other pyramidal cells (Anderson & Martin, 2009; Bock et al., 2011; Kisvárday et al., 1986b; Kisvárday & Eysel, 1992; McGuire et al., 1991; Melchitzky et al., 1998, 2001), but they also innervate the dendrites of smooth dendritic cells (Bopp et al., 2014; Kisvárday et al., 1986a; Kisvárday et al., 1986b; Melchitzky & Lewis, 2003). Pyramidal neurons release glutamate, which through fast ionotropic receptors acts as an excitatory neurotransmitter by depolarisation, and facilitates the firing of target neurons. However, the actions of glutamate through G-protein coupled metabotropic glutamate receptors (mGluRs) have diverse effects on synaptic transmission and neuronal firing, which cannot be translated into simple excitation or inhibition. In addition to spiny pyramidal cells, smooth-dendritic GABAergic projection neurons have also been described in the neocortex of rodents (McDonald & Burkhalter, 1993; Tomioka et al., 2005) and cats (Higo et al., 2007; Matsubara & Boyd, 1992).

Interneurons

The defining feature of interneurons is that their axon does not leave the neocortex. Interneurons comprise the remainder 30% of neurons in the neocortex. A type of glutamatergic interneuron are the spiny stellate cells in layer IV of primary sensory areas. In contrast to pyramidal cells, spiny stellate cells do not possess an apical dendrite, but rather emit dendrites in all directions, which gives them a star-like shape (Jones, 1975; Lorente De Nó, 1922; Lund, 1973; Valverde, 1971). They are the main target neurons of the specific thalamic afferents (Ahmed et al., 1994; saint Marie & Peters, 1985; Staiger et al., 2004; White & Rock, 1980) and

their axon projects to the supra-granular and infra-granular layers, where they mostly innervate the spines and dendritic shafts of pyramidal cells in the same column (Lübke et al., 2000).

The majority of neocortical interneurons are GABAergic neurons, whose dendrites can be smooth or sparsely spiny. They have been found in all layers of the neocortex and they show great diversity and specialization in the distribution of their dendrites and axon, their synaptic relationships, molecular content and electrical behaviour (Ascoli et al., 2008; Gonchar & Burkhalter, 1997; Gupta et al., 2000; Jiang et al., 2015; Kubota et al., 2011; Markram et al., 2004; Rudy et al., 2011; Somogyi et al., 1998), which reflects their adaptation to specific functional roles in the neocortical circuit. Several types of interneurons were identified based on the spatial distribution of their processes, particularly their axon in relation to neocortical layers, most of which have been observed across multiple cortical areas and in many different species (de Carlos et al., 1987; DeFelipe et al., 1986; Feldman & Peters, 1978; Jones, 1975; Kisvárday et al., 1990; Lund, 1987; Lund & Wu, 1997; Lund & Yoshioka, 1991; Marin-Padilla, 1987; Marin-Padilla & Stibitz, 1974; Meyer, 1983, 1987; Ramón y Cajal, 1899a, 1909; Valverde, 1971, 1976, 1978). Some interneurons distribute their axon mainly in the layer, where their cell body is located. These include large multipolar stellate cells, chandelier cells and spiderweb cells, among others. Multipolar stellate cells, found in layers II-VI, have a wide axonal arbour extending to several hundred microns horizontally, in some cases also giving radially oriented collaterals, descending or ascending to adjacent layers (Kisvárday et al., 1987). The characteristic axon of chandelier cells forms short vertical rows of boutons, which are connected by boutonless segments, giving the appearance of candlesticks in a chandelier (del Río & DeFelipe, 1997a; Jones, 1975; Szentágothai & Arbib, 1974). Spiderweb, or neurogliaform cells, provide dense innervation in the close vicinity of their cell bodies (Jones, 1975; Kisvárday et al., 1990; Ramón y Cajal, 1899b; Tamás et al., 2003). Canopy cells, and some neurogliaform cells have both their dendrites and axon restricted to layer I (Schuman et

al., 2019). Other types of interneuron, have axon mostly oriented radially, and provide innervation across multiple layers (Jones, 1975; Kisvárday et al., 1987; Ramón y Cajal, 1899a). These include interneurons with several different dendritic arborisations, such as bitufted, bipolar and multipolar cells. Yet other types of interneuron, such as Martinotti cells, are located in layers III-V and have an ascending axon, which strongly innervates layer I (Lund, 1973; Martinotti, 1890; Ramón y Cajal, 1909).

Interneurons also specialise in innervating different subcellular domains of their target cells, which is partly reflected in the characteristic shape of their axon and boutons. For example, chandelier cells innervate exclusively the axon initial segment of pyramidal cells, hence they are also called axo-axonic cells (Fairén & Valverde, 1980; Freund et al., 1983; Kisvárday, Adams, et al., 1986; Somogyi, 1977; Somogyi et al., 1982). Multiple interneuron types with horizontal or radial axonal distribution, called basket cells, innervate the somata and proximal dendrites of pyramidal cells and interneurons (DeFelipe & Fairén, 1982; Ekstrand et al., 2001; Kisvárday et al., 1985, 1993; Martin et al., 1983; Somogyi et al., 1983; Tamás et al., 1997a, 1998). Martinotti and neurogliaform cells, preferentially innervate the oblique dendrites and the apical dendritic tuft of pyramidal cells (Kisvárday et al., 1990; Tamás et al., 2003; Wang et al., 2004). There are also interneurons with less specific synaptic targeting of dendritic spines, shafts, somata and axon (DeFelipe & Fairén, 1988). Although most of these GABAergic interneuron types preferentially innervate pyramidal cells, they also provide innervation to other interneurons and themselves (Tamás et al., 1997b, 1998). Some types of GABAergic interneuron preferentially innervate other GABAergic interneurons, thus specialising in disinhibition (Acsády et al., 1996a; Acsády et al., 1996b; Freund et al., 1986; Jiang et al., 2013; Letzkus et al., 2015; Meskenaite, 1997a; Pi et al., 2013; Xu et al., 2013).

Furthermore, GABAergic interneurons can be grouped based on differential expression of calcium-binding proteins and neuropeptides (Gonchar et al., 2008; Gonchar & Burkhalter,

1997; Kubota et al., 2011; Rudy et al., 2011). Parvalbumin (PV), Somatostatin and 5-HT3 receptors are expressed by distinct GABAergic interneuron populations, which cover virtually all GABAergic neurons in the neocortex of mice (Rudy et al., 2011). Each group includes multiple interneuron types with different axonal distributions, however, these can be further differentiated based on co-expression of other molecules. For example, parvalbumin expressing neurons include basket cells, dendrite-targeting cells and axo-axonic cells (DeFelipe et al., 1989b; Kawaguchi, 1993; Kawaguchi & Kondo, 2002; Kawaguchi & Kubota, 1998). Axo-axonic cells in humans co-express calbindin, whereas those in monkeys do not (del Río & DeFelipe, 1997a), and a subpopulation of axo-axonic cells in monkeys express corticotropin releasing factor (Lewis & Lund, 1990). Conversely, at least two types of basket cells can be differentiated based on their molecular expression: those, which express PV, and those which express cholecystokinin (Armstrong & Soltesz, 2012; Freund et al., 1986). The latter also express the cannabinoid receptor type I along their axonal membrane (Katona et al., 1999; Neu et al., 2007; Somogyi et al., 2004), and a subpopulation co-expresses vasoactive intestinal polypeptide (VIP) (Ekstrand et al., 2001). Interneurons expressing somatostatin include Martinotti cells (Wang et al., 2004), and other interneuron types (Kawaguchi & Kubota, 1996; McGarry et al., 2010; Riedemann et al., 2018; Xu et al., 2013). The group of interneuorns, expressing 5-HT 3 receptor, includes neurogliaform cells, among multiple other types, which co-express VIP, calretinin, CCK or a combinations of these molecules (Bayraktar et al., 2000; Caputi et al., 2009; Cauli et al., 2000; Férézou et al., 2002; Freund et al., 1986; Kubota & Kawaguchi, 1997; Porter et al., 1998; Rudy et al., 2011).

Finally, based on their evoked firing patterns, interneurons have been grouped into different groups, such as fast-spiking, regular-spiking, irregular-spiking, bursting and low-threshold firing, among many others, which correlate with their molecular expression (Kawaguchi, 1993; Kawaguchi & Kubota, 1993, 1996, 1998; Krimer et al., 2005).

Parvalbumin-expressing interneurons, such as basket cells and axo-axonic cells have a fast-spiking firing pattern characterised by short duration action potentials and continuous high frequency firing (Kawaguchi & Kubota, 1998; Povysheva et al., 2013; Zaitsev et al., 2005). On the other hand, interneurons with diverse axonal distributions, expressing neuropeptides, such as VIP, CCK and somatostatin, have either regular-, irregular-, or bursting firing patterns, characterised by slower action potentials and lower evoked firing rate (Kawaguchi & Kubota, 1996, 1998). Importantly, interneurons expressing the same neuropeptide can have different firing patterns (Kawaguchi & Kubota, 1996). Some interneurons expressing calretinin also have an irregular firing pattern in rats (Kubota et al., 2011) and monkeys (Zaitsev et al., 2005). In contrast, those expressing calbindin show a low-threshold firing phenotype (Kawaguchi & Kubota, 1993). Interneurons with a low-threshold firing pattern also include neurogliaform cells, among other types in rats (Kawaguchi, 1993).

The anatomical, molecular and electrophysiological diversity of GABAergic interneurons reflects their functional specialisation for specific roles in the neocortical circuit. Hence, interneuron types can only be defined by simultaneous characterisation using anatomical, molecular and electrophysiological techniques, which is challenging.

1.1.4 Definition of double bouquet cells

Among GABAergic interneurons, of particular interest are double bouquet cells (DBCs), because of their relative abundance and highly regular distribution in humans and nonhuman primate species (Ballesteros Yáñez et al., 2005). The term double bouquet (bipenachadas in Spanish, bitufted in English) was first introduced by Ramon y Cajal to describe neurons with a bitufted dendritic tree branching extensively on the superficial and deep sides of the cell body, in layers II and upper III of the visual, motor and auditory cortices of human infants (Ramón y Cajal, 1899a) and cat (Ramón y Cajal, 1899b). The majority of such cells had radially oriented axon, some of them forming pericellular baskets, but also some with axon restricted to a small

region around the cell body. He also described small multipolar cells with narrow radially oriented axon, but did not refer to them as double bouquet cells. Later, Jones (1975) defined type III cells, which were located in layer II and upper III of the primary sensory cortex of the squirrel monkey, as neurons with multipolar and bitufted dendrites and radially oriented axon, which forms narrow bundles and aligns with the radial fasciculi of pyramidal cell apical dendrites, and stated that they are the double bouquet cells defined by Ramon y Cajal. Valverde (1976; 1978) also defined neurons with class V axon in layers II and III of the visual cortex of the mouse (Valverde, 1976), and monkey (Valverde, 1978), forming radial bundles, and compared them to the double bouquet cells of Cajal and the type III cells of Jones (1975), however he found them rarely in the mouse. The term "horsetail" for the radial axon bundle of such neurons was introduced by Szentagothai (1975), who also described spiny neurons in layer IV with both ascending and descending bundles of horsetail-shaped axon. The term "horsetail cell" was also used by Meyer (1983), who found these neurons in the visual cortices of the cat (Meyer, 1983; Meyer & Ferres-Torres, 1984), but not in the motor cortex of man (Meyer, 1987). In subsequent studies double bouquet cells were defined as small neurons with various dendritic trees in layers II and upper III with a radially oriented axon, restricted to a narrow cortical column descending through multiple layers in the neocortex of the monkey and human (DeFelipe et al., 1989a; DeFelipe & Jones, 1992; del Río & DeFelipe, 1995; del Río & DeFelipe, 1997c) and the visual cortex of cat and monkey (Somogyi & Cowey, 1981). Somogyi et al. (1981) demonstrated that a population of GABAergic neurons existed in upper layers III and II which could be labelled from the deep layers by retrograde axonal transport of 3H-GABA in the monkey (Somogyi et al., 1981). Intracellularly recorded and labelled neurons *in vitro* with radially oriented axon were also described in the visual cortex of the cat (Tamás et al., 1997a, 1998), frontal cortex of rats (Kawaguchi & Kubota, 1996) and visual cortex of mice (Jiang et al., 2015), and some aspects of the molecular content, electrical behaviour and synaptic

connections of these neurons were studied, although the axonal distribution of the double bouquet cells in these studies, particularly those in rodents does not appear to correspond to the specific horsetail bundles of double bouquet cells described in primates and humans. Furthermore, the axonal distribution, membrane properties, molecular content and synaptic connections of double bouquet cells in humans, where these cells are thought to be the most numerous (Ballesteros Yáñez et al., 2005) has not been characterised. In this thesis I studied double bouquet cells in the human neocortex, defined as neurons located in layers II and upper III, whose axon forms a radially oriented bundle, resembling a horsetail, distributed in a narrow (10 – 20 μm) cortical column, crossing multiple layers while descending towards the white matter (DeFelipe, 2002; Somogyi & Cowey, 1981).

1.1.5 The columnar organisation of the neocortex

It was suggested that the neocortex is composed of columnar modules, local neural circuits, each composed of the same set of neurons, repeated iteratively across the extent of the neocortex with specific modifications in neuronal components, afferent and efferent projections, and local synaptic wiring according to the functional specialisation of the area (Casanova & Casanova, 2019; Hubel & Wiesel, 1969; Mountcastle, 1997; Öngür et al., 2003; Szentágothai, 1975). A presumed basic unit of a module is the minicolumn, consisting of ~80 – 100 interconnected neurons in a narrow radial column (Buxhoeveden & Casanova, 2002; Mountcastle, 1957; Mountcastle, 1997). Neocortical modules (or columns) are thought to be formed of multiple minicolumns interconnected by short horizontal connections.

Several developmental, structural and functional features of the neocortex reflect a columnar principle of organisation. First, immature postmitotic neurons generated serially at the same locus in the germinal epithelium during cortical development migrate radially along the same or adjacent radial glia. These neurons form a radial unit (Rakic, 1974, 2008). Radial

organization of cortical development has also been imaged in humans (McKinstry et al., 2002). It should be noted, however, that tangential migration, particularly of GABAergic interneurons also occurs during development, prior to their radial migration (Fishell et al., 1993; Nadarajah et al., 2002).

Second, structural organisation of several components is in the radial direction. In the primary sensory cortices and particularly in the barrel cortex of mice, specific thalamic afferents, carrying information from a single whisker, terminate on spiny stellate cells in a circumscribed patch of cortex of 0.5 -1.0 mm diameter in layer IV (van der Loos & Woolsey, 1973; Woolsey & van der Loos, 1970). Spiny stellate cells in turn transmit this information through radially oriented axons to the supragranular layers (Lübke et al., 2000; Staiger et al., 2004). Similarly restricted termination patterns of thalamic afferents has also been observed in the primary visual cortex of monkeys (Blasdel & Lund, 1983; Freund et al., 1989; Hubel & Wiesel, 1969, 1972). The termination patterns of cortico-cortical projections also show a columnar organisation (Goldman-Rakic & Schwartz, 1982; Jones et al., 1975; McGuire et al., 1991; Selemon & Goldman-Rakic, 1988), similarly to the neurons of origin (Jones et al., 1975). Furthermore, the apical dendrites of pyramidal cells located in layer II to V bundle together to form narrow radial columns (Fleischhauer et al., 1972; Peters & Walsh, 1972; Peters & Yilmaz, 1993), similar in size to minicolumns (Mountcastle, 1997). Radial bundles are also formed by the myelinated axons of pyramidal cells located in a narrow cortical column, and are alternately spaced with the dendritic bundles (del Río & DeFelipe, 1997c; Peters & Sethares, 1996). Finally, radial organisation of the axons of GABAergic interneurons (Kisvárday et al., 1987; Szentágothai, 1973, 1978), most noticeably that of double bouquet cells (Somogyi & Cowey, 1981; Tamás et al., 1997a), which I study in detail in this thesis, provide further evidence for columnar organisation in the neocortex.

Third, functionally related neurons located in different layers, are also organised in columns. For example, in the visual cortex of monkeys and cats neurons selective for the same orientation are arranged in radial columns across the depth of the cortex (Hubel & Wiesel, 1959, 1968), which has also been demonstrated anatomically (Hubel et al., 1978). Similarly, neurons selective for stimulation of one eye or the other (LeVay et al., 1975), and others selective for different colours (Livingstone & Hubel, 1984), are also arranged in radial columns. Functional columns exist not only in the somatosensory (Mountcastle, 1957), and the primary auditory cortex (Abeles & Goldstein, 1970), but also in the motor cortex (Asanuma, 1975), and association cortices (Albright et al., 1984; Mountcastle et al., 1975; Perrett et al., 1992).

1.1.6 Comparative aspects of neocortical structure and function with special focus on humans

The neocortex is greatly expanded in humans compared to other mammals (Clark et al., 2001; DeFelipe et al., 2002; de Winter & Oxnard, 2001; Nieuwenhuys, 1994). This expansion is thought to be the result of the addition of more neurons, and multiplication of columnar modules, while neuronal density is relatively constant (Bugbee & Goldman-Rakic, 1983; DeFelipe, 2011; Haug, 1987; Mountcastle, 1997). An increase in the number of neurons in humans is particularly evident in the supragranular layers (DeFelipe, 2011). However, the number of neurons in the neocortex was suggested not to be different between humans and other primates (Azevedo et al., 2009). Nevertheless, the proportion of GABAergic neurons in the neocortex is higher in humans and nonhuman primates than in other mammals (Beaulieu, 1993; Beaulieu et al., 1992; Hendry et al., 1987), and they have different developmental origins (Jakovcevski et al., 2011; Letinic et al., 2002).

Differences in the dendritic structure of pyramidal neurons have also been reported. For example, human pyramidal neurons have increased dendritic complexity (Elston et al., 2001; Mohan et al., 2015), and increased spine density (Benavides-Piccione et al., 2002; Elston et al.,

2001) compared to pyramidal neurons in other mammals. Furthermore, dendritic spines in humans are larger and have longer necks than those in mice (Benavides-Piccione et al., 2002). In accordance with these structural differences in dendritic structure, human layer V pyramidal cells show increased dendritic compartmentalisation of electrical signals, compared to those in mice (Beaulieu-Laroche et al., 2018). In addition, pyramidal cells in layers II and III have been found to conduct electrical signals more effectively in humans than in mice (Eyal et al., 2016). Differential ion channel expression between pyramidal cells in humans and mice results in hyperpolarisation activated cation currents altering dendritic signal processing in human pyramidal cells, but not in mice (Kalmbach et al., 2018). Most interestingly, novel calcium-mediated dendritic potentials in human pyramidal cells have been found to be most effectively generated in response to excitatory inputs of a specific strength, while being suppressed by stronger or weaker excitation, a phenomenon not observed in rodent pyramidal cells before (Gidon et al., 2020).

Differences in synaptic transmission have also been observed between humans and rodents. For example, short-term depression in pyramidal to pyramidal cell connections is more pronounced in humans than in mice (Testa-Silva et al., 2014). Excitatory synaptic transmission from pyramidal cells onto fast-spiking interneurons is also more efficient in humans than in rats (Molnár et al., 2016), and may underly the initiation of polysynaptic complex events of excitation and inhibition in human neocortical networks (Molnár et al., 2008; Szegedi et al., 2016, 2017).

Finally, single cell and in situ RNA sequencing of thousands of neurons in mice and humans shows an increased molecular diversity of both glutamatergic and GABAergic neurons (Hodge et al., 2019; Zeng et al., 2012), in parallel with an increased diversity of intra- and subcortical efferent projections in humans (Bakken et al., 2021). Moreover, a novel GABAergic

interneuron type, the rosehip cell has been described in layer I of the human neocortex (Boldog et al., 2018) which also exhibits specific GABAergic tonic inhibition (Field et al., 2021).

1.2 Group III metabotropic glutamate receptors (mGluR)

Glutamate is the most abundant neurotransmitter in the mammalian brain (Balazs et al., 2010; Deutch, 2013), activating receptors in neurons and glial cells. Ionotropic glutamate receptors, such as the α-amino-3-hydroxy-5-methyl-4-isoxazole propionic acid (AMPA), N-methyl-D-aspartate (NMDA) and kainate (KA) receptors are cation channels which mediate fast (millisecond timescale) depolarisation of the neuronal membrane in response to binding of glutamate. For this reason, glutamate is often referred to as 'excitatory', although glutamate can have inhibitory effects on neuronal activity. It was discovered very early that glutamate could also induce long-term (seconds to hours) metabolic responses in neurons and glial cells involving the phosphoinositide pathway and mobilisation of calcium (Ahmed et al., 1990; Murphy & Miller, 1988; Nicoletti, Iadarola, et al., 1986; Nicoletti, Meek, et al., 1986; Nicoletti, Wroblewski, et al., 1986; Pearce et al., 1986; Sladeczek et al., 1985). The receptors mediating these slower effects were named metabotropic glutamate receptors (mGluR), and they mediate the effects of glutamate through G-proteins and intracellular signalling cascades.

1.2.1 General aspects and differentiation from group I and group II mGluRs

Metabotropic glutamate receptors, along with $GABA_B$, calcium sensing, pheromone and taste receptors are the family C G-protein coupled receptors (GPCRs) characterised by a large extracellular N-terminal domain (the Venus Flytrap domain), which includes the agonist binding site. They have seven transmembrane domains, which are often targets of allosteric modulators, and an intracellular domain, which is linked to G-proteins and other intracellular or membrane proteins (Hermans & Challiss, 2001; Jingami et al., 2003; Nicoletti et al., 2011; Pin et al., 2003). Eight genes have been identified coding for different subtypes of mGluRs (mGluR1 - 8), which based on sequence homology, ligand selectivity and G protein coupling, have been separated into three groups. Group I mGluRs include mGluR1 and mGluR5 and are selectively activated by (S)-3,5-dihydroxyphenylglycine (DHPG). They are predominantly

coupled to G_q/G_{11} proteins, which activate phospholipase C_β (PLC_β), leading to accumulation of inositol trisphosphate (IP_3) and diacyl-glycerol (DAG). The result of this cascade is mobilisation of calcium and activation of protein kinase C (PKC) (Aramori & Nakanishi, 1992). Group II mGluRs include mGluR2 and mGluR3, they are selectively activated by (2R,4R)-4-Aminopyrrolidine-2,4-dicarboxylate (2R,4R-APDC or LY314593) and are predominantly coupled to $G_{i/o}$ proteins resulting in the inhibition of adenylyl-cyclase. This leads to a decrease in the concentration of cyclic adenosine-monophosphate (cAMP), which results in decreased phosphorylation of other enzymes and receptors. Finally, group III mGluRs include mGluR4, mGluR6, mGluR7 and mGluR8, and their selective orthosteric agonist is L-(+)-2-Amino-4-phosphonobutyric acid (L-AP4). Group III mGluRs are also predominantly coupled to $G_{i/o}$ proteins (Conn & Pin, 1997; Nakanishi, 1992; Nicoletti et al., 2011; Pin & Duvoisin, 1995; Schoepp et al., 1999). Importantly, in addition to these classical signal transduction pathways, mGluRs have been shown to couple to G-proteins other than their preferred one (Choi & Lovinger, 1996; Kammermeier & Ikeda, 1999; McCool et al., 1998; Wright & Schoepp, 1996), as well as to directly interact with multiple intracellular and membrane proteins, such as ion channels and receptors, independently of G-protein activation (Bertaso et al., 2006; Boss et al., 1994; Calò et al., 2005; Far et al., 2000; Flajolet et al., 2003; Hermans & Challiss, 2001; Heuss et al., 1999; Holler et al., 1993; Kammermeier et al., 2000; Kato et al., 1998; Nicoletti et al., 2011; Rose et al., 2008; Seebahn et al., 2008; Tu et al., 1998, 1999). Historically, mGluRs were thought to function as homodimers, but recently functional heterodimers between subtypes of the same and of different groups have also been reported in heterologous expression systems (Doumazane et al., 2011; Levitz et al., 2016) and in native tissue (Kammermeier, 2012; Xiang et al., 2021; Yin et al., 2014).

Another important difference between different groups of mGluRs is their subcellular location in functionally distinct parts of the neuronal membranes, because this partly determines

the range of molecules with which the receptor can interact. Group I mGluRs are mainly expressed postsynaptically, in the dendritic membrane of neurons, where they are located in the extra-synaptic membrane surrounding the synaptic junction (Baude et al., 1993; Luján et al., 1996, 1997; Millán et al., 2002), but presynaptic mGluR1 action has also been reported in synaptosomes (Manahan-Vaughan et al., 1999; Sistiaga & Sánchez-Prieto, 2000). Group II mGluRs can be located both postsynaptically, in the somato-dendritic membrane, and presynaptically in the axonal membrane of neurons, and similarly to group I mGluRs are located outside the synaptic active zone (Neki et al., 1996; Shigemoto et al., 1997). Finally, group III mGluRs are mainly expressed presynaptically in the axonal membrane, but in contrast to group I and II mGluRs, they are located inside the active zone of synapses (Dalezios et al., 2002; Shigemoto et al., 1996; Somogyi et al., 2003), in close proximity to the N- and Q-type Ca-channels involved in neurotransmitter release (Wheeler et al., 1994).

1.2.2 Pharmacology

Group III mGluRs are selectively activated by L-AP4 and L-serine-O-phosphate (L-SOP), but other related compounds also show similar selectivity towards group III mGluRs compared to other receptor groups (Schoepp et al., 1999; Selvam et al., 2007; Sibille et al., 2007). The potency of L-AP4 is in the submicromolar range for mGluR8, 4 and 6, and in the submilimolar range for mGluR7 (Schoepp et al., 1999). Similarly, mGluR8, 4 and 6 have higher affinity for glutamate than mGlur7 (Schoepp et al., 1999). Subtype-selective agonists include S-3,4-DCPG for mGluR8 (Thomas et al., 2001) and Z-cyclopentyl AP4, for mGluR4 (Johansen et al., 1995). Low-potency, selective group III orthosteric antagonists include (*S*)-2-Amino-2-methyl-4-phosphonobutanoic acid (MAP4) and (*RS*)-α-Methylserine-*O*-phosphate (MSOP) (Mercier & Lodge, 2014), but the group II preferring antagonists LY341495 and (*RS*)-α-Cyclopropyl-4-phosphonophenylglycine (CPPG) also have an antagonistic effect on group III mGluRs with higher potency (Niswender et al., 2008). Furthermore, several subtype-selective

allosteric modulators have been developed, such as *N*-Phenyl-7-(hydroxyimino)cyclopropa[*b*]chromen-1a-carboxamide (PHCCC), VU0155041 and VU0080421, positive allosteric modulators (PAM) of mGluR4, and AMN082, a selective PAM of mgluR7. A selective negative allosteric modulator of mGluR7 is 6-(4-Methoxyphenyl)-5-methyl-3-(4-pyridinyl)-isoxazolo[4,5-*c*]pyridin-4(5*H*)-one hydrochloride (MMPIP). Other pharmacological agents have been reviewed extensively by Niswender and Conn (2010) and Mercier and Lodge (2014).

1.2.3 Expression pattern and subcellular location in the cerebral cortex

Anatomical studies using immunohistochemistry and in situ hybridization, done mostly in rodents have shown that group III mGluRs are selectively expressed across the entire CNS, including the cortex, basal ganglia, thalamus, cerebellum, brainstem and spinal cord, and are mainly located in the presynaptic active zone of synapses (Bradley et al., 1996, 1998; Corti et al., 1998; Iskhakova & Smith, 2016; Kinoshita et al., 1998; Kinoshita, Ohishi, Neki, et al., 1996; Kinoshita, Ohishi, Nomura, et al., 1996; Kinzie et al., 1995; Ohishi et al., 1995; Shigemoto et al., 1997). One exception is mGluR6, which is exclusively expressed on the dendrites of ON bipolar cells in the retina (Nakajima et al., 1993; Nomura et al., 1994; Vardi et al., 2000). In all brain areas studied expression of group III mGluR subtypes is segregated among different neuronal populations and synaptic pathways. The widest expression is shown by mGluR7, and the most restricted is that of mGluR6.

In the hippocampus and neocortex, expression of mGluR7 is the most abundant among group III mGluRs. In the perforant path, the main synaptic input from the neocortex to the hippocampus, mGluR7 is selectively expressed in glutamatergic axons originating from pyramidal cells of the medial entorhinal cortex (medial perforant path), where it is co-expressed with mGluR2. In contrast, axons originating in the lateral entorhinal cortex selectively express mGluR8 (Shigemoto et al., 1997). Other major glutamatergic synaptic pathways in the

hippocampus, such as the mossy fibre pathway, consisting of granule cell axons from the dentate gyrus projecting to the CA3 region of the hippocampus, and the Schaffer collateral pathway, consisting of axons of CA3 pyramidal cells projecting to CA1, also express mGluR7 (Shigemoto et al., 1997). Correspondingly, nerve terminals in the dendritic layers of the hippocampus (str. oriens, str. radiatum and str. lacunosum-moleculare) show different mGluR7 expression levels in the CA1 and CA3 regions (Bradley et al., 1996), being higher in str. radiatum and oriens in CA1, where the Schaffer collaterals terminate, than in stratum lacunosum-moleculare. Conversely, expression of mGluR7 in CA3 is higher in the str. lacunosum moleculare, and lower in strata radiatum and oriens (Kinoshita et al., 1998). In the hippocampus mGluR7 is exclusively expressed in the presynaptic active zone of type I and type II synapses (Bradley et al., 1996; Kinoshita et al., 1998; Shigemoto et al., 1997), the majority of the latter being GABAergic. Although Bradley et al. (1996) reported instances of immunolabelling of dendrites and spines in the neuropil, this was most likely resulting from artefact. These mGluR7 expressing type I and type II synapses innervate dendritic spines, and spiny and smooth dendritic shafts of pyramidal cells and interneurons (Shigemoto et al., 1997). Moreover, in the dendritic layers of the hippocampus and the molecular layer of the dentate gyrus, mGluR7 expressing synapses are not uniformly distributed. Instead, some very strongly immunopositive terminals decorate certain dendrites densely, whereas they omit others (Bradley et al., 1996; Shigemoto et al., 1997). Specifically, pyramidal cell synapses innervating smooth dendrites of interneurons, which express high levels of mGluR1α in their dendritic membranes have 10 fold higher expression of mGluR7 in the presynaptic active zone than synapses targeting dendrites, which do not express mGluR1α, even along single axon collaterals (Shigemoto et al., 1996). This suggests that the level of mGluR7 expression in the pre-synaptic terminals is regulated by the post-synaptic dendrites (Shigemoto et al., 1996) possibly through Elfn-1 (Stachniak et al., 2019). A similar target-cell type-dependent

expression of mGluR7 in GABAergic synapses targeting mGluR1α expressing interneuron dendrites was also observed in the hippocampus (Somogyi et al., 2003).

Expression of mGluR4 and mGluR8 are more restricted in hippocampus than that of mGluR7 (Shigemoto et al., 1997). Correspondingly, immunoreactivity for mGluR8 was found in the outer third of the molecular layer of the dentate gyrus, but not the middle, or inner thirds. Conversely, mGluR4 is selectively expressed in the inner third of the molecular layer, which corresponds to the termination zone of the commissural projections (Shigemoto et al., 1997). Occasionally, selective decoration of dendrites can be observed both with mGluR4 and mGluR8 in the molecular layer of the dentate gyrus, although to a lesser extent than with mGluR7 (Shigemoto et al., 1997). Electron microscopic analysis shows that mGluR4 and mGluR8 are also located in the pre-synaptic active zone of both type I and type II synapses (Corti et al., 2002; Kinoshita, Ohishi, Neki, et al., 1996; Kogo et al., 2004; Shigemoto et al., 1997). Furthermore, mGluR8 expressing type I and type II nerve terminals in str. oriens of the hippocampus selectively innervate a subset of GABAergic neurons, which express type II muscarinic acetyl-choline receptor (M2R) in their somato-dendritic membranes (Ferraguti et al., 2005). A subset of mGluR8 expressing GABAergic synapses in the hippocampus co-express mGluR7, whereas a different subset of these are immunoreactive for vasoactive intestinal polypeptide (VIP) (Ferraguti et al., 2005), a neuropeptide selectively expressed in a subset of GABAergic interneurons, which specifically innervate other GABAergic interneurons (Acsády et al., 1996b).

In neocortical areas, including the entorhinal, piriform, cingulate and primary somatosensory cortex, group III mGluRs are most abundantly expressed in layer I, followed by layers II and III, followed by layer V as assessed by immunohistochemistry. Weak to no expression of group III mGluRs was observed in layers IV and VI (Corti et al., 2002; Kinoshita et al., 1998; Kinoshita, Ohishi, Neki, et al., 1996; Shigemoto et al., 1997). Similarly to the

hippocampus, selective decoration of dendrites by mGluR7 expressing nerve terminals was also observed in the neocortex, particularly in layers II and III, suggesting selective innervation of certain neuron types by mGluR7 expressing synapses (Kinoshita et al., 1998), which was demonstrated by Dalezios et al. (2002). In layer Ia of the piriform cortex mGluR7 and mGluR8 is localised to the presynaptic active zone of type I synapses made by Mitral cells of the olfactory bulb, innervating dendrites of pyramidal cells (Kinoshita, Ohishi, Neki, et al., 1996; Kinzie et al., 1997).

1.2.4 Synaptic effects

The most common effect of group III mGluR activation is inhibiton of synaptic transmission at both glutamatergic (Ayala et al., 2008; Baskys & Malenka, 1991; Capogna, 2004; Gerber et al., 2000; Koerner & Cotman, 1981; McCaffery et al., 1999; Pisani et al., 1997; Turner & Salt, 1999; W. F. White et al., 1979; Xiang et al., 2021; Xi et al., 2003) and GABAergic synapses (Bonci et al., 1997; Chu & Moenter, 2005; Cuomo et al., 2009; Doi et al., 2002; Gereau IV & Conn, 1995; Giustizieri et al., 2005; Kyuyoung & Huguenard, 2014; Matsui & Kita, 2003; Mitchell & Silver, 2000; Panatier et al., 2004; Schrader & Tasker, 1997; Turner & Salt, 2003; Valenti et al., 2003; Wittmann et al., 2001) in many different regions of the brain, although measurements in the neocortex are rare (McCaffery et al., 1999; Xiang et al., 2021). In the hippocampus, suppression of GABAergic synaptic transmission by group III mGluRs is target cell type-dependent in that it is more pronounced at inputs to GABAergic interneurons than to pyramidal cells (Kogo et al., 2004; Semyanov & Kullmann, 2000). The amount of depression also varies depending on the concentration of the agonist used (Kogo et al., 2004), suggesting the involvement of different group III mGluR subtypes. This is in accordance with the target cell type-selective expression of group III mGluRs, as demonstrated by Shigemoto et al. (1996). Target cell-dependent suppression of glutamatergic transmission by mGluR7 has also been demonstrated in mossy fiber synapses to CA3 pyramidal neurons vs synapses of the

same axons onto stratum lucidum interneurons in the hippocampus (Pelkey et al., 2006). Similarly, group III mGluR activation suppresses glutamatergic synaptic transmission from CA3 pyramidal cells onto CA1 interneurons, but not pyramidal cells (Scanziani et al., 1998). In the neocortex, excitatory synaptic inputs to layer V pyramidal cells originating either from the thalamus or other brain regions, are differentially suppressed by mGluR4 activation (Xiang et al., 2021). The suppression of synaptic transmission is primarily mediated by inhibition of neurotransmitter release, which has been directly demonstrated in synaptosomes for glutamatergic (East et al., 1995; Rodríguez-Moreno et al., 1998; Vázquez & Sánchez-Prieto, 1997) and GABAergic synapses (Lafon-Cazal et al., 1999; Schaffhauser et al., 1998; Summa et al., 2013). Although some authors reported examples of group III mGluR activation leading to increase of glutamate or GABA release (Marabese et al., 2005; Ren et al., 2011), this is unlikely to be a direct enhancement of neurotransmitter release, but rather the result if suppression of GABAergic inhibition of glutamatergic or monoaminergic neurons resulting in increased release from those neurons.

Suppression of neurotransmitter release is mediated through inhibition of calcium entry into the terminals via N- and P/Q-type Ca-channels (Giustizieri et al., 2005; Guo & Ikeda, 2005; Pelkey et al., 2006; Rusakov et al., 2004; Takahashi et al., 1996), which can occur together with or independently of modifications in cAMP concentration (Herrero, 1996; Martín et al., 2007; Schoppa & Westbrook, 1997). Furthermore, group III mGluRs may suppress neurotransmitter release independently of Ca-channels through activation of potassium channels (Cochilla & Alford, 1998) and direct modulation of the vesicle release machinery (Erdmann et al., 2012).

Although most studies looked at the short-term modulation of synaptic transmission by group III mGluRs, these receptors have also been implicated in long-term synaptic plasticity. For example, mGluR7 was shown to gate long-term depression of glutamatergic inputs to CA3 interneurons from mossy fibres (Pelkey et al., 2005) and CA3 pyramidal cells (Laezza et al.,

1999). Group III mGluR activation has also been found to induce long-term depression in the hippocampus in vivo (Naie et al., 2006).

1.2.5 Roles in behaviour

The behavioural roles of group III mGluRs have been studied by genetic deletion of different subtypes. Mice with genetic deletion of mGluR4 showed deficit in learning and executing complicated motor tasks (Pekhletski et al., 1996), in accordance with the abundant expression of this subtype in the cerebellum, but also show deficits in a hippocampus dependent spatial memory task (Gerlai et al., 1998). Genetic ablation of mGluR7 selectively impairs short-term working memory in a hippocampus dependent spatial memory task, which is associated with altered theta-frequency oscillations in the hippocampus (Hölscher et al., 2005), but does not affect long-term memory (Hölscher et al., 2004). Mice lacking mGluR7 also show deficits in various conditional learning paradigms (Goddyn et al., 2008). Genetic deletion of mGluR8 results in altered anxiety-related behaviour (see below). Importantly, in these genetic mutants, the respective mGluR subtypes were deleted from the entire brain and body, not just the particular brain area involved in the behavioural response studied. Thus the observed behavioural alterations and deficits are probably not exclusively the result of mGluR disfunction in a single brain area.

1.2.6 Related pathological processes and therapeutic potential

Mental disorders are highly prevalent and disabling diseases, and impose a great social and economic burden (Fayyad et al., 2017; Wittchen et al., 2011; Yang et al., 2021). Current treatments are only effective in a fraction of cases and their use is limited by side effects, thus new therapeutic targets are constantly investigated (Hecking et al., 2021; Nieman, 2015; Park et al., 2015; Sanacora et al., 2012; Tsai & Coyle, 2002; Wijeratne & Sachdev, 2008). Group III mGluRs have been investigated as potential drug targets for the treatment of mental disorders

(Ferraguti, 2018; Kalinichev et al., 2014; Maksymetz et al., 2017; Park et al., 2015; Robbins et al., 2007), neurodegenerative disorders, such as Parkinsons disease (Amalric, 2015; Charvin, 2018), neurological disorders, such as epilepsy (Sansig et al., 2001) and neuroinflammation (Fallarino et al., 2010).

Genetic and pharmacological studies in rodents suggest that group III mGluRs may play a role in the pathophysiology of epilepsy (Mercier & Lodge, 2014). Mice lacking mGluR7 show higher susceptibility to seizures than healthy littermates (Sansig et al., 2001). Conversely, mice lacking mGluR4 show resistance against absence seizures induced by GABA-A receptor antagonists (X. Wang et al., 2005). A history of seizures also alters group III mGluR function in the hippocampus of mice (Dammann et al., 2018). Activation of group III mGluRs by central administration of agonists has been shown to have anticonvulsive effects in multiple different epilepsy models (Chapman et al., 2001; Folbergrová et al., 2001, 2003, 2008; Suzuki et al., 1996) either by their own action or by enhancing the anticonvulsive effects of ionotropic glutamate receptor blockers (de Sarro et al., 2002). A decrease in group III mGluR function has also been reported in the human epileptic hippocampus (Dietrich, 1999).

Through their inhibitory effect on neurotransmitter release, group III mGluRs show neuroprotective potential. Intracerebroventricular injection of L-AP4 has neuroprotective effects and improves cognitive performance after brain injury in rats (Zhou et al., 2003). Systemic injection of an mGlur4 PAM also has neuroprotective effects against 1-methyl-4-phenyl-1,2,3,6- tetrahydropyridine (MPTP)-induced toxicity in the substantia nigra (Battaglia et al., 2006). Activation of group III mGluRs by endogenous glutamate also protects against excitotoxicity in the hippocampus induced by intracerebral injection of 4-aminopyridine (4-AP) (Vera & Tapia, 2012).

Different subtypes of group III mGluRs in the amygdala, have been implicated in fear learning and anxiety (Mercier & Lodge, 2014). For example, genetic deletion of mGluR7 in mice causes deficiency in the expression of cued fear conditioning (Masugi et al., 1999), whereas deletion of mGluR8 disrupts contextual fear expression (Fendt et al., 2013). Accordingly, selective activation of mGluR8 in the amygdala inhibited the acquisition and expression of fear (Schmid & Fendt, 2006). Although the fear-related responses studied are amygdala dependent processes, the genetic modifications were not restricted to the amygdala. Interestingly, genetic deletion of mGluR7 appears to have anxiolytic effects (Cryan et al., 2003a), while deletion of mGluR8 increases anxiety in mice (Linden et al., 2002), as evaluated by the elevated plus maze. Furthermore, administration of both group III mGluR antagonists (Stachowicz et al., 2007) and agonists (Pałucha et al., 2004; Stachowicz et al., 2009) has been found to have anxiolytic effects in mice.

Finally, pharmacological agents acting on group III mGluRs, and particularly PAMs of mGluR4, show promise in the treatment of Parkinsons's disease (Amalric, 2015; Amalric et al., 2013). Antiparkinsonian effects are either by mGluR4 selective PAMs on their own or in combination with l-DOPA (Jones et al., 2012), and are thought to be mediated by modulation of synaptic transmission at the cortico-striatal (Gubellini et al., 2014), striato-pallidal (Beurrier et al., 2009; Lopez et al., 2007; MacInnes et al., 2004; Marino et al., 2003; Valenti et al., 2003), or subthalamo-nigral synapses (Lopez et al., 2012). Their neuroprotective effects may also contribute (Betts et al., 2012). Recently, an mGluR4 PAM, foliglurax, showed promise in alleviating the symptoms of Parkinson's disease by inhibiting neurotransmitter release at striato-pallidal synapses in pre-clinical rodent and primate models, and was introduced into clinical trials (Charvin, 2018; Charvin et al., 2017, 2018). However, the drug failed in phase III, because of inefficiency as compared to placebo (Doller et al., 2020).

1.3 Rationale and aims

The motivation of my studies was twofold. First, evolutionary expansion and diversification in the human neocortex involves cell types and synaptic connections (Bakken et al., 2021; Boldog et al., 2018; DeFelipe, 2011), which may not be present in rodents, the most commonly used mammals for neuroscience research. Second, despite many drugs acting on mGluRs showing promise in rodents for treatment of many neuropathological conditions, none of them have been introduced into clinical practice. In rodents, group III mGluRs show a brain area and cell type-selective expression (Ferraguti & Shigemoto, 2006), and inhibit GABAergic and glutamatergic synaptic transmission in a cell type-specific manner (Kogo et al., 2004; Pelkey et al., 2005; Scanziani et al., 1998; Semyanov & Kullmann, 2000). However, nothing is known of their effects in human neocortical networks. Direct investigation of group III mGluR function in human neuronal networks may uncover human-specific network organisation and may help to explain the effects of drugs acting on group III mGluRs, or the lack thereof, in human mental disorders and could facilitate development of more efficacious drugs. The aim of my studies was to investigate GABAergic interneuron types and their synaptic connections in human neocortex and to explore the roles of group III mGluRs in the regulation of GABAergic synaptic transmission in identified GABAergic cell types, using in vitro patch clamp in acute cortical slices from patients.

The specific aims were to:

1. Record and identify GABAergic interneuron types based on the distribution of their axon and dendrites, molecular expression and electrical behaviour.
2. Test which GABAergic interneuron types are synaptically connected.
3. Test if different GABAergic interneuron types specialise in synaptic targeting of other select neurons and their subcellular domains.

4. Test if activation of group III mGluRs differentially suppresses spontaneous GABAergic synaptic transmission onto different types of GABAergic interneuron and pyramidal cells.

2 Experimental procedures

2.1 Ethical approval and patient consent

For this thesis human tissue samples were collected from patients undergoing neurosurgery at the John Radcliffe Hospital (Oxford) for the treatment of brain tumours or temporal lobe epilepsy (table 2.1). All samples were collected and used in accordance with the Human tissue Act 2004 (UK), under the ethical licence (15/SC/0639) of the Oxford Brain Bank (OBB), Department of Neuropathology, John Radcliffe Hospital, Oxford, UK, and for the purpose of the project entitled "Dis-inhibitory circuits in the human cerebral cortex**"** (ERC grant 694988). Patients consented to providing the samples after they were fully informed by a medical professional not involved in the study. All collected samples represented "access tissue", that is tissue necessarily removed in order to access the diseased part of the brain, but not directly affected by the pathological process, which otherwise would have been discarded. An additional six tissue samples were imported through the OBB from the laboratory of professor Gábor Tamás, at the University of Szeged, Hungary, which were collected after informed consent of patients in the Department of Neurosurgery, University of Szeged, Hungary, under the ethical licence (75/2004), as specified by Hungarian law and the University of Szeged.

Table 2.1 Patient information

patient code	sex	age range	cells	cortical region	diagnosis (type)	cortical infiltration	intracranial pressure/ oedema
A	M	50-54	PMC 14	rITG	Diffuse glioma (WT)	Not known	Not known
B	F	65-69	AAC 1 RH 1	rITG	Glioblastoma (WT)	Yes	No
C	F	40-44	DBC 1	rMFG	Glioblastoma (IDH1 mutant)	No	No
D	M	75-79	AAC 2	rSTG	Glioblastoma (WT)	No	No
E	F	55-59	DBC 2,3	rITG	Metastatic melanoma (WT)	No	No
F	M	65-69	NGC 1	lSFG	Metastatic melanoma (WT)	No	No
G	M	65-69	DBC 27,28	rSPL	Glioblastoma (WT)	NC	No
H	M	50-54	AAC 3, 4	lSFG	Subependymoma (WT)	No	No
I	F	30-35	AAC 5 NGC 2	rITG	TLE (n.a.)	No	No
J	M	50-54	PMC 8	rF	Glioblastoma (WT)	Yes	Yes
K	F	18-20	DBC 4, 5, 6 NGC 3	rMTG	Focal epilepsy (n.a.)	No	No
L	M	50-54	NGC 4	rF	Metastatic adenocarcinoma (WT)	NC	Yes
M	M	80-84	DBC 29	rT	Glioblastoma (WT)	Yes	Yes
N	M	60-64	DBC 7, 8, 9	POL	Metastatic adenocarcinoma (WT)	Yes	Yes
O	F	65-69	DBC 10,30 PMC 12	rT	Glioblastoma (WT)	NC	Yes
P	M	50-54	DBC 11, 12 AAC 6 NGC 5	rP	Glioblastoma (WT)	NC	Yes
Q	F	70-74	DBC 13 CTR 1 AAC 7 NGC 6	rSFG	Metastatic melanoma (WT)	No	No
R	F	45-49	NGC 7	rSTG	Meningioma (WT)	No	No
S	F	60-64	CTR 2	rITG	Glioblastoma (WT)	Yes	Yes
T	M	40-44	DBC 14 NGC 8	rSTG	Oligodendroglioma (WT)	Yes	No
U	M	50-54	DBC 15 NGC 9	rITG	TLE (n.a)	No	No
V	M	40-44	PMC 13 NGC 10	rITG	Oligodendroglioma (WT	Yes	yes

patient code	sex	age range	cells	cortical region	diagnosis (type)	cortical infiltration	intracranial pressure/ oedema
W	M	60-64	PMC 1 CTR 3	rMTG	Glioblastoma (WT)	NC	Yes
X	F	30-34	PMC 5	lMFG	Astrocytoma (IDH1 mutant)	Yes	No
Y	F	55-59	PMC 2 NGC 11	rMTG	Meningioma (n.a.)	NC	No
Z	F	60-64	DBC 16, 17 CTR 4,5 NGC 12, 13, 14	lMFG	Glioblastoma (WT)	NC	No
AA	M	60-64	PMC 3, 4, 6, 7	lMTG	Glioblastoma (WT)	NC	Yes
BB	M	50-54	CTR 6	rITG	Glioblastoma (WT)	No	No
CC	F	35-39	PMC 9	rITG	Anaplastic astrocytoma (IDH1 mutant)	NC	Yes
DD	F	50-54	DBC 18, 31 PMC 10, 11 CTR 7 NGC 15, 16	lITG	Glioblastoma (WT)	Yes	No
EE	M	60-64	DBC 19, 20, 25, 32 NGC 17, 18	rIPL	Dysembryoplastic neuroepithelial tumour (n.a.)	No	No
FF	M	60-64	DBC 26 NGC 19, 20	rITG	Anaplastic astrocytoma (IDH1 mutant)	No	No
GG	F	55-59	DBC 21, 22, 23, 24 NGC 21, 22	rITG	Anaplastic astrocytoma (IDH1 mutant)	NC	No
HH	F	55-59	-	rT	Subarachnoid haemorrhage (n.a.)	n.a.	-
II	F	45-49	-	rF	Subarachnoid haemorrhage (n.a.)	n.a.	-
JJ	M	55-59	-	rF	Metastatic tumour (not known)	-	-
KK	M	18-20	PYR 1	rMTG	Trauma (n.a.)	n.a.	Yes
LL	M	25-29	PYR 2	lMTG	Intraventricular haemorrhage (n.a.)	n.a.	
MM	M	65-69	PYR 3	lMTG	Supratentorial tumour (not known)	-	-

Samples HH – MM were imported provided by prof. Gábor Tamás at the University of Szeged, Hungary. ITG – inferior temporal gyrus; MTG – middle temporal gyrus; STG – superior temporal gyrus; MFG – middle frontal gyrus; SFG – superior frontal gyrus; SPL – superior parietal lobule; IPL – inferior parietal lobule; POL – parieto-occipital lobe; T – temporal; F – frontal; P – parietal; l – left; r – right; DBC – double bouquet cell; PMC – parvalbumin-expressing multipolar cell; AAC – axo-axonic cell; NGC-neurogliaform cell; RHC – rosehip cell; PYR – pyramidal cell; CTR – pharmacological control; WT – wild type; IDH – isocitrate dehydrogenase 1; NC – not conclusive; empty cells – not known

patient code	seizures (onset)	anticonvulsive medication	steroid medication	other medication	medical history
A	Partial (not known)	Carbamazepine; levetiracetam	None	None	Posterior fossa astrocytoma; radiotherapy; traumatic brain injury; left temporal meningioma
B	No (n.a.)	None	Dexamethasone	Amitriptyline lansoprazole; bendrofluzothiazide; atorvastatin	HTN; anxiety
C	No (n.a.)	Levetiracetam	Dexamethasone	Omeprazole; Sertraline	Depression
D	Yes (5m)	Levetiracetam	Dexamethasone	folic acid; omeprazole; ramipril; simvastatin	HTN
E	No (n.a.)	None	Dexamethasone	None	Melanoma surgically removed
F	No (n.a.)	Levetiracetam	Dexamethasone	Dalteparin; Omeprazole; iron; allopurinol	Melanoma; Immunotherapy; Bilateral pulmonary embolisms
G	No (n.a.)	None	Dexamethasone	Amlodipine; lansoprazole; atorvastatin	HTN
H	No (n.a.)	None	Dexamethasone	None	None
I	Yes (13y)	Carbamazepine; Lamotrigine; Pregabalin; Perampanel	None	None	None
J	Yes (not known)	Levetiracetam	Dexamethasone	Nicotine; omeprazole; lactulose	None
K	Yes (2.5y)	Levetiracetam; lacosamide; carbamazepine	Dexamethasone	Depo injection contraceptive	None
L	No	None	Dexamethasone	Metformin; salbutamol; glicazide	Colorectal metastasis resected; asthma; Type II DM
M	Yes (not known)	Levetiracetam	Dexamethasone	Metformin; salbutamol	Asthma (mild); Type II DM
N	No (n.a.)	Levetiracetam	Dexamethasone	None	Metastatic lung cancer; AKI
O	No (n.a.)	None	Dexamethasone	Amlodipine	HTN
P	No (n.a.)	Levetiracetam	Dexamethasone	None	None
Q	Yes (not known)	Levetiracetam	Dexamethasone	lansoprazole	None

patient code	seizures (onset)	anticonvulsive medication	steroid medication	other medication	medical history
R	Yes (not known)	Levetiracetam	Dexamethasone	fluoxetine fostair inhaler; salbutamol inhalor	None
S	No (n.a.)	None	None	Amlodipine	HTN
T	Yes (3y)	Lamotrigine	Dexamethasone	None	None
U	Yes (5y)	Carbamazepine; clobazam; lamotrigine; levetiracetam	None	Beclometasone inhaler	Asthma
V	Yes (5y)	Levetiracetam	Dexamethasone	Hydrocoison; mirtazapine; testosterone; paracetamol; adcal-D3; levothyroxine	Secondary Addison's
W	No (n.a.)	Levetiracetam	Dexamethasone	Amlodipine; loratadine; paracetamol	HTN
X	Yes (4m)	Levetiracetam	none	Beclometasone; salbutamol	Asthma
Y	Yes (2m)	levetiracetam	None	None	None
Z	No (n.a.)	None	dexamethasone	Atorvastatin	High cholesterol
AA	Yes (15d)	Levetiracetam	Dexamethasone	None	None
BB	No (n.a.)	Levetiracetam	Dexamethasone	None	None
CC	Yes (10d)	Levetiracetam	Dexamethasone	None	None
DD	Yes (2m)	Levetiracetam	None	Doxycycline	None
EE	No (n.a.)	None	Dexamethasone	None	None
FF	Yes (6y)	Levetiracetam	Dexamethasone	Amlodipine, atorvastatin; gliclazide; indapamide, metformine; perindopril	HTN; Diabetes; High cholesterol

patient code	seizures (onset)	anticonvulsive medication	steroid medication	other medication	medical history
GG	No (n.a.)	None	None	Amlodipine; ramipril; sertraline	Depression,; HTN
HH	-	-	-	-	-
II	-	-	-	-	-
JJ	-	-	-	-	-
KK	-	-	-	-	-
LL	-	-	-	-	-
MM	-	-	-	-	-

HTN – hypertension

2.2 Sample collection and slice preparation

All surgeries were performed between 10 am and 8 pm, the vast majority being performed between 10 AM and 2 PM (UK time). After opening of the skull and the dura mater, the area of access was determined by the surgeon. Four cuts were made perpendicular to the surface to a depth of 1-2 cm around the sample area using a surgical scalpel, and the sample (size 1-2 cm^3), including all layers and white matter, was removed by cutting through the base with a spatula and dropped into ice-cold cutting artificial cerebrospinal fluid (ACSF) saturated with carbogen (95 % O_2, 5 % CO_2). Electrical cauterization of the blood vessels around the sample was only performed after the removal of the sample, unless deemed necessary by the surgeon. The average time from the first cut until the sample was immersed in cutting ACSF was 1 minute.

Two different cutting ACSFs were used. First, for samples collected before June 2018 the cutting ACSF contained the following (in mM): 65 sucrose, 85 NaCl, 25 $NaHCO_3$, 2.5 KCl, 1.25 NaH_2PO_4, 0.5 $CaCl_2$, 7 $MgCl_2$, 10 glucose. The pH was adjusted to ~7.3, and the final osmolality was ~300 mOsm/L (Bocchio et al., 2019). Second, from June 2018 onward, the cutting ACSF contained the following (in mM): 92 N-methyl-D-glucamine (NMDG), 2.5 KCl, 1.25 NaH_2PO_4, 30 $NaHCO_3$, 20 4-(2-hydroxyethyl)-1-piperazineethanesulfonic acid (HEPES), 25 glucose, 2 thiourea, 5 Na-ascorbate, 3 Na-pyruvate, 0.5 $CaCl_2 \cdot 4H2$ O and 10 $MgSO_4 \cdot 7H_2O$ (pH ~7.3 , ~300 mOsm/L) (Ting et al., 2018).

The samples were further cut into 2-3 smaller blocks at the hospital in ice-cold cutting ACSF constantly bubbled with carbogen, in order to create a flat surface perpendicular to the pia, parallel to which the slicing was then performed. One or two blocks were then transported to the laboratory at the Department of Pharmacology, in the same solution saturated with carbogen, in a sealed transport bottle. The transport took 10-15 minutes, during which the

solution was not bubbled with carbogen. Any remaining pieces were immediately immersed in an ice-cold fixative solution containing 4% (wt/vol) paraformaldehyde (PFA, Sigma Aldrich), 0.05% (wt/vol) glutaraldehyde (GA, TAAB Laboratories Equipment Ltd.), and 15% (vol/vol) saturated picric acid (Sigma Aldrich) in 0.1 M phosphate buffer (PB) at pH ~7.2.

Immediately after arrival at the department of the live sample, slices of ~350 µm thickness were cut on a vibratome (VT1200, Leica Instruments; or Hyrax v50, Zeiss; or Microm HM 650 V, Thermo Fisher Scientific) in ice-cold cutting ACSF, and were left to recover in the same solution at ~37 ºC for 15-25 minutes. After this the cutting ACSF was gradually replaced by either recording ACSF (before June 2018), or storing ACSF (after June 2018), and were kept in this solution at room temperature until recording. The recording ACSF contained the following (in mM): 126 NaCl, 2.5 KCl, 1.2 NaH_2PO_4, 26 $NaHCO_3$, 3 $CaCl_2$, 1.5 $MgCl_2$, 10 glucose, (pH ~7.3, ~300 mOsm/L). The storing ACSF contained the same components as the NMDG-based cutting ACSF except the NMDG was replaced with 92 mM NaCl. All solutions were continuously bubbled with carbogen.

2.3 Electrophysiology

2.3.1 Whole-cell patch-clamp recordings

Electrophysiological recordings were performed similarly to what was described earlier (Bocchio et al., 2019; Field et al., 2021), with some modifications, over 10-16 hours after slicing between 12 PM and 4 AM the next day. Slices were transferred to the recording chamber where they were stabilised with a plastic string harp, and were perfused continuously with recording ACSF saturated with carbogen at a flow rate of ~4 ml/min using a peristaltic pump (Gilson). The time required for the solution to reach the chamber was 45-60 seconds. Recordings were made using chlorided silver electrodes. Glass capillaries of 4-6 MΩ resistance were prepared from borosilicate glass capillaries (1.2 mm; GC120F, Harvard Apparatus) using a horizontal

puller (DMZ Universal, Zeitz-Instrument). Capillaries were filled with an internal solution containing the following (in mM): 126 K-gluconate, 4 KCl, 4 ATP-Mg, 0.3 GTP-Na_2, 10 Na_2-phosphocreatine, 10 HEPES, and 0.05% biocytin, with osmolality of 270–280 mOsmol/L without biocytin, at pH ~7.3 adjusted with KOH. The slices and neurons were visualised with a differential interference contrast (DIC) microscope (Olympus BX51WI) using a LUMPlanFL 60x water objective (Olympus) and equipped with a digital camera (Zyla, ANDOR), connected to a desktop computer. Whole-cell patch-clamp recordings were performed from neurons in layers II and III, at 33-37 ^{o}C, using either an EPC-10 triple patch clamp amplifier and Patchmaster software (HEKA), or a Multiclamp 700B amplifier and pClamp software (Molecular Devices). With the former, data was digitized at 50 or 100 kHz for current-clamp recordings and at 50 kHz for voltage-clamp recordings. With the latter, data was digitized at 10 kHz for both current-clamp and voltage-clamp recordings. The reported voltage values are not compensated for a 16 mV junction potential between the ACSF and the internal solution, as calculated using Igor Pro software (WaveMetrics).

Before patching, pipette resistance was continuously monitored through a 10 ms voltage step of 10 mV amplitude. After achieving successful cell attached configuration, as assessed by achieving the "Gigaseal", a pipette resistance over 1 GΩ, and compensation of the fast capacitance component, break into the cell was achieved by carefully sucking on the recording pipette through an attached tube. After break-in, if stable access to the cell was achieved, the cell was held in current-clamp mode with a holding current between 0 and -100 pA, to maintain a membrane potential of approximately -60 mV. Voltage responses to a series of 800 ms long current steps starting from -100 pA relative to the initial holding current until rheobase +100 pA with 20 pA increments between sweeps were recorded at the beginning of each recording (I-V traces). The initial holding current was aimed to be a multiple of 20 pA. Bridge balance was not adjusted during current clamp recordings.

For paired recordings, whole-cell configuration was established for two neurons simultaneously. After recording the voltage responses of both neurons in response to current injection steps, each cell was tested for postsynaptic responses evoked by the other neuron. A pair or a train of five action potentials (APs) 50 ms apart were evoked in one neuron by brief (1-5 ms) square pulses of current injection of 300-800 pA amplitude. In order to detect GABA-A receptor mediated unitary evoked inhibitory postsynaptic currents (eIPSCs), the other neuron was held at just subthreshold potentials (-40 - -45 mV) in voltage-clamp mode, to provide the driving force for the primarily chloride ion current flowing through GABA-A receptors ($E_{Cl^-} \approx$ -94 mV as calculated through the Nernst equation). Synaptic connectivity was assessed visually during the recording, by checking the sweeps for fast upward current deflections in the postsynaptic cells with sharp rising phase and a slower, exponential decay phase, consistent with GABA-A receptor mediated postsynaptic currents, within 5 ms of the peak of the presynaptic AP. A paired- or train-pulse protocol was used in order to assess the short-term plasticity of the connections, by comparing the amplitudes and failure rates of the postsynaptic responses at the first and subsequent APs in the sweep. If a train-pulse protocol was used, 1 s after the last presynaptic AP, a test AP was evoked to evaluate the recovery of the postsynaptic response from the short-term plasticity during the train. At the end of each sweep a 10 ms current step of -100 pA relative to the baseline holding current, which was between 0 and -100 pA, was applied to the cell held in current-clamp mode, whereas a 10 ms step of -10 mV relative to the clamp potential was applied to the cell held in voltage-clamp, to monitor the uncompensated series resistance (Rs). Connectivity was tested in both directions. At least 15 sweeps were recorded for each tested connection with intervals of 15 seconds. Ionotropic glutamate receptors were not blocked during these experiments.

In single neurons, spontaneous inhibitory postsynaptic currents (sIPSCs) were recorded by continuously clamping the neurons to just subthreshold membrane potentials (-40 - -45 mV)

for the same reason as described above. After a stable recording of baseline synaptic activity (3-5 minutes), group III mGluRs were activated by bath application of either 50 or 300 μM of the prototypical orthosteric agonist, L-2-amino-4-phosphonobutyric acid (L-AP4) for 4-5 minutes. At the lower concentration, L-AP4 is thought to activate only the high affinity sybtypes, mGluR 4 and 8, whereas at the higher concentration it would also activate mGluR7 (Cartmell & Schoepp, 2000; Kogo et al., 2004). Finally, the drug was allowed to wash out for 5-15 minutes, by perfusion of recording ACSF. Uncompensated series resistance was monitored every minute by application of a 10 ms voltage step of -10 mV. Action potentials and ionotropic glutamate receptors were not blocked during these experiments, thus sIPSCs represented both AP- dependent and independent IPSCs. To demonstrate that both spontaneous and evoked IPSCs recorded in these experimental configurations were mediated by $GABA_A$ receptors, gabazine (16 μM) was perfused into the recording chamber, which completely abolished fast outward currents in both experimental settings (see fig. 3.1).

2.3.2 Drugs and compounds

Sucrose, KCl, NaH_2PO_4, $MgCl_2$, NMDG, thiourea, Na-ascorbate, Na-pyruvate, K-gluconate, ATP-Mg, Na_2-phosphocreatine and biocytin were purchased from Sigma-Aldrich. NaCl, $NaHCO_3$, $CaCl_2$, $CaCl_2 \cdot 4H_2O$ and $MgSO_4 \cdot 7H_2O$ were purchased from Scientific Laboratory Supplies (SLS). D-glucose, HEPES, GTP-Na_2 and HCl were purchased from Merck Life Sciences. Sodium azide, NaOH and KOH were purchased from VWR International. Finally, gabazine was purchased from TOCRIS Bioscience, and L-AP4 was purchased from TOCRIS Bioscience, Enzo Life Sciences and Abcam.

2.3.3 Data analysis and inclusion criteria

The following criteria were applied for inclusion of the cells' current-voltage traces in the analysis: 1. After break-in, the holding current was between 0 and -100 pA for holding the cell

below -60 mV; 2. At least one overshooting AP could be elicited by depolarising current injections; 3. The fast capacitance associated to the contact surface between the bath solution and the pipette surface was successfully compensated and no oscillation artefacts were observed in the voltage traces. The following additional criteria were applied for inclusion of the eIPSCs and sIPSCs in the analysis: 1. Series resistance, calculated as the ratio of the applied -10 mV voltage step and the peak initial current deflection, was less than 35 MΩ during the entire recording and did not change more than 25%; 2. there were no sudden shifts in Rs. If the Rs was initially acceptable, but fell outside the inclusion parameters later during the experiment, the data acquired before the first excluding parameter shift were still analysed.

PatchMaster (.dat) files were opened in Igor Pro software v7.0.8.1 (WaveMetrics) using Patchers's Power Tools (Department of Membrane Biophysics, Max Planck Institute for Biophysical Chemistry, Göttingen, Germany[1]). The intrinsic membrane parameters calculated in Igor Pro from the I-V traces recorded at the beginning of each recording, were the following (voltage traces were digitally adjusted to remove the artefact resulting from the bridge balance): Input resistance (IR) was calculated as the slope of the linear fit to the subthreshold steady state voltage responses and the injected current ($V = a + b*I$, where V is the steady state voltage response, I is the injected current, and b is the input resistance). Resting membrane potential (Vm), was measured as the steady state voltage in response to 0 pA current injection, or was calculated as the constant (variable 'a' in the formula above) of the linear fit to the subthreshold steady state voltage responses and the injected current steps. The membrane time constant (τ) and whole-cell capacitance (C_m) were calculated from the current-clamp recordings, as described in Golowasch et al. (2009): τ was calculated as the time constant of the slowest component of a double-exponential fit to the voltage deflection in response to holding current

[1] http://www3.mpibpc.mpg.de/groups/neher/index.php?page=aboutppt

-100 pA current injection step from the beginning of the step until the peak negative deflection; to get C_m, t was divided by the voltage deflection amplitude associated to the slowest exponential term ($V_m(t) = V_0 + \sum_{i=1}^{2} V_i e^{-t/\tau}$, where V_0 is the baseline membrane potential and V_i is the amplitude of the voltage deflection associated to each exponential term)(Golowasch et al., 2009). The sag ratio was calculated as the ratio of the maximum voltage deflection over the difference of the steady state voltage and the baseline voltage, in response to holding current -100 pA current injection. The rheobase was measured as the current injected at the first step, when an AP was generated.

For the measurement of single AP parameters, the voltage traces were exported as a text file, and were imported into Matlab R2020a (MathWorks). Using a custom written script, the first AP was detected by threshold search for each cell, and the following measurements were made. Threshold was measured as the membrane potential at which the rate of change in membrane voltage exceeded 20% of the maximum rate of change. Amplitude was calculated as the difference between the peak membrane voltage and the threshold. Afterhyperpolarisation amplitude (AHP) was calculated as the difference between the threshold and the lowest membrane voltage after the peak. Half-width was calculated as the time difference between the membrane voltage reaching a value halfway between the peak and the threshold on the depolarising phase and the same membrane voltage on the repolarising phase of the AP. All the above measurements were made on the first AP elicited at rheobase current injection for each cell. Average firing frequency, spike frequency adaptation, spike amplitude accommodation, and the coefficient of variation of the inter-spike intervals (ISI CV) were calculated from the voltage response to rheobase +100 pA current injection in Igor Pro, after threshold detection of the APs. Average firing frequency was calculated by dividing the number of APs with the duration of the stimulation (800 ms). Frequency adaptation was calculated as the last ISI over

the first, and amplitude accommodation was calculated as the amplitude of the last AP over the amplitude of the first.

Evoked IPSCs were detected with TaroTools toolbox for Igor Pro (https://sites.google.com/site/tarotoolsregister), using a threshold detection method, followed by visual inspection. The threshold was adjusted for every recording and was between 4 and 7 pA. The time of onset and time of peak of the events were detected automatically. Trials in which no eIPSC was detected, were considered as failures. Response delay (lag) was measured as the time elapsed from the peak of the first presynaptic AP until the onset of the first IPSC (IPSC1). In the case of pair 3 (see chapter 3.2.2; fig. 3.8 K, L), the lag was calculated from the peak of the first AP in the presynaptic burst. The mean amplitude of IPSC1 and IPSC2 were calculated from all trials, including failures, as the average difference between the current at onset and the current at the time of peak. The failure rate (FR) was calculated as the number of failures over the number of trials . By default, FR was only calculated for IPSC1, except in the case of pair 2 (see chapter 3.2.2; fig. 3.8 E, G), where it was also calculated for IPSC2. The paired-pulse ratio, an indicator of presynaptic release probability, was calculated as the mean amplitude of IPSC2 over the mean amplitude of IPSC1, including failures. The half-width and the risetime (20-80%) were calculated automatically by the software from IPSC1.

For the analysis of spontaneous IPSCs the relevant traces were exported as text files and were imported into Clampfit v10.7.0.3 (Molecular Devices). Analysed periods included all 3-5 minutes of baseline recordings, whereas for group III mGluR activation, only periods after 2 minutes of drug application were analysed, to allow for the drug to reach maximum concentration in the recording chamber and achieve reasonable penetration into the slice. Washout of L-AP4 was allowed for 5-15 minutes, but in some cases a loss of stability or too large a change in Rs was observed, and thus this period could not be analysed. For the detection of sIPSCs, first a typical IPSC was visually identified in the baseline period, and was used as a

template for automatic detection in Clampfit. Detection threshold was adjusted for each recording and was between 4 and 5. After the first round of detection, events with an amplitude smaller than 5 pA, and a risetime (20-80%) longer than 5 ms were removed, and the remaining events were averaged to create a second template. This template was the used in a second round of event detection. The frequency of sIPSCs was calculated as the number of events over the duration of the respective period. The median sIPSC amplitude was calculated for each period.

Because no reliable measurements could be made of the period after the washout of L-AP4 due to instability, to control for changes induced in sIPSC frequency and amplitude by factors not related to the application of L-AP4, including changes in Rs, slice degradation, and rundown of synaptic events due to dilution of the intracellular composition of neurons by the internal pipette solution, recordings were made in which instead of application of L-AP4, only the vehicle recording ACSF was continuously applied for 15-20 minutes. These control recordings were alternating with test recordings during every recording session, so that the wide range of recording times and slice survival periods were covered. All traces recorded in voltage-clamp were filtered with a 2 kHz lowpass Bessel (8-pole) filter, and with boxcar smoothing (11 points) in Clampfit or IgorPro before analysis.

2.3.4 Statistics

All statistical tests were carried out in Origin Pro (v 94E 2017, OriginLab), and are reported in full in the results. Values are reported as mean ± standard deviation, unless stated otherwise in the text.

2.4 Anatomical analysis

Recorded neurons were intracellularly labelled by the spontaneous diffusion of the biocytin included in the internal pipette solution (0.05% w/v). After completion of the electrophysiological recording, slices were immersed and left overnight in fixative, containing 4% (w/v) PFA and 15% (v/v) saturated picric acid in 0.1 M PB at pH ~7.2 at 4ºC. Slices were thoroughly washed and stored in 0.1M PB containing 0.05% w/v sodium azide until further processing. For resectioning, slices were embedded in 20% w/v gelatine (Sigma), postfixed with the fixative described above for 20 minutes, and resectioned into 3 to 5, ~70 µm thick sections on a vibratome (VT1000s, Leica instruments). Sections were either further processed for immunohistochemistry or stored in 0.1M PB with 0.05% w/v sodium azide at 4ºC.

2.4.1 Streptavidin visualisation and immunohistochemistry

I performed ~50% of the reactions, whereas the remainder were performed by Emily Hunter and Michael Howarth, research assistants. Every reaction was planned by me.

After resectioning, from each slice two sections were selected for fluorescent visualization, including the one, in which the soma was predicted to be found. These were first thoroughly washed (3 x 10 min) in tris buffered saline containing 0.3% (w/v) Triton X-100 detergent (TBS-Tx, Sigma Aldrich), then incubated in 1 ml of streptavidin-conjugated Alexa 488 fluorophore in TBS-Tx for 4-6 hrs at room temperature, or overnight at 4ºC. After washing (3 x 10 min) the sections were mounted on glass slides in a mounting medium for fluorescent microscopy, vectashield (Vector laboratories), covered with a coverslip and sealed with nail varnish. All additional sections selected for fluorescent visualisation went through the same process.

The expression of multiple molecules in labelled cells and in control tissue were tested using immunohistochemistry. Multiple immunohistochemical reactions were performed on

single 70 µm thick sections. First sections were washed in TBS-Tx, and nonspecific antibody binding sites were blocked with 20% (v/v) normal horse serum (NHS, Vector laboratories) in TBS-Tx. Up to three different primary antibodies (ab), produced in different host species, against the epitopes of the molecules of interest were added in appropriate dilutions (table 2.2) to TBS-Tx containing 1% (v/v) NHS. Sections were incubated in primary ab. solution for 48 hrs at 4ºC, or overnight at room temperature. Subsequently, sections were washed in TBS-Tx. Secondary abs raised in donkey against immunoglobulin G of the host species of the primary ab, conjugated to different fluorophores, were added at appropriate dilutions (Alexa405/DyLight405 (blue)- and cyanine5 (Cy5)/DyLight649 (infra-red)-conjugated abs in 1:250; Alexa488 (green)-conjugated abs in 1:1000; Cy3 (red)-conjugated abs in 1:400) to TBS-Tx, containing 1% (v/v) NHS. Sections were incubated in secondary ab solutions for 4 hrs at room temperature, or overnight at 4ºC. Finally, sections were washed in TBS-Tx and mounted as described above for fluorescent microscopy. Up to five different primary antibodies were used on any single section. For the majority of slices, the expression of different molecules was tested sequentially, thus sections were repeatedly mounted and demounted. All washing steps consisted of 3 x 10 min washes, except after demounting, when sections were washed for at least 3x20 minutes to remove the Vectashield, and the entire procedure, including blocking was repeated with a different ab. For a list of all primary abs used in this study see table 2.2. All secondary abs raised in donkey were purchased from Jackson Immuno Research.

Biocytin labelling was distinguished from endogenous biotin by the continuous cytoplasmic labelling and greater signal strength of the former. The specificity of the primary antibodies was not tested here. I evaluated the specificity of the reactions partly based on the specific subcellular localisation and tissue-wide distribution of the labelling, specific to the particular epitope. For example, the immunoreaction against the neuropeptide somatostatin (SM) gave a granular labelling in the cell body and axonal boutons of cells, consistent with the

localisation of the peptide in the Golgi apparatus and in synaptic vesicles. Conversely, immunoreactions to parvalbumin (PV), a calcium-binding protein, gave a uniform labelling in the cell bodies and processes of neurons, consistent with its cytoplasmic location. For the first reaction with a primary ab on a given specimen, I also performed a negative control, by leaving out the primary ab from the reactions, using a different piece of the same tissue, and a positive control, by adding a mouse or rat brain section, on which the antibody was previously successfully used, to the same vial in which the human section was incubated.

2.4.2 Wide field epifluorescence and confocal laser scanning microscopy.

Cells visualised with streptavidin-conjugated Alexa 488 and fluorescent immunoreactions were first evaluated in a wide field epifluorescent microscope (Leitz DMRB, Leica) using PL FLuotar 20x/0.5 and 40x/0.7 lenses. The light source was either a mercury arc lamp (HBO, Osram) or a pE-300 LED lamp (CoolLED). In case of the Hg arc lamp, the light was spectrally separated by dichroic mirrors to obtain optimal excitation and emission bandwidths for each fluorophore as follows: for Alexa405 and DyLight405 fluorophores – 405/460/425; Alexa488 – 480/527/505; Cy3 – 545/610/565; Cy5 and DyLight647 – 620/700/660 (excitation/emission/beam splitter threshold in nm). Photographs were taken with an ORCA ER digital camera (Hamatsu Photonics) controlled by OpenLab software (Improvision).

For higher resolution imaging of small structures, such as individual boutons, labelled cells and immunoreactions were further documented by confocal laser scanning microscopy. The higher resolution of this technique compared to epifluorescence microscopy is achieved by focusing the illuminating laser light by the objective lens, and passing the emitted light through a confocal aperture (pinhole) in the imaging plane, which eliminates the out-of-focus light along the Z optical axis. The detected point-like image is quantitatively described by the point spread function. Confocal laser scanning microscopy was done using an LSM 710 axioImager.Z1

microscope (Zeiss) and DIC M27 Plan-Apochromat 40x/1.3, 63x/1.4 and alpha Plan-Apochromat 100x/1.46 oil immersion objective lenses, controlled by ZEN 2008 software (v 5, Zeiss). Signal from each fluorophore was recorded in separate scanning tracks and channels, using the following lasers: for Alexa405 and DyLight405 a 405 nm solid state laser; for Alexa488 a 488 nm argon laser; for Cy3 a 543 nm He-Ne laser; for Cy5 and DyLight647 a 633 He-Ne laser. Pinhole size was adjusted optimally for similar optical slice thickness between tracks. The step size along the Z imaging axis was set to half of the thickness of the optical slices, as per the Nyquist criterion for optimal sampling. Details of the optical slice thickness are given in the figure descriptions.

Some neurons visualised with streptavidin-conjugated Alexa488 were imaged in the entire ~60 μm thick section to demonstrate the distribution of their dendrites and axon (chapter 3.1.1, fig. 3.1 B; and chapter 3.1.3, fig. 3.2 A)**.** However, a specific issue of imaging fluorescent signals in PFA-fixed human tissue is the intense autofluorescence of the abundant lipofuscin, which has a broad emission spectrum and thus is detected in every channel. This obscures the visibility of thin axonal processes at low magnification. In order to remove the autofluorescence of the lipofuscin, these sections were imaged in a spectral scanning mode, using the 488 nm argon laser for excitation and detecting emission in the entire spectrum of the detector (λ-stack mode in ZEN software). The pinhole was opened completely, to allow maximum detection of the emitted light. Next, regions of interest including the labelled processes of neurons, lipofuscin and the background respectively were selected to determine the emission spectra of each. This was used to separate the signals into different pseudo channels by spectral linear unmixing (Dickinson et al., 2001), which was performed in the ZEN software.

Table 2.2 Primary antibody information

molecule	host species	antigen	clonality	internal ref.	dilution	stock protein concentration (mg/ml)
calbindin	rabbit	recombinant rat calbindin D-28k	polyclonal	989	1:5000	antiserum
calbindin	goat	mouse calbindin D-28k (NM009788) expressed in bacteria	polyclonal	1427	1:500	200
cannabinoid type 1 receptor (CB1)	guinea-pig	mouse CB1, C-terminal 31 aa (NM007726)	polyclonal	1274	1:5000	200
CB1	rabbit	synthetic peptide aa residues 443-473, mouse and human	polyclonal	1558	1:10000	10000
cholecystokinin (CCK)	mouse	gastrin-17	monoclonal	1052	1:1000	5000
calretinin (CR)	goat	human recombinant calretinin	polyclonal	1116	1:1000	antiserum
hexaribonucleotid binding protein-3 (NeuN)	mouse		monoclonal	842	1:1000	1000
parvalbumin (PV)	guinea-pig	rat recombinant protein aa 1-110	polyclonal	1310	1:1000-1:5000	antiserum
PV	goat	rat muscle parvalbumin	polyclonal	1258	1:1000	antiserum
PV	mouse	purified carp II parvalbumin	monoclonal	922	1:1000	ascites
somatostatin (SM)	sheep	somatostatin conjugated to carrier protein	polyclonal	1085	1:500-1:5000	5000
SM	mouse	somatostatin-14 conjugated to carrier protein	monoclonal	1276	1:400	140
vesicular GABA transporter (VGAT)	guinea-pig	rat recombinant protein aa 2-115	polyclonal	1321	1:500-1:1000	antiserum
vasoactive intestinal polypeptide (VIP)	rabbit	porcine VIP coupled to bovine thyroglobulin with carbodiimide linker	polyclonal	1523	1:5000	antiserum
VIP	mouse	VIP	monoclonal	1053	1:25000	antiserum
γ-aminobutyric acid (GABA)	rabbit	GABA-bovine serum albumin conjugate	polyclonal	9	1:1000	antiserum

molecule	host species	source	product code	specificity reference
calbindin	rabbit	SWANT	CB-38	(Airaksinen et al., 1997)
calbindin	goat	Frontier Institute	Calbindin-Go-Af1040	(Nakagawa et al., 1998)
cannabinoid type 1 receptor (CB1)	guinea-pig	Frontiers Institute	CB1-GP-Af530	(Fukudome et al., 2004)
CB1	rabbit	Immunogenes	Anti-CB1 (Rabbit) Polyclonal Antibody	(Dudok et al., 2015)
cholecystokinin (CCK)	mouse	CURE/Digestive Diseases research Center, Antibody/RIA Core, NIH Grant #DK41301	9303	(Geerling et al., 2006; Ohning et al., 1996)
calretinin (CR)	goat	SWANT	CG1	(Schiffmann et al., 1999)
hexaribonucleotid binding protein-3 (NeuN)	mouse	Chemicon International	MAB377	(Tippett et al., 2007)
parvalbumin (PV)	guinea-pig	Synaptic Systems	195 004	synaptic systems
PV	goat	SWANT	PVG-213	(Schwaller et al., 1999)
PV	mouse	SWANT	235	(Celio et al., 1988)
somatostatin (SM)	sheep	Cortex Biochem	CR2056SP	
SM	mouse	Genetex	GTX71935	(Kubota et al., 2011)
vesicular GABA transporter (VGAT)	guinea-pig	Synaptic Systems	131 004	(Ramer, 2008)
vasoactive intestinal polypeptide (VIP)	rabbit	Immunostar	20077	Immunostar
VIP	mouse	CURE/Digestive Diseases research Center, Antibody/RIA Core, NIH Grant #DK41301	55	(Wong et al., 1996)
GABA	rabbit	produced by Prof. Somogyi	n.a.	(Hodgson et al., 1985)

2.4.3 Peroxidase reactions

Some sections, after being used for immunohistochemistry, were ultimately converted by avidin-biotin horseradish peroxidase (HRP) reaction with 3,3'-diaminobenzidine (DAB) as chromogen for the visualisation of biocytin, and embedded in epoxy resin (Sigma) for conventional light microscopic examination. This method provides high signal intensity and contrast and allows visualisation of processes such as thin axons collaterals and terminals, which were not detectable by fluorescent visualisation. Immunofluorescent sections were demounted and washed 3x20 minutes in TBS-Tx, then incubated in biotinylated peroxidase complex (B) 1:100 v/v (Vectastatin ABC elite kit, Vector Laboratories) in TBS-Tx for 4 hrs at room temperature, washed for 3x10 minutes in TBS-Tx, then incubated in avidin + B (A+B)1:100 v/v (Vectastatin ABC elite kit, Vector Laboratories) in TBS-Tx over 36 hrs at 4ºC. Sections were washed 3x10 minutes in TBS and pre-incubated in 0.5 mg/ml DAB in Tris Buffer without saline (TB) for 10 minutes in dark. Subsequently, 0.002% w/v H_2O_2 substrate was added to initiate precipitation of DAB. After 12 to 20 minutes of conversion, depending on the intensity of the labelling, reactions were stopped and sections were washed 4x10 minutes in 0.1M PB. For contrast enhancement, sections were incubated in 0.5% w/v Osmium solution in 0.1M PB for 1 hour at room temperature, after which they were thoroughly washed (4x10 minutes). Before mounting, sections were dehydrated using increasing concentrations of ethanol (50% for 10 min, 70% for 10 min, 90% for 5 min, 95% for five min and 100% for 2x10 min) and a final step of propylene oxide (Sigma) for 2x10 min. From propylene oxide, sections were quickly transferred into Durcupan epoxy resin (Sigma) and left for 12 hrs at room temperature. Sections were mounted on glass slides in resin and left at ~60ºC for 48 hrs, until polymerization of the resin.

Some sections, containing parts of the labelled cells, which were not used for immunohistochemistry, were used for electron-microscopic study of their synaptic targets.

These were stored in 0.1 M PB and sodium azide until processing. After washing (3 x 10 min) in 0.1 M PB, sections were postfixed with the same fixative as before with the addition of 0.05% (vol/vol) GA for 2 hrs at 4ºC. Sections were washed again in PB, then were incubated in 20% sucrose (Sigma Aldrich) in 0.1M PB for 2 hrs at room temperature for cryoprotection. This was followed by quickly freezing the sections in liquid nitrogen and thawing them in PB, in order to make the cell membranes permeable to the reagents. The freeze-thaw process was repeated 2-3 times. All following steps were the same as for HRP reactions on fluorescent sections with the exception that the buffer did not contain detergent, in order to preserve the lipid membranes and the subcellular structure of the cellular organelles, which would be examined by electron-microscopy. During dehydration, these sections were also stained with 1% (w/v) uranyl acetate (UA) dissolved in 70% ethanol for 40 min in dark for further enhancement of contrast for electron-microscopy.

2.4.4 Light microscopy and reconstruction of labelled cells

Transmitted light microscopy of HRP-converted sections was performed using a Leitz Dialux22 microscope (Leica), equipped with NPL Fluotar 10x/0.3, 25x/0.55, 40x/0.78 dry and PL Apo 100x/1.32 oil immersion objective lenses. Images were taken using a Canon EOS 40D digital camera controlled by EOS Canon Utility software. Some neurons were reconstructed in order to demonstrate the distribution of their dendrites and axon across different neocortical layers, as well as for the identification of their axonal boutons, which were later examined using electron-microscopy. For 2D reconstruction of labelled cells (chapter 3.1.5, fig. 3.4 A; and chapter 3.2.1, fig. 3.7 A), neurons were manually traced using a drawing tube attached to a transmitted light microscope (Leitz Dialux22, Leica), equipped with a Pl Apo 63x/1.4 oil immersion objective. Neurons were traced in 2-3 consecutive sections, and cut ends of their processes were marked on both surfaces. Occasionally, alignment of consecutive sections required enlargement of the tracing from Tx-treated sections, because they shrunk more during

dehydration than freeze-thaw sections. After alignment, the drawings were overlayed and copied onto a single sheet of paper, which was digitised using a digital camera (EOS 40D, Canon). The reconstruction was then further processed in Adobe Photoshop. Digital 3D reconstruction of some neurons (chapter 3.2.1, fig. 3.6 A) was performed with Neurolucida software (v 2020.2.2 MBF Bioscience) and an Axioskop 2 mot plus (Zeiss) equipped with a Plan Apochromat 100x/1.4 Oil lens and Retiga 2000R (QImaging) digital camera, or with a v 2021.1.3 software and a Leica DMR microscope equipped with a HCX PL Fluotar 100x/1.30 Oil lens and Lumina HR (mbf bioscience) digital camera. A total of 24 neurons were reconstructed, of which I reconstructed 10, including DBCs 1 , 4, 5, 10, 22, 23, 25, PMC 14, and PYRs 2 and 3. Two (PMC 1 and 5) were reconstructed by Dr. Sawa Horie; one AAC and one CB1+ cell by Miss Rhukshanda Habib; DBC 14, one AAC and one CB1+ cell by Mr. Ilyés Zalán; PMC 8 and one pyramidal cell by Mr. Puneet Pareek; 2 pyramidal cells by Mr. Michael Howarth; one CB1+ cell by Mrs. Qianru Zhao; and DBC 2 by Miss Emily Hunter. Pyramidal cell 1 was reconstructed in Prof. Gábor Tamás' lab.

2.5.5 Serial section electron microscopy of labelled cells and reconstruction of target dendrites

After the labelled neurons were reconstructed, some were selected for electron-microscopic study of their synapses (see table 3.1; chapter 3.2.1, figs. 3.6 and 3.7). Coverslips from freeze-thawed HRP-converted sections were removed with a razor blade, and pieces from the sections containing the 'horsetail'-like axon of DBCs and the descending axon of pyramidal cells in layer III were cut out and re-embedded in cylindrical blocks of epoxy resin and left at ~60 ºC until polymerisation. Blocks were then trimmed with a razor blade around the embedded piece of tissue to form a trapezoid shape with one right angle, which would help in orientation of the electron-microscopic sections. Excess resin was trimmed from above the section with a glass knife on an ultramicrotome (Ultracut UCT, Leica). Ultra-thin electron-microscopic

sections (~50 nm) were cut using an Ultra 45 Diatome diamond knife (TAAB), and mounted on pioloform-coated copper slot grids (2x1 mm, 10-20 sections/grid). Grids were examined using either a Fei Tecnai 12 transmission electron microscope (TEM) at 12 keV accelerating voltage and photographed with a Gatan OneView CMOS camera controlled by Gatan Digital Micrograph software (GMS3), or using a Jeol-1011 microscope at 80 keV accelerating voltage and photographed with a TRS Sharp Eye camera controlled by iTEM software. The labelled processes were traced in the serial sections and serial images were taken of the synapses and their targets at three different magnifications in order to study the identity of the postsynaptic structures. Serial photomicrographs of some of the targets were then imported into TrackEM2 reconstruction plugin of ImageJ software. The sections were aligned using an automatic non-linear alignment method, based on block correspondence in TrackEM. After alignment the axon and bouton of the labelled cell, the target structure and the synaptic specialisation was traced through the serial sections and was rendered into a 3D reconstruction (chapter 3.2.1, fig. 3.6 L; and chapter 3.2.3, fig. 3.10 F).

2.5.6 Post-embedding immunohistochemistry for GABA

Three blocks fixed with 4% (w/v) PFA, 2.5% (w/v) GA and 15% (v/v) PA were kindly provided by Prof Gabor Tamas, at the University of Szeged, Hungary. From these, ~70 μm thick sections were cut on a vibratome, washed in PB, treated with 1% (w/v) Osmium for 1h, dehydrated, and stained with 1% (w/v) UA for 35 min, and mounted in epoxy resin. Pieces of these sections containing layer III re-embedded in cylinders of resin. From these blocks ~60 nm thick sections were cut with an ultramicrotome and mounted on pioloform coated nickel slot grids (2x1 mm). Post-embedding immunohistochemistry was performed as described by Somogyi and Hodgson (1985). Grids were placed on drops (100-200 μl) of each reagent in a petri dish. A wet tissue was also placed in the petri dish to prevent the drops from drying up during incubation. Sections were placed for 10 min on drops of 1% periodic acid to etch the

resin and reveal the tissue surface for the antibodies. After washing the sections by several dips in double-distilled water, osmium was removed from the tissue with 1% sodium periodate for 10 min. Sections were again washed by several dips and then placed on drops of TBS for 10 min. Next, non-specific ab binding sites were blocked with 20% normal goat serum (NGS) in TBS, after which sections were placed on drops containing the primary ab against GABA-glutaraldehyde complex, raised in rabbit (Somogyi & Hodgson, 1985) in 1:1000 dilution and 1% (v/v) NGS in TBS for 2 hrs at room temperature. Sections were then washed by placing them on drops of TBS containing 1% NGS for 3 x 10 min, followed by 10 min on drops of TB. Sodium chloride salt was washed out before the next step and was also omitted from the buffer of the secondary ab solution, because it causes precipitation of the colloidal gold in the secondary ab. Next, grids were placed on drops of secondary ab solution, containing colloidal 6 nm gold-coupled anti rabbit IgG raised in donkey (AURION) in 1:100 dilution and 1% NGS in TB for 2 hrs at room temperature. Sections were washed by several dips in double-distilled water followed by 2 x 10 min on double-distilled water. Gold particles were silver enhanced, using a silver enhancement kit (AURION) for 1 h at room temperature in dark, for easier visualisation in EM. Before examination in EM, sections were stained (5 min) with Reynolds' lead citrate for contrast enhancement, containing 0.27 g of lead nitrate (BDH) and 0.35 g of tri-sodium citrate (BDH) in 10 ml of solution, dissolved in double-distilled water and titrated with 0.4 ml of 4M NaOH, after which they were thoroughly washed by several dips in double-distilled water. Some sections were also stained with 1% (w/v) UA dissolved in double-distilled water for 20 min.

3 Results

3.1 GABAergic cell types in the human neocortex

3.1.1 Recorded cells and samples

We collected a total of 56 neocortical samples from 52 tumour and 4 epilepsy patients undergoing neurosurgery at the John Radcliffe Hospital, Oxford. Of these, I collected 42, the remainder being collected by Professor Peter Somogyi. The samples were obtained from 17 different cortical regions, in which I recorded and labelled a total of 561 neurons and 9 glial cells, using *in vitro* patch-clamp electrophysiology in acute slices. Further 13 neurons were recorded and labelled by Dr Ruggiero Francavilla in our lab. Of the 574 neurons, 511 were visualised and fully or partially recovered for anatomical analysis. In addition to these specimens, further 6 samples were imported from the laboratory of Professor Gábor Tamás at the University of Szeged, Hungary, through the Oxford Brain Bank (OBB), in which an additional 3 neurons were recorded and labelled by Dr Márton Rózsa.

Of the total of 514 visualised neurons 311 (~61 %) were smooth dendritic or sparsely spiny interneurons, and 203 (~39 %) were spiny pyramidal cells. These proportions do not represent the true ratio of cell classes as many of the cells were selectively targeted based on their appearance in live DIC imaging. The cell bodies were located in either layer II or III due to our selection (fig. 3.1 B), with 1 exception, a neuron located in layer I. Layers were determined by the density, size and shape of either unlabelled neuronal cell bodies in osmium-treated sections with transmitted light microscopy (fig. 3.1 A) and in fluorescent sections by the autofluorescence of the lipofuscin, or neuronal cell bodies immunolabelled for NeuN (fig. 3.1 B) or calcium-binding proteins. The boundary between layers II and III is not sharp, but

that between layers I and II is well defined by the sudden change in the density of cell bodies. The cytoarchitectonic area corresponding to the cortical regions sampled were not determined. However, in some samples from the middle temporal gyrus, a clear inner granular layer (IV) could be distinguished (fig. 3.1 A), indicating that those samples likely come from a sensory area. In most samples from other cortical regions (see table 2.1) no clear layer IV could be identified.

All visualised pyramidal neurons had typical dendritic trees with an apical dendrite ascending radially toward the pial surface, forming an apical tuft in layer I; and multiple basal dendrites, which were densely covered by spines. Their axon originated from the base of the cell body, or in some cases from the main trunk of a basal dendrite, and descended towards the white matter emitting collateral branches at various depths, which provided innervation to the neuropil surrounding their cell bodies and to a lesser extent also innervating layer I (fig. 3.9). Recovered interneurons showed great diversity in the spatial distribution of their axon and boutons, as well as in their dendritic structure, which I studied to identify different populations. The majority (~ 76%) of the recovered interneurons could not be allocated to a cell type based on the visual assessment of the spatial distribution of their axon.

A total of 86 neurons were analysed in this thesis, selected to answer questions on synaptic organisation and physiology. Of these, I identified 76 as belonging to one of 5 previously described GABAergic neuron types, based on the distribution of their axon; 6 were identified as pyramidal cells based on their densely spiny dendrites and pyramidal-shaped soma; and 4 neurons remained unidentified, but had smooth dendrites, and lacked a projection axon, thus were likely GABAergic interneurons. These neurons were recorded in samples from 36 patients, including 12 different cortical areas and 15 different diagnoses (see table 2.1).

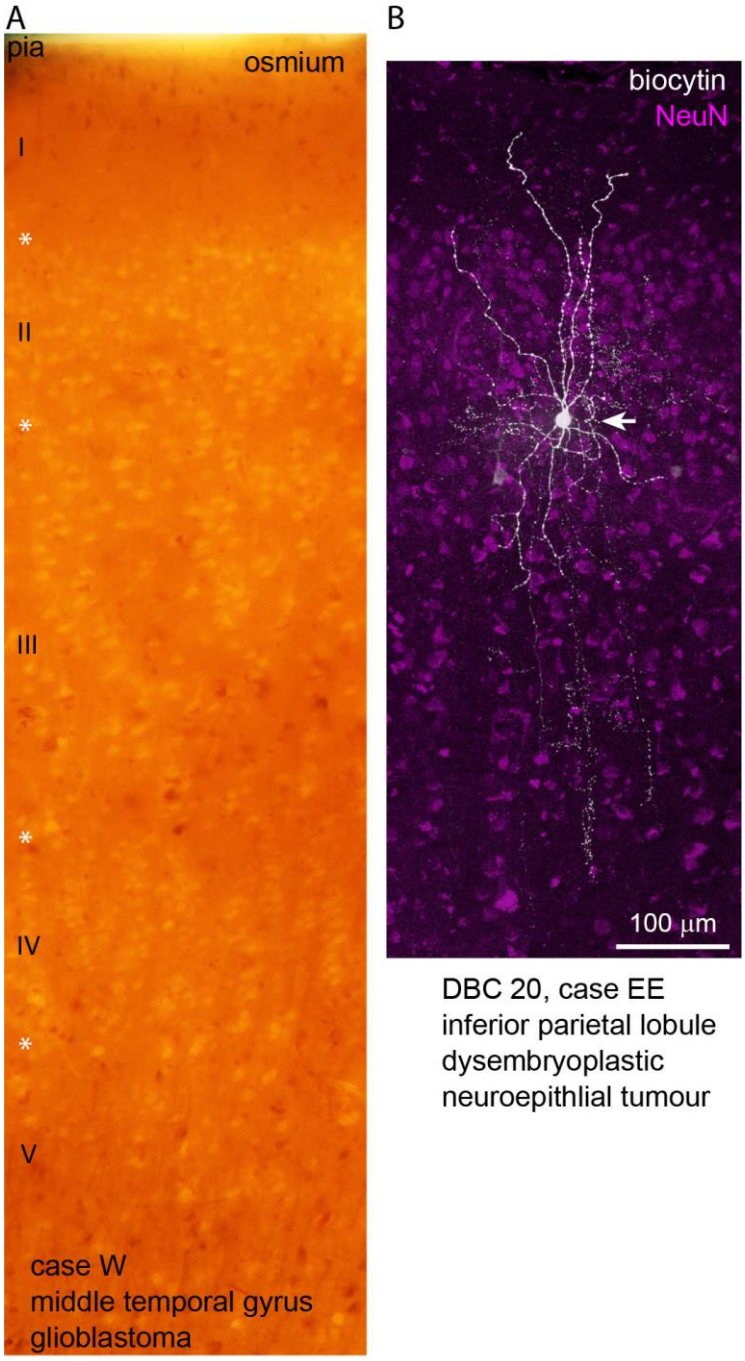


Figure 3.1: Identification of neocortical layers and the location of recorded neurons. A. Transmitted light micrograph of a ~60 μm thick resin-embedded section of an immersion-fixed block, stained with 1% osmium, taken with a 10x/0.3 NA objective. Light-coloured unstained neuronal cell bodies are visible. Roman numbers indicate the neocortical layers determined based on the density, shape and size of the cell bodies. Layer boundaries are indicated by asterisks. Note the presence of a distinct inner granular layer (layer IV) with a high density of small, round neuronal cell bodies. **B.** Tiled confocal fluorescent image (λ mode) of a neuron (DBC 20) labelled with biocytin (white) and visualised with streptavidin-conjugated Alexa 488, and immunoreaction for NeuN (magenta), visualised with Cy3-conjugated secondary antibody (Z stack of 44 optical slices of 1.8 μm thickness each, total depth: 40.5 μm). Layers can be determined as in A. The cell body (arrow) is located at the border of layer II with III. Scale bar applies to both panels.

3.1.2 Interneuron types identified based on the spatial distribution of their axons

The largest group of cells analysed in this thesis, were double bouquet cells (DBC, n = 32, fig. 3.2), identified based on their radially oriented axonal plexus forming a tight bundle, resembling a horsetail, restricted to a narrow (10-20 μm) cortical column, descending through layers II to V (DeFelipe, 2011, 2002; Somogyi & Cowey, 1981). Another population of neurons had widely distributed axon (> 200 μm) in every direction from the soma with a relatively uniform density, which also had large, multipolar dendritic trees. Subsequent analysis showed that these cells express the calcium binding protein, parvalbumin (PV, see chapter 3.1.5), thus to refer to them, I use the term parvalbumin-expressing multipolar cells (PMC, n = 14, fig. 3.4). We studied the dendritic and axonal distributions, firing patterns, molecular expression and synaptic connections of these two groups of cells in detail using whole-cell patch-clamp electrophysiology, immunohistochemistry and electron-microscopy, which are described in detail in the following chapters (3.1.3 through 3.1.6, 3.2.1 and 3.3), in order to better understand their possible functions in the human neocortical circuit.

Further, among the recovered interneurons I identified 7 axo-axonic cells (AAC), based on the short (10 – 20 μm), radially oriented bouton cartridges, which were interconnected by bouton-less axon segments, giving the axon an overall appearance of candlesticks in a chandelier (Szentágothai & Arbib, 1974). Their axon was mostly distributed in layers II-III, and projected 100 – 200 μm laterally and radially, but never entered layer I, consistent with reports that they exclusively innervate the axon initial segments of pyramidal cells. This was confirmed by immunoreaction to ankyrin G, a marker of the axon initial segment, which aligned with the bouton cartridges of the cells. Their dendrites were smooth, travelling in every direction from the soma, and typically entered layer I. Out of the 6 AACs tested, 5 were double-immunopositive for the calcium-binding proteins PV and calbindin in the soma (n=1), dendrites

(n=1) or boutons (n=3), consistent with immunohistochemical reaction patterns of these two molecules in human neocortex (del Río & DeFelipe, 1997a); whereas for one cell the immunoreaction for PV was inconclusive. One AAC was only tested for calbindin and it was immunopositive. Two AACs tested were immunopositive for the vesicular GABA transporter (VGAT) in their boutons. When continuously depolarised by current injection in whole-cell current-clamp, AACs typically fired action potentials with a significant delay after the beginning of the current injection step, which persisted even at high (rheobase + 100 pA) injected currents and their firing showed no spike frequency adaptation. In response to hyperpolarising current injection, AACs did respond with a voltage sag.

Other interneurons, identified as neurogliaform cells (NGC, n=22), had a dense axonal plexus distributed relatively uniformly around their cell body in every direction, with a wavy appearance and small boutons, and which could also enter layer I (Oláh et al., 2007, 2009). Neurogliaform cells typically fired regular trains of action potentials in response to continuous depolarisation, with no frequency adaptation or amplitude accommodation. Importantly, at very high current injections (> rheobase + 100 pA) some but not all NGFs (n=5) entered a continuous spontaneous firing state, which persisted after the end of the current injection step, confirming previous observations of persistent NGF firing (Krook-Magnuson et al., 2011). Similarly to AACs, NGFs did not show voltage sag in response to hyperpolarising current injection.

One interneuron that I recorded was identified as a rosehip cell (RHC), based on the dense and compact axonal plexus restricted to the close vicinity of its soma (< 100 μm), but which in contrast to NGFs had large boutons (Boldog et al., 2018). The soma, located in layer I, and the proximal segments of its short dendrites were sparsely spiny. Its dendrites and axon were present in both layers I and II. These cells were recently discovered in layer I of the human neocortex (Boldog et al., 2018), but their defining RNA expression pattern also predicts them to be present in layers II and III (Hodge et al., 2019). The RHC fired a regular train of action

potentials when continuously depolarised, with amplitude accommodation and showed large amplitude voltage sag in response to hyperpolarising current injection.

Although the functions of some GABAergic cell types in neocortical circuits, such as basket and axo-axonic cells, have been extensively studied in different species and cortical areas, there are few studies on the activity and functions of DBCs, which were done in cats (Tamás et al., 1997a, 1998) and primates (Krimer et al., 2005; Zaitsev et al., 2005), but not in human. Studying DBCs in humans is of particular importance because of the striking spatial specificity of their axon, the apparent bias in their synaptic targets and their relative abundance in humans (Ballesteros Yáñez et al., 2005; DeFelipe, 2011), suggesting that they may be important for human cognitive capabilities. Whether a homologue cell type exists in rodents (Jiang et al., 2013, 2015; Kawaguchi & Kubota, 1996, 1997; Kubota et al., 2007, 2011), is not yet clear.

3.1.3 Anatomical and molecular characterization of DBCs and the relationship of their 'horsetail' axons to calbindin immunoreactive radial bundles

The distinguishing feature of DBCs is their 'horsetail' axon (DeFelipe, 2011; Jones, 1975; Somogyi & Cowey, 1981), formed of at least three, but often more, interwoven axon branches traveling in the radial direction from the soma in the supragranular layers, towards layers V and VI, forming a 10-20 μm wide columnar plexus (fig. 3.2 A; fig. 3.6 A). I visualised 32 DBCs for anatomical and immunohistochemical analysis. Of these, the current-voltage (I-V) traces of 29 DBCs were analysed (table 3.1), three being excluded because of bad capacitance compensation.

The cell bodies of all DBCs were located in either layer II or layer III, at a distance of ~ 740 ± 268 μm (n = 12) from the pial surface. The axon of DBCs could be traced as deep as layer V (see fig. 3.6 A). The number of branches in the 'horsetails' varied between 3 and 7.

Occasionally, short collaterals branched from the 'horsetail' at different depths and travelled laterally but remained within 100 μm from the 'horsetail' (see fig. 3.6 A). The majority of DBC boutons were *en-passant*, but all DBCs had a few *en-termineux* boutons on axonal side branches. In addition to the 'horsetail' DBCs also had axon around the cell body and in layer I, where it did not form a columnar structure, but spread to 100 - 500 μm laterally (fig. 3.2 A, fig. 3.6 A). The axon of 22 DBCs entered layer I, with one (DBC 19) exclusively innervating a narrow subpial band. The axon of 9 DBCs spread uniformly across the depth of layer I, whereas another 9 innervated only the deep half. Three DBCs had only a few collaterals entering layer I. The dendrites of 29 DBCs were recovered, of which 24 were smooth, whereas the remainder were sparsely spiny. The dendritic trees were usually small with a median of 4 (range: 2 - 7) main branches originating from the soma, which travelled mostly towards the pial surface, and less than 100 μm laterally. The distribution of the dendrites was in most cases unipolar towards the pia (n = 18), or bipolar in the radial direction (n = 9). Two DBCs had uniformly distributed dendritic trees around their soma. All, except DBC 1 had dendrites in layer I.

Previous studies have demonstrated calbindin immunopositive radial axonal columns in human (Ballesteros Yáñez et al., 2005; DeFelipe et al., 2006; del Río & DeFelipe, 1995; del Río & DeFelipe, 1997c) and monkey cortex (DeFelipe et al., 1989a, 1990a; Peters & Sethares, 1997) which were predicted to originate from DBCs. I have confirmed the presence of such calbindin immunopositive axon bundles reminiscent of the 'horsetail' axon of DBCs, in the temporal, frontal and parietal areas of the human neocortex. By labelling individual DBCs with biocytin I was able to test directly their immunoreactivity for calbindin and establish the relationship of DBC 'horsetails' to axonal bundles revealed by immunoreaction against calbindin. Furthermore, interneurons with descending axons were found to be immunoreactive to the calcium-binding protein calretinin (CR) and the vasoactive intestinal polypeptide (VIP) in rat (Kawaguchi & Kubota, 1997), monkey (Condé et al., 1994; Lund & Lewis, 1993;

Meskenaite, 1997; Zaitsev et al., 2005) and human (Varga et al., 2015). I also tested if human DBCs were immunoreactive for these molecules. Other neuropeptides, such as somatostatin (SM) and cholecystokinin (CCK) were also tested, because of their co-expression with calbindin in rodents (Kubota et al., 2011; Rogers, 1992) and primates (González-Albo et al., 2001). Finally, the calcium binding protein parvalbumin (PV) was also tested, which was also found to be co-expressed with calbindin in rodent (Kubota et al., 1994; Kubota & Jones, 1993) and human neocortex (del Río & DeFelipe, 1997a).

All DBCs were tested for calbindin and 24 (75 %) were immunopositive (CB+) in all three compartments (axon, soma and dendrites, n = 11), only in their axons (n = 8), only in their somata (n = 1), or in their somata and axons (n = 4). Eleven of these, tested for CR on their axon (n = 8), soma (n = 1) or both (n = 2) were immunonegative. Two DBCs were immunopositive for CR in their axons, and these were immunonegative for calbindin (CB-). Six DBCs were immunonegative for both CR and calbindin (CR+/CB+). None of the 14 tested DBCs (8 calbindin+, 2 calretinin+, 4 double immunonegative) were immunopositive for VIP in their axons (n = 11), somata (n = 1), or both (n = 2). Similarly, none of the 6 - 6 DBCs tested were immunopositive for PV in their axons or CCK in their somata. Of the 18 DBCs tested, only one (DBC 18) was immunopositive for SM and this cell was also immunopositive for calbindin (fig. 3.2 A, D, F). Interestingly, although there was granular immunoreactivity for SM in the soma of DBC 18, characteristic of peptides found in the Golgi apparatus (fig. 3.2 A inset), not all of its boutons were SM-immunoreactive (fig. 3.2 D). All 16 DBCs tested were immunopositive for the vesicular GABA transporter in their boutons (VGAT, fig. 3.2 E, F). Immunohistochemical profiles of the cells are shown in fig. 3.2 F.

We found CB+ DBCs in the temporal (n = 13), frontal (n = 4), parietal (n = 4) and parieto-occippital (n = 3) cortices. Calbindin immunonegative DBCs were found in the temporal (n =

4) and parietal (n = 4) cortices. One CR+ DBC was found in the temporal, whereas the other in the parietal cortex. The only somatostatin immunopositive DBC was in the temporal cortex.

The 'horsetail' axons of the recorded and biocytin-labelled CB+ DBCs always aligned with the calbindin immunopositive axonal bundles, where they intermingled with calbindin immunopositive axons from unknown neurons (fig. 3.3 B 1st and 2nd columns). Furthermore, The axons of CR+ and CB-/CR- double immunonegative DBCs also aligned with and travelled within calbindin immunopositive bundles (fig. 3.3 B, 3rd column and fig. 3.3 C). While most DBCs' axon formed one 'horsetail', DBCs 1 and 4 formed two, whereas DBC 20 formed three separate horsetails, each aligned with a different calbindin bundle (fig. 3.3 B, 2nd column). Cells with a single main 'horsetail' also gave off collateral branches leaving the main calbindin bundle and entering a neighbouring one, forming boutons also between bundles. Finally, in one case, where two DBCs (27 and 28) were labelled close to each other in the same slice, their axons intermingled in a single bundle. Both of them were immunonegative for calbindin, CR and VIP.

These results show that the cortical columns determined by the calbindin immunopositive bundles are complex structures formed by the 'horsetail' axons of multiple cells, including CB+ as well as CR+ DBCs, among other cells.

Figure 3.2. In vitro recorded and biocytin labelled double bouquet cell in the human inferotemporal neocortex

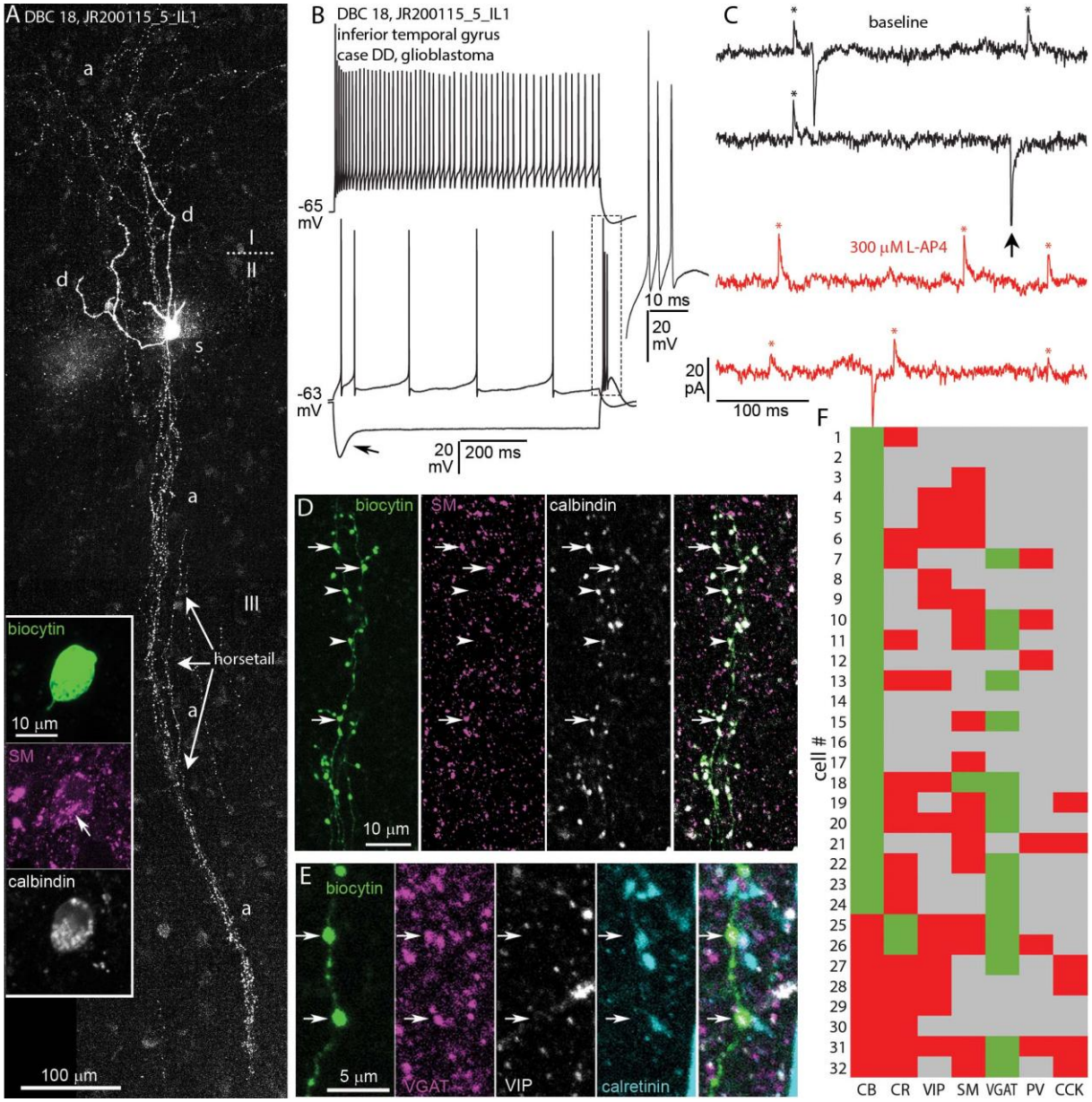


Figure 3.2. In vitro recorded and biocytin labelled double bouquet cell in the human inferotemporal neocortex. A. Tiled confocal fluorescent image (λ mode) of the cell with descending columnar 'horsetail' axon. The cell body (s) is located in layer II with dendrites (d) penetrating layer I. The axon (a) diffusely innervates layer I (Z stack of 50 optical slices of 1.8 μm thickness, total depth: 45.9 μm); roman numbers indicate layers; inset: the cell body showing immunoreactivity for somatostatin (SM, Golgi apparatus, magenta, arrow) and calbindin (white) in the cytoplasm (Z stack of 5 optical slices of 0.9 μm thickness, total depth, 2.4 μm). **B.** Voltage responses of the cell in A to current injections of rheobase (RB), RB +100 pA, and holding current -100 pA, showing a voltage sag (arrow) and rebound spikes (boxed area, inset) in response to hyperpolarising current injection and firing with spike frequency adaptation and strong spike amplitude accommodation when continuously depolarised; inset showing the expanded rebound burst from the boxed area. **C**. Example current traces recorded at -50 mV clamping potential, showing spontaneous inhibitory (asterisks, upward deflections) and excitatory (arrow, downward deflections) postsynaptic currents in baseline condition (black) and after bath application of 300 μM L-AP4 (red). **D**. Boutons of the cell in A are immunopositive for SST (magenta, arrows) and calbindin (white); note that not all boutons are immunopositive for somatostatin (arrowheads) (Z stack of 3 optical slices of 0.9 μm thickness, total depth, 1.8 μm). **E.** Boutons (arrows) of the cell in A are immunopositive for the vesicular GABA transporter (VGAT, magenta), and immunonegative for vasoactive intestinal polypeptide (VIP, white) and calretinin (cyan) (Z stack of 3 optical slices of 0.9 μm thickness, total depth, 1.8 μm). **F**. Immunoreactivities in all recovered and tested neurons with descending axon bundles: green, immunopositive; red, immunonegative; grey, not tested/inconclusive.

Figure 3.3. Examples of recorded and labelled DBCs

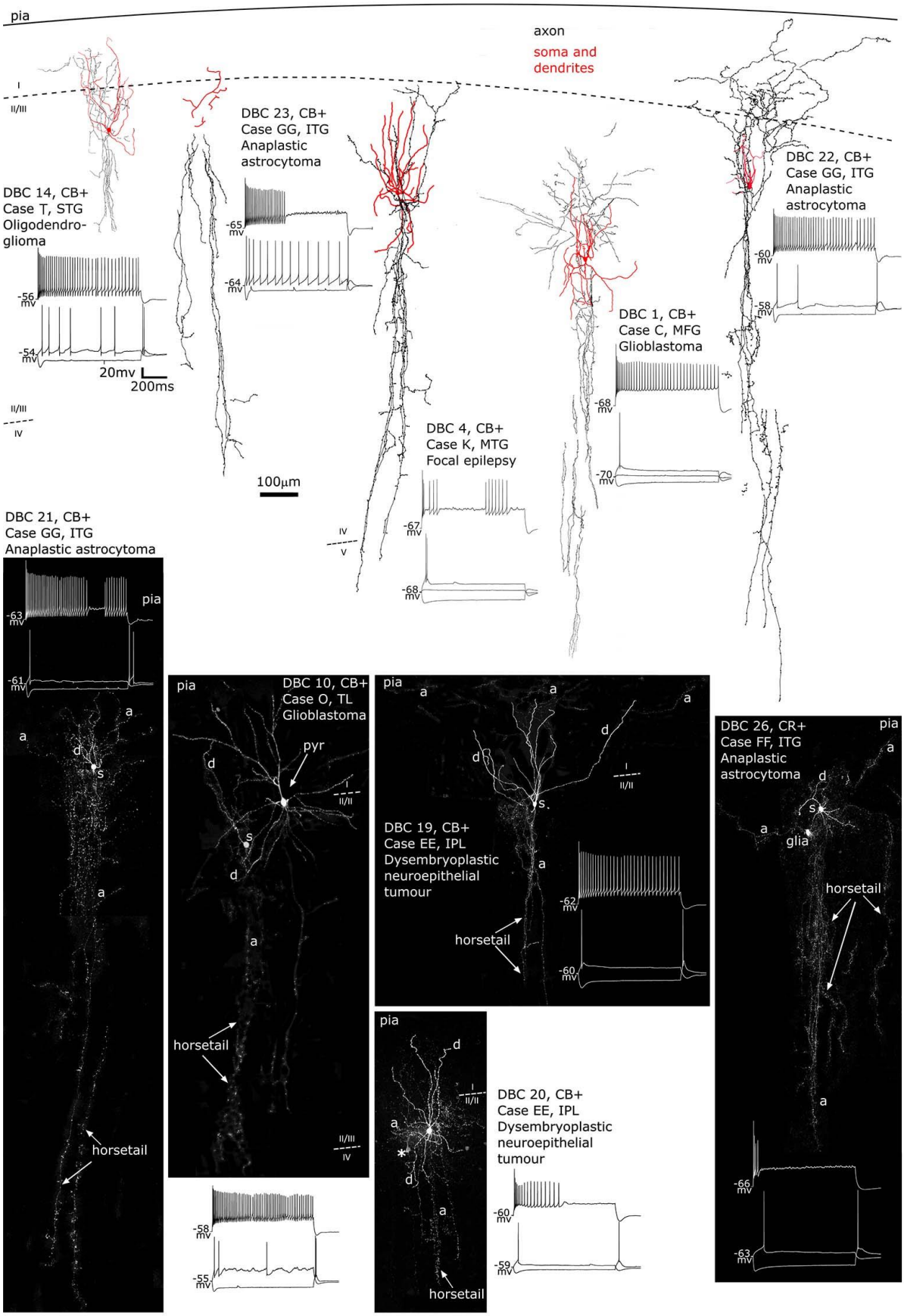


Figure 3.3. Examples of recorded and labelled DBCs. Top. Reconstructions of individual DBCs from 2 - 3 ~60 μm thick transmitted light microscopic sections. Axon is shown in black, dendrites and somata are shown in red. DBCs 1 and 14 were reconstructed using a drawing tube, DCBs 4, 22 and 23 were reconstructed with Neurolucida software (see methods). **Bottom.** Tiled confocal fluorescent (λ-stack) images of DBCs visualised with Alexa488-conjugated streptavidin in single ~70 μm thick sections. The cell bodies (s), dendrites (d), and axons (a) of the cells are indicated. The 'horsetail' axons are indicated by arrows. Note the presence of a recorded and labelled pyramidal neuron (pyr) next to DBC 10. Roman numerals indicate layers, dashed lines indicate layer boundaries. Voltage responses of each DBC in response to current injections of holding current - 100 pA, RB and RB + 100 pA. The cortical areas and pathologies are shown. Scale bars apply to all cells.

Figure 3.4. Diversity of double bouquet cells with 'horsetail' axons

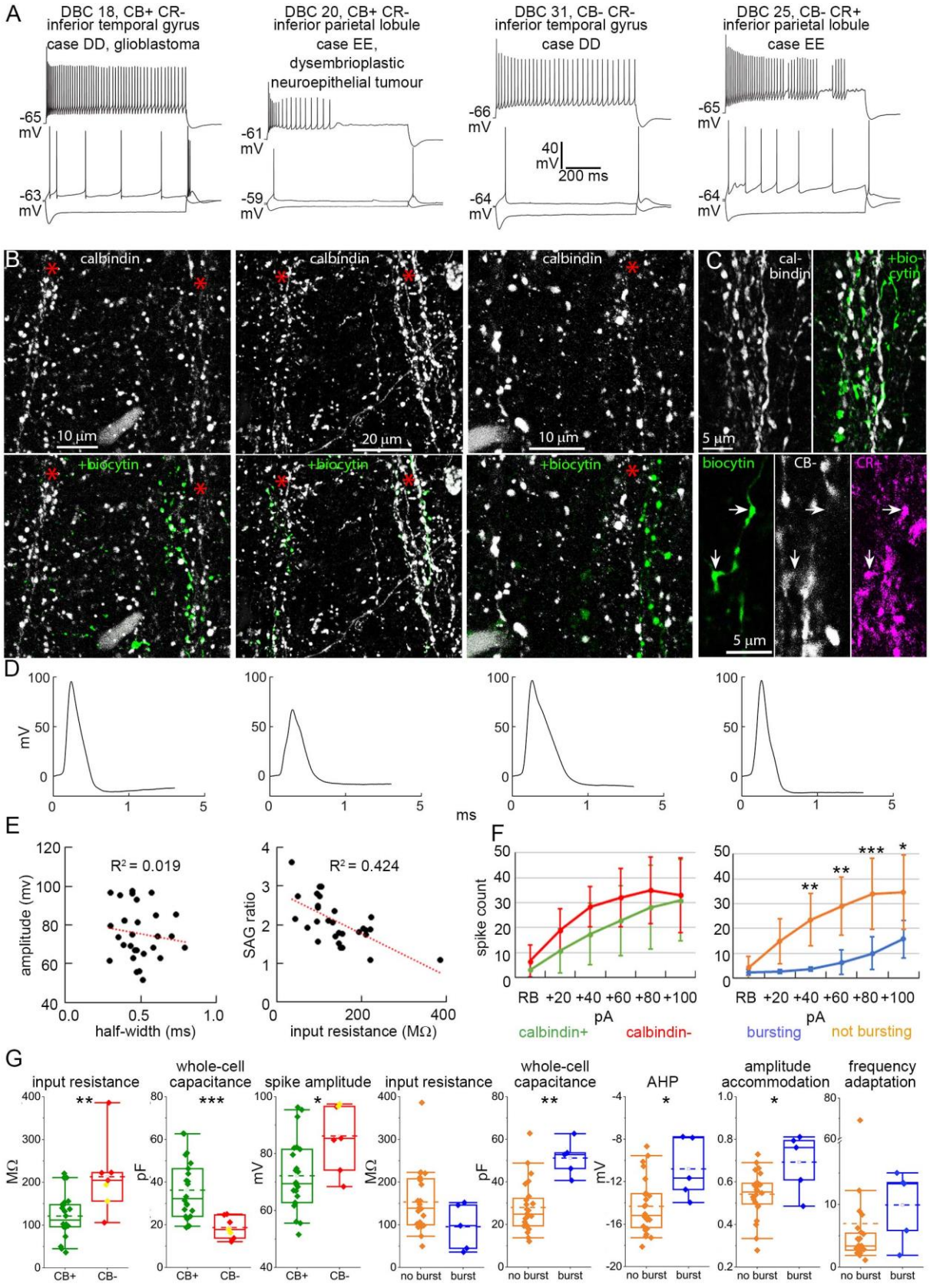


Figure 3.4. Diversity of double bouquet cells with 'horsetail' axons. **A.** Voltage responses of double bouquet cells to current injections (RB, RB + 100 pA, and holding current – 100 pA steps). Immunoreactivity to calbindin (CB) and calretinin (CR) are noted. **B.** Confocal fluorescent images of immunoreaction to calbindin (top, white) and overlayed visualisation of biocytin (bottom, green), revealing the contribution of individual double bouquet axons to calbindin positive axonal columns (asterisk; for DBC 18\20\31 respectively: Z stacks of 32\25\7 optical slices of 0.9\0.9\0.7 μm thickness, total depth, 13.3\11.2\3.0 μm). **C.** Top: Immunoreaction to calbindin (white) and overlayed axonal biocytin (green) for the calretinin immunopositive DBC 25 above (Z stack of 14 optical slices of 0.9 μm thickness, total depth, 5.2 μm); Bottom: Calretinin positive boutons of DBC 25 (arrows) are intermingled with but immunonegative for calbindin (Z stack of 3 optical slices of 0.9 μm thickness, total depth, 1.6 μm). **D.** Voltage traces of the first action potentials evoked at rheobase current injection for each cell. **E.** Scatter plots of action potential amplitude vs. half-width (left, Pearson's correlation: $p = 0.405$); and sag ratio vs. input resistance (right, Pearson's correlation: $p < 0.001$) of all DBCs ($n = 29$). **F.** Firing index (number of spikes elicited by current step) of calbindin immunopositive (green) vs. calbindin immunonegative (red) DBCs (left, two-way repeated measures ANOVA, within subjects effect of current step: $F = 50.712$, $p < 0.001$; within subjects effect of interaction: $F = 1.353$, $p = 0.255$; between subjects effect of immunoreactivity: $F = 2.164$, $p = 0.153$) and of bursting (blue) vs. non-bursting (orange) DBCs (right, two-way repeated measures ANOVA, within subjects effect of current step: $F = 28.365$, $p < 0.001$; within subjects effect of interaction: $F = 7.201$, $p = 0.012$; between subjects effect of bursting: $F = 13.840$, $p < 0.001$, Tukey pairwise comparisons: bursting vs not bursting within each current step: * $p < 0.05$, ** $p < 0.01$, *** $p < 0.001$; whiskers represent SD). **G.** Comparison of passive and active membrane properties between calbindin immunopositive (CB+, green, $n = 22$) and immunonegative (CB-, red, $n = 7$) DBCs (calretinin immunopositive cells, yellow), and between bursting (blue, $n = 5$) and non-bursting (regular firing, orange, $n = 24$) DBCs. Boxes represent median and IQR, whiskers represent 5 and 95 percentiles, mean is indicated by dashed line. For all CB+ vs CB-, and the AHP and AP amplitude accommodation comparisons student's t-test was used, for the remainder Mann-Whitney U-test, * $p < 0.05$, ** $p < 0.01$, *** $p < 0.001$.

3.1.4 Electrophysiological characterization of DBCs

I have found that DBCs express firing phenotypes that distinguish them from PMCs and other cell interneuron types in the neocortex. All DBCs, except DBCs 28 and 29, responded with a prominent voltage sag (fig. 3.2 B, fig. 3.3 A, sag ratio: 2.07 ± 0.58, n = 29) and 19 of 32 DBCs also fired rebound spikes after continuous hyperpolarisation (fig. 3.3 A). Five of 32 DBCs showed burst firing either at rheobase current injection and/or as rebound after continuous hyperpolarisation (fig. 3.2 B), and all five were CB+. The CB- DBCs did not show burst firing. When continuously depolarised by rheobase + 100 pA current injection, 14 DBCs fired a regular train of action potentials (Fig. 3.3 A, DBCs 18 and 31), 5 showed depolarisation block (fig. 3.3 A, DBC 20), and 7 fired either irregular or stuttering action potential trains (fig. 3.3 A, DBC 25). All DBCs showed strong spike amplitude accommodation (average: 0.57 ± 0.12), and spike frequency adaptation (median: 3.43, IQR: 3.52). At rheobase + 100 pA current injection, DBCs fired at an average firing rate of 38.1 ± 19.7 Hz, but their coefficient of variation of the inter-spike-intervals (ISI-CV), a measure of the regularity of the spike train, varied between 9.5 for the most regularly firing cell (DBC 24) to 206.2 for DBC 11, with a stuttering firing pattern (average: 45.2 ± 37.9).

The action potential (AP) kinetics of DBCs was variable (fig. 3.3 D). Action potential amplitude varied between 52 and 97 mV, the average being 75 ± 2.5 mV (n = 29), and the AP half-width varied between 0.29 and 0.79 ms, the average being 0.48 ± 0.02 ms, as measured on the first elicited AP at rheobase current injection. There was no correlation between AP amplitude and half-width (fig. 3.3 E, left, Pearson corr. -0.13642, p = 0.48041). Input resistance and sag ratio also varied across DBCs and were inversely correlated (fig. 3.3 E, right, Pearson corr. -0.65118, $p = 1.3 * 10^{-4}$).

Next I compared the firing patterns, the passive and active membrane properties of CB+ (n = 22) vs CB- DBCs (n = 7), and bursting (n = 5) vs regular (n = 24) firing DBCs. The firing

index plots (number of action potentials per current step) indicated no difference in input gain between CB+ and CB- DBCs (fig. 3.3 F, left, two-way repeated measures ANOVA, within subjects effect of current step: $F = 50.71227$, $p = 1.17 * 10^{-7}$; within subjects effect of interaction: $F = 1.3527$, $p = 0.25498$; between subjects effect of immunoreactivity: $F = 2.16395$, $p = 0.15284$). Furthermore, those CB+ DBCs which showed a bursting phenotype fired significantly fewer action potentials than regular firing DBCs, which include both CB+ and CB- DBCs, at every current injection step above rheobase +20 pA (fig. 3.3 F, right, two-way repeated measures ANOVA, within subjects effect of current step: $F = 28.3653$, $p = 1.27 * 10^{-5}$; within subjects effect of interaction: $F = 7.20052$, $p = 0.01229$; between subjects effect of bursting: $F = 13.84007$, $p = 9.23 * 10^{-4}$, Tukey pairwise comparisons: bursting vs not bursting within each current step: * $p < 0.05$, ** $p < 0.01$, *** $p < 0.001$). Indeed, bursting DBCs often ceased firing after the initial burst even at large depolarising current injections. The input resistance of CB+ DBCs was lower than that of CB- DBCs (fig. 3.3 G, 121.1 ± 50.7 MΩ for CB+ DBCs vs 212.9 ± 86.8 MΩ for CB- DBCs, student's t-test $t(27) = -3.48614$, $p = 0.00169$). Conversely, whole-cell capacitance was higher in CB+ DBCs than in CB- ones (36.2 ± 13.8 pF for CB+ DBCs vs 18.6 ± 5.1 pF for CB- DBCs, Welch's t-test $t(26.07) = 4.97888$, $p = 3.5 * 10^{-5}$), indicating that CB+ DBCs are larger cells with bigger surface. Finally, action potential amplitude was larger in CB- DBCs than in CB+ ones (72.2 ± 12.5 mV for CB+ DBCs vs 86.2 ± 11.6 mV for CB- DBCs, student's t-test $t(27) = -2.61352$, $p = 0.01447$). The sag ratio, AP threshold, AP half-width, AHP, and the ISI CV were not different between CB+ and CB- DBCs (fig. 3.3 G).

Bursting DBCs had similar input resistance to regular firing (not bursting) DBCs (fig. 3.3 G, median: 138.5, IQR: 110.2 MΩ for not bursting vs median: 97.8, IQR: 108.6 MΩ for bursting, Mann-Whitney U test $Z(88) = 1.58771$, $p = 0.11235$), whereas the whole-cell capacitance was higher in bursting DBCs than in regular firing ones (median: 24.8, IQR: 13.4

pF for not bursting vs median: 52.8, IQR: 14.7 pF for bursting, Mann-Whitney U test Z(8) = -2.97335, p = 0.00295). The amplitude of the AHP was larger in not bursting DBCs than in bursting ones (-14.3 ± 2.6 mV for not bursting vs -10.8 ± 2.8 mV for bursting, student's t-test t(27) = -2.71015, p = 0.01154). Finally, not bursting DBCs showed stronger AP amplitude accommodation than bursting DBCs (0.54 ± 0.11 for not bursting vs 0.69 ± 0.14 for bursting, student's t-test t(27) = -2.72043, p = 0.01127), whereas AP frequency adaptation was not different (fig. 3.3 G; median: 3.36, IQR: 2.78 for not bursting vs median: 13.3, IQR: 10.39 for bursting, Mann-Whitney U test Z(30) = -1.70318, p = 0.08853).

3.1.5 Anatomical and molecular characterization of PMCs

I have fully recovered 14 (12 cells in temporal and 2 cells in the frontal cortex) cells with large, multipolar, smooth dendritic trees and extensive axon spreading uniformly in all directions from the soma (figs. 3.4 A and 3.7 A), 12 of them recorded and labelled by Dr Ruggiero Francavilla. The cell bodies of these cells were located in layer III at an average distance of ~ 1000 ± 430 μm (n = 3) from the pia. The 6 – 8 main dendrites travelled radially on average to ~ 375 ± 37 μm (n = 4) from the soma and had a relatively straight course (figs. 3.4 A and 3.7 A). The axons of these cells were even more extensive and travelled to ~ 500 ± 97 μm on average uniformly in every direction (figs. 3.4 A and 3.7 A). Importantly, the axons did not project to layer I and formed mostly *en-passant* and only few *en-termineux* boutons, which occasionally contacted neuronal somata (fig. 3.4 G).

Neurons with such dendritic and axonal distributions have been described previously in humans and other species as large basket cells (Kisvárday et al., 1993; Somogyi & Soltész, 1986) and dendrite-targeting cells (Tamás et al., 1997a). Basket cells by definition innervate the somata and the proximal dendrites of pyramidal neurons, however they also innervate distal dendrites and some dendritic spines (Kisvárday et al., 1987, 1990, 1993; Somogyi et al., 1983),

and have been demonstrated previously to be of at least two types in rodents, which can be differentiated based on immunoreactivity to parvalbumin (PV) or cholecystokinin (CCK)(Armstrong & Soltesz, 2012; Freund et al., 1983, 1986; Kawaguchi & Kubota, 1998; Somogyi et al., 2004). Those that are immunopositive for CCK have been found to be also immunopositive for the cannabinoid receptor type I (CB1R) along the axonal membrane in the hippocampus (Katona et al., 1999). Thus, I tested multipolar cells for immunoreactivity to PV and CB1, as well as to calbindin, as the latter was found previously in interneurons co-expressed with PV or CCK (Gulyás et al., 1991; Kubota et al., 1994).

Nine out of 12 tested multipolar cells were immunopositive for PV as shown either in their cell body (n = 2) or the boutons (n = 10; fig. 3.4 D, E, H), whereas none of the 5 PV immunopositive, 3 PV immunonegative, and one PV-untested cells were immunopositive for CB1 along their axons (fig. 3.4 H). Eight of the nine PV+ multipolar cells were immunonegative for calbindin in their boutons (n = 5) or soma (n = 3, fig. 3.4 E); one was immunopositive in the soma. Two PV-immunonegative multipolar cells tested were also immunonegative for calbindin in their boutons. The boutons of two PV+ and one PV- multipolar cell were tested for VIP and they were immunonegative. Finally, I tested the bouotns of multipolar cells for VGAT and showed that all 11 neurons tested were immunopositive (fig. 3.4 F, H).

The expression of parvalbumin by the majority (75 %) of the multipolar cells studied by me and their axonal and dendritic structures are characteristic of large basket cells, and dendrite targeting cells described in other species. Nevertheless, because I only found a small proportion of the multipolar cells' synapses to innervate somata (see chapter 3.2.1), instead of referring to them as basket cells, which might be misleading, I refer to them as parvalbumin-expressing multipolar cells (PMCs).

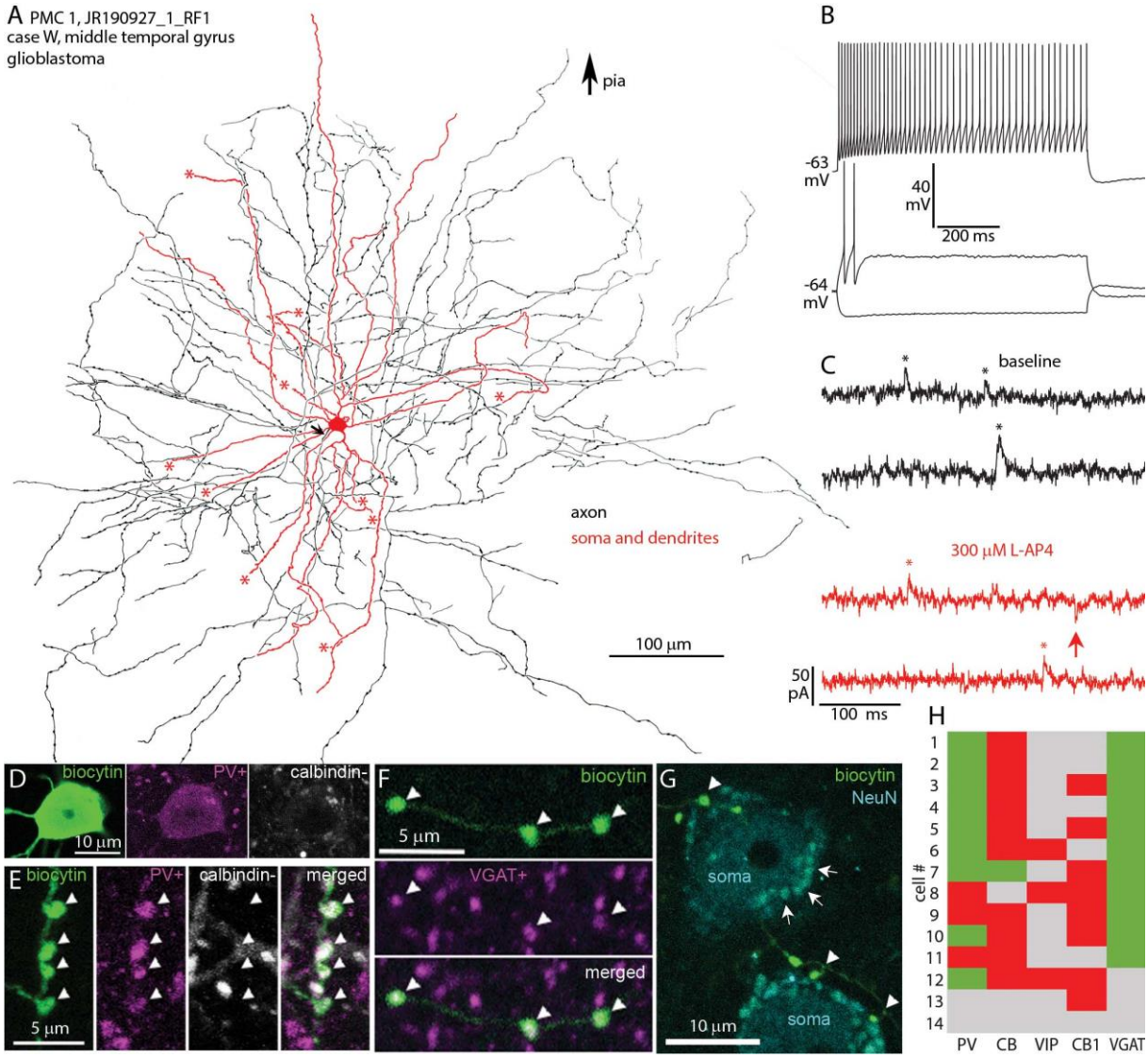


Figure 3.5. In vitro recorded and biocytin labelled basket cell in the human temporal neocortex. **A**. Partial 2D reconstruction (2 sections of ~ 60 µm thickness) of the cell with cell body in layer III; the axon did not enter layer I. The axon initial segment (arrow) and cut ends of dendrites (asterisks) are indicated. **B**. Voltage responses of the cell in A to current injections in whole-cell patch-clamp (+150, +300, and -150 pA steps). Firing is a regular train of action potentials with spike frequency adaptation and small spike amplitude accommodation. There is a minimal voltage sag and no rebound spikes in response to hyperpolarising current injection. **C**. Example current traces recorded at -50 mV clamping potential, showing spontaneous inhibitory (asterisks, upward deflections) and excitatory (arrow, downward deflections) postsynaptic currents in baseline condition (black) and after bath application of 300 µM L-AP4 (red). **D**. The cell body is immunopositive for parvalbumin (PV, magenta) and immunonegative for calbindin (white) in the cytoplasm (Z stack of 9 optical slices of 0.9 µm thickness, total depth, 4.7 µm). **E.** Boutons of the cell in A are immunopositive for PV (magenta, arrowheads) and immunonegative for calbindin (white) (Z stack of 13 optical slices of 0.9 µm thickness, total depth, 7.9 µm). **F**. Boutons (arrowheads) of the cell in A are immunopositive for the vesicular GABA transporter (VGAT, magenta) (single optical slice of 0.7 µm thickness). **G.** Boutons (arrowheads) of the cell in A (biocytin, green) are in close proximity with NeuN (cyan) immunopositive cell bodies (soma), which also contain autofluorescent lipofuscin granules (e.g. arrows). (Z stack of 4 optical slices of 0.7 µm thickness, total depth, 2.4 µm). **H**. Immunoreactivities in all recovered and tested neurons with multipolar dendrites: green, immunopositive; red, immunonegative; grey, not tested/inconclusive.

3.1.6 Electrophysiological characterization of PMCs

Based on recording quality, the current-voltage responses of 11 of these neurons were analysed (table 3.1). Several active and passive membrane parameters were different between PMCs and DBCs; PMCs showed a smaller amplitude voltage sag in response to hyperpolarising current injection than DBCs, and lacked rebound spikes after the hyperpolarising steps (fig. 3.5 A, B, C, sag ratio: PMCs 1.11 ± 0.06 vs. DBCs 2.07 ± 0.58, Welch's t-test, $p = 1.6 \times 10^{-9}$). Only the PV+/CB+ double immunopositive PMC 7 fired rebound spikes. During continuous depolarisation, PMCs fired a regular train of APs with less spike amplitude accommodation than DBCs (fig. 3.5 D; PMCs 0.85 ± 0.07 vs. DBCs 0.57 ± 0.12, Student's t-test, $p = 2.6 \times 10^{-8}$); spike frequency adaptation tended to be smaller in PMCs than in DBCs (fig. 3.5 E; PMCs median: 2.45, IQR: 1.83, DBCs median: 3.43, IQR: 3.52, Kolmogorov-Smirnov test, p = 0.0738). Two PMCs developed depolarisation block at RB + 100 pA current injection. In contrast to DBCs, only one cell, PMC 2, responded with a burst of 4 APs, all other PMCs fired 1 or 2 action potentials to RB current (e.g. fig. 3.4 B, PMC 1 and fig. 3.5 A, PMC 9). The mean firing rate of PMCs at RB +100 pA current injection was similar to that of DBCs (fig. 3.5 F, PMCs 36.9 ± 18.3 Hz vs. DBCs 38.1 ± 19.7 Hz, Student's t-test, p = 0.87), but the regularity of the AP trains were different, as the coefficient of variation of the inter-spike intervlas (ISI CV) was smaller in PMCs than DBCs (PMCs median: 20.3, IQR: 7.6 vs. DBCs median: 33.2, IQR: 33.4, Kolmogorov-Smirnov test, p = 0.02123).

Parvalbumin-expressing cells in the cortex of other species are also referred to as fast-spiking cells, because of their short duration action potentials (AP) and high frequency firing *in vivo* and *in vitro* (Baranyi et al., 1993; Erisir et al., 1999; Kawaguchi, 1995; McCormick et al., 1985). In this study PMCs had a mean AP half-width of 0.48 ± 0.12 ms, similar to that of DBCs (fig. 3.5 G, H; 0.48 ± 0.11 ms, Student's t-test, p = 0.99). The AP threshold of PMCs was not different from that of DBCs (fig. 3.5 I; PMCs -40.1 ± 3.4 mV vs. DBCs -39.1 ± 3.8

mV, Student's t-test, p = 0.45). On average PMCs had smaller AP amplitude (fig. 3.5 J; PMCs 60.2 ± 7.9 vs. DBCs 75.6 ± 13.3 mV, Student's t-test, p = 0.00119) and larger AHP amplitude (fig. 5 K; PMCs 20 ± 3.4 mV vs. DBCs 13.7 ± 2.9 mV, Student's t-test, $p = 1.44 \times 10^{-6}$) than DBCs.

Whole-cell capacitance of PMCs was larger than that of DBCs (fig. 3.5 L; PMCs 78.3 ± 21.8 pF vs. DBCs 31.9 ± 14.1 pF, Student's t-test, $p = 2.93 \times 10^{-9}$), reflecting their cell bodies and longer dendrites. Their input resistance (IR) and membrane time constant was not different from those of DBCs (fig. 3.5 M IR; PMCs 135 ± 50 MΩ vs. DBCs 143 ± 70 MΩ, Student's t-test, p = 0.733; fig. 3.5 N tau; PMCs 9.4 ± 2.5 ms vs. DBCs 7.9 ± 2.1 ms, Student's t-test, $t_{(38)} = -1.82$, p = 0.077). Furthermore, PMCs had larger rheobase than DBCs (fig. 3.5 O; PMCs 36.5 ± 45.5 pA vs. DBCs -5.5 ± 28.4 pA, Welch's t-test, p = 0.01697), whereas their resting membrane potentials tended to be smaller, but was not significantly different (fig. 3.5 P; PMCs -62.2 ± 7.4 mV vs DBCs 56.9 ± 4.3 mV, Welch's t-test, $t_{(12.49)} = 2.133$, p = 0.05339).

Figure 3.6. Comparison of membrane properties of DBCs and PMCs

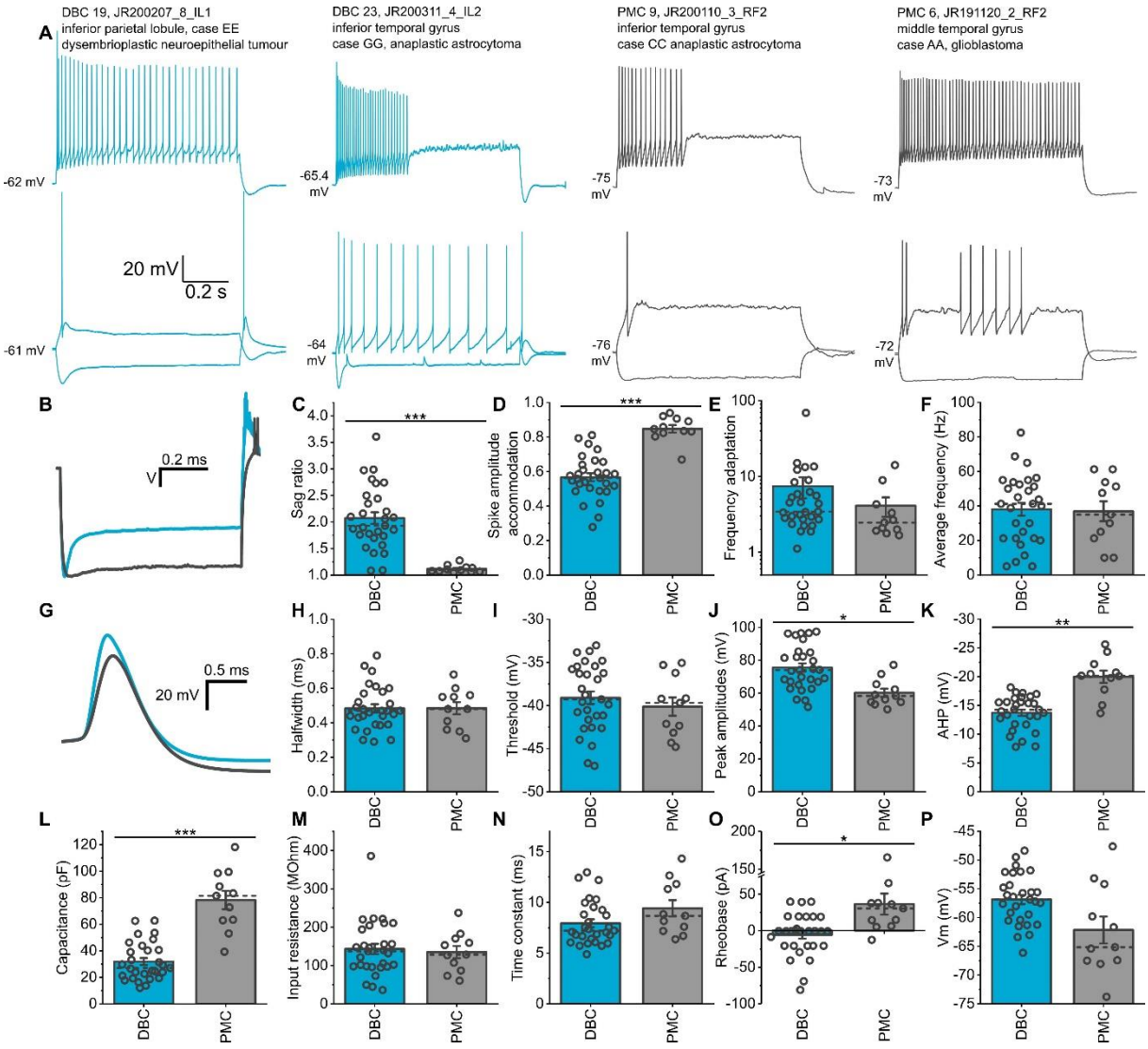


Figure 3.6. Comparison of membrane properties of DBCs and PMCs. a. Example traces from two DBCs (blue) and two PMCs (grey) showing voltage responses to current injections of rheobase, holding current -100 pA and rheobase +100 pA. **b.** Average waveforms of the voltage responses of the DBCs (blue, n = 29) and PMCs (grey, n = 11) in response to holding current -100 pA current injection. The average traces were normalised such that the initial baseline values and the lowest points on the voltage responses are equal. **c.** Ratios of the sags in the voltage responses to stimulation with holding current -100 pA, calculated as the peak voltage deflection divided by the amplitude of the steady state voltage response (Welch's t-test, $t_{(29.9)} = 8.55$, $p < 0.001$). **d.** Spike amplitude accommodation ratios, calculated by dividing the amplitude of the last action potential by the amplitude of the first generated in response to rheobase +100 pA current injection (Student's t-test, $t_{(38)} = -6.98$, $p < 0.001$). **e.** Firing frequency adaptation ratios calculated by dividing the last inter-spike interval with the first one of the response to rheobase +100 pA current injection (Kolmogorov-Smirnov test, $D = 0.429$, $Z = 1.21$, $p = 0.074$). **f.** Average frequencies of action potentials generated in an 800 ms response to rheobase +100 pA current injection (Student's t-test, $t_{(38)} = 0.161$, $p = 0.87$). **g.** Average waveforms of the first action potentials generated at rheobase current injection for each cell. **h - j.** Halfwidths (**h**, Student's t-test, $t_{(38)} = -0.00799$, $p = 0.99$), thresholds (**I**, Student's t-test, $t_{(38)} = 0.76$, $p = 0.45$), and amplitudes (**j**, Student's t-test, $t_{(38)} = 3.5$, $p = 0.001$), of the first action potential generated in response to rheobase current injection for each cell. **k.** Afterhyperpolarisation amplitudes of the first action potential for each cell at rheobase current injection, calculated relative to the threshold of that action potential (Student's t-test, $t_{(38)} = 5.71$, $p < 0.001$). **l.** Whole cell capacitances, calculated from the voltage amplitude and the time constant associated with the slowest component of a double exponential fit to the initial voltage deflections of the responses to holding current -60 pA current injection (Student's t-test, $t_{(38)} = -7.69$, $p < 0.001$). **m.** Comparison of input resistances (Student's t-test, $t_{(38)} = 0.343$, $p = 0.733$). **n.** Membrane time constants, measured as the slowest component of the double exponential fit described in **l** (Student's t-test, $t_{(38)} = -1.82$, $p = 0.077$). **o.** The amount of current required to elicit at least one action potential within an 800 ms period of stimulation for each cell (Welch's t-test, $t_{(12.89)} = -2.74$, $p = 0.017$). Note that 20 pA current injection steps were used, and the rheobase was taken as the holding current of the first step to elicit an action potential. **p.** The membrane voltage of each cell recorded in response to a 0 pA current injection, or estimated based on the cell's current-voltage relationship if no 0 pA step was recorded (Welch's t-test, $t_{(12.49)} = 2.133$, $p = 0.053$).

3.2 Cell type-specific synaptic targeting in the human neocortex

3.2.1 Synaptic targets of DBCs and PMCs

In non-human species DBCs innervate both pyramidal cells and interneurons (DeFelipe et al., 1989a; Kawaguchi & Kubota, 1998; Somogyi & Cowey, 1981; Tamás et al., 1998), in agreement with my paired eIPSC recordings in humans (see chapter 3.2.2). In order to explore the synaptic targets of the 'horsetail' axon of DBCs, I used serial section electron microscopy of individual DBCs' axonal boutons to study their synaptic targets and compared their frequency distributions to the synaptic targets of PMCs, which have a very different axonal distribution. I studied the 'horsetail' axons of 4 CB+ DBCs (DBCs 5, 10, 22 and 23), and one CR+ DBC (DBC 25). All samples were taken from layer III and included small collateral side branches (fig. 3.6 A). All CB+ DBCs examined were recorded in the temporal neocortex, whereas the CR+ DBCs was recorded in the inferior parietal lobule. One DBC (DBC 5) was recorded from a temporal lobe epilepsy patient, and the rest from tumour patients (see tables 2.1 and 3.1).

Synaptic junctions were identified based on well-established electron microscopic criteria. These included the electron opaque synaptic cleft, a regular and uniform apposition of the presynaptic and postsynaptic membranes, the slight widening of the extracellular space, accumulation of synaptic vesicles at the pre-synaptic active zone and the presence of a varying width of postsynaptic density (fig. 3.6 E – J). I examined a total of 132 boutons (20 - 34 from each DBC), of which 100 were found to form synaptic junctions. For 32 boutons the synaptic junctions could not be identified because of an incomplete series of sections or because of the unfavourable cutting angle to the synaptic junctions. Three boutons formed two separate synaptic junctions each, all other boutons (97 %) formed just one synapse, thus the total number of identified synaptic junctions was 103. In 9 instances the synaptic junction was identified, but

the small diameter target structure could not be defined, so a total of 94 synaptic targets were identified. All synapses made by DBCs were of Gray's type II, or symmetric (Colonnier, 1968; Gray, 1959), with a thin if any postsynaptic density (fig. 3.6 E - J), consistent with the GABAergic nature of DBCs shown here. The shape and size of vesicles could not be studied in the labelled boutons, being covered by the electron opaque DAB/OsO4 precipitate (fig. 3.6 E - J). All examined synaptic junctions were made with dendritic spines or dendritic shafts; no synapse was found on soma. Small diameter processes of triangular or elongated shapes and without mitochondria were identified as spines if the process could be followed to its end in one direction through serial sections (fig. 3.6 E, G, H, J; total no. of spines: 39). Some spines (33 %) contained a spine apparatus, a membranous structure with multiple cisternae (fig. 3.6 H). All dendritic spine targets were also innervated by an additional unlabelled type I (asymmetric) synapse (fig. 3.6 E, G, H, J). I followed spine targets through serial sections in an attempt to identify the parent dendritic shaft to predict its origin from an interneuron or a pyramidal cell. Due to loss of sections and the very thin and long shape of some of the spine necks, only 9 spines could be traced back to their parent shafts. Three of these dendritic shafts emitted spines other than the one innervated by the DBC and none of these dendrites received type I synapses on their shaft, thus most likely belonged to pyramidal cells. Nevertheless, given the abundance of dendritic spines on pyramidal cells relative to interneurons, it is likely that the vast majority of spine targets belong to pyramidal cells. In the case of the CB+ DBC 5, one postsynaptic dendrite was innervated by two labelled boutons, both of them targeting spines. These spines also received a type I synapse each. Two other spines on the same target dendrite received a single type I synapse each (fig. 3.6 K, L).

Dendritic shafts postsynaptic to DBCs could not be followed to an end in either direction and contained mitochondria and/or microtubules amongst other organelles (fig. 3.6 F, I). I identified a total of 55 dendritic shaft synaptic targets and followed them through serial sections.

Of these 10 had at least 4 (6.4 ± 2.6 SD) type I and type II additional synapses covering their surface densely. As no spines originated from these dendrites, I identified them as belonging to GABAergic interneurons. I grouped 23 dendritic shaft targets with at least 3 innervating synapses (including the labelled synapse) and lacking spines as originating from GABAergic interneurons. On 32 dendritic shaft targets, either no, or only one additional synapse could be found due to short and incomplete series of sections; 3 of these also emitted spines. These three dendrites were grouped as pyramidal cell dendrites, whereas 29 postsynaptic dendritic shafts remained unidentified. The average diameter of the target shafts was of median 623, IQR: 454 nm diameter, and some were of very small diameter (e.g. fig. 3.6 F), corresponding to distal dendrites.

Among the CB+ DBCs the average proportion of dendritic spine targets was 48 ± 15 % (DBCs 5, 10, 22 and 23, n = 23, 22, 18 and 13 respectively), the remainder (52 ± 14 %) being dendritic shafts. The CB-/CR+ DBC 25 had the lowest proportion (17 %) of dendritic spine targets (3/18), the majority of postsynaptic elements (83 %) being dendritic shafts (fig. 3.6 M). The frequency distribution of synaptic targets was different between all DBCs, including the CB-/CR+ DBC 25 ($X^2_{(4,\ N\ =\ 94)}$ = 11.31372, p = 0.02326), meaning that the proportion of dendritic shaft and spine targets depends on the identity of the presynaptic DBCs. When looking at only the CB+DBCs no such dependence was observed ($X^2_{(3,\ N\ =\ 76)}$ = 5.51408, p = 0.1378). Among the targets of CB+ DBCs identified as originating from GABAergic interneurons or pyramidal cells, the average proportion of pyramidal cell targets was 76.5 ± 18 %, whereas that of identified interneuron targets was 23.5 ± 18 % (DBCs 5, 10, 22 and 23, N = 17, 11, 11 and 6 respectively). On the other hand, the proportion of pyramidal cell targets for the CB-/CR+ DBC No 25 was only 21.4 %, the majority of the targets (78.6 %) being interneurons. These synaptic target distributions are similar to what was reported in other species (DeFelipe &

Jones, 1992; Kubota et al., 2007; Somogyi & Cowey, 1981; Tamás et al., 1997a, 1998), but the homology of cell types is difficult to establish (see discussion).

A total 104 boutons from 3 PMCs (3, 4 and 5) were studied by Dr Sawa Horie, and a total of 63 synaptic junctions with 62 postsynaptic structures were identified (fig. 3.7), one bouton forming two synaptic junctions. In the case of 38 boutons the synapse could not be found due to incomplete series of sections or unfavourable cutting angle; in the case of 5 synapses the postsynaptic structure could not be defined. The PMCs 3 and 4 were recorded in the temporal cortex, whereas PMC 5 in the frontal cortex. All samples came from tumour patients. All synapses made by PMCs were of Gray's type II (fig. 3.7 F - K), but in contrast to DBCs, PMCs also targeted somata in addition to dendrites. Based on the presence of the nucleus (fig. 3.7 E) or on the size of the profile, a total of 8 targets were identified as soma; 4 of the somata were identified as pyramidal cells, based on the presence of only additional type I synapses. Next, 41 targets were dendritic shafts (fig. 3.7 G, H, J), of which 36 (88 %) were identified as pyramidal cell dendrites (fig. 3.7 H), and 5 as interneuron dendrites (fig. 3.7 G, J), based on the same criteria as described above. Finally, 13 targets were identified as dendritic spines (fig. 3.7 K), of which 6 (46 %) contained a spine apparatus. One soma was found to be innervated by two boutons of a single PMC. Interestingly, PMC 4 had a higher proportion of spine targets (40 %) compared to the other two (13.3 and 12.5 % for PMC 3 and 5 respectively; fig. 3.7 E). The average frequency of soma targets was 12.8 ± 3.4 % for PMCs, whereas that of dendritic shafts and spines was 65.2 ± 13.9 % and 21.9 ± 16.7 % respectively (fig. 3.7 E). When comparing this with the target frequency distributions of calbindin immunopositive DBCs, I found that there was significant correlation between the cell type and the frequency of different synaptic targets ($X^2_{(12, N = 126)} = 28.06643$, $p = 0.00541$), thus calbindin immunopositive DBCs and PMCs have different synaptic target preferences in the human neocortex. Although PMCs innervate somata to some extent, the majority of their synapses are onto dendrites, similarly to DBCs. To test

whether different dendritic domains are innervated by these two cell types, the diameters of target dendrites were measured. I found no difference in the diameter of target dendrites innervated by DBCs and PMCs (DBCs median: 623, IQR: 454 nm vs. PMCs median: 726, IQR: 550 nm, Mann-Whitney U-test U = 378, Z = -1.42972, p = 0.1528), suggesting that DBCs and PMCs may innervate overlapping dendritic domains.

I conclude that CB+ DBCs have different synaptic target preference from the CB- DBC and PMCs in the human neocortex, and dedicate a high proportion of their synapses to dendritic spines of pyramidal cells. While PMCs also innervate dendritic spines, the majority of their targets are dendritic shafts and they also innervate somata, which DBCs omit. The dendritic domains targeted by DBCs and PMCs overlap.

Figure 3.7. Synaptic targets of double bouquet cells in layer III of the human neocortex

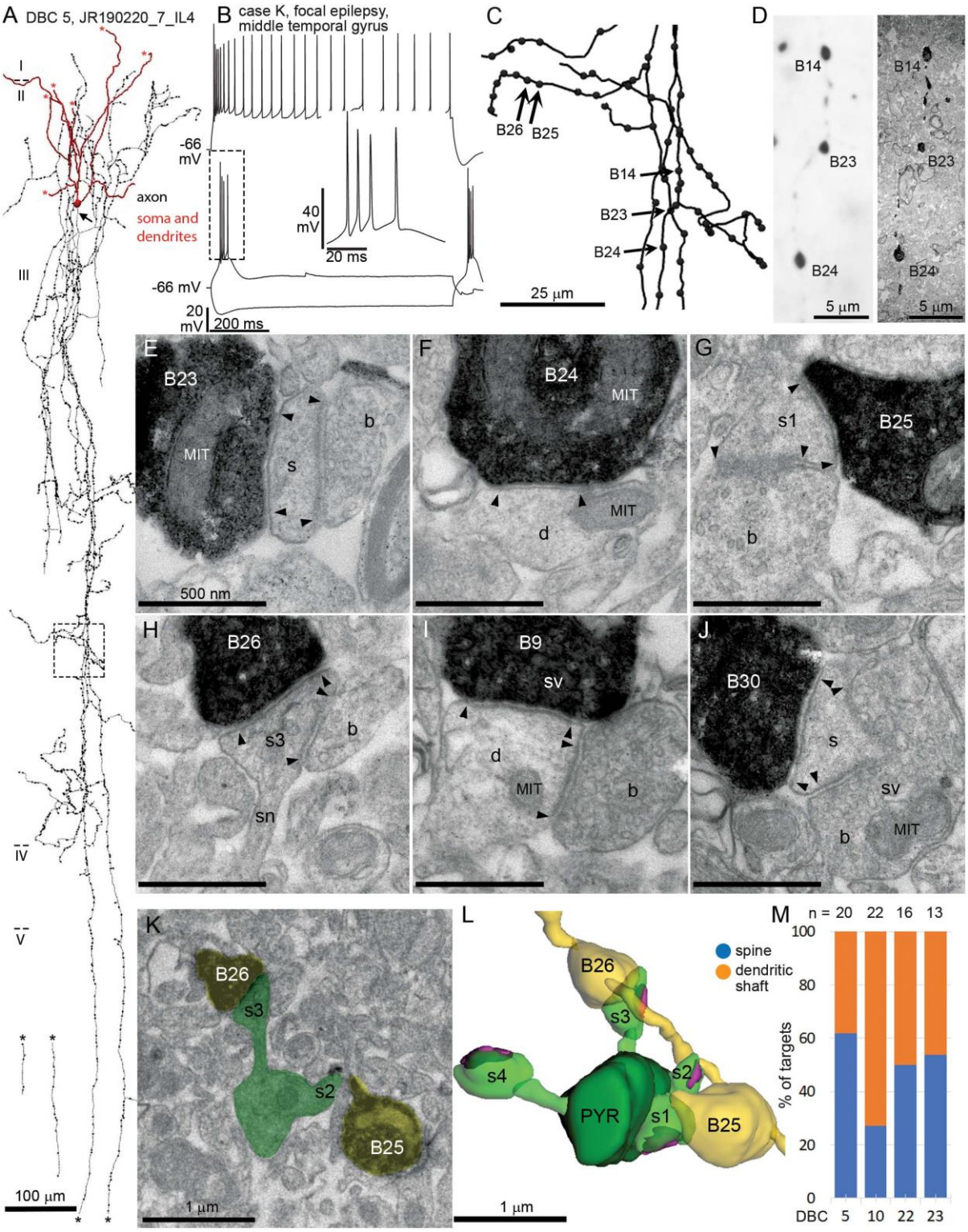
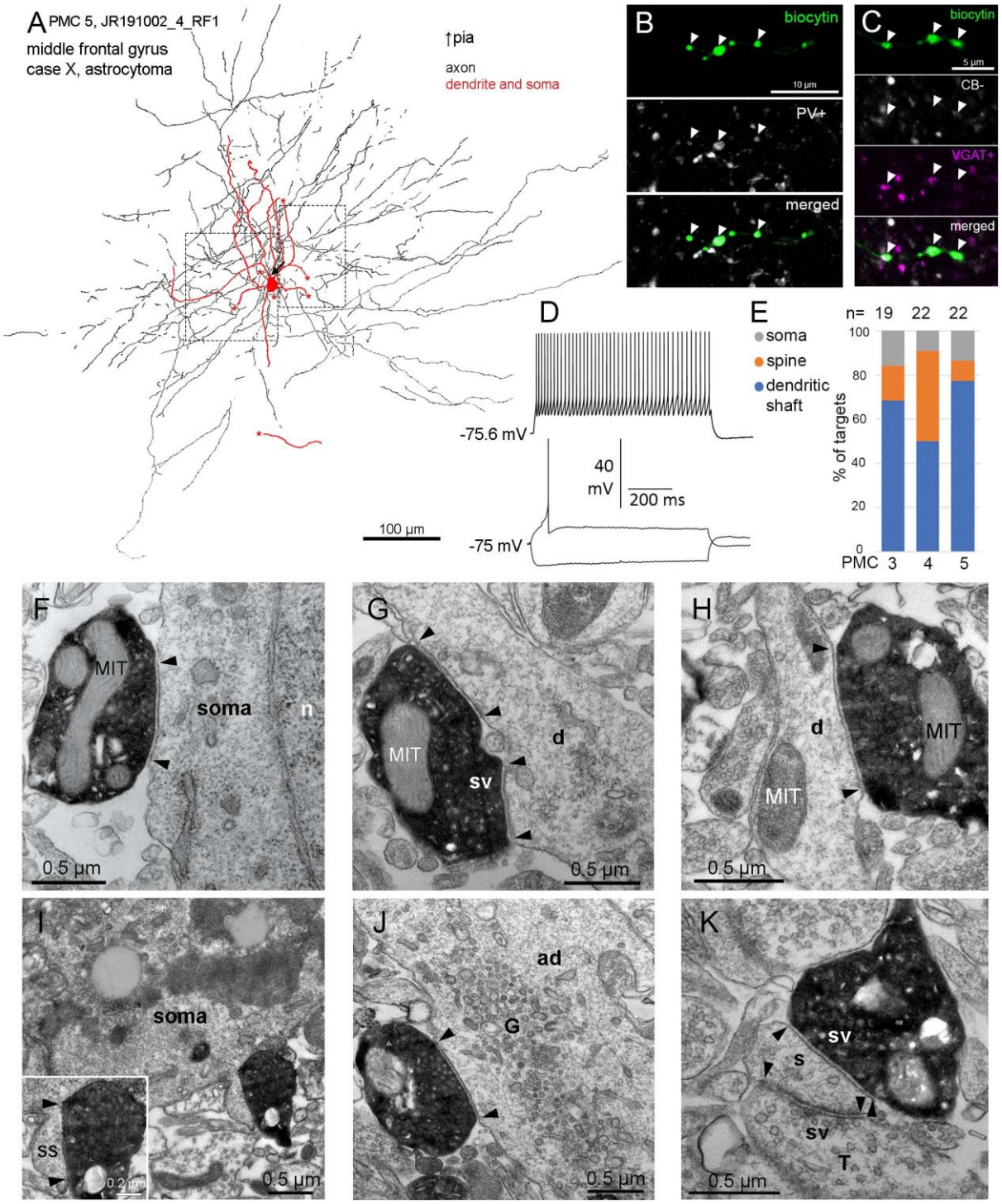


Figure 3.7. Synaptic targets of double bouquet cells in layer III of the human neocortex. A. Partial 3D reconstruction (3 sections of ~ 60 μm thickness) of a supragranular double bouquet cell with dendrites entering layer I, and a "horsetail" axon (arrow, initial segment) descending to layer V (asterisks indicate cut ends of axon and dendrites); note short lateral collaterals in layer III. B. Voltage responses of the cell to current injections (+60, +160 and -100 pA steps) in whole-cell patch-clamp; inset showing the burst in boxed area. C. Enlarged view of the boxed area in A, included in serial electron microscopic analysis; numbered boutons are shown in E- H, K-L. D. Left: Light micrograph of a descending axon collateral with three boutons visualised by HRP reaction product (single optical section within a ~60 μm thick osmium treated section); Right: low power electron micrograph of the same boutons in a 50 nm thick resin section. E-J. High power electron micrographs of the boutons of the cell in A forming type-2 synapses with their targets. The edges of synapses are indicated by black arrowheads. Note the smooth apposition of the pre- and postsynaptic membranes and synaptic vesicles (sv) at the pre-synaptic active zones. Boutons 23, 25, 26 and 30 innervate dendritic spines (s), whereas Boutons 9 and 24 innervate dendritic shafts (d). All targets, except the dendrite in F are innervated by additional boutons (b) forming type-1 synapses (arrowheads). MIT: mitochondrion; sn: spine neck. K - L. electron micrograph (K) and 3D reconstruction (L) of the axon with two boutons (B25, B26, yellow) and their target spiny pyramidal cell dendrite (PYR, green). The target of B25 (s1) is a stubby spine (see G), that of B26 (s3) is a mushroom spine (see H). Two other spines were also identified (2, 4). All four spines receive a type 1 synapses (magenta). M. Proportion of synaptic targets (n, shown on top) of four double bouquet cells (cell numbers as in Fig. 3.2).

Figure 3.8. Synaptic targets of Parvalbumin-positive multipolar cells in layer III of the human neocortex. A. Partial 2D reconstruction from 2 sections of ~60 μm thickness of a parvalbumin positive multipolar cell (PMC 5) with dendrites (red) and axons (black) extending in every direction uniformly around the cell body in layer III. The axon initial segment (arrow), cut ends of dendrites (asterisks) and the direction of the pial surface are indicated. Boxes indicate the areas re-embedded for electron-microscopy. **B.** Boutons (arrowheads) of the cell in **A** are immunopositive for parvalbumin (PV, white) (single optical slice of 0.4 μm thickness). **C.** Boutons (arrowheads) of the cell are immunopositive for vesicular GABA transporter (VGAT, magenta) and immunonegative for calbindin (white)(single optical slice of 0.4 μm thickness). **D.** Voltage responses of the cell held in current-clamp mode to current injections of rheobase, holding current -100 pA and rheobase +100 pA. **E.** Proportion of synaptic targets for PMCs 3, 4 and 5 (n = 19, 22 and 22 respectively), as identified by serial section electron microscopy. **F-K.** Electron micrographs of labelled boutons (black, electron opaque) of PMC 5 (**F-H**) and PMC 4 (**I-K**), forming type II synaptic junctions with somata (**E, I),** inset in **I** shows the bouton innervating a somatic spine (ss), dendritic shafts (d, ad; **G, H, J**), and a dendritic spine (s, **K**). Edges of the synaptic junctions are indicated by arrowheads. The spine in **K** also receives a type I synapse (arrowheads) from an unlabelled terminal (T). n: nucleus, MIT: mitochondrion, d: dendritic shaft, ad: apical dendrite; ss: somatic spine, sv: synaptic vesicles, G: Golgi apparatus

Figure 3.8. Synaptic targets of Parvalbumin-positive multipolar cells in layer III of the human neocortex



3.2.2 Unitary postsynaptic currents evoked by DBCs

The target cell types and subcellular target domains of DBC efferent synapses and their postsynaptic effects are not known in humans. Following pervious work in other species (Jiang et al., 2015; Tamás et al., 1997a), I tested unitary synaptic interactions between pairs of neurons consisting of one DBC and one other GABAergic interneuron or a pyramidal cell within a 50 μm distance from the DBC soma. I tentatively identified DBCs during the recordings based on their characteristic firing. I succeeded in testing 12 unitary synaptic connections from DBCs to interneurons and 4 connections to pyramidal cells, and detected postsynaptic responses in 3 interneurons (DBC-to-IN) and one pyramidal cell (DBC-to-PYR), a 25% connectivity ratio (fig. 3.8). I also found two unitary synaptic connections from interneurons to DBCs out of 9 tested.

The identity of presynaptic DBCs (n=5) was confirmed by light microscopy based on their 'horsetail' axon (fig. 3.8 A). Three of them (DBCs 2, 6 and 12) were immunopositive for calbindin (fig, 3.8 C), the other two (DBCs 28 and 29) were CB-/CR- double immunonegative (see fig. 3.2 F). The cell bodies of the recorded cell pairs were located in layers II or III. One of the postsynaptic interneurons (pair 4), was also identified as a CB-/CR- double immunonegative DBC (DBC 27); there was no detectable connection from DBC 27 to DBC 28. I was not able to determine the cell type of the other three postsynaptic interneurons. One of them (pair 2), had a bipolar dendritic tree originating from two main trunks at the superficial and deep poles of the soma (fig. 3.8 A), and its axon had loose branches descending towards deeper layers. Its firing pattern was stuttering and showed spike amplitude accommodation; it showed no voltage sag (fig. 3.8 B). In rodents, similar neurons were found to express VIP. However this postsynaptic human interneuron was double immunonegative for VIP as well as for calbindin. In pair 3 the postsynaptic cell had a firing pattern resembling that of multipolar basket cells, such as high frequency regular firing and depolarisation block (fig. 3.8 K), had a small voltage sag and a multipolar dendritic tree. In contrast, the postsynaptic interneuron in pair 5 had a slow

irregular firing pattern and showed no voltage sag. Its dendrites were oriented radially. This cell was immunonegative for CR, VIP and calbindin. The axons of two postsynaptic interneurons (pairs 3 and 5) were not recovered. In pair 1, the postsynaptic pyramidal cell was identified based on its densely spiny dendrites.

In order to test for unitary synaptic connections I evoked pairs or, in the case of pair 2, a train of five action potentials 50 ms apart in one cell held in current clamp between -70 and -75 mV by brief (1 – 5 ms) current injections of 100 – 500 pA, while recording the other neuron in voltage-clamp mode at just below firing threshold potentials (-45 - -50 mV,see chapter 2.3.1). The peak amplitude of the evoked Inhibitory postsynaptic currents (eIPSCs), the paired-pulse ratio (PPR, amplitude of eIPSC2 / amplitude eIPSC1) and the failure rate of the first eIPSC were evaluated, as well as the 20 to 80 % risetime and the half-width of the first eIPSC. In pair 2, single APs evoked 50 ms apart in the presynaptic DBC did not elicit IPSCs in the postsynaptic cell; only evoking a presynaptic AP burst resulted in detectable bursts of postsynaptic IPSCs (fig. 3.8 D, E). In this case the PPR was not available. In all other pairs, single APs elicited IPSCs in the postsynaptic cells. However, in pair 3, although single APs could elicit detectable IPSCs, the first presynaptic stimulus was always a burst of 2-3 APs, even at the lowest current injection (fig. 3.8 L).

I found large variability in the response parameters of the 5 synaptic connections made by DBCs onto interneurons and pyramidal cells. The mean amplitude of the first eIPSC in the DBC-to-PYR connection (pair 1) was 21 ± 1.7 pA (n = 17, including failures), with a failure rate of 0.12 and a PPR of 0.52. In the DBC-to-IN connections, the amplitude was 16.2 ± 3.8 pA (n = 20, including failures) in pair 2, it was significantly higher in pair 4 (27.4 ± 3.1 pA, n = 20, including failures) and was significantly lower in pairs 3 (5 ± 0.9 pA, n = 12, including failures) and 5 (4 ± 0.3 pA, n = 20, including failures; One-way ANOVA, $F_{(72,4)} = 16.22$, $p = 4.7 * 10^{-8}$, Tukey post-hoc test; $p < 0.05$ for pairs 4 vs. 2; $p < 0.01$ for pairs 5 vs. 2; $P < 0.001$ for pairs 4

vs. 3 and 4 vs. 5; fig. 3N, IPSC 1 amplitude). Conversely, eIPSC1 failure rates were low in pairs 4 and 5 (0.05 and 0.1 respectively), and higher in pairs 2 and 3 (0.55 and 0.33 respectively; fig. 3.8 N, IPSC1 FR). All pairs, except pair 2 showed paired-pulse depression of eIPSC amplitude, the PPR being 0.66, 0.6 and 0.56 for pairs 3, 4 and 5 respectively (fig. 3.8 N, PPR), indicating a decrease of release probability from the first to the second action potential. In contrast, in pair 2, where the presynaptic input was a burst of APs, the delay between the first and second APs within the burst varied around ~10 ms. Here I measured paired-pulse facilitation, from 16.2 ± 3.8 pA (n = 20, including failures) of eIPSC1 to 32.2 ±1.9 pA (n = 20, including failures) of IPSC2 (fig. 3.8 E, G). This paired-pulse facilitation was accompanied by a decrease in failure rate of eIPSC2 compared to eIPSC1 from 0.55 to 0.5 (fig. 3.8 G). The increased release probability at the second action potential is likely explained by the short (~ 10 ms) delay between the first two APs in the burst and accumulation of intracellular calcium.

I also analysed the response kinetics of these connections. The largest response delay (from AP peak to eIPSC onset) was in pair 2 (2.5 ± 0.2 ms, n = 9 eIPSCs, omitting failures; fig. 3.8 F), and the shortest in pair 3 (0.6 ± 0.1 ms, n = 8 eIPSCs, omitting failures; fig. 3.8 M); eIPSC1 delay in pairs 1, 4 and 5 was 1.2 ± 0.1 (n = 15), 1.6 ± 0.05 (n = 19) and 1.8 ± 0.1 (n = 18) ms respectively (One-way ANOVA, $F_{(69,5)} = 34.75243$, $p = 2.1 * 10^{-15}$, Tukey post-hoc test, $p < 0.05$ for all comparisons). The mean 20 – 80 % risetime was the shortest in pair 4 with 0.36 ± 0.039 ms (n = 19 eIPSCs, no failures). Pairs 3 and 5 had a risetime of 0.61 ± 0.1 (n = 8) and 0.67 ± 0.1 (n = 18) ms respectively. In pair 1, the risetime was 0.87 ± 0.058 ms (n = 15) (One-way ANOVA, $F_{(69,5)} = 7.37265$, $p = 3 * 10^{-4}$, Tukey post-hoc test, $p < 0.05$ for pairs 5 vs. 1; $p < 0.001$ for pairs 4 vs. 1; fig. 3.8 N, 20-80% risetime). Finally, I found no difference in half width between the four connections (pair 2 excluded due to burst) (One-way ANOVA, $F_{(60,4)} = 0.46589$, $p = 0.70724$; fig. 3.8 N, half-width).

In Summary, the most reliable connection was made in between DBC 28 and DBC 27 (pair 4), and this synapse also showed the fastest kinetics. Connections made by calbindin immunopositive DBCs to interneurons were less reliable than other connections. Finally, the connection by the calbindin immunopositive DBC onto the pyramidal cell was also reliable, but showed slower kinetics than the connection in pair 4.

Figure 3.9. Unitary eIPSCs evoked by DBCs

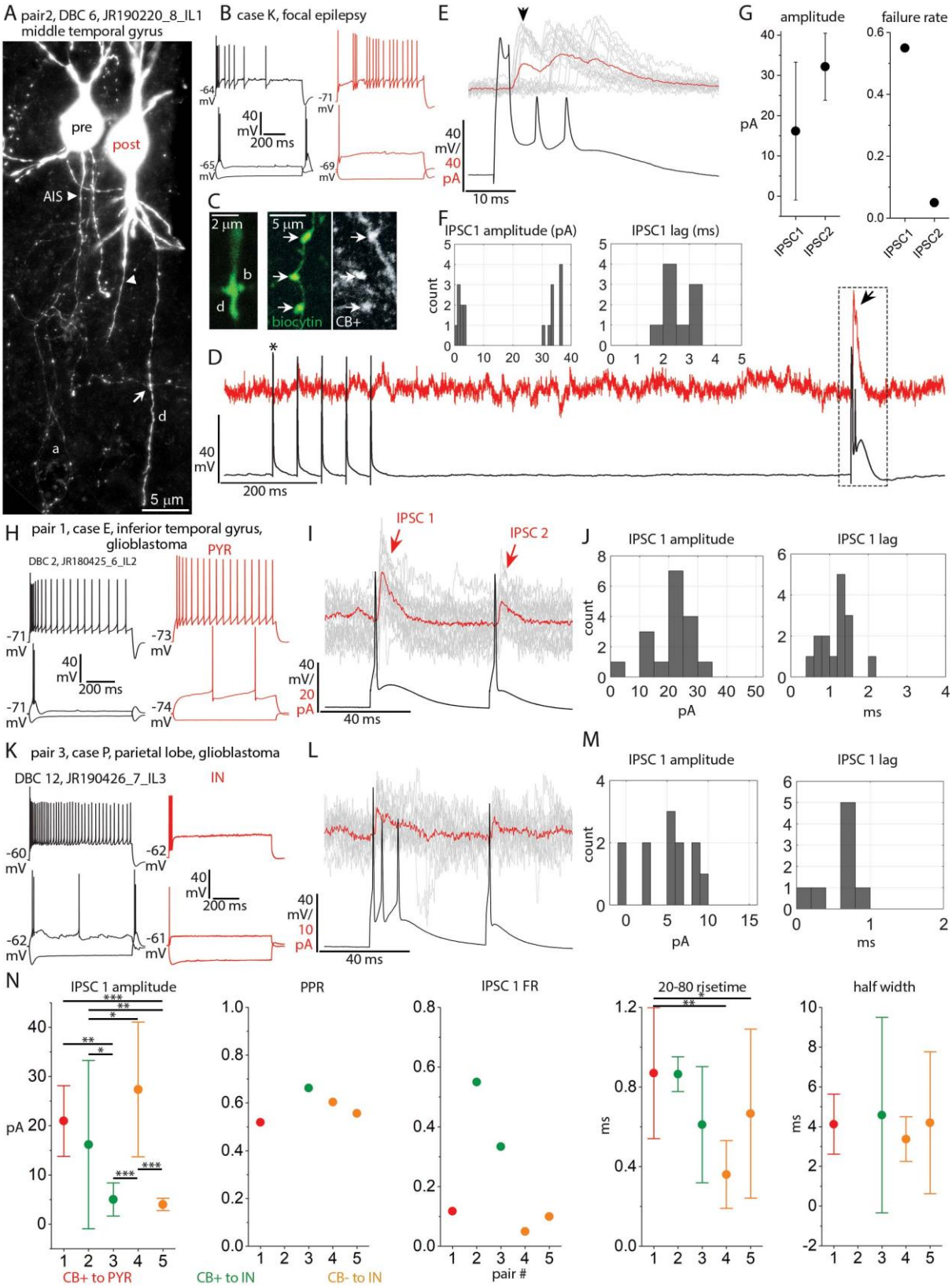


Figure 3.9. Unitary eIPSCs evoked by DBCs. A. Fluorescent image of two simultaneously recorded synaptically connected interneurons (pair 2). The presynaptic double bouquet cell (pre) has a horsetail axon (a) and a collateral forms a bouton in close apposition to the dendrite (d, arrow) of the postsynaptic interneuron (post). Axon initial segments (AIS), arrowheads. (Z stack of 16 optical slices of 14.3 μm thickness, total depth, 42.8 μm). **B**. Voltage responses of the pre- (black) and postsynaptic (red) cells in A to current injections of RB, RB +100 pA and holding current -100 pA. **C. Left: Fluorescent** image of one contact site (arrow in A) showing the putative presynaptic bouton (b) in close juxtaposition with the postsynaptic dendrite (d, single optical slice of 0.7 μm thickness). **Right:** Boutons (arrows) of the presynaptic DBC (green) are immunopositive for calbindin (grey) (single optical slice of 0.9 μm thickness). **D.** Example of the current response in the postsynaptic cell (red, single sweep) voltage clamped at -47 mV to a train of single action potentials (APs, asterisk) 50 ms apart and an action potential burst (boxed area) evoked in the presynaptic DBC (black) in current clamp. There is a postsynaptic IPSC response to the burst (arrow) but not to the single APs (failures). **E.** Current responses in the postsynaptic cell (single responses in grey, arrow 1st response, average of 20 responses in red) to the action potential burst in the presynaptic DBC (black, single sweep). **F.** Distributions of peak amplitude (n = 20 including failures) and response lag (n = 9 excluding failures) of the response to the first AP in the burst (bin width: 1 pA for amplitude and 0.5 ms for lag). **G.** Mean response amplitude including failures (left,) and failure rate (right) of the IPSCs to the first and second APs in the burst (n = 20 for each of IPSC 1 and 2, whiskers represent SD). **H.** Voltage responses of the presynaptic DBC 2 (black) and postsynaptic pyramidal cell (red) of Pair 1 to current injections of RB, RB +100 pA and holding current -100 pA. **I.** Current responses in the postsynaptic cell (single responses in grey, average of 17 responses in red) to a pair of APs evoked in the presynaptic DBC 2 (black) 50 ms apart. **J.** Distribution of peak amplitude (n = 17 including failures) and response lag (n = 15 excluding failures) of response 1 (bin width: 5 pA for amplitude and 0.2 ms for lag). **K-M.** Same as **H-J** for pair 3 (bin width: 1 pA for amplitude and 0.2 ms for lag; n = 12 including, n = 8 excluding failures). The postsynaptic cell is an interneuron (IN) and the presynaptic DBC fires AP bursts to rheobase current injection. **N.** Mean amplitude (including failures) of IPSC 1 (n = 17, 20, 12, 20 and 20 responses for neuron pairs 1-5 respectively; One-way ANOVA, $F = 16.22$, $p < 0.001$, Tukey post-hoc test; $p < 0.05$ for pairs 4 vs. 2 and 3 vs. 2; $p < 0.01$ for pairs 5 vs. 2 and 3 vs. 1; $P < 0.001$ for pairs 4 vs. 3, 4 vs. 5 and 5 vs. 1), paired-pulse ratio (PPR, average response2/response1 mean amplitude), failure rate, 20-80 % rise-time (One-way ANOVA, $F = 7.37$, $p < 0.001$, Tukey post-hoc test, $p < 0.05$ for pair 5 vs. 1; $p < 0.001$ for pair 4 vs. 1) and half-width (One-way ANOVA, $F = 0.47$, $p = 0.707$) of IPSC 1 for 5 DBC synapses onto different types of postsynaptic neuron. Whiskers represent SD, plots are colour coded according to immunoreactivity of the presynaptic DBC for calbindin (CB) and the postsynaptic neuron class (PYR: pyramidal cell; IN: interneuron).

3.2.3 Local synaptic targets of pyramidal cells

The distribution of the axon of individual DBCs is similar to that of individual pyramidal cells in the supragranular layers in that they have a broad arbour around the cell body and a narrow long descending set of boutons. The descending main axons from multiple functionally related pyramidal cells form radial bundles, called radial fasciculi, which have been shown to overlap with calbindin- and calretinin immunoreactive axonal bundles of putative DBCs in the human neocortex (del Río & DeFelipe, 1997c; Peters & Sethares, 1997). Whether the horsetail axon of DBCs and the descending axon of pyramidal cells innervate similar or different postsynaptic structures in humans is not known. In order to clarify this, I examined the synaptic targets of three biocytin labelled pyramidal cells (fig. 3.9 and 3.10) using electron-microscopy, and compared their synaptic target frequency distributions to that of DBCs.

The soma of all three pyramidal cells were situated in layers II-III and their dendrites were densely covered with spines. All three cells had an apical dendrite that emitted side branches and ended in a tuft in layer I, but had different proportions of their dendritic tree in that layer. The main axon originated at the basal side of the soma, and descended relatively straight towards the white matter (fig. 3.9 arrows). During its course it emitted several collateral branches that formed a dense plexus with boutons *en passant* and *en termineux* in the neuropil around the cell. A small proportion (not quantified) of the axon of PYR 1 and 2 entered layer I, whereas the axon of PYR 3 did not (fig. 3.9). Some collaterals travelled laterally away from the soma up to a distance of 600 µm (fig. 3.9, PYR 3).

An area including the main descending axon of the cells and several collateral branches were selected for electron-microscopic examination of the boutons as shown in figure 3.9. The labelled axon was traced through consecutive electron-microscopic sections and boutons and the synaptic junctions were identified based on criteria described earlier (fig. 3.10; see chapter 3.2.1). I examined a total of 144 boutons. For 12 boutons either the synaptic specialization or

the target structure could not be identified due to degeneration processes. One bouton formed 2 synaptic specialisations, both with spines, thus I identified a total of 133 synapses (33, 52 and 48 for PYR 1, 2 and 3 respectively). All synapses showed characteristic features of Gray's type I synapses (Gray, 1959), specifically, an asymmetrical appearance of the extensive post-synaptic density and round synaptic vesicles (fig. 3.10 A, B, D). The targets of identified synapses were either dendritic spines (fig. 3.10 C, D) or shafts (fig. 3.10 A, B), recognised based on criteria described above (chapter 3.2.1. Similarly to DBCs no somata or axons were among the targets. Targets were followed through consecutive sections in an attempt to identify the dendrite as originating from pyramidal cells or interneurons, based on criteria described above (chapter 3.2.1). Although most spines (74 %) could not be traced to their parent dendritic shaft, they are likely to originate from pyramidal cells, as these provide the vast majority of spines in the neuropil of the neocortex. The majority of the synaptic targets of PYR 1 and 3 were dendritic spines (64 and 69 % respectively), the remainder being on dendritic shafts, whereas only 46 % of the synapses of PYR 2 were onto dendritic spines. The proportion of synaptic targets was not significantly different between the three cells ($X^2_{(3, N = 133)} = 5.70542$, $p = 0.05769$; fig. 3.10 E). The average proportion of spine targets among pyramidal cells was 60 ± 12 %, whereas among CB+ DBCs it was 48 ± 15 %, however, target frequency was not different between pyramidal cells and CB+ DBCs ($X^2_{(2, N = 209)} = 2.4812$, $p = 0.11521$).

Furthermore, among the 12 dendritic shaft targets of PYR 1, 9 were identified as belonging to interneurons, and one as belonging to a pyramidal cell; in two cases the cell type origin of the shaft could not be determined. In the case of PYR 2, which had a higher proportion of shaft targets compared to the other two cells, of the 28 target dendritic shafts, 12 were identified as belonging to interneurons, and 4 as belonging to pyramidal cells. One spine innervated by PYR 2 was traced to a shaft, which had no other spines and was densely covered by synapses on its shaft. This spine target was grouped as belonging to an interneuron.

Interestingly, 6 target dendrites had multiple spines, but were also densely innervated on their shafts, thus showing both pyramidal cell and interneuron dendrite characteristics. For PYR 3, 4 target shafts were identified as belonging to interneurons and 2 as belonging to pyramidal cells, whereas 9 remained unidentified. Two target dendrites of PYR 2 were reconstructed as shown in fig. 3.10 F. One of the dendrites (left) lacked spines and received additional type I synapses on its shaft, identifying it as originating from an interneuron. The other target (right) emitted four spines, each of which received a type I synapse, including the one from the labelled pyramidal cell, and no additional synapses were located on its shaft, therefore it was identified as originating from a pyramidal cell.

Taking all the above observations into account, the average proportion of pyramidal cell synapses targeting pyramidal cell dendrites was 76 ± 12 % (n = 31, 40 and 39 for PYR 1, 2 and 3 respectively), the remainder targeted interneurons. In comparison, pyramidal cell dendrites were on average 77 ± 18 % of the synaptic targets of calbindin immunopositive DBCs, the remainder being interneuron dendrites. These results suggest that beyond the highly overlapping spatial distribution of their axon and synaptic boutons, the postsynaptic targets of DBCs and pyramidal cells are also similar, a high proportion of which are dendritic spines of other pyramidal cells. This raises the question whether pyramidal cell axons and DBC axons co-descending in the same radial bundle innervate the same or different population of dendritic spines. Only one of the 78 total spine targets of pyramidal cells examined here received an additional type II synapse. The observation that in the rat prefrontal cortex so-called DBC axons innervate spines targeted by thalamocortical afferents (Kubota et al., 2007) suggests that human DBCs may also be selective in their target spine selection.

Figure 3.10. Spatial distribution of the dendrites and axons of three pyramidal cells

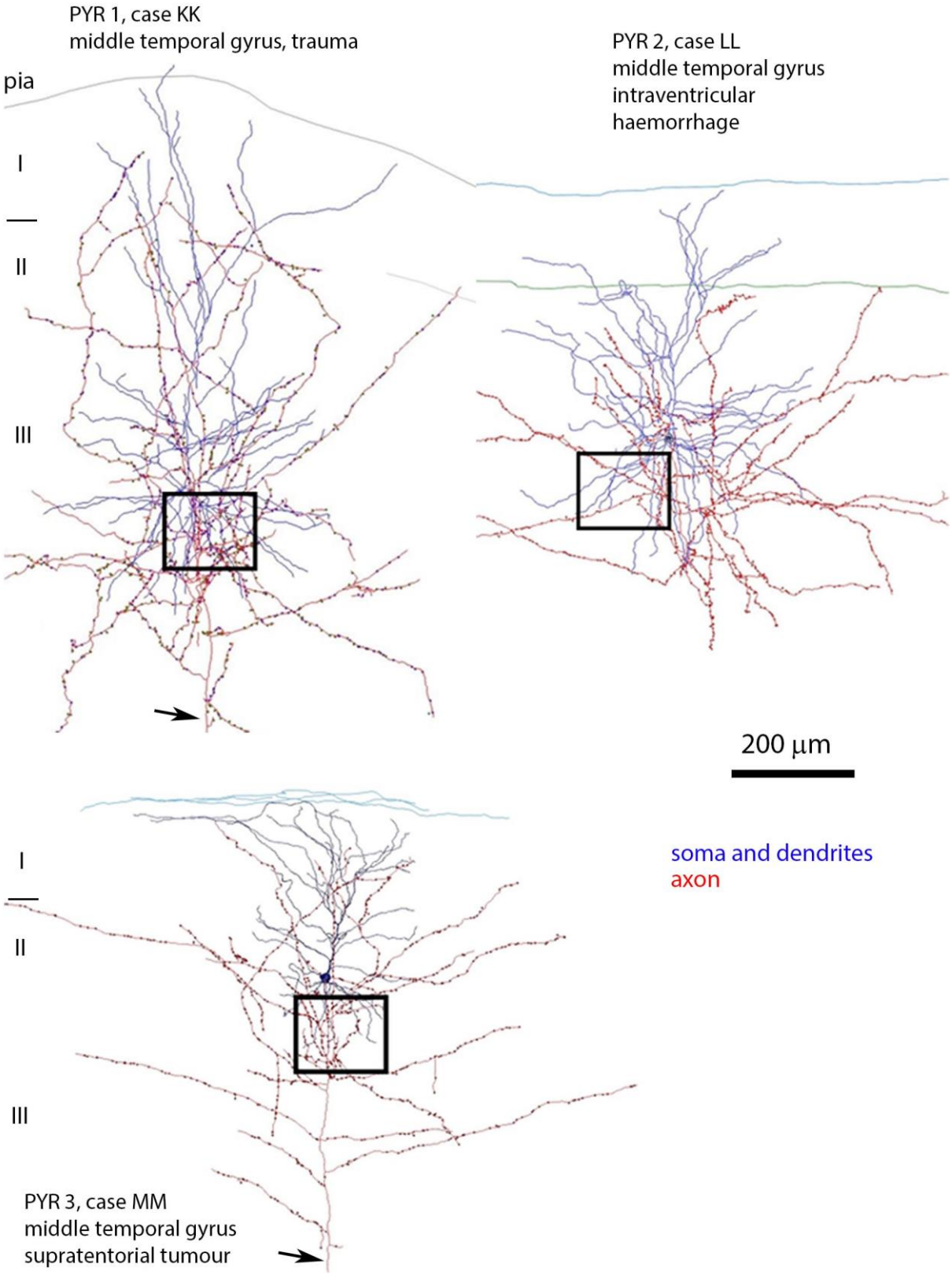
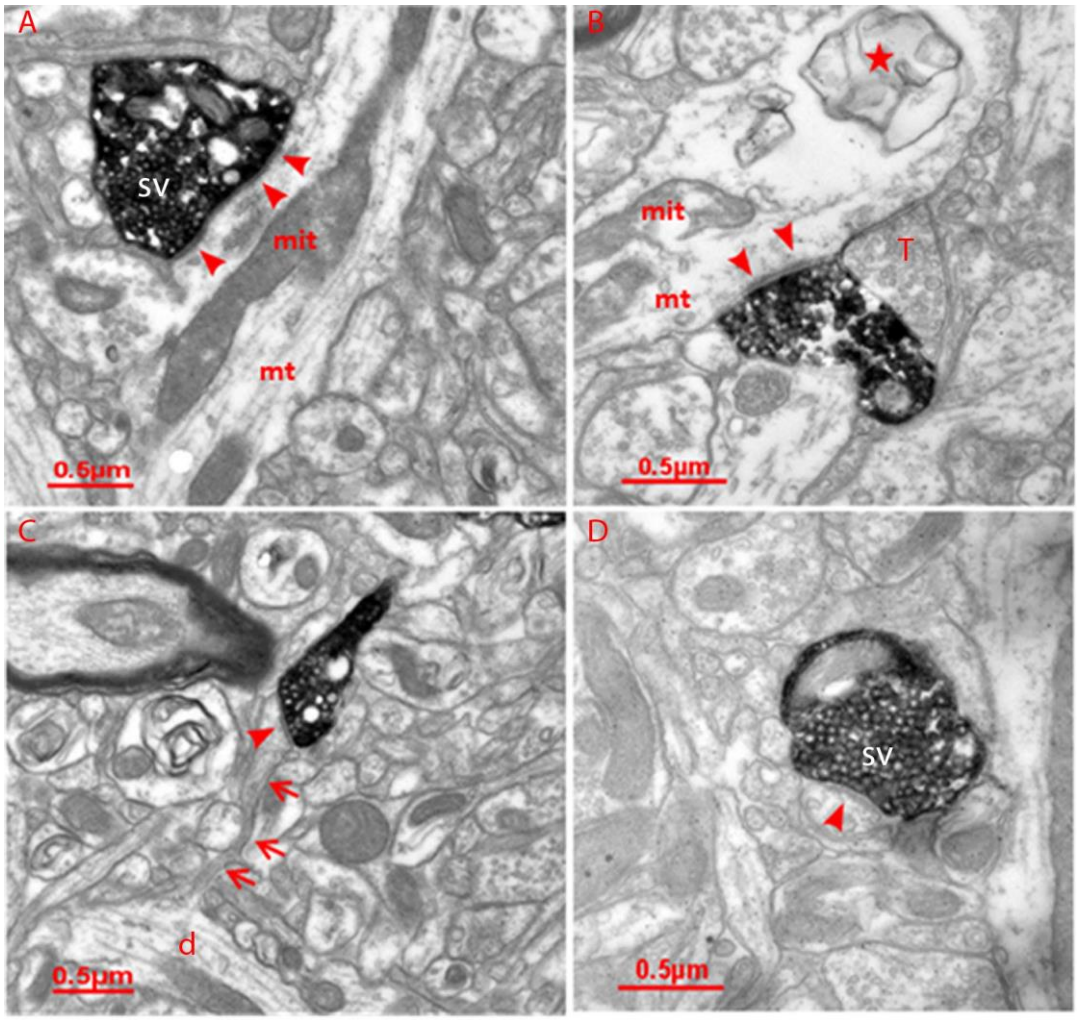
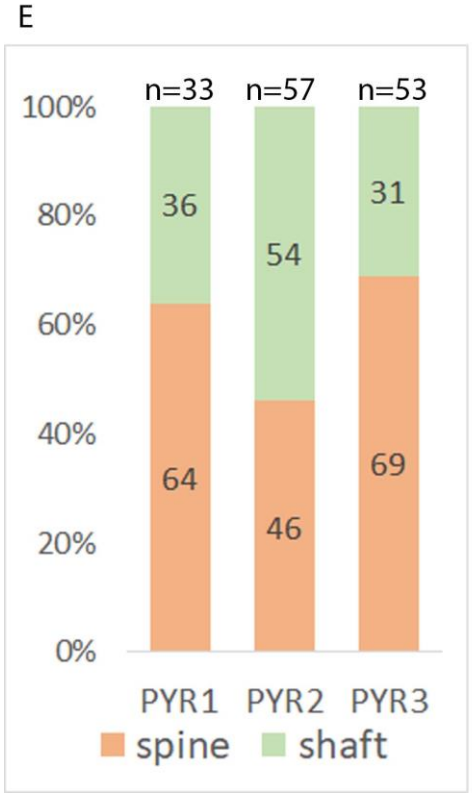


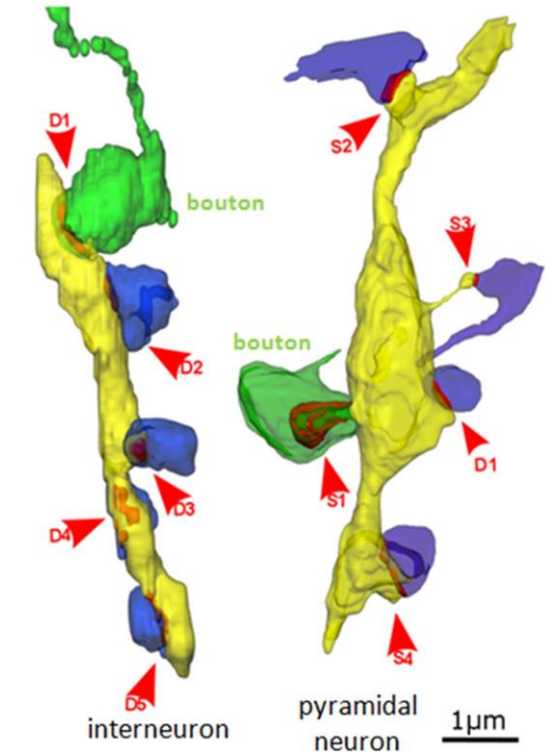
Figure 3.10. Spatial distribution of the dendrites and axons of three pyramidal cells. 3D Neurolucida reconstructions of pyramidal cells, recorded and labelled by Dr Márton Rózsa in the laboratory of prof Gábor Tamás at the University of Szeged, Hungary. Each cell was reconstructed from three ~70 μm thick sections. Cortical layers are indicated by roman numbers. Grey line for PYR 1 and blue lines for PYRs 2 and 3 indicate the pial surface, green line for PYR 3 indicates the boundary between layers I and II. Axons are shown in red and boutons are represented by varicosities. Dendrites are shown in blue. The cell bodies of PYRs 1 and 2 are located in layer III, whereas that of PYR 3 is in layer II. All three cells have numerous dendrites in layer I. The axon of PYRs 1 and 3, but not PYR 2 enters layer I. The main axon (arrow) of PYRs 1 and 3 descends radially towards the white matter; the main axon of PYR 2 also descended, but was cut near the most ventral dendritic tips. All three cells provide dense innervation to the neuropil surrounding their cell bodies, while soma branches travel laterally to several hundred microns. Black boxes show the areas re-embedded for electron-microscopic examination of the synaptic targets. The figure was modified from my graduation thesis at the University of Medicine and Pharmacy of Targu Mures, titled "Local synaptic targets of individual pyramidal neurons in layers II-III of the human neocortex".

Figure 3.11. Local synaptic targets of pyramidal cells. A-D. Electron micrographs of the axonal boutons of PYR 3, showing the electron-opaque osmium-labelled DAB-precipitate inside the terminals (black material), filled with round synaptic vesicles (sv). The boutons form type I synapses, exhibiting thick postsynaptic specialisations (indicated by arrowheads), with dendritic shafts (A, B) and dendritic spines (C, D). Arrows in C indicate the spine neck connecting the innervated spine head to its parent shaft (d). In b, the target dendrites receives an additional type II synapse from an unlabelled terminal (T). Star in B indicates a myelin figure, representing degrading lipid membranes. mit: mitochondrion, mt: microtubules. **E.** Proportion (in %) of dendritic spines and shafts as the synaptic targets of PYRs 1, 2 and 3. The number of synapses examined for each cell is indicated at the top of the bars. **F.** Serial section 3D reconstructions of two dendrites (yellow) innervated by synaptic terminals of PYR 3. The dendrite on the left lacks spines and the synaptic junction formed by the labelled bouton (green) is with the dendritic shaft (D1). Four additional synaptic junctions are formed on its shaft by unlabelled boutons (blue, D2-5), therefore it was identified as belonging to an interneuron. The dendrite on the right has 4 spines (S1-4), each innervated by synapses (purple), including the labelled bouton (S1, green), whereas only one additional synapse is formed with its shaft (D1), therefore it was identified as belonging to a pyramidal neuron. The synaptic specialisations are indicated in red. The figure was modified from my graduation thesis at the University of Medicine and Pharmacy of Targu Mures, titled "Local synaptic targets of individual pyramidal neurons in layers II-III of the human neocortex".

Figure 3.11. Local synaptic targets of pyramidal cells







3.2.4 Targets of GABAergic and non-GABAergic synapses in the neuropil of layer III

I have shown that a large proportion (48 %) of the synaptic targets of calbindin immunopositive DBCs in the human neocortex are dendritic spines. In contrast, only 22 % of the synaptic targets of PMCs are dendritic spines. I next tested if synapses of calbindin immunopositive DBCs represent a unique population of GABAergic synapses in the neuropil, by comparing their synaptic target frequency distribution with the overall distribution of GABAergic synapses on dendritic spines and shafts in the neuropil of layers II and III.

I used post-embedding immuno-gold reactions with antibodies to GABA to label GABAergic neuronal elements in electron-microscopic sections in order to determine the distribution of GABAergic synapses on spines and shafts. In this method, the secondary antibody is absorbed on the surface of colloidal gold particles and is used to visualize the primary antibody that recognizes GABA-glutaraldehyde complex, hence the tissue is fixed with fixative containing 2.5 % glutaraldehyde (see methods). Boutons were identified as GABAergic based on the enrichment of gold particles over their surface, particularly over mitochondria (fig. 3.11 A-D). Enrichment of gold particles was also observed over mitochondria in GABAergic postsynaptic dendrites (fig. 3.11 C, D), but this signal was usually weaker than in boutons. Neuronal elements immunopositive for GABA were consistently labelled in multiple consecutive sections (fig. 3.11 A-D). Boutons making type I synapses, dendritic spines, spiny dendrites and most dendritic shafts usually lacked gold particles (fig. 3.11 B). Boutons immunopositive for GABA contained flattened and ellipsoid vesicles and established typical type II (symmetric) synapses with thin post-synaptic densities (fig. 3.11 A-D), targeting dendritic spines (fig. 3.11 A, B) and shafts (fig. 3.11 C, D). Most boutons not labelled for GABA contained round vesicles and established typical type I (asymmetric) synapses with thick post-synaptic densities (fig. 3.11 B) (Gray, 1959).

For an unbiased estimation of the proportion of spine and dendritic shaft targeting synapses in the neuropil I used a stereological counting method based on direct counting of synapses in a defined volume through serial sections (DeFelipe et al., 1999; Sterio, 1984; West, 1999). I counted synapses in samples from three patients. Two samples were taken from the frontal cortex and one from the temporal cortex (cases HH, II and JJ, table 2.1). A total of 199 synapses were counted in a total volume of 434.2 μm^3 (144.7 ± 42.4 μm^3/sample, mean ± SE, as below), corrected for a 21 % compression of the serial ultrathin sections measured in the direction of the cutting. The mean numerical density of all synapses across all samples was 4.5 ± 0.3 * $10^8/mm^3$ (n = 3 samples), similar to what was recently reported for the human entorhinal cortex (Domínguez-Álvaro et al., 2021). The mean density of synapses appeared to be lower in the temporal (3.7 * $10^8/mm^3$) than in the frontal neocortex (4.9 and 5 * $10^8/mm^3$ for the two samples respectively). Similarly to the neocortex of other species, the majority of synapses were non-GABAergic (85 ± 2.5 %, mean density: 3.8 ± 0.2 * $10^8/mm^3$), and 15 ± 2.5 % (mean density: 0.7 ± 0.2 * $10^8/mm^3$) were GABAergic (fig. 3.11 E). Domínguez-Álvaro et al. (2021) reported higher proportion of asymmetric (non-GABAergic) synapses (∼ 92%,) in the entorhinal cortex. Interestingly, in our temporal neocortex sample, the proportions were more similar to those reported by Domínguez-Álvaro et al. (2021)(90 % non-GABAergic vs. 10 % GABAergic), whereas in the frontal cortices the proportion of GABAergic synapses was higher (20.7 % and 14.2 % in the two samples respectively). Dendritic spines were the targets of 68.3 ± 1.6 % (mean density: 3.1 ± 0.2 * $10^8/mm^3$) of all synapses, whereas dendritic shafts were the targets of the remainder 31.7 ± 1.6 % (mean density: 1.5 ± 0.2 * $10^8/mm^3$) (fig. 3.11 F). However, the target frequency distribution of GABAergic and non-GABAergic synapses were different. Only 16.1 ± 2 % of GABAergic synapses targeted spines, the majority (83.9 ± 2 %) targeted dendritic shafts (fig. 3.11 H). Conversely, the majority of non-GABAergic synapses targeted dendritic spines (77.6 ± 0.4 %) and only 22.4 ± 0.4 % targeted dendritic shafts (fig.

3.11 G). On average 3.5 ± 0.7 % of spines received double innervation from a GABAergic and a non-GABAergic bouton.

These results show that the frequency distribution of synaptic targets of DBCs is significantly different from the target frequency distribution of the total population of GABAergic synapses ($X^2_{(1, 104)}$ = 9.46165, p = 0.0021). This difference strongly suggests that DBCs provide a unique population of GABAergic synapses specifically targeting dendritic spines more frequently than do other GABAergic interneurons, and that a significant proportion of spine-innervating GABAergic synapses are provided by DBCs. As only a small fraction of dendritic spines receive GABAergic input, and they all receive glutamatergic innervation as well. Indeed in the rat neocortex, Kubota et al. (2007) showed that dendritic spines innervated by thalamic afferents (VGlut-2 immunopositive) are more frequently targeted by GABAergic synapses than those innervated by cortical pyramidal cells (VGlut-1 immunopositive). Whether subtypes of DBCs specialise to target specific subpopulations of dendritic spines receiving specific input, remains to be investigated.

Figure 3.12. Synaptic targets of GABAergic synapses in the neuropil of layer III

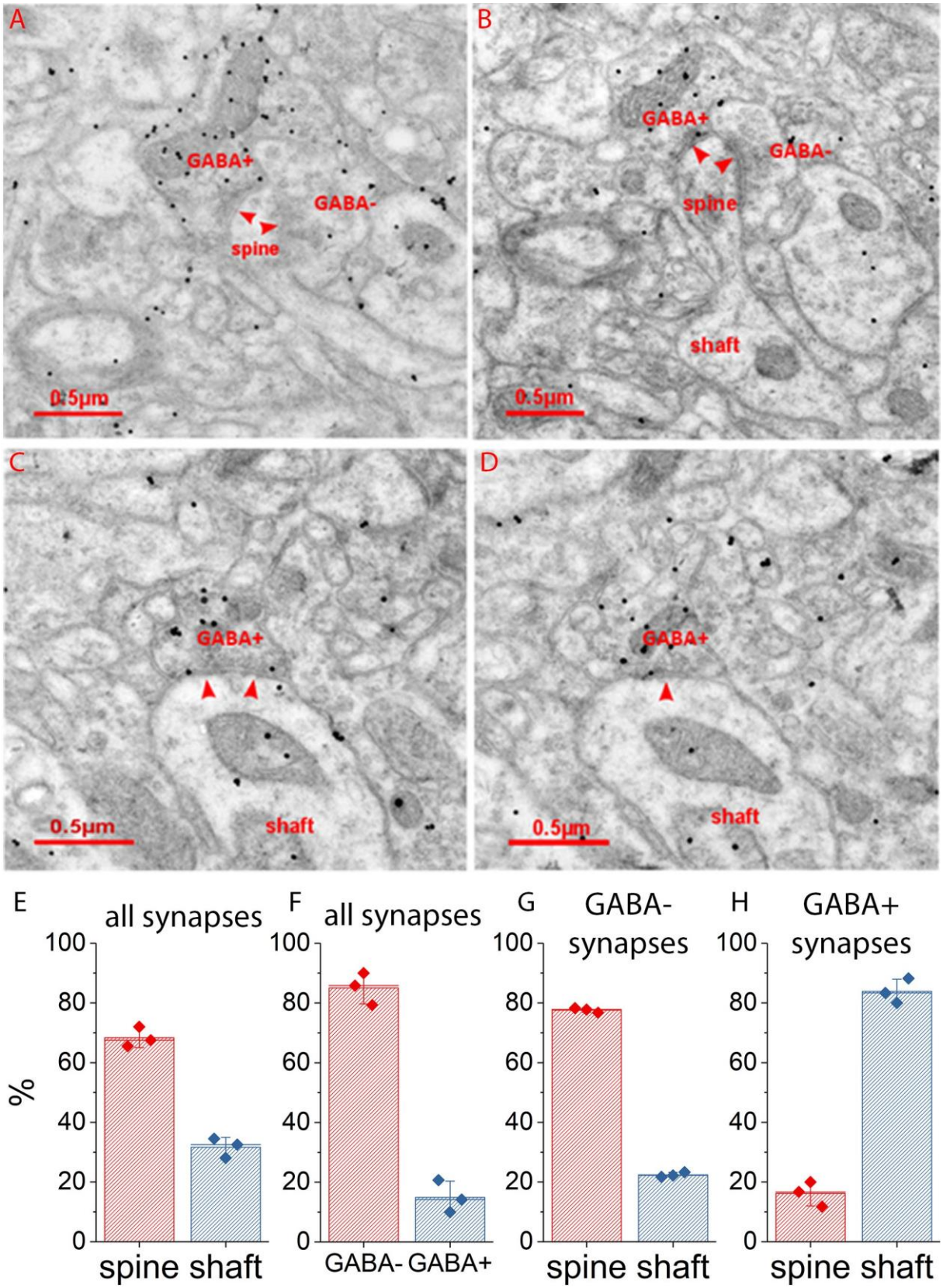


Figure 3.12. Synaptic targets of GABAergic synapses in the neuropil of layer III. A-D. Electron-micrographs of post-embedding immuno-gold reactions for GABA**. A-B.** Two sections of a dendritic spine receiving innervation from a GABAergic (GABA+) bouton, as indicated by the enrichment of silver-enhanced gold particles (electron-dense dots), and another bouton, which is immunonegative for GABA (GABA-). Note that in B, the spine can be traced to its parent shaft. **C-D.** Two sections of a dendritic shaft innervated by a GABAergic (GABA+) bouton. Note that the enrichment of silver-enhanced gold particles over a profile and not others, is consistent across different sections. Arrows indicate the synaptic specialisation. **E-F.** Proportion of dendritic spines and shafts as synaptic targets of all synapses (E), and proportion of GABA+ to GABA- synapses (F) in the neuropil. Proportion of GABA- (G) and GABA+ (H) synapses targeting dendritic spines vs. shafts in the neuropil. The figure was modified from my graduation thesis at the University of Medicine and Pharmacy of Targu Mures, titled "Local synaptic targets of individual pyramidal neurons in layers II-III of the human neocortex".

3.2.5 Evoked and spontaneous (IPSCs) are mediated by $GABA_A$ receptors

I recorded spontaneous (chapter 3.3) and evoked unitary postsynaptic currents (chapter 3.2.2) in different types of neuron, as fast transient outward and inward currents. I recorded these currents at a somatic nominal membrane potential clamped between -45 and -50 mV, and a -94 mV equilibrium potential for chloride (see chapter 2.3.1), which suggested that the outward currents were IPSCs mediated by $GABA_A$ receptors. In order to test the GABAergic nature of these currents, I recorded spontaneous (n = 4) IPSCs in 3 interneurons and 1 pyramidal cell, and monosynaptic unitary eIPSCs in one additional interneuron. Bath application of the $GABA_A$ receptor antagonist gabazine (16 μM) completely abolished the phasic outward currents (fig. 3.12 A) and eIPSCs (fig. 3.12 B), demonstrating that the outward currents recorded in these experimental conditions were mediated by $GABA_A$ receptors, and I consider them to represent IPSCs. Although I did not test if the spontaneous outward currents recorded in DBCs or the DBC-evoked eIPSCs recorded in other neurons were mediated by $GABBA_A$ receptors, these were recorded under the same experimental conditions and exhibited the same kinetics, thus I consider them to be GABAergic IPSCs.

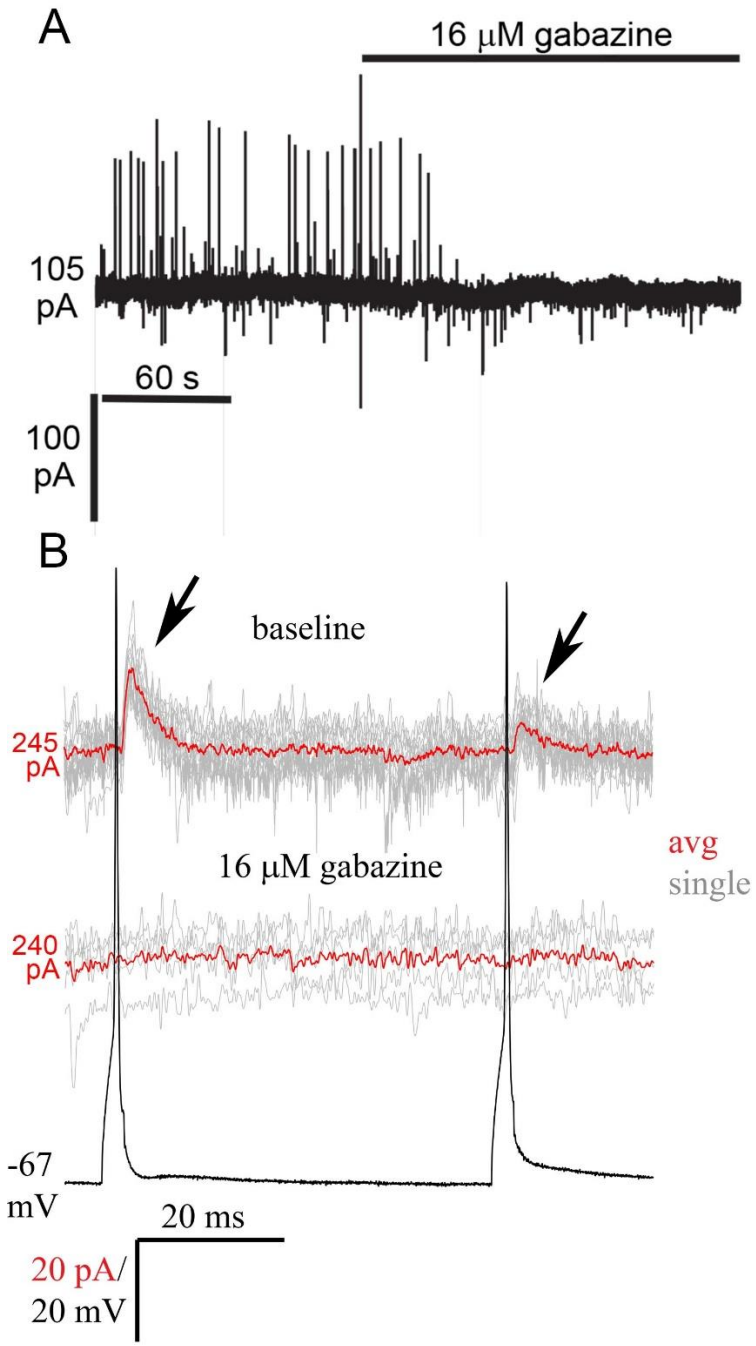


Figure 3.13. Spontaneous and evoked outward currents are IPSCs are mediated by GABAA receptors. A. Continuous voltage-clamp recording of an unidentified interneuron at -50 mV membrane potential and E_{Cl} = -94 mV. Outward currents, represented by upward spikes, correspond to sIPSCs, whereas inward currents (downward spikes) represent sEPSCs. Bath application of 16 μM gabazine, a $GABA_A$ receptor antagonist, blocks sIPSCs, but not sEPSCs. **B.** Two action potentials evoked in an unidentified interneuron (black trace) recorded in current-clamp mode, elicited monosynaptic eIPSCs (arrows, top trace: red – avg. of 15 sweeps) in another unidentified interneuron, recorded in voltage-clamp mode, at -50 mV. Bath application of 16 μM gabazine completely abolished eIPSCs in the postsynaptic neuron (middle trace: red – avg. of 5 sweeps). Both recordings are from case H, superior frontal gyrus, subependyoma.

3.3 Differential regulation of GABAergic inputs to DBCs and PMCs by group III mGluRs in the human neocortex

I have shown that in the human neocortex two distinct types of GABAergic interneuron, DBCs and PMCs, have distinct axonal and dendritic distributions and innervate different subcellular compartments of their target cells. Furthermore, differences in the dendritic distribution and passive and active membrane properties between DBCs and PMCs suggest that they receive and process synaptic inputs differently. The synaptic inputs of DBCs are not known.

Group III metabotropic glutamate receptors (mGluRs) are pre-synaptic regulators of both GABAergic and glutamatergic synaptic transmission in many distinct forebrain neuronal circuits in rodents. Synaptic pathway- and cell type-specific expression of group III mGluRs in the rodent cortex (Dalezios et al., 2002; Ferraguti et al., 2005; Shigemoto et al., 1996; Shigemoto & Kinoshita, 1997; Somogyi et al., 2003) is thought to result in the differential inhibition of GABAergic synaptic transmission to different types of interneuron and pyramidal cells (Kogo et al., 2004; Semyanov & Kullmann, 2000). However, neither the subcellular localisation nor the functions of group III mGluRs are known in the human neocortex.

We tested if GABAergic synaptic transmission to different types of interneuron in the human neocortex is differentially regulated by group III mGluRs. Specifically, we tested if activation of group III mGluRs by the orthosteric agonist *L-2-amino-4-phosphonobutyric acid* (L-AP4), depresses the frequency and/or amplitude of GABA-A receptor mediated spontaneous inhibitory postsynaptic currents (sIPSCs), as has been shown in rodents (Bonci et al., 1997; Cuomo et al., 2009; Giustizieri et al., 2005; Mitchell & Silver, 2000). It is important to note, that action potentials and fast glutamatergic synaptic transmission were not blocked in these experiments. We recorded sIPSCs in whole-cell voltage clamp, at just below firing threshold

potential (-50 - -45 mV), using a low Cl^- (4 mM) concentration in our internal pipette solution. In this setting sIPSCs presented as upward deflections in the holding current with a fast rising phase and an exponential decay (fig. 3.2 C and 3.4 C), and we also recorded AMPA receptor mediated spontaneous excitatory postsynaptic currents (sEPSCs, fig. 3.2 C), but these were not analysed. We recorded sIPSCs in a total of 185 neurons and tested the effects of L-AP4 on 133, of which 65 were analysed, including 49 putative interneurons and 16 putative pyramidal cells. The remainder 68 cells did not pass technical criteria to be included in the study (see chapter 2.3.3). After microscopic examination of the visualised and pharmacologically tested cells, we identified 7 DBCs (fig. 3.13 A left, and see fig. 3.2), 7 PMCs (recorded by Dr Ruggiero Francavilla) (fig. 3.13 B left, and see fig. 3.4), 2 NGCs, 1 RHC (Boldog et al., 2018), and 1 AAC, based on the specific distribution of their axon. The identity of 29 cells could not be determined, and 2 cells were not recovered. Four pyramidal cells were confirmed visually, based on their densely spiny dendrites. We compared the effects of L-AP4 on sIPSCs in DBCs and PMCs as these two groups had enough identified cells to study the effects at the population level (fig. 3.13). To control for spontaneous rundown of synaptic activity *in vitro*, and variability in slice conditions and technical parameters, the effects were compared to vehicle-treated control cells, including 4 interneurons (1 DBC) and 3 pyramidal cells.

Median sIPSC frequency was 2.0 Hz (IQR: 3.6 Hz, n = 18) in interneurons and 1.6 Hz (IQR: 1.3 Hz, n = 14) in pyramidal cells, whereas median amplitude was 9.0 pA (IQR: 5.5 pA) in interneurons and 12.3 pA (IQR: 5.7 pA) in pyramidal cells. In three out of 7double bouquet cells, bath application of L-AP4 (50 μM, n = 3; or 300 μM, n = 4) unexpectedly shifted the cumulative distribution of sIPSC inter-event intervals to the left (e.g. fig. 3.13 C left, two sample Kolmogorov-Smirnov test, p = 0.00117, n = 854 IPSCs), meaning that the proportion of shorter inter-event intervals increased compared to longer ones, corresponding to an increase in the frequency of sIPSCs. In the other 4 DBCs, the inter-event interval did not change significantly.

However, the leftward shift in the distribution of sIPSC intervals was still present when averaged across all DBCs (fig. 3.13 G, two sample Kolmogorov-Smirnov test, $p = 4.8 * 10^{-5}$, n = 100 bins). At the population level, the frequency of sIPSCs increased from median 3.25 Hz (IQR: 7.08 Hz) at baseline to median 4.4 Hz (IQR: 7.6 Hz; Wilcoxon signed rank test, p = 0.02249, n = 7; fig. 3.13 E). Although in individual DBCs L-AP4 shifted the cumulative distribution of sIPSC amplitudes to the left in 4 cells (smaller amplitudes, e.g. fig. 3.13 C right, two sample Kolmogorov-Smirnov test, p = 0.0466, n = 854 IPSCs); to the right (larger amplitudes) in one, and did not change in the remaining two, and the average cumulative distribution of sIPSC amplitudes also shifted towards smaller amplitudes (fig. 3.13 H, two sample Kolmogorov-Smirnov test, $p = 3.2 * 10^{-4}$, n = 100 bins), the change in amplitude was not significant at the population level (fig. 3.13 F, baseline median: 6.7, IQR: 1.7 pA vs. L-AP4 median: 6.6, IQR: 1.5 pA, Wilcoxon signed rank test, p = 0.21875). Washout of L-AP4 from the bath did not lead to the recovery of the baseline frequencies or amplitudes. These results are in contrast with previous studies in rodents, where L-AP4 suppressed spontaneous and evoked IPSCs (Cuomo et al., 2009; Drew & Vaughan, 2004; Gerber et al., 2000; Lu, 2007; Matsui & Kita, 2003).

In contrast to DBCs, in PMCs bath application of 300 μM L-AP4 shifted the cumulative distribution of sIPSC inter-event intervals to the right, corresponding to lower sIPSC frequency (e.g. fig. 3.13 D left, two sample Kolmogorv-Smirnov test, p = 0.0479, n = 100 IPSCs) in 2 out of 7 cells, whereas in 5 cells the distribution did not change. However, averaged across all PMCs the distribution of sIPSC intervals shifted to the right, upon application of L-AP4 (fig. 3.13 K, two sample Kolmogorov-Smirnov test, $p = 5.7 * 10^{-10}$, n = 100 bins). At the population level, although the median frequency changed from 0.46 Hz (IQR: 4 Hz) in baseline to 0.48 Hz (IQR: 3.9 Hz) after application of L-AP4, the pairwise change was a significant decrease (fig. 3.13 I, Wilcoxon signed rank test, p = 0.0313), as expected from rodent studies. The average

cumulative distribution of sIPSC amplitudes did not change upon application of L-AP4 (fig. 3.13 L, two sample Kolmogorov-Smirnov test, p = p = 0.0994,n = 100 bins), nor did the median amplitude at the population level (fig. 3.13 J, baseline median: 12.6, IQR: 10.4 pA vs. L-AP4 median: 12.2, IQR: 17.4 pA, Wilcoxon signed rank test, p = 0.375, n = 7).

I further assessed whether the changes measured upon L-AP4 application are different from spontaneous changes in frequency and amplitude due to changing slice conditions, technical parameters, and synaptic rundown. I compared the baseline normalised changes measured in DBCs and PMCs to the changes measured in vehicle treated control cells (n = 7; fig. 3.13 M, N). The median change in sIPSC frequency was to 103 % (IQR: 26 %) of baseline in vehicle treated controls, and it was significantly higher in DBCs (median: 130, IQR: 30 %, Conover post hoc test, adjusted by the Holm FWER method, p = 0.011 for controls vs DBCs), whereas it was significantly lower in PMCs (median: 92 %, IQR: 46 %, Conover post hoc test, adjusted by the Holm FWER method, p = 0.043)(fig. 3.13 M). The changes were also different between DBCs and PMCs (Conover post hoc test, adjusted by the Holm FWER method, p = 0.0001). Conversely, normalised change in sIPSC amplitude in DBCs and PMCs did not differ from the change in vehicle treated controls (fig. 3.13 N, Kruskal-Wallis test, p = 0.382495). These comparisons show that the effects of L-AP4 are more robust on the frequency than on the amplitude of sIPSCs, which indicates that L-AP4 primarily acts through modulation of neurotransmitter release at the level of axon terminals, in accordance with previous studies in rodents (Cuomo et al., 2009; Drew & Vaughan, 2004; Gerber et al., 2000; Kogo et al., 2004; Matsui & Kita, 2003; Semyanov & Kullmann, 2000). However, because in our experiments action potentials and fast glutamatergic synaptic transmission were not blocked, such conclusions could not be drawn and the unexpected increase of sIPSC frequency in DBCs is likely the result of a complex effect of group III mGluRs acting at both GABAergic and glutamatergic synapses and probably multiple levels of synaptic connections. Although these

results suggest that activation of group III mGluRs differentially modulates spontaneous local inhibitory synaptic inputs onto two distinct types of GABAergic interneuron in the human neocortex, the small number of cells tested in this thesis require future confirmation of the effects observed here.

Figure 3.14. Effects of group III mGluR activation on sIPSCs in DBCs and PMCs.

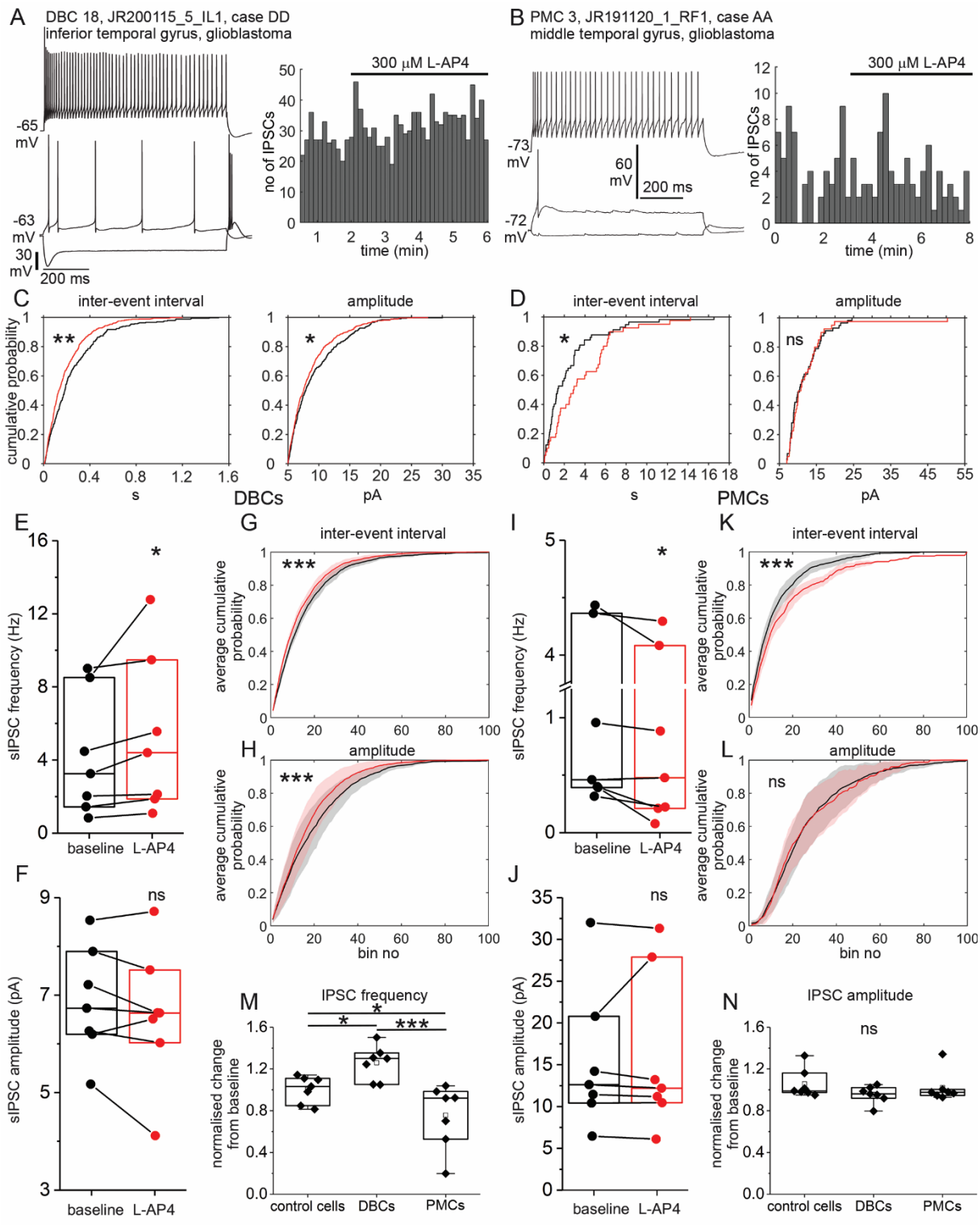


Figure 3.14. Effects of group III mGluR activation on sIPSCs in DBCs and PMCs. A. Effect of group III mGluR activation on a DBC. Left: Voltage responses of DBC 18 to current injections of RB, RB +100 pA, and holding current -100 pA; right: event time histogram of sIPSCs recorded from DBC 18 during baseline and bath application of 300 μM L-AP4 (n = 1326 events, bin width: 8 s). **B.** Effect of group III mGluR activation on PMCs. Left: Voltage responses of PMC 3 to current injections of RB, RB +200 pA and holding current -100 pA; right: event time histogram of sIPSCs recorded from PMC 3 during baseline and bath application of 300 μM L-AP4 (n = 140 events, bin width: 10 s). **C.** Cumulative probability distribution of sIPSC inter-event intervals (left) and amplitudes (right) in baseline (black, n = 326) vs. L-AP4 (red, n = 528) conditions in DBC 18 (Kolmogorov-Smirnov test, p = 0.001for intervals and p = 0.047 for amplitudes). **D.** same as C for PMC 3 (baseline, black, n = 59 vs. L-AP4, red, n = 41; Kolmogorov-Smirnov test, p = 0.048 for intervals and p = 0.876 for amplitudes). **E.** Mean sIPSC frequency of DBCs in baseline vs. L-AP4 conditions (paired sample Wilcoxon signed rank test, p = 0.016, boxes represent median and IQR). **F.** Median sIPSC amplitude of all DBCs in baseline vs. L-AP4 conditions (paired sample Wilcoxon signed rank test, p = 0.219). **G.** Mean cumulative probability distribution (line) and 95 % CI (shaded areas) of sIPSC inter-event intervals across all DBCs in baseline (black) vs. L-AP4 (red) conditions (100 bins/cell, Kolmogorov-Smironov test, $p < 0.001$). **H.** Average cumulative probability distribution of sIPSC amplitudes across all DBCs (100 bins/cell, Kolmogorov-Smironov test, $p < 0.001$). **I-L.** Same as E-H for PMCs (I,J: paired sample Wilcoxon signed rank test, p = 0.031 for intervals, p = 0.375 for amplitudes; K,L: Kolmogorov-Smirnov test, $p < 0.001$ for intervals and p = 0.099 for amplitudes). **M-N.** Normalised change from baseline to L-AP4 in sIPSC frequency (M) and amplitude (N) in control cells (n = 7), DBCs (n = 7), and PMCs (n = 7) (Kruskal-Wallis ANOVA test, for frequency, p = 0.002, Conover post hoc test, adjusted by the Holm FWER method, p = 0.011 for controls vs DBCs, p = 0.043 for controls vs PMCs, $p < 0.001$ for DBCs vs PMCs; for amplitude, p = 0.382, boxes represent median and IQR, square symbol, mean, whiskers, SD).

3.4 Effects of patient- and sample-related factors on the change in sIPSC frequency in responses to group III mGluR activation

In this thesis I identified a total of 76 neurons as belonging to one of 5 GABAergic interneuron types (see chapter 3.1.2). Of these, the intrinsic membrane properties of 40 (29 DBCs and 11 PMCs) were analysed and compared (see chapter 3.1.6). These 40 neurons were recorded in 22 samples of different cortical regions, of tumour (n = 20) and epilepsy (n = 2) patients, of different age, sex and medical history (see table 2.1). Samples from tumour patients were taken as far from the MRI-imaged tumour mass as possible and in deep tumours cortical tissue was not affected by infiltration, as assessed by MRI. However, some samples showed some degree of infiltration and/or oedema (table 2.1). Furthermore, chemical signals and activity patterns may not be limited to structures directly infiltrated by the tumour mass. Particularly, seizures associated with brain tumours and epilepsy can spread through the entire neocortex. Different medications received by the patients could also affect the measured parameters.

Of the 20 tumour patients, 10 (50 %) had seizures by the time of surgery, and 14 (70 %) received anti-epileptic medication. Both TLE patients received anti-epileptic medication and had seizures. Of all 22 patients, two (9 %) received psychiatric medication and 16 (73 %) received anti-inflammatory steroid medication. Half of the patients were male. More than half of the neurons (24, 60 %) were recorded in the temporal cortex, 10 (25 %) in the parietal and 6 (15 %) in the frontal cortex. Most cells were recorded in glioblastoma samples (19, 47.5 %), 6 (15 %) in astrocytoma samples, 4 (10 %) in dysembrioblastic neuroepithelial tumour samples, 1 (2.5 %) oligodendroglioma, 1 in meningioma and 5 (12.5 %) in metastatic tumour samples. Only 4 cells (10 %), all DBCs, have been recorded in TLE samples.

I tested if variability in intrinsic membrane parameters of DBCs and PMCs was explained by factors related to the sample, pathology or the medical history of patients by generating multiple linear regression models for each of the intrinsic membrane parameters. The independent variables included in the models were the following: cell type (DBC = 1), age, sex (M = 1), cortical area (temporal = 1), pathology (glioblastoma, TLE, metastasis or anaplastic astrocytoma), seizures at time of surgery, presence of oedema in the sample, hypertension in the medical history, and medication history (treatment with levetiracetam or dexamethasone). From diagnosis, medical history and medication history, only those were included, from which at least 5 data points were collected, except for TLE, which only had 4 data points. Models significantly different from a constant were found for the sag ratio (R^2 (COD): 0.75, F = 5.98, p = $5.56*10^{-5}$), whole-cell capacitance (R^2 (COD): 0.69, F = 4.47, p = $5.71*10^{-4}$), action potential threshold (R^2 (COD): 0.58, F = 2.8, p = 0.012), AHP (R^2 (COD): 0.57, F = 2.62, p = 0.018), spike amplitude-accommodation (R^2 (COD): 0.82, F = 8.89, p = $1.5*10^{-6}$) and rebound spikes (R^2 (COD): 0.53, F = 2.29, p = 0.035). The model for spike amplitude-accommodation explained most of the variability in the parameter, for which the most significant factor, among the 13 independent variables, was the cell identity (i.e. being DBC, t = -6.7, p = $4.09*10^{-7}$). However, two other factors, age (t = -2.39, p = 0.024) and the pathology being metastasis (t = 2.34, p = 0.027) were also significant factors. For whole-cell capacitance (t = -4.64, p = $8.59*10^{-5}$) and AHP (t = 2.92, p = 0.007) the only significant factor was the cell identity, whereas for sag ratio the cell identity (t = 3.44, p = 0.002) and hypertension (t = -2.7, p = 0.012) were significant factors. Similarly, for rebound spikes the cell identity (t = 3.99, p = $4.78*10^{-4}$) and the presence of oedema (t = 2.44, p = 0.022) were significant factors. Indeed, DBCs had larger amplitude voltage sags, smaller whole-cell capacitance, and showed stronger spike amplitude-accommodation than PMCs (see fig. 3.5). Interestingly, for the action potential threshold, the cell identity was not a significant factor. However, several other factors were significant, such

as the cortical region ($t = -2.2$, $p = 0.037$), the pathology being glioblastoma ($t = -2.82$, $p = 0.009$) or anaplastic astrocytoma ($t = -3.09$, $p = 0.005$), the presence of oedema in the sample ($t = 2.2$, $p = 0.037$), seizures ($t = 2.43$, $p = 0.022$) and hypertension ($t = 3.9$, $p = 6.09*10^{-4}$), of which the most significant was hypertension. Importantly, the cell identity was consistently the most significant predictor for the value of the sag ratio, whole-cell capacitance, spike amplitude-accommodation, AHP and rebound spikes, indicating that these parameters were cell type-specific and did not vary with pathology, patient history or cortical region. It is important to note, however, that for some parameters, including the spike amplitude-accommodation, sag ratio and rebound spikes, other factors than the cell identity were also significant. These included the pathology being a metastatic tumour, presence of oedema and hypertension, all of which could directly or indirectly lead to increased pressure. Because not all cortical areas and pathologies were equally sampled, it cannot be excluded that these may have a larger effect on the variability of the intrinsic membrane properties, than observed in our sample.

I tested similarly if the effect of group III mGluR activation, measured as the normalised change in sIPSC frequency, was explained by sample- and patient-related factors. I generated several multiple linear regression models, which included different sets of independent variables, in order to find the ones which explain the variability in the data best. However, due to the low number of pharmacologically tested neurons (n = 14 cells, 7 DBCs, 7 PMCs, see chapter 3.3), and the uneven frequency of the different cortical areas and pathologies, the predictive value of these models is limited. Almost all pharmacological response data came from patients between 50 – 66 years of age with the exception of one outlier (age: 31 years; mean: 57.5 ± 2.4 yrs.). Furthermore, 9 (64 %) cells were recorded in samples from glioblastoma patients, and none in samples from TLE patients. Similarly, 11 cells (79 %) were recorded in the temporal, 2 (14 %) in the frontal and only one (7 %) in the parietal cortex. Of the 7 models generated (table 3.2), models 1 (Adj. R^2: 0.47, $F = 4.79$, $p = 0.026$), 4 (Adj. R^2: 0.75, $F = 6.44$,

p = 0.019), 5 (Adj. R^2: 0.83, F = 8.51, p = 0.027), 6 (Adj. R^2: 0.88, F = 14.74, p = 0.002) and 7 (Adj. R^2: 0.47, F = 3.93, p = 0.04) were significantly different from a constant. All models included the cell identity as a factor. Model 1 included the age and sex in addition to the cell identity, model 4 included the age, sex, cortical region, pathology, the presence of oedema in the sample, and seizures, and model 5 included all parameters, except hypertension as factors. Model 6 included age, sex, the presence of oedema, seizures and treatments with anticonvulsive and steroid medication, but not the cortical region and the pathology, whereas model 7 only included age, sex and hypertension in addition to the cell identity (table 3.2). In models 1 and 7 the cell identity was the only factor significantly different from zero, contributing to the pharmacological response, however these models explained less than half of the variance in the data (table 6.1). In model 5, seizures were a significant factor in addition to the cell identity. Interestingly, in model 4 all factors, except age and pathology were significant. In model 6, in addition to the cell identity and age, seizures and anticonvulsive medication were significant factors with seizures adding to the increase in sIPSC frequency induced by L-AP4 (0.67 ± 0.14, p = 0.003), and anticonvulsive treatment having the opposite effect (-0.6 ± 0.17, p = 0.013; table 6.1). model 6 also explained the most of the variability in the change in sIPSC frequency (Adj. R^2: 0.88). In all the different models, the most consistently significant factor was the cell identity, however seizures were also significant in three models. Although these models support that the effect of group III mGluR activation on sIPSC frequency is cell type-specific, considering the small number of data points, it cannot be excluded that other factors, such as seizures and various medications might also have an effect on the measured responses.

Consistent with these models, the change in sIPSC frequency in response to group III mGluR activation was not different in males and females (fig. 3.14 A, Mann-Whitney U-test, p = 0.0824), nor it was different in the temporal neocortex vs. other cortical regions (fig. 3.14 B, Mann-Whitney U-test, p = 0.585). Furthermore, responses to L-AP4 were similar between

patients with seizures and patients without (fig. 3.14 C, Mann-Whitney U-test, $p = 0.4812$), as well as between samples with and without oedema (fig. 3.14 F, Mann-Whitney U-test, $p = 0.1743$). Finally, the change in sIPSC frequency was not different between patients receiving vs. not receiving anticonvulsive (fig. 3.14 D, Mann-Whitney U-test, $p = 0.12$) or steroid (fig. 3.14 E, Mann-Whitney U-test, $p = 0.52$) medication.

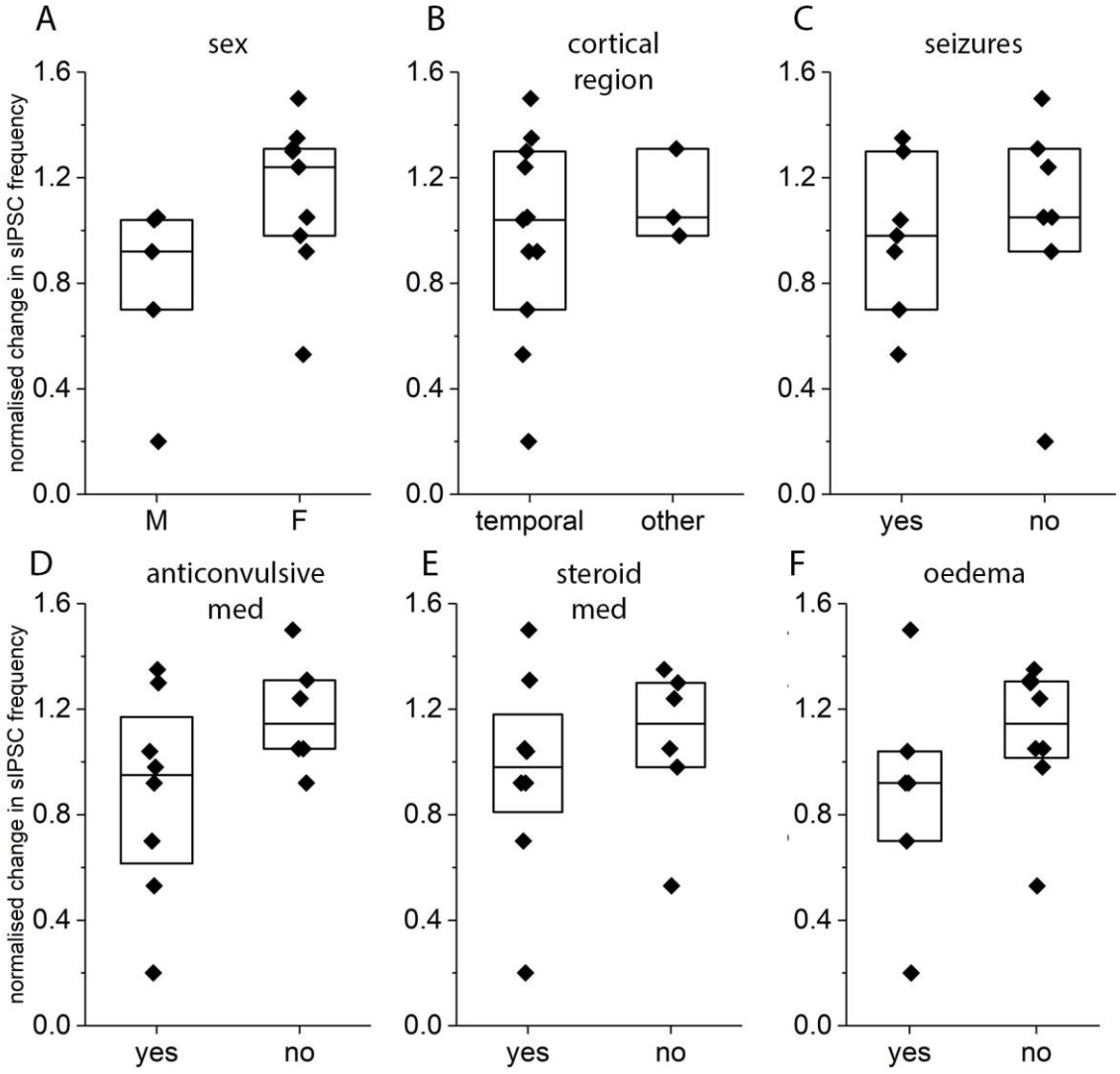


Figure 3.15. Effects of sample- and patient-related parameters on L-AP4 induced changes in sIPSC frequency. The distributions of the baseline-normalised change in sIPSC frequency in response to group III mGluR activation by L-AP4 are shown for each cell. **A.** males vs females (Mann-Whitney U-test, U = 36, p = 0.08); **B.** temporal cortex vs other cortical regions (Mann-Whitney U-test, U = 12.5, p = 0.58); **C.** patients with seizures vs without seizures at the time of surgery (Mann-Whitney U-test, U = 30.5, p = 0.48); **D.** patients who received anticonvulsive medication vs those, who did not (Mann-Whitney U-test, U = 11.5, p = 0.12); **E.** patients who received steroid medication vs. those who did not (Mann-Whitney U-test, U = 18.5, p = 0.52); and **F.** samples showing signs of oedema vs no oedama detectable (Mann-Whitney U-test, U = 13, p = 0.17).

Table 3.1 Information on recorded and labelled DBCs, PMCs, pyramidal cells, and cells used for pharmacological control measurements

cell #	patient	cell code	data collected	
			anatomy	electrophysiology
DBC 1	C	JR180119_3_IL6	reconstruction, IHC	I-V
DBC 2	E	JR180425_6_IL2	IHC	IV; eIPSC (pair1)
DBC 3	E	JR180425_7_IL1	IHC	I-V
DBC 4	K	JR190220_7_IL3	reconstruction; IHC	I-V
DBC 5	K	JR190220_7_IL4	reconstruction; EM; IHC	I-V
DBC 6	K	JR190220_8_IL1	IHC	I-V; eIPSC (pair2)
DBC 7	N	JR190410_1_IL4	IHC	I-V
DBC 8	N	JR190410_2_IL5	IHC	-
DBC 9	N	JR190410_3_IL1	IHC	I-V
DBC 10	O	JR190424_5_IL4	EM; IHC	I-V; sIPSC (L-AP4)
DBC 11	P	JR190426_3_IL3	IHC	I-V
DBC 12	P	JR190426_7_IL3	IHC	I-V; eIPSC (pair3)
DBC 13	Q	JR190515_3_IL3	IHC	I-V
DBC 14	T	JR190628_1_IL2	IHC	I-V
DBC 15	U	JR190731_9_IL2	IHC	I-V
DBC 16	Z	JR191030_1_IL1	IHC	I-V
DBC 17	Z	JR191030_5_IL1	IHC	I-V; sIPSC (L-AP4)
DBC 18	DD	JR200115_5_IL1	IHC	I-V; sIPSC (L-AP4)
DBC 19	EE	JR200207_8_IL1	IHC	I-V
DBC 20	EE	JR200207_10_IL2	IHC	I-V; sIPSC (L-AP4)
DBC 21	GG	JR200311_1_IL1	IHC	-
DBC 22	GG	JR200311_2_IL1	reconstruction; EM; IHC	I-V; sIPSC (L-AP4)
DBC 23	GG	JR200311_4_IL2	reconstruction; EM; IHC	I-V; sIPSC (L-AP4)
DBC 24	GG	JR200311_6_IL1	IHC	I-V
DBC 25	EE	JR200207_11_IL4	EM; IHC	I-V
DBC 26	FF	JR200219_10_IL2	IHC	I-V
DBC 27	G	JR181026_3_IL3	IHC	I-V; eIPSC (pair4)
DBC 28	G	JR181026_3_IL4	IHC	I-V; eIPSC (pair4)
DBC 29	M	JR190403_1_IL2	IHC	I-V; eIPSC (pair5)
DBC 30	O	JR190424_8_IL3	IHC	-
DBC 31	DD	JR200115_6_IL4	IHC	I-V; sIPSC (L-AP4)
DBC 32	EE	JR200207_1_IL7	IHC	I-V
PMC 1	W	JR190927_1_RF1	reconstruction; IHC	I-V; sIPSC (L-AP4)
PMC 2	Y	JR191017_5_RF1	IHC	I-V; sIPSC (L-AP4)
PMC 3	AA	JR191120_1_RF1	EM; IHC	I-V; sIPSC (L-AP4)
PMC 4	AA	JR191120_4_RF4	EM; IHC	I-V
PMC 5	X	JR191002_4_RF1	reconstruction; EM; IHC	I-V; sIPSC (L-AP4)
PMC 6	AA	JR191120_2_RF2	IHC	I-V; sIPSC (L-AP4)
PMC 7	AA	JR191120_6_RF1	IHC	I-V; sIPSC (L-AP4)
PMC 8	J	JR190206_5_IL1	reconstruction; IHC	I-V

cell #	patient	cell code	data collected	
			anatomy	electrophysiology
PMC 9	CC	JR200110_3_RF2	IHC	I-V
PMC 10	DD	JR200115_3_RF2	IHC	I-V
PMC 11	DD	JR200115_4_RF1	IHC	I-V
PMC 12	O	JR190424_1_IL3	IHC	sIPSC (L-AP4)
PMC 13	V	JR190904_3_RF1	IHC	-
PMC 14	A	JR171103_12_IL3	reconstruction	-
CTR 1	Q	JR190904_4_IL1	-	sIPSC (control)
CTR 2	S	JR190918_3_IL1	-	sIPSC (control)
CTR 3	W	JR190927_2_IL2	-	sIPSC (control)
CTR 4	Z	JR191030_3_IL2	-	sIPSC (control)
CTR 5	Z	JR191030_6_IL1	-	sIPSC (control)
CTR 6	BB	JR191213_2_RF1	-	sIPSC (control)
CTR 7	DD	JR200115_7_IL2	-	sIPSC (control)
PYR1	KK	-	reconstruction; EM	-
PYR2	LL	-	reconstruction; EM	-
PYR3	MM	-	reconstruction; EM	-

DBC – double bouquet cell; PMC – parvalbumin-expressing multipolar cell; CTR – sIPSC control cell; PYR – pyramidal cell; EM – electron microscopy; IHC – immunohistochemistry; I-V – current – voltage relationship; IPSC – inhibitory postsynaptic current (s – spontaneous, e - evoked)

Table 3.2 Multiple linear regression models for the effect of group III mGluR activation on sIPSC frequency.

factor	model 1	model 2	model 3	model 4	model 5	model 6	model 7
intercept	0.92 ± 0.46, p = 0.076	0.92 ± 0.49, p = 0.093	1.02 ± 0.47, p = 0.061	0.36 ± 0.5, p = 0.504	0.27 ± 4.72, p = 0.957	1.43 ± 0.36, **p = 0.008**	0.74 ± 0.49, p = 0.161
DBC	0.45 ± 0.16, **p = 0.018**	0.44 ± 0.17, **p = 0.033**	0.46 ± 0.17, p = 0.0.25	0.86 ± 0.17, **p = 0.003**	0.58 ± 0.2, **p = 0.043**	0.65 ± 0.1, **p = 0.0007**	0.43 ± 0.16, **p = 0.024**
age	-0.002 ± 0.009, p = 0.864	-0.0009 ± 0.01, p = 0.926	-0.004 ± 0.009, p = 0.652	0.004 ± 0.009, p = 0.666	0.02 ± 0.15, p = 0.88	-0.02 ± 0.007, **p = 0.044**	0.003 ± 0.01, p = 0.743
sex	-0.13 ± 0.18, p = 0.477	-0.14 ± 0.19, p = 0.487	-0.16 ± 0.18, p = 0.403	-0.42 ± 0.15, **p = 0.03**	0.1 ± 0.68, p = 0.896	-0.18 ± 0.11, p = 0.154	-0.21 ± 0.19, p = 0.296
temporal	-	-0.03 ± 0.19, p = 0.864	-0.1 ± 0.19, p = 0.614	-0.4 ± 0.16, **p = 0.045**	-1.03 ± 3.66, p = 0.792	-	-
glio-blastoma	-	-	0.23 ± 0.16, p = 0.2	-0.2 ± 0.17, p = 0.308	0.36 ± 0.81, p = 0.685	-	-
oedema	-	-	-	0.74 ± 0.26, **p = 0.028**	1.18 ± 3.3, p = 0.74	0.31 ± 0.13, p = 0.054	-
seizures	-	-	-	0.49 ± 0.17, **p = 0.03**	0.69 ± 0.16, **p = 0.013**	0.67 ± 0.14, **p = 0.003**	-
leveti-racetam	-	-	-	-	-0.7 ± 0.35, p = 0.114	-0.6 ± 0.17, **p = 0.013**	-
dexa-methasone	-	-	-	-	-1.39 ± 5.43, p = 0.811	0.26 ± 0.15, p = 0.129	-
hyper-tension	-	-	-	-	-	-	-0.17 ± 0.16, p = 0.311
Df	10	9	8	6	4	6	9
Residual sum of squares	0.65	0.65	0.52	0.19	0.08	0.09	0.58
R2	0.59	0.59	0.67	0.88	0.95	0.95	0.64
Adj. R2	0.47	0.41	0.47	0.75	0.83	0.88	0.47
ANOVA F	4.79	3.25	3.27	6.44	8.51	14.74	3.93
p	**0.026**	0.065	0.067	**0.019**	**0.027**	**0.002**	**0.04**

For each independent variable (factor) its coefficient is given as mean ± SE and the p-values are listed. ANOVA statistics for each model are given at the bottom. DBC – double bouquet cell.

4 Discussion

Neocortical functions supporting human behaviour emerge from the complex interactions of billions of neurons forming diverse but specific synaptic connections within and outside the neocortex. Explaining how neocortical functions and their various pathological states emerge requires the definition of the diversity of the neurons and their synaptic connections in the network. The functional specialisation of neurons is reflected in the diversity of their gene expression patterns and molecular composition, determining which other neurons they form connections with and how electrical and molecular signals received from other neurons are processed and transmitted to their downstream target neurons. Conversely, how individual neurons support neocortical functions can be inferred from studying their gene expression, molecular composition, electrical signal processing and synaptic connections, preferably all in combination. Importantly, studying neurons from only one perspective is not enough, and often leads to different grouping and naming of the same type of neuron based on the particular method used to study them (DeFelipe et al., 2013; The Petilla Interneuron Nomenclature Group, 2008).

Anatomical studies revealed a diverse population of interneurons with distinct spatial distribution of their axon and dendrites, prompting their classification into morphological types, such as multipolar, double bouquet (or bitufted), chandelier and neurogliaform cells (de Carlos et al., 1987; Jones, 1975; Kisvárday et al., 1990; Lund & Wu, 1997; Marin-Padilla & Stibitz, 1974; Meyer, 1983, 1987; Valverde, 1976). Interneuron types defined based on their specific synaptic targets include axo-axonic cells (Somogyi, 1977), which innervate exclusively the axon initial segment of pyramidal cells, basket cells, which innervate the cell bodies and proximal dendrites of pyramidal cells and interneurons (DeFelipe & Fairén, 1982; Kisvárday et

al., 1993; Somogyi et al., 1983) and dendrite targeting cells, which innervate the distal dendrites of pyramidal cells and interneurons (Tamás et al., 1997a) among many others. Intracellular *in vitro* and *in vivo* electrophysiological recordings and labelling of individual neurons revealed distinct firing phenotypes, such as fast-spiking, regular-spiking and burst-spiking neurons among others, corresponding to different morphological types (Kawaguchi, 1995; Kawaguchi & Kubota, 1993; Krimer et al., 2005). Furthermore, interneurons can be grouped based on their molecular content of calcium-binding proteins, such as parvalbumin, calbindin and calretinin and neuropeptides, such as somatostatin, cholecystokinin and vasoactive intestinal polypeptide as detected by immunohistochemistry or more recently RNA sequencing (Kawaguchi & Kubota, 1998; Kubota et al., 1994, 2011; Rudy et al., 2011).

However, it is difficult to establish the one-to-one correspondence between these different classes of neurons defined by different techniques. Recent studies, using large scale single cell and in situ RNA sequencing revealed even larger molecular diversity of neurons across different cortical areas and species than previously captured by traditional immunohistochemical or in situ hybridisation techniques (Alon et al., 2021; Bakken et al., 2021; Berg et al., 2020; Gouwens et al., 2020; Kalmbach et al., 2018; Tasic et al., 2018; Yuste et al., 2020).

4.1 Identification of GABAergic cell types

The great diversity of neurons in the neocortex makes it difficult to assign functions to cell types that can be systematically compared across different species and physiological or pathological states. It is hoped that an integrated analysis of neurons using molecular, electrophysiological and anatomical techniques leads to better and more robust identification of functionally relevant neuronal entities, or cell types, and allows for better understanding of their roles health and disease (Callaway et al., 2021). In order to systematically map and catalogue the molecular and structural diversity of neurons across multiple cortical areas and species, large scale studies combining molecular techniques such as patch-seq (Lipovsek 2021), genetic labelling, in vitro electrophysiological recording and labelling of individual neurons were carried out in mice (Gouwens et al., 2020) and humans (Boldog et al., 2018; Hodge et al., 2019) complemented with computational modelling (Nandi et al., 2020). Although these results are paving the way for better understanding of the neocortical circuit, they still only represent a static cross section, a catalogue of the components of a dynamic complex system. Notwithstanding the complex multidisciplinary analyses currently undertaken, relatively little effort is dedicated to revealing the pharmacological differences between human cortical cell types, which is essential for explaining the mechanisms of drug action (Bocchio et al., 2019; Field et al., 2021; Kroon et al., 2019; Obermayer et al., 2018; Szegedi et al., 2016). It was with this perspective that I undertook the challenge of studying GABAergic neuron types in the human neocortex. I used electrophysiological recording and labelling, immunohistochemistry and electron microscopy, to describe and identify distinct neuron types based on their axonal distributions, firing patterns, molecular content and synaptic connections. Importantly, I also investigated how a group of metabotropic glutamate receptors changes synaptic communication in these cell types.

I recorded and labelled individual neurons in the human neocortex *in vitro*, and identified 5 distinct interneuron types, based on the spatial distribution of their dendrites and axon: double bouquet cells (DBC), parvalbumin-expressing multipolar cells (PMC), chandelier cells (axo-axonic cells, AAC), neurogliaform cells (NGC) and one rosehip cell (RHC) (see chapter 3.1). All AACs had a delayed-firing phenotype and high rheobase, which was observed previously in the neocortex of monkeys (Krimer et al., 2005) and rats (Kawaguchi, 1995; Kawaguchi & Kubota, 1998; Povysheva et al., 2013), but not in mice (Jiang et al., 2015). AACs were double-immunopositive for the calcium-binding proteins PV and calbindin. Co-expression of PV and calbindin in AACs was reported previously in human neocortex (del Río & DeFelipe, 1997a) but not in monkeys (DeFelipe et al., 1989b; Gabbott & Bacon, 1996) or rodents (Kawaguchi & Kubota, 1993). In monkeys a subpopulation of AACs are immunoreactive for corticotropin releasing factor (Lewis & Lund, 1990), but I did not test this on my cells. Neurogliaform cells had a regular, non-adapting firing pattern and showed no voltage sag in response to hyperpolarising current injection. This is consistent with previous reports in human neocortex (Boldog et al., 2018; Oláh et al., 2007). In rodents, NGCs were found to have late-spiking firing patterns in rats (Kawaguchi, 1995; Kawaguchi & Kubota, 1998; Molnár et al., 2014; Ozsvár et al., 2021; Simon et al., 2005) or show spike frequency-adaptation in mice (Jiang et al., 2015). In some NGCs I observed persistent firing after several steps of depolarising current injection-induced firing, similar to what was observed previously in rodents (Krook-Magnuson et al., 2011) and human (unpublished observation by Márton Rózsa and colleagues). I did not test study the molecular expression and synaptic targets of NGC, but they have been shown to express nitric oxide synthase (Armstrong et al., 2012) and innervate dendritic spines and shafts and occasionally somata of pyramidal cells and interneurons in rodents (Kawaguchi & Kubota, 1998; Kubota et al., 2007; Oláh et al., 2009; Tamás et al., 2003) and humans (Kisvárday et al., 1990). Rosehip cells were discovered recently in humans and have not been observed before in

other species (Boldog et al., 2018). I identified the only rosehip cell in this study based on its dense axon and large boutons in layer I.

In this thesis DBCs and PMCs were studied more extensively using anatomical, molecular and electrophysiological techniques (chapters 3.1 and 3.2) and the effects of group III mGluR activation were tested on their GABAergic synaptic inputs (chapter 3.3). The results are discussed in detail below.

4.2 Comparison of DBCs and PMCs across different species

4.2.1 Molecular expression

I studied the molecular expression, evoked firing patterns and synaptic connections of individual double bouquet cells (DBCs) recorded and labelled *in vitro* in layers II and III of the human neocortex. I recognised and defined DBCs based on their radially oriented axonal plexus, also called a DBC 'horsetail', distributed in a narrow (10 – 20 μm) bundle descending towards the white matter (DeFelipe, 2002; Lund & Wu, 1997; Somogyi & Cowey, 1981). Double bouquet cells were first described in the human neocortex by Ramon y Cajal at the end of the 19th century (Ramón y Cajal, 1899b, 1899a), and were later reported in the primate (Jones, 1975; Somogyi & Cowey, 1981; Valverde, 1978), and cat neocortex (Meyer, 1983; Somogyi & Cowey, 1981) using Golgi impregnation. In rodents, using *in vitro* recording and intracellular labelling of single cells, neurons with radially oriented axonal plexus were named as DBCs (Jiang et al., 2013, 2015; Karube et al., 2004; Kawaguchi & Kubota, 1996) but the 'horsetail' axons have not been documented. Detailed correlative anatomical, electrophysiological and/or molecular studies of individual cells have only been done in rodents (Jiang et al., 2013, 2015; Karube et al., 2004; Kawaguchi & Kubota, 1996, 1997; Kubota et al., 2007) and cats (Tamás et al., 1997a, 1998), but not in humans, where these cells are thought to be the most numerous (Ballesteros Yáñez et al., 2005; DeFelipe, 2011).

I have found that 75 % of recorded and labelled DBCs were immunopositive for calbindin. This is in line with the evidence that immunoreactions for calbindin reveal DBC-like bundles of axons in humans and nonhuman primate species (Ballesteros Yáñez et al., 2005; DeFelipe et al., 1989a, 1990, 1999, 2006; del Río & DeFelipe, 1997c; Ferrer et al., 1992). While similar axonal bundles are revealed by immunoreaction to calbindin in carnivores, this is not the case in rodents, lagomorphs and artiodactyls (Ballesteros Yáñez et al., 2005). Possible

explanations for this are that DBCs in rodents do not express calbindin, or calbindin-expressing DBCs are absent in rodents. It is also possible that DBC-like neurons in rodents are less specialised and their axon does not form typical 'horsetails' observed in primates and humans. Indeed, the axon of neurons visualised in rat neocortex, which have been named as DBCs does not form narrow 'horsetails', but rather it is more widely and irregularly distributed (Jiang et al., 2015; Karube et al., 2004; Kawaguchi & Kubota, 1996, 1997). Furthermore, some neurons named DBCs recorded in rodents and primates were shown to be immunoreactive for vasoactive intestinal polypeptide (VIP) and/or calretinin (CR) and/or corticotropin releasing factor (CRF) (Karube et al., 2004; Kawaguchi & Kubota, 1996; Meskenaite, 1997), and cholecystokinin (CCK) (Freund et al., 1986). Only a few examples of calbindin-immunoreactive neurons with radially oriented axonal plexus were recorded in monkeys (Zaitsev et al., 2005). Although no individual DBCs have been shown to be immunoreactive for the tachykinin family of neuropeptides, such as substance P, immunoreactions to tachykinins also reveal axonal bundles similar to those revealed by calbindin in monkey (DeFelipe et al., 1990). I found no immunoreactivity for VIP or CCK in any of the DBCs tested here, and because 90 % of CRF-immunoreactive cells in layers II-III in rats are also immunopositive for VIP (Karube et al., 2004), I did not test CRF on the cells recorded in humans. I also did not test immunoreactivity of DBCs to any of the tachykinin family proteins because the antibodies available to us produced no specific immunoreaction.

Some of the human DBCs tested here (25%) were immunonegative for calbindin, and of these, 2 were immunopositive for CR, the remainder being immunonegative for both calbindin and CR. Those DBCs immunopositive for CR were immunonegative for VIP, despite the relatively high degree of overlap reported in the expression of these two molecules in rodents (Kawaguchi & Kubota, 1997; Kubota et al., 1994, 2011; Rogers, 1992) and monkey (Gabbott & Bacon, 1997). It is possible that CB/CR double immunonegative cells in our sample

genuinely do not express either of these molecules, or that expression was undetectable by our method due to a genuine variation in the expression level by cell type and/or cortical area. However, because I found CB+ DBCs in multiple cortical areas, variation by cortical area is an unlikely explanation, at least in the areas sampled in this thesis (see table 1). It is also possible that calbindin or CR was diluted by the internal solution in the recording pipette to undetectable levels, which is the most likely scenario. To reduce this risk, in most cases the axonal boutons were immunoreacted, which are further from the soma and less likely to be dialysed.

Co-expression of calbindin with other calcium binding proteins, such as parvalbumin (PV) and CR, in neocortical non-pyramidal neurons has been reported in humans and other species. In rats the vast majority of PV-immunoreactive neurons are also immunoreactive for calbindin, particularly in layers II-III (Kubota et al., 1994; Kubota & Jones, 1993; van Brederode et al., 1991). In the human temporal neocortex this overlap is smaller, and the pattern of labelled axons is reminiscent of that of axo-axonic cells (del Río & DeFelipe, 1997a), whereas in cats (Demeulemeester et al., 1991; Hendry & Jones, 1991) and primates (Condé et al., 1994; van Brederode et al., 1990) the two molecules were reported to be expressed in distinct GABAergic neuronal populations. I did not find expression of PV in any of the calbindin immunopositive or immunonegative DBCs tested in this study. Similarly, co-expression of calbindin and CR has also been reported in a small fraction of neocortical GABAergic neurons in humans (del Río & DeFelipe, 1996; Fonseca & Soriano, 1995; Leuba & Saini, 1997) and rats (Kubota et al., 1994), however, none of the DBCs studied here were double-immunopositive.

Furthermore, most calbindin-expressing GABAergic neurons co-express the neuropeptide somatostatin (SM) in the neocortex of rodents (Gonchar & Burkhalter, 1997; Kawaguchi & Kubota, 1997; Kubota et al., 1994; Rogers, 1992), cats (Demeulemeester et al., 1988) and humans (González-Albo et al., 2001). I found that only one of the 14 calbindin-

immunopositive DBCs tested was immunoreactive, and none of the 4 calbindin-immunonegative DBCs tested were immunoreactive for SM. Interestingly, SM immunoreactivity was present in the cell body of DBC 18, but only some of its boutons were immunoreactive, possibly indicating a genuine localisation of SM only in certain boutons of the same cell.

The majority of PMCs (75 %) that I studied in this thesis were immunopositive for PV, and immunonegative for calbindin, except for PMC 7, which was also immunopositive for calbindin. Parvalbumin is typically expressed by fast-spiking basket cells, dendrite targeting and axo-axonic cells (AACs) in rodents (Kawaguchi, 1997; Kawaguchi & Kondo, 2002; Kawaguchi & Kubota, 1993, 1998; Kubota et al., 1994), cats (Kisvárday et al., 1993) and monkeys (Condé et al., 1994; DeFelipe et al., 1989b; Gabbott & Bacon, 1996; Lewis & Lund, 1990; Zaitsev et al., 2005) and these cells were reported to lack calbindin expression. Human PMCs were immunonegative for both the cannabinoid receptor type 1 (CB1) and cholecystokinin (CCK), molecules expressed in other species by a specific population of basket cells, which are immunonegative for PV (Freund 1986, Armstrong & Soltesz, 2012).

I conclude that the vast majority of DBCs in humans express the calcium-binding protein, calbindin alone, and a small proportion express CR, but unlikely both, and neither subpopulations express PV. Conversely, PMCs express PV, but rarely calbindin, whereas axo-axonic cells express both calbindin and PV. I demonstrated the GABAergic nature of all three cell types by their immunoreactivity to vesicular GABA transporter and also by their synaptic effect (see below). Whether DBCs express any neuropeptides remains less clear. Further research of individually labelled DBCs is necessary with more sensitive detection of neuropeptide expression, such as patch-seq (Lipovsek et al., 2021), in situ hybridization and in situ sequencing, particularly in humans.

4.2.2 Intrinsic membrane properties

The function of different GABAergic cells in the neocortex is also determined by how they process electrical signals, and what action potential patterns they generate in response to depolarising stimuli. These characteristics in turn depend on the combinations of ion channels the cells express in their membranes, as well as the physical parameters of their processes and cytoplasm. Although DBCs have been known for more than a century, how they process electrical signals has not been reported in humans. I studied the responses of DBCs and PMCs to sustained hyperpolarising and depolarising current injections, and found that these two group of cells respond markedly differently to such stimuli, which predicts that they also process electrical signals differently *in vivo.*

One of the most common features of DBCs was the large amplitude voltage sag in response to hyperpolarising current injections, which was significantly larger in DBCs than in PMCs, and is likely to result from the expression of hyperpolarisation-activated cation channels in the DBCs' membranes (Ludwig et al., 1998; Maccaferri et al., 1993; McCormick & Pape, 1990). The presence of such channels in neurons is thought to regulate rhythmic firing (Pape & McCormick, 1989), resting membrane potential (McCormick & Pape, 1990), excitability and dendritic integration (Berger et al., 2001; Magee, 1998) in different types of neuron. Indeed, 5 of 29 DBCs showed burst firing either at the beginning of a depolarising current injection, or after the end of a hyperpolarising current injection as a rebound (see figs. 1 and 2), and even non-bursting DBCs fired at least one rebound spike after continuous hyperpolarisation. I did not study whether individual DBCs can switch between burst and non-burst firing. Conversely, PMCs did not show either burst firing, nor rebound spikes. In agreement with the likely presence of high levels of hyperpolarisation activated cation channels in DBCs, they were also more excitable than PMCs, as indicated by their lower rheobase, and the tendency of DBCs to having more depolarised resting membrane potentials.

Further differences were also found between DBCs and PMCs. All DBCs showed strong spike amplitude accommodation and spike frequency-adaptation, and some DBCs even entered depolarisation block in response to continuous depolarisation, whereas PMCs did not show amplitude accommodation and frequency adaptation also tended to be smaller than in DBCs. The adaptation of the firing frequency during continuous depolarisation could be attributed to various voltage dependent and Ca-activated potassium channels (Faber et al., 2001; Lancaster & Nicoll, 1987; Louise Faber & Sah, 2003), which mediate the fast and slow components of the afterhyperpolarisation (AHP) following single action potentials. Spike-frequency adaptation is in general correlated with the amplitude of the slow component of the AHP, whereas the fast AHP reflects the fast repolarisation following an action potential (Louise Faber & Sah, 2003; Sah & Faber, 2002). The slow AHP was not measured here, however the fast AHP was larger in PMCs than in DBCs, and did not correlate with the observed difference in spike frequency adaptation between the two groups. Action potential threshold, half-width, input resistance and average firing frequency were similar in the two groups.

The larger whole-cell capacitance measured in PMCs compared to DBCs, may be explained by the former group having larger dendritic trees, and consequently a larger membrane surface, which was only evaluated semi-quantitatively. The lateral spread of the dendritic tree was larger for PMCs than for DBCs. The median number of dendrites originating from the soma was also larger in PMCs than in DBCs (see chapter 3.1).

The most prominent features of evoked DBC firing, which differentiate them from PMCs in humans, namely the large amplitude voltage sag, burst firing, amplitude accommodation and frequency adaptation, correlate with the differential expression of calbindin and PV by these two interneuron types. These firing phenotypes also correlate with calcium-binding protein expression in monkeys (Zaitsev et al., 2005) and rodents (Cauli et al., 1997; Kawaguchi & Kondo, 2002; Kawaguchi & Kubota, 1993). However, these firing patterns are not unique for

DBCs, as many other GABAergic neurons with different axonal distributions and molecular expression share one or more of these features, as do pyramidal cells (Connors & Gutnick, 1990; Kawaguchi, 1993). For example in rodents calbindin and SM double-immunoreactive Martinotti cells in layer V with ascending axonal arbour, VIP-expressing arcade cells and CCK-expressing basket cells show burst firing (Kawaguchi & Kubota, 1996, 1998). Furthermore, CR-expressing cells in layer I and SM-expressing cells in layers II and III with widely distributed axon show strong spike frequency adaptation (Kawaguchi & Kubota, 1998; Kubota et al., 2011). In the monkey, some calbindin-expressing neurons, other than DBCs with wide axonal arbours show spike frequency adaptation (Zaitsev et al., 2005). In addition, novel and previously unknown GABAergic cell types in humans, such as rosehip cells (Boldog et al., 2018) and other interneurons in layers I and II show large amplitude voltage sags and rebound spikes (Field et al., 2021) Conversely, neurons named as DBCs in rodents and monkeys typically do not show any of these evoked firing characteristics (Jiang et al., 2015; Zaitsev et al., 2005), or were not fully studied (Kawaguchi & Kubota, 1996). In contrast, the firing patterns of PV-expressing neurons, which are mostly identified as basked or axo-axonic cells are more similar across species, in that they do not show burst firing, spike amplitude accommodation, or strong spike frequency adaptation.

4.2.3 Synaptic targets

Specialised GABAergic neuron types innervate different subcellular domains of their target cells (DeFelipe, 2002; Markram, 2000; Somogyi et al., 1998). We studied the synaptic targets of two types of GABAergic neuron in human neocortex with different spatial axonal distribution, intrinsic membrane properties and molecular expression, the DBCs and PMCs, and showed that they indeed innervate different subcellular domains of their target cells. Double bouquet cells had axons and boutons distributed in a narrow cortical column spanning multiple layers, and approximately half of their synaptic targets in layers II and III are dendritic spines

most likely originating from pyramidal neurons, the other half targeting dendritic shafts of both pyramidal cells and interneurons (see chapter 3.2.1). In contrast, PMCs had widely distributed axon spanning multiple cortical columns, but mostly restricted to layers II and III, where the majority of their synaptic targets were dendritic shafts of mostly pyramidal cells and also interneurons, and to a lesser extent dendritic spines most likely originating from pyramidal cells. Importantly, a small proportion of PMC boutons also innervated somata of pyramidal cells and interneurons, which DBCs did not innervate.

The synaptic targets of individually labelled DBCs have been unknown in human. However studies of the synapses made by calbindin immunoreactive axon bundles showed similar, although somewhat smaller frequency (41 %) of dendritic spine targets in layers II and III of the temporal neocortex in humans (del Río & DeFelipe, 1995) and in the primary sensory cortex of the macaque monkey (38%; DeFelipe et al., 1989a). Similar to my results, no somata were found among the synaptic targets in these studies. In another study, only 28 % of synaptic targets were found to be dendritic spines in the striate cortex of rhesus monkeys, the majority of targets being dendritic shafts, and a small proportion also targeted somata (Peters & Sethares, 1997). It is important to note however, that there are multiple distinct types of GABAergic calbindin expressing neuron in the primate (DeFelipe et al., 1999; Gabbott & Bacon, 1996) and human (Bakken et al., 2021; Gouwens et al., 2020; Hodge et al., 2019), each of which may have different synaptic target distributions, which contribute to an average in population calbindin EM immunoreaction analysis. In addition, approximately 30 % of calbindin immunopositive neurons in layers II and III of the macaque somatosensory cortex are pyramidal cells (DeFelipe & Jones, 1992), which also have descending axons and intermingle with DBC axons (del Río & DeFelipe, 1997c), and although they form type I synapses as opposed to the type II synapses formed by DBCs, these may not be always differentiated due to unfavourable angle of the synapse in the section plane or various technical issues. Furthermore, DeFelipe & Jones (1992)

also report a proportion of calbindin immunoreactive nonpyramidal cells, which are not GABAergic, the synapses of which could further skew the target distribution (DeFelipe & Jones, 1992). Further differences in the proportion of synaptic targets may arise from the different cortical areas studied. All four calbindin immunopositive DBCs studied for their synaptic targets were recorded in the middle temporal gyrus, which likely corresponds to auditory sensory areas, as indicated by the presence of a distinct inner granular layer (layer IV). These areas might also correspond to the areas studied by del Rio & DeFelipe (1995), however I did not determine the exact Brodmann in my samples.

Other studies also showed variability in the synaptic target preference of individually labelled DBCs. In particular, Somogyi & Cowey (1981) examined the synaptic targets of Golgi impregnated DBCs in the striate cortex of the rhesus monkey, and found that the proportion of dendritic spine targets was similar (40 %) to that reported in the somatosensory cortex of the macaque (DeFelipe et al., 1989a). Interestingly, Somogyi and Cowey (1981) also studied the synaptic targets of three putative DBCs in the striate cortex of the cat, however the proportion of dendritic spine targets was only 5 %, the vast majority of synapses innervating dendritic shafts (86 %) of mostly smooth dendritic cells. Furthermore, a significant proportion of synapses were found innervating nonpyramidal somata in the cat (Somogyi & Cowey, 1981). In the absence of molecular data on the Golgi impregnated neurons, it is not clear if the cells studied in the cat were homologous to the calbindin positive cells in the monkey and humans. In a different study of the synaptic connections of individually labelled DBCs and other GABAergic interneuron types, including basket and dendrite targeting cells in the cat visual cortex, more than half (69 %) of the synaptic targets of DBCs were dendritic spines, the remainder being dendritic shafts and no somata were targeted (Tamás et al., 1997a). This target distribution is most similar to the synaptic target distribution of DBC 5 (61 % spine), although higher than the average proportion of spine targets for all calbindin immunopositive DBCs

presented in this thesis. Tamás et al. (1998) also reported that a DBC in the cat visual cortex, which had different dendrites and thicker axon than the DBCs in Tamás et al. (1997), only had 38 % of its synapses on dendritic spines, the majority being on dendritic shafts (Tamás et al., 1998); this is similar to the synaptic target distribution of DBC 10 in this thesis. Since both in this thesis and in the studies mentioned above DBCs with different synaptic target frequencies were observed within a single cortical area, this suggests that there could be multiple subtypes of DBCs. Indeed, I found variation in the target frequencies within calbindin immunopositive DBCs, although this was not significant (see chapter 3.2.1). I found significant difference between the target distribution of calbindin and calretinin immunopositive DBCs, however from the latter group only one cell was examined. In the prefrontal cortex of the rat, the synaptic targets of calretinin or CRF-immunoreactive neurons with radial axon, named as DBCs were also studied, and 28 – 44 % of the synaptic target were dendritic spines in layer III (Kubota et al., 2007). This is lower than that of calbindin immunopositive DBCs in humans. Two CR-immunoreactive cells in the rat also innervated somata, as reported for Golgi impregnated DBCs in the cat.

The target frequency distribution of the synapses of PMCs was most similar to the synaptic target distributions of so-called dendrite-targeting cells in the cat visual cortex (Tamás et al., 1997a), and to the distribution of one fast-spiking neuron in the rat frontal cortex (Kubota et al., 2007). Because the dendritic and axonal distributions, firing patterns and the molecular content of dendrite targeting cells show remarkable similarity in all three species, they likely represent a distinct and highly conserved cell type. Importantly, dendrite targeting cells can only be differentiated from fast-spiking basket cells by their synaptic target specificity towards dendrites instead of somata (DeFelipe et al., 1986; Kawaguchi & Kubota, 1998; Kisvárday et al., 1993; Somogyi et al., 1983; Tamás et al., 1997a). Despite this, in almost all studies of genetically labelled parvalbumin-expressing neurons, they are considered to be either axo-

axonic or basket cells, in spite of not making ‘basket’-like formations by their terminals. But other GABAergic neurons do make basket formations (DeFelipe et al., 1986; Kawaguchi & Kubota, 1998; Kisvárday et al., 1993; Somogyi et al., 1983; Somogyi & Soltész, 1986; Tamás et al., 1997a), therefore the genuine basket and dendrite targeting cells should be considered distinct cell types with different synaptic effects.

The postsynaptic effect of GABAergic synapses and their spatial integration depends on the localization of the synapses along the somatodendritic compartment of the target neurons, as has been shown in the somatosensory (Tamás et al., 2002, 2004) and frontal (Kubota et al., 2015) cortices of the rat, in the visual cortex of the cat (Tamás et al., 1997a), and in the hippocampal CA1 field in rats (Maccaferri et al., 2000). Furthermore, perisomatic GABAergic synapses can have a strong effect on action potential generation, and are able to phase the firing of postsynaptic pyramidal cells (Cobb et al., 1995; Tamás et al., 2000, 2004). In contrast, the postsynaptic effects of GABAergic synapses targeting distal dendritic segments are localised to separate dendritic segments, as has been shown for the rosehip cells in humans, which innervate the apical tufts of pyramidal cells in layer I (Boldog et al., 2018), or can be localised to single dendritic spines (Chiu et al., 2013). Consequently, the postsynaptic effects of DBCs and PMCs are likely to be different, because of the differential localization of their synapses on dendritic spines and shafts. For example, DBCs are well suited to control synaptic plasticity in populations of individual spines, whereas PMCs are better suited to regulate calcium signals and dendritic integration in entire dendritic branches. Although both DBCs and PMCs studied in this thesis had dendritic spines among their synaptic targets, these spines likely belong to different functional populations, and participate in different neocortical processes, because of the different spatial distribution of the presynaptic axons.

4.2.4 Postsynaptic effects of DBCs

The postsynaptic effects of DBCs have only been recorded previously in the visual cortex of the cat in 1 connection to a pyramidal cell (Tamás et al., 1997a) and in mice (Jiang et al., 2015), although the homology of the cell type in the mouse is questionable. Here I showed by simultaneous recording of pairs of interneurons, that DBCs are synaptically connected with ~ 25 % connectivity ratio to both interneurons (3 of 12 tested) and pyramidal cells (1 of 4 tested). The similarity in connectivity rates is in contrast with the postsynaptic target distribution determined by electron-microscopy, which was ~ 75 % to pyramidal cells, and ~ 25 % to interneurons, but I could only test a low number of neuronal pairs. Therefore, this may not be a representative sample. Furthermore, postsynaptic responses of inputs to distal dendrites are more difficult to detect in pyramidal cells than in interneurons using somatic whole-cell recordings due to dendritic filtering and the difficulty of clamping distal compartments to the desired potential (space-clamp problem). In comparison, the average connection probability of so-called DBCs to pyramidal cells in layers II and III in the mouse visual cortex, was 39.4 %, whereas the average connectivity rate to interneurons was 21.3 %, slightly lower than in our sample (Jiang et al., 2015). Among the four innervated postsynaptic interneurons in this thesis, was one DBC, one interneuron with bipolar dendritic tree, one fast-spiking interneuron and one unidentified interneuron. Similarly, Jiang et al. (2015) found that postsynaptic interneurons to DBCs in layers II and III were other DBCs, bipolar cells and basket cells, in descending order of connection probability (Jiang et al., 2015). It is important to note here, that Jiang et al. (2015) used four different genetic mouse lines, in which VIP, SM, PV, or GABAergic neuron populations were fluorescently tagged, which could bias the sampling towards particular interneuron types. Connectivity ratio in the cat visual cortex was not evaluated, however DBCs were found to innervate pyramidal cells, basket cells and dendrite targeting cells and even the

number and location of the synaptic junctions were determined, which correlated with the amplitude of the postsynaptic effect (Tamás et al., 1997a, 1998).

The monosynaptic IPSCs evoked by DBCs recorded at just subthreshold membrane potentials (-45 - -55 mV), were outward currents with a short latency and fast kinetics (see chapter 3.2.2), similar to $GABA_A$ receptor mediated currents (Edwards et al., 1990; Farrant & Kaila, 2007; Farrant & Nusser, 2005; Kuffler & Edwards, 1958; Mozrzymas, 2004; Nusser et al., 1997), consistent with the GABAergic nature of these neurons as demonstrated by immunoreactivity to VGAT This suggests that DBCs have an inhibitory effect on their postsynaptic targets at these membrane potentials. The mean amplitude of the eIPSCs was variable and it did not depend on the immunoreactivity of the presynaptic DBC to calbindin, or the postsynaptic cell type. For instance, both the largest and smallest eIPSCs were evoked by CB-/CR- double immunonegative DBCs in potsynaptic interneurons. The kinetics of the response, more specifically, the risetime was also variable between connections, whereas half-width was less variable. These parameters are indicative of the postsynaptic dendritic filtering of the synaptic responses, and indicate that the synaptic junctions were made at different distances from the soma along the dendritic trees of the postsynaptic neurons, consistent with the electron-microscopic observation that DBCs made synapses with both proximal and distal dendrites of large and small diameter, respectively. Similarly, one indicator of pre-synaptic release probability, the eIPSC failure rate was also variable, and appeared to correlate with the pre- and post-synaptic neuron identities, such that the failure rate was smallest in connections of CB-/CR- DBCs to interneurons, and was also small in the calbindin immunopositive DBC to pyramidal cell connection, indicating that these connections were mediated by high release probability synapses. In contrast, failure rate was higher in the connections of calbindin immunopositive DBCs to interneurons, indicating that these synapses were in a different state, which may either be a genuine biological difference, or may be these synapses were more

sensitive to *in vitro* conditions. Patient history and cortical area may also have an effect of the observed differences. These results are consistent with the differential synaptic target preference of calbindin immunopositive DBCs and the one calretinin immunopositive DBC, as determined by electron-microscopy. Specifically, pyramidal cell dendrites were more frequently the targets of calbindin immunopositive DBCs, than interneuron dendrites, and the inverse was true for the calretinin immunopositive DBC. Thus the chance of multiple synapses converging on the same pyramidal cell is higher for calbindin immunopositive DBCs, which would increase transmission efficacy, whereas for calretinin immunopositive DBCs the chance of multiple convergent boutons to the same postsynaptic interneuron is higher. Indeed, I could prove one example of convergent input to the same postsynaptic pyramidal cell dendrite from the calbindin immunopositive DBC 5, but no convergent input to interneuron dendrites. Conversely, I found two examples of convergent input to postsynaptic interneuron dendrites from the calretinin immunopositive DBC 25, but no convergence onto pyramidal cell dendrites. These results, however, come from a small sample, and are very time consuming and technically demanding to obtain with the methods I used. Future studies, possibly with high resolution live imaging will be needed to confirm these potential differences.

Tamás et al. (1997a and 1998) and Jiang et al. (2015) recorded evoked inhibitory postsynaptic potentials (IPSPs) in current-clamp mode, rather than eIPSCs, thus comparison of the amplitudes would not be meaningful. The postsynaptic neurons in Tamás et al. (1997a) were held at similar membrane potentials to postsynaptic neurons in our experiments. In agreement with my suggestion above, the DBC to pyramidal cell connections (Tamás et al., 1997a) were mediated by more synaptic junction sites than connections from DBCs to basket cells (Tamás et al., 1998). The postsynaptic responses to inputs from DBCs were only recorded in pyramidal cells (Tamás et al., 1997a), but not in basket cells (Tamás et al., 1998). In Tamás et al. (1997) DBC-evoked IPSPs in postsynaptic pyramidal cells had smaller amplitudes and slower kinetics

than those evoked by other types of interneuron the ‘dendrite targeting cells’ and basket cells, consistent with their more distal placement on the pyramidal cell dendrites (Tamás et al., 1997a). We could not test the unitary postsynaptic effects of PMCs in our study, a cell type that I propose correspond to ‘dendrite targeting cells’ in the cat (Tamás et al., 1997a).

In the visual cortex of the mouse, Jiang et al. (2015) held the postsynaptic neurons at more negative membrane potentials (−57 ± 3 mV), using the same internal chloride concentration (4 mM) during eIPSP recording. They found that on average eIPSP amplitude in postsynaptic interneurons, evoked by the so-called DBCs, was larger than in postsynaptic pyramidal cells. This is in contrast with the results of Tamás et al. (1997a and 1998) and with our results. However, more molecular data is required to establish possible homology of DBCs in humans, carnivores and rodents.

4.2.5 Unique effects of group III mGluR activation on GABAergic inputs to DBCs

We have tested the effects of group III mGluR activation by the non-selective group III orthosteric agonist L-AP4 on spontaneous inhibitory synaptic currents (sIPSCs) arriving onto different types of GABAergic neuron in the human neocortex. Although I have tested many neuronal types, we focused our comparison on two distinct cell types, DBCs and PMCs, which had a large enough sample size for statistical comparison.

We found unexpectedly that group III mGluR activation increased the frequency of sIPSCs onto DBCs, which was not accompanied by a change in the amplitude of the IPSCs. Importantly, voltage-gated Na channels were not blocked in our experiments, thus the recorded sIPSCs represented both action potential-dependent, and action potential-independent GABA release from presynaptic terminals. It is also important to note that ionotropic glutamate receptors and thus fast glutamatergic synaptic transmission was not blocked in our experiments

(see chapter 2.3.1). Under these conditions, the observed effects may be the result of the combined activation group III mGluRs at GABAergic, glutamatergic and possibly other synapses, which are not restricted to monosynaptic inputs.

Such an increase in spontaneous GABAergic synaptic transmission by group III mGluR activation has not been reported before and virtually all previous studies found that group III mGluRs inhibit both evoked and spontaneous GABAergic synaptic transmission in every brain region studied *in vitro* (Bonci et al., 1997; Chu & Moenter, 2005; Cuomo et al., 2009; Giustizieri et al., 2005; Matsui & Kita, 2003; Mitchell & Silver, 2000; Panatier et al., 2004; Rusakov et al., 2004; Schrader & Tasker, 1997; Summa et al., 2013; Turner & Salt, 2003; Valenti et al., 2003; Wittmann et al., 2001) and *in vivo* (MacInnes & Duty, 2008; Marabese et al., 2005; Naie & Manahan-Vaughan, 2005; Salt & Eaton, 1995). However, there are two studies, which reported that activation of group III mGluRs increased the frequency of spontaneous and miniature excitatory postsynaptic currents (sEPSCs and mEPSCs respectively) in layer V neurons in the entorhinal cortex of rats *in vitro* (Evans et al., 2000; Woodhall et al., 2007). In these experiments, similarly to ours, neither GABA nor glutamate ionotropic receptors were blocked, except for NMDA receptors in Evans et al. (2000), thus both GABAergic and glutamatergic synaptic and extrasynaptic signalling were left intact. In the vast majority of studies on GABAergic synaptic transmission *in vitro*, either the frequency of spontaneous miniature IPSCs is measured while TTX is used to block action potential-dependent neurotransmitter release, or the amplitude and paired-pulse ratio of extracellularly evoked IPSCs is measured while ionotropic glutamate receptors are blocked. These conditions allow the measurements of the drug effects on monosynaptic inputs. With both of these methods however, multiple GABAergic inputs are measured, thus the specific presynaptic neuron types mediating the effects are not possible to determine.

The observed changes in sIPSC frequency in DBCs and PMCs were not accompanied by a change in the amplitude of sIPSCs in either cell type, which indicates that the changes in frequency were the result of changes in GABA release from presynaptic terminals and not changes in the membrane properties of the postsynaptic cells. Parameters, such as the input resistance, or the membrane potential (indirectly assessed by measuring the holding current) could affect sIPSC amplitude by changing the dendritic membrane conductance, or the driving force for GABA-A receptor mediated currents, were probably not affected. I did not test these possibilities directly. The presynaptic nature of the effects reported here are consistent with the presynaptic localisation of group III mGluRs (Dalezios et al., 2002; Shigemoto et al., 1996, 1997; Somogyi et al., 2003). In the vast majority of observations in multiple brain regions of animals the presynaptic site of action of group III mGluRs through inhibition of neurotransmitter release from synaptic terminals is further supported by changes in the frequency of miniature spontaneous IPSCs (Chu & Moenter, 2005; Doi et al., 2002; Giustizieri et al., 2005), or changes in the paired-pulse ratio of evoked postsynaptic events (Bonci et al., 1997; Cuomo et al., 2009; Matsui & Kita, 2003). Miniature sIPSCs are the result of stochastic spontaneous fusion of single vesicles with the presynaptic membrane that is not dependent on the arrival of an action potential, and changes is their amplitude frequency indicate changes in quantal size (Turrigiano et al., 1998) and presynaptic release probability (Padamsey et al., 2019; Taylor et al., 2020) respectively (Kavalali, 2014), regardless of the somatodendritic excitation of the neuron. Conversely, the paired-pulse ratio of evoked postsynaptic events depends on the difference in Ca^{2+} ion concentration in the terminal on the arrival of two successive action potentials, and thus changes in the paired-pulse ratio indicate changes in presynaptic neurotransmitter release (Blatow et al., 2003; Hashimoto & Kano, 1998; McNaughton, 1982; Rozov et al., 2001; Wu & Saggau, 1994; Zucker, 1989).

Considering all the above, the observed increase in sIPSC frequency in DBCs is likely the result of a summed action of group III mGluRs at multiple GABAergic and glutamatergic synapses in the entire local network, rather than a direct action at monosynaptic GABAergic inputs to the recorded cell enhancing neurotransmitter release. Although it is not possible to determine from these experiments which GABAergic interneuron types and/or pyramidal cells and synapses contribute to the effect, the increase is target cell type-selective, because in PMCs group III mGluR activation decreased the frequency of sIPSCs (see chapter 3.3). One possible way how such an increase in GABAergic synaptic transmission onto DBCs could occur at the network level is if activation of group III mGluRs disinhibited GABAergic neurons providing monosynaptic input to DBCs via suppression of GABAergic synaptic transmission onto those presynaptic neurons. The GABAergic synaptic inputs to DBCs in humans are not known. Although, I have shown earlier that, similarly to putative DBCs in rodents (Jiang et al., 2015), GABAergic neurons innervating DBCs include other DBCs, they cannot be the presynaptic neuron type increasing their GABAergic input to other DBCs, as they themselves receive increased GABAergic input and so likely are inhibited after group III mGluR activation. On the other hand, immunohistochemical studies have shown that more than half of the neurons immunoreactive for calbindin in the monkey visual and temporal cortex, receive synaptic input from calretinin-immunoreactive neurons, whereas approximately one third of them receive synaptic inputs from PV-immunoreactive neurons (DeFelipe et al., 1999). Because, PMCs in humans are immunoreactive for PV and they are disinhibited by group III mGluR activation, as we have shown here, it is possible that they contribute to the increased GABAergic synaptic input to DBCs. However, whether such circuit indeed exists in the human neocortex and mediates the effects of group III mGluR activation needs more specifically aimed experiments. I intended to test the effects of group III mGluR activation on unitary synaptic inputs to DBCs from indentified GABAergic interneuron types by recording synaptically connected pairs of

DBCs and other interneuron types. However, due to the difficulty of finding the same types of both pre- and postsynaptic interneuron without any cell type-specific labelling in the slices, and the relatively low frequency of samples, the study could not have been concluded within the limits of my DPhil.

My analysis has shown that group III mGluR activation suppressed the frequency of sIPSCs in PMCs, an effect consistent with inhibition of GABA release reported in other species (see references above), and which is likely explained by suppression of GABA release from monosynaptic GABAergic inputs to PMCs. Such inputs would include VIP-expressing neurons, a subset of which are known to selectively innervate other GABAergic neurons (Acsády et al., 1996b), including those that express PV in the neocortex of mice (Hioki et al., 2013) and rats (Dávid et al., 2007). Consistent with such hypothesis, VIP-expressing neurons in non-human species have been shown to also express high levels group III mGluRs, particularly the high affinity subtype, mGluR8, as well as the low affinity mGluR7 (Dalezios et al., 2002; Katona et al., 2020). Multiple datasets of single cell RNA sequencing in human neocortex also shows selective expression of mGluR8 in some VIP-, SM-, and PV-expressing GABAergic transcriptomic cell types. These can be browsed and analysed at: *https://portal.brain-map.org/atlases-and-data/rnaseq*.

It is important to note, that we only recorded and analysed the effects of group III mGluR activation in a small number of neurons in each group, which came from samples of different cortical areas and patients with different medical history and treatments (see table 2,1), and thus these results should be interpreted cautiously. Indeed, changes in group III mGluR function have been reported in animal models of various pathologies, including absence seizures (Snead et al., 2000) and epilepsy (Sansig et al., 2001), as well as depression and anxiety (Cryan et al., 2003b; Stachowicz et al., 2008). Furthermore, the effects on sIPSC frequency reported here were small in individual cells, and were only significant in a proportion of cells in each group

at the event numbers I succeeded in recording. Nevertheless, they were consistent at the group level, and small receptor activation effects may still have biological modulatory activity. The small effect size may be partly explained by endogenous activity of group III mGluRs, or by allosteric modulation of these receptors by the bivalent cations in the ACSF. Some variability in effect size may also be explained by variability in patient-related parameters, however, because of the small number of cells involved, we could not reliably exclude or confirm an effect of the variability of the samples on the observed effects of group III mGluR activation (see chapter 3.4).

In summary, we have observed a unique effect of group III mGluR activation in the human neocortex, which has not been reported in other species and which is specific to a GABAergic neuron type, the double bouquet cell, a particularly abundant cell type in humans and nonhuman primates. Although most of the details of how DBCs are involved in neocortical function and what are the consequences of group III mGluR activation in the wider neocortical circuit in humans still remain to be explored, our results highlight the potential differences between human neuronal networks and those of other animals, as well as point to why drug development may benefit from more direct research of human tissue.

4.3 Local synaptic targets of pyramidal cells

The layer III pyramidal cells that I studied made type I synaptic junctions with either dendritic spines or shafts of both pyramidal cells and interneurons, whereas no somata were targeted, similar to DBCs (see chapter 3.2.1). The proportion of dendritic spine targets among pyramidal cell synapses were 60 ± 12 %, the remainder being dendritic shafts, of which some also belonged to pyramidal cells, thus, assuming that all postsynaptic spines originated from pyramidal cells, raising the proportion of innervated dendrites belonging to pyramidal cells to 76 ± 12 %. Intriguingly, this proportion or pyramidal vs. smooth dendritic targets is similar to that found in the visual cortex of the mouse (Bopp et al., 2014), but lower than what was reported in the visual cortex of the cat (Kisvárdayet al., 1986b). In the latter, ~ 95 % of the synaptic targets of individual pyramidal cell axons were dendrites of other pyramidal cells, and only 5 % were dendrites of interneurons. In the primary visual cortex of the macaque (McGuire et al., 1991) ~ 75 % of the synapses made by intracellularly labelled pyramidal cells were on dendritic spines, the remainder being on dendritic shafts, some of which also originated from spiny pyramidal cells. In another study on the prefrontal area 9 of the cynomolgus monkey, local dendritic spine targets of biotinylated dextran amine (BDA) labelled pyramidal cell axons, representing a large population of pyramidal cells, not single neurons, were ~ 50 % of the synaptic targets, the remainder being dendritic shafts, including those of parvalbumin-expressing GABAergic neurons (Melchitzky et al., 2001). Surprisingly, one study of the synapses of Golgi-impregnated pyramidal cell axons in the somatosensory cortex of the rhesus monkey, only found 40 % of the targets to be dendritic spines, the remainder being dendritic shafts of smooth dendritic cells, a result similar to a study of pyramidal cells in the primary visual cortex of the mouse, where only 49 % of the synaptic targets were dendritic spines, the rest suggested to originate from smooth dendrites belonging to interneurons (Bock et al., 2011). These studies and our results indicate that the proportion of dendritic spines among the synaptic

targets of the recurrent axon collaterals of pyramidal cells in the supragranular layers varies greatly between 40 and 87 % across different species, cortical areas and probably also on subtypes of pyramidal cells, being the lowest in the visual cortex of the mouse, highest in the visual cortex of the cat, and varying in between in various cortical areas in primates and human. However, this is in striking contrast with the frequency of dendritic spines among the synaptic targets of all type I (mostly glutamatergic) synapses in the supragranular layers of the prefrontal and parietal association cortex of rhesus monkeys, which was found to be as high as 95 % (Melchitzky et al., 1998). Interestingly, Bopp et al. (2014) also estimated that dendritic spines accounted for more than 90 % of the synaptic targets of type I synapses in the neuropil surrounding the labelled pyramidal cells in the mouse visual cortex, and concluded that recurrent collaterals of individual pyramidal cells preferentially innervate smooth dendritic cells, rather than forming synaptic connections randomly in the neuropil based on the relative abundance of dendritic spines of pyramidal cells and smooth dendrites of interneurons. This, however, may not be the case for the human temporal neocortex, as it was recently estimated that dendritic spines constitute ~ 62 % of the synaptic targets of type I synapses in layers II and III of the entorhinal cortex (Domínguez-Álvaro et al., 2021), and ~ 75 % in layer III of the temporal neocortex (Brodmann area 9) (Cano-Astorga et al., 2021), which is in accordance with the proportion of dendritic spine targets of the local collaterals of individual pyramidal cells found here.

Studies of functional connectivity in the neocortex indicate that local synaptic connections between neighbouring neurons are not random (Lefort et al., 2009; Song et al., 2005), but see (Packer & Yuste, 2011; Yuste, 2011). Pyramidal neurons in the primary visual cortex of mice are preferentially connected to neurons with similar response properties (Cossell et al., 2015; Iacaruso et al., 2017; Ko et al., 2011; Lee et al., 2016; Rossi et al., 2020). Furthermore, local recurrent synaptic connections of pyramidal neurons are thought to support

working memory in higher order association cortices (Mongillo et al., 2008), and feature selectivity in the primary visual cortex (Olshausen & Field, 1996; Pernice & Silveira, 2018). However, how the synaptic target preference of individual pyramidal neurons correlates with such functional connectivity, and whether the same connectivity rules apply in other species, will require further research. Our results, however, suggest that local, recurrent synaptic connections of pyramidal cells in higher order association areas of the human neocortex might follow similar rules to those in primary sensory areas of mice.

4.4 Neocortical dendritic spines are selectively targeted by GABAergic DBCs

My analysis of the distribution of DBC synapses on dendritic spines vs. shafts (chapter 3.2.1) and my estimation of the density and distribution of all GABAergic synapses on dendritic spines vs. shafts in the neuropil of layer III in the temporal and frontal neocortex (chapter 3.2.4), predicts that neocortical dendritic spines are selectively targeted by DBCs in the human neocortex.

Across the two cortical areas the average density of all synapses was $4.5 \pm 0.3 * 10^8/mm^3$ and was higher in the frontal than in the temporal association cortex. This value is lower than that found in layer III of the temporal neocortex (Cano-Astorga et al., 2021), and layer II of the transentorhinal cortex (Domínguez-Álvaro et al., 2018) by ~32 % and ~12 % respectively, but is similar to what was found in III of the entorhinal cortex in humans (Domínguez-Álvaro et al., 2021). Other studies reported higher synaptic densities in layers II and III of the middle temporal gyrus by ~62 % (Davies et al., 1987), and in layer III of the middle frontal gyrus by ~144 % (Peter R., 1979), or lower densities across all layers of Heschl's gyrus and middle frontal gyrus by ~22 and ~25 % respectively (Huttenlocher & Dabholkar, 1997) and across all layers in multiple cortical areas by ~40 % (Tang et al., 2001) in humans. In non-human species, higher total synaptic density was reported in layer III of the somatosensory cortex of rat by ~108 % (Merchán-Pérez et al., 2014), across multiple layers in the somatosensory cortex of mice by ~97 % (Kasthuri et al., 2015), in layers II and III of the visual cortex of macaques by ~18 % (Beaulieu et al., 1992), whereas lower total synaptic densities were reported in all layers of the visual cortex of the cat by ~38 % (Beaulieu & Colonnier, 1985) and the macaque by ~16 % (O'Kusky & Colonnier, 1982), and across all layers of the prefrontal cortex of rhesus monkeys by ~18 % (Bourgeois et al., 1994), and similar total synaptic densities in layers II and

III of the prefrontal cortex of rhesus monkeys (Peters et al., 2008), and primary visual cortex of macaque monkeys (Bourgeois & Rakic, 1993). Although some of these differences may reflect biological differences, it should also be noted that different microscopy and counting methods (DeFelipe, 1999; Merchán-Pérez et al., 2009) as well as differently processed samples were used in these studies. Generally, higher synaptic densities were reported from biopsy than from autopsy samples (Cano-Astorga et al., 2021). Synapse densities were smaller in Alzheimer disease samples compared to controls in some of the studies (Davies et al., 1987), but not in others (Domínguez-Álvaro et al., 2018), and density also decreased with ageing (Adams, 1987; Peter, 1979; Peters et al., 2008). Interestingly, synaptic density was also lower in the visual cortex of cats living in enriched, compared to those living in deprived environment (Beaulieu & Colonnier, 1987).

The second measurement I have taken into account is the proportion of GABAergic synapses (15 ± 2.5 %), which was lower in the temporal cortex sample by 10 % than in the frontal cortex, but on average was similar to that found in layers II and III of the visual cortex of monkeys (17.4 %; Beaulieu et al., 1992). I am unaware of any previous studies that quantified the proportion of GABAergic synapses using immunohistochemistry. Most other studies used the thickness of the postsynaptic density as observed in electron microscopic sections to differentiate type I and type II synapses, which may correspond to non-GABAergic (mostly glutamatergic) and GABAergic synapses respectively in the cortex of humans (Adams, 1987; Cano-Astorga et al., 2021; Domínguez-Álvaro et al., 2018, 2019, 2021), monkeys (Peters et al., 2008; Rakic et al., 1986), and rodents (Kasthuri et al., 2015; Merchán-Pérez et al., 2014). However, it is uncertain to what degree these qualitative features correspond to GABAergic and non-GABAergic synapses, as some monoaminergic synapses also have type I or type II characteristics, as do cholinergic synapses. Furthermore, in some cases preservation quality and unfavourable cutting angle of the synaptic junctions can render it difficult to unequivocally

differentiate type I from type II synapses. Compared to my results, the proportion of type II synapses was reported to be lower (4 – 8 %) in the somatosensory cortex of rodents (Kasthuri et al., 2015; Merchán-Pérez et al., 2014), and in the temporal neocortex (4 – 8 %) of humans (Cano-Astorga et al., 2021; Domínguez-Álvaro et al., 2018, 2021), but it was more similar (~ 13%) (Peters et al., 2008), or even higher (~ 20%) (Bourgeois et al., 1994) in the prefrontal cortex, and it was also higher in the visual cortex (Bourgeois & Rakic, 1993) of monkeys. Other studies used the shape of vesicles as a proxy for GABAergic and non-GABAergic synapses, which contain pleomorphic and round vesicles respectively (Beaulieu & Colonnier, 1985, 1987). They found that the proportion of synaptic boutons with pleomorphic vesicles was between 11 and 16 % in layers II and III of the visual cortex of monkeys. It should be noted, however that some 5 % of GABAergic boutons do not contain pleomorphic vesicles in the visual cortex of cats (Beaulieu & Somogyi, 1990).

The third factor I measured was the proportion of GABAergic synapses innervating dendritic spines (average: 16.1 ± 2%), which was lower than what was found in the visual cortex of monkeys by ~41 % (Beaulieu et al., 1992). Moreover, Beaulieu et al. (1992) also counted synapses targeting somata, thus the difference is even larger for synapses only in the neuropil. This large discrepancy may be due to genuine biological differences in the synaptic connectivity of the visual cortex and higher order temporal and frontal association areas in monkeys and humans. Unfortunately, I am unaware of data on the proportion of targets of GABAergic synapses in the human primary visual cortex. Other studies in humans found that the proportion of electron microscopically classified type II synapses innervating dendritic spines was somewhat higher (~ 19%) in layer III of the lateral temporal neocortex (Cano-Astorga et al., 2021), or lower (~ 8%) (Domínguez-Álvaro et al., 2019, 2021) in layers II and III of the entorhinal and transentorhinal cortices. Interestingly, similar proportions to our GABAergic results were reported for type II synapses innervating dendritic spines in the somatosensory

cortex of juvenile mice (Kwon et al., 2019), but a higher proportion of type II synapses were reported in the visual cortex of cats (Beaulieu & Colonnier, 1985; Beaulieu & Somogyi, 1990).

Previous studies show great variability in the distribution and proportion of proven or assumed GABAergic synapses in the neuropil of layers II and III across different species and cortical areas, as well as changes in these proportions due to ageing, environmental factors and various pathologies. However they agree in that the majority of dendritic spines are innervated by non-GABAergic synapses, most of which are glutamatergic, and that only a low proportion of GABAergic synapses (5 – 30%) innervate dendritic spines, which, considering the high density of spines, is still a very significant number. In the context of the above summary, approximately half of the synaptic targets of the GABAergic DBCs in humans being dendritic spines, similar to DBCs in cats (Tamás et al., 1997a) shows a clear bias in postsynaptic target selection. The significance of this finding is not reduced by the fact that only a small fraction of dendritic spines receive GABAergic innervation; in my samples 3.5 ± 0.7 %, in rodents ~10 % has been reported (Kubota et al., 2007). Together these results show that DBCs selectively target dendritic spines, as opposed to other postsynaptic structures, and their boutons constitute a unique population of GABAergic synaptic terminals in the neuropil.

5 Conclusions

I have identified double bouquet cells in the human neocortex as neurons in layers II and upper III with a ‘horsetail’ axon descending through several layers in a narrow cortical column, and confirmed that they express calbindin unlike putative DBCs identified in rodents (Jiang et al., 2015; Kawaguchi & Kubota, 1996, 1997; Kubota et al., 2007, 2011). Furthermore, I have demonstrated that human DBCs show distinct evoked firing patterns different from those in rodents, and that they innervate dendritic spines in a higher proportion that their proposed rodent homologues (Kubota et al., 2007). In primates, DBCs are electrophysiologically, molecularly and synaptically more similar to DBCs in humans. Taken together these unique features contribute to how DBCs functions in the brain during different behavioural states I propose that DBCs in humans and nonhuman primates should be considered a distinct cell type from those proposed previously in rodents. This is also supported by the lack of identification of DBCs as a distinct cell type in recent studies of large number of neurons in mice, using combined molecular, electrophysiological and anatomical cell typing (Gouwens et al., 2019, 2020; Peng et al., 2021).

I have found that DBCs in humans are immunohistochemically and electrophysiologically diverse, and different subtypes may be differentiated based on calbindin and calretinin content, which may correlate with differential synaptic targeting of dendritic spines and shafts. Surprisingly, a clear transcriptomic and electorphysiological identification of DBCs has not yet been achieved in humans recently (Bakken et al., 2021), although there was more focus on glutamatergic cell types than on GABAergic ones. More large scale and focused cell type-specific research is needed to elucidate the roles of these enigmatic neurons in humans.

The columnar structure of the human and primate neocortex is highlighted by the regularly spaced radial bundles of calbindin immunoreactive axons and dendrites, which consistently overlap with bundles of myelinated axons, called radial fasciculi, formed by the main descending axons of functionally related pyramidal cells located in different layers (Ballesteros Yáñez et al., 2005; DeFelipe et al., 1989a, 1990; del Río & DeFelipe, 1995; del Río & DeFelipe, 1997c). I have found that the 'horsetail' axon of calbindin immunopositive, calretinin immunopositive and CB-/CR- double immunonegative DBCs contribute to these radial bundles, and that these bundles contain the horsetail axon of more than one DBC. This means that the synaptic boutons formed by the beam of descending pyramidal cell and DBC axons are distributed in the same narrow column of cortical tissue. Furthermore, I also showed that calbindin immunopositive DBCs and pyramidal cells have the same synaptic target preference in that they innervate dendritic spines and shafts with similar probability. I hypothesise that pyramidal cells and DBCs with axon in the same radial bundle innervate the same dendritic spines. However, I could not test this hypothesis as no such pairs of pyramidal cells and DBCs were recovered in our samples, and a much more targeted double recording/labelling strategy would be required using not only two, but multiple simultaneous recording as carried out elsewhere (Jiang et al., 2015; Tamás et al., 1997a, 1997b, 1998). The results of Kubota et al. (2007) that GABAergic cells in the prefrontal cortex of rat, including DBC-like neurons with radial axon, innervate dendritic spines targeted by thalamocortical afferents, as shown by immunoreactivity to VGlut2, provides an alternative hypothesis, namely that on single dendritic spines subcortical glutamatergic and DBC boutons converge. However, this input pairing in the human association cortex is less likely as thalamocortical terminals are likely to be differently distributed from DBC terminals. On the other hand, I found that one calretinin immunopositive DBC preferentially innervated dendritic shafts of smooth dendritic cells over dendritic spines, similar to CR-expressing neurons described by others (del Río &

DeFelipe, 1997b; Meskenaite, 1997) and to some DBCs in the cat neocortex (Somogyi & Cowey, 1981). How the synaptic targets of such DBCs relate to the synaptic targets of pyramidal cells in the same radial bundle remains unknown and needs further research.

Finally, I have shown a unique facilitatory effect of group III mGluR activation on GABAergic synaptic input to DBCs, which is in contrast to effects reported in rodents and suggests human-specific network organisation. However, more cellular and pharmacological studies of DBCs and other specialised GABAergic neurons in humans are needed to elucidate the mechanisms of this effect and to uncover human-specific network organising principles. Such studies may also help to explain the effects of drugs in human health and disease.

References

Abeles, M., & Goldstein, M. H. (1970). Functional architecture in cat primary auditory cortex: columnar organization and organization according to depth. *Journal of Neurophysiology*, *33*(1), 172–187.

Acsády, L., Arabadzisz, D., & Freund, T. F. (1996a). Correlated morphological and neurochemical features identify different subsets of vasoactive intestinal polypeptide-immunoreactive interneurons in rat hippocampus. *Neuroscience*, *73*(2), 299–315.

Acsády, L., Görcs, T. J., & Freund, T. F. (1996b). Different populations of vasoactive intestinal polypeptide-immunoreactive interneurons are specialized to control pyramidal cells or interneurons in the hippocampus. *Neuroscience*, *73*(2), 317–334.

Adams, I. (1987). Comparison of synaptic changes in the precentral and postcentral cerebral cortex of aging humans: A quantitative ultrastructural study. *Neurobiology of Aging*, *8*(3), 203–212.

Ahmed, Z., Lewis, C. A., & Faber, D. S. (1990). Glutamate stimulates release of Ca2+ from internal stores in astroglia. *Brain Research*, *516*(1), 165–169.

Airaksinen, M. S., Eilers, J., Garaschuk, O., Thoenen, H., Konnerth, A., & Meyer, M. (1997). Ataxia and altered dendritic calcium signaling in mice carrying a targeted null mutation of the calbindin D28k gene. *Proceedings of the National Academy of Sciences of the United States of America*, *94*(4), 1488–1493.

Albright, T. D., Desimone, R., & Gross, C. G. (1984). Columnar organization of directionally selective cells in visual area MT of the Macaque. *Journal of Neurophysiology*, *51*(1), 16–31.

Alon, S., Goodwin, D. R., Sinha, A., Wassie, A. T., Chen, F., Daugharthy, E. R., Bando, Y., Kajita, A., Xue, A. G., Marrett, K., Prior, R., Cui, Y., Payne, A. C., Yao, C.-C., Suk, H.-J., Wang, R., Yu, C.-C. (Jay), Tillberg, P., Reginato, P., … Boyden, E. S. (2021). Expansion sequencing: Spatially precise in situ transcriptomics in intact biological systems. *Science*, *371*(6528).

Amalric, M. (2015). Targeting metabotropic glutamate receptors (mGluRs) in Parkinson's disease. *Current Opinion in Pharmacology*, *20*, 29–34.

Amalric, M., Lopez, S., Goudet, C., Fisone, G., Battaglia, G., Nicoletti, F., Pin, J. P., & Acher, F. C. (2013). Group III and subtype 4 metabotropic glutamate receptor agonists: Discovery and pathophysiological applications in Parkinson's disease. *Neuropharmacology*, *66*, 53–64.

Anderson, J. C., Douglas, R. J., Martin, K. A. C., & Nelson, J. C. (1994). Synaptic output of physiologically identified spiny stellate neurons in cat visual cortex. *Journal of Comparative Neurology*, *341*(1), 16–24.

Anderson, J. C., & Martin, K. A. C. (2009). The synaptic connections between cortical areas V1 and V2 in macaque monkey. *Journal of Neuroscience : The Official Journal of the Society for Neuroscience*, *29*(36), 11283–11293.

Andjelic, S., Gallopin, T., Cauli, B., Hill, E. L., Roux, L., Badr, S., Hu, E., Tamás, G., & Lambolez, B. (2009). Glutamatergic nonpyramidal neurons from neocortical layer VI and their comparison with pyramidal and spiny stellate neurons. *Journal of Neurophysiology*, *101*(2), 641–654.

Aramori, I., & Nakanishi, S. (1992). Signal transduction and pharmacological characteristics of a metabotropic glutamate receptor, mGluRl, in transfected CHO cells. *Neuron*, *8*(4), 757–765.

Armstrong, C., Krook-Magnuson, E., & Soltesz, I. (2012). Neurogliaform and Ivy cells: A major family of nNOS expressing GABAergic neurons. *Frontiers in Neural Circuits*, *6*, 23.

Armstrong, C., & Soltesz, I. (2012). Basket cell dichotomy in microcircuit function. *The Journal of Physiology*, *590*(4), 683–694.

Asanuma, H. (1975). Recent developments in the study of the columnar arrangement of neurons within the motor cortex. *Physiological Reviews*, *55*(2), 143–156.

Ascoli, G. A., Alonso-Nanclares, L., Anderson, S. A., Barrionuevo, G., Benavides-Piccione, R., Burkhalter, A., Buzsáki, G., Cauli, B., DeFelipe, J., Fairén, A., Feldmeyer, D., Fishell, G., Fregnac, Y., Freund, T. F., Gardner, D., Gardner, E. P., Goldberg, J. H., Helmstaedter, M., Hestrin, S., … Yuste, R. (2008). Petilla terminology: Nomenclature of features of GABAergic interneurons of the cerebral cortex. *Nature Reviews Neuroscience*, *9*(7), 557–568.

Ayala, J. E., Niswender, C. M., Luo, Q., Banko, J. L., & Conn, P. J. (2008). Group III mGluR regulation of synaptic transmission at the SC-CA1 synapse is developmentally regulated. *Neuropharmacology*, *54*(5), 804–814.

Azevedo, F. A. C., Carvalho, L. R. B., Grinberg, L. T., Farfel, J. M., Ferretti, R. E. L., Leite, R. E. P., Filho, W. J., Lent, R., & Herculano-Houzel, S. (2009). Equal numbers of neuronal and nonneuronal cells make the human brain an isometrically scaled-up primate brain. *Journal of Comparative Neurology*, *513*(5), 532–541.

Bakken, T. E., Jorstad, N. L., Hu, Q., Lake, B. B., Tian, W., Kalmbach, B. E., Crow, M., Hodge, R. D., Krienen, F. M., Sorensen, S. A., Eggermont, J., Yao, Z., Aevermann, B. D., Aldridge, A. I., Bartlett, A., Bertagnolli, D., Casper, T., Castanon, R. G., Crichton, K., … Lein, E. S. (2021). Comparative cellular analysis of motor cortex in human, marmoset and mouse. *Nature*, *598*(7879), 111–119.

Balazs, R., Bridges, R. J., Cotman, C. W., & Cotman, C. A. (2010). *Excitatory Amino Acid Transmission in Health and Disease*. Oxford University Press.

Ballesteros Yáñez, I., Muñoz, A., Contreras, J., Gonzalez, J., Rodriguez-Veiga, E., & DeFelipe, J. (2005). Double bouquet cell in the human cerebral cortex and a comparison with other mammals. *Journal of Comparative Neurology*, *486*(4), 344–360.

Baranyi, A., Szente, M. B., & Woody, C. D. (1993). Electrophysiological characterization of different types of neurons recorded in vivo in the motor cortex of the cat. II. Membrane parameters, action potentials, current-induced voltage responses and electrotonic structures. *Journal of Neurophysiology*, *69*(6), 1865–1879.

Baskys, A., & Malenka, R. C. (1991). Agonists at metabotropic glutamate receptors presynaptically inhibit EPSCs in neonatal rat hippocampus. *The Journal of Physiology*, *444*(1), 687–701.

Battaglia, G., Busceti, C. L., Molinaro, G., Biagioni, F., Traficante, A., Nicoletti, F., & Bruno, V. (2006). Pharmacological activation of mGlu4 metabotropic glutamate receptors reduces nigrostriatal degeneration in mice treated with 1-methyl-4-phenyl-1,2,3,6-tetrahydropyridine. *The Journal of Neuroscience : The Official Journal of the Society for Neuroscience*, *26*(27), 7222–7229.

Baude, A., Nusser, Z., Roberts, J. D. B., Mulvihill, E., Jeffrey Mcllhinney, R. A., & Somogyi, P. (1993). The metabotropic glutamate receptor (mGluRlα) is concentrated at perisynaptic membrane of neuronal subpopulations as detected by immunogold reaction. *Neuron*, *11*(4), 771–787.

Bayraktar, T., Welker, E., Freund, T. F., Zilles, K., & Staiger, J. F. (2000). Neurons immunoreactive for vasoactive intestinal polypeptide in the rat primary somatosensory cortex: Morphology and spatial relationship to barrel- related columns. *Journal of Comparative Neurology*, *420*(3), 291–304.

Beaulieu, C. (1993). Numerical data on neocortical neurons in adult rat, with special reference to the GABA population. *Brain Research*, *609*(1–2), 284–292.

Beaulieu, C., & Colonnier, M. (1985). A laminar analysis of the number of round-asymmetrical and flat-symmetrical synapses on spines, dendritic trunks, and cell bodies in area 17 of the cat. *Journal of Comparative Neurology*, *231*(2), 180–189.

Beaulieu, C., & Colonnier, M. (1987). Effect of the richness of the environment on the cat visual cortex. *Journal of Comparative Neurology*, *266*(4), 478–494.

Beaulieu, C., Kisvarday, Z., Somogyi, P., Cynader, M., & Cowey, A. (1992). Quantitative distribution of gaba-immunopositive and -immunonegative neurons and synapses in the monkey striate cortex (area 17). *Cerebral Cortex*, *2*(4), 295–309.

Beaulieu, C., & Somogyi, P. (1990). Targets and Quantitative Distribution of GABAergic Synapses in the Visual Cortex of the Cat. *European Journal of Neuroscience*, *2*(4), 296–303.

Beaulieu-Laroche, L., Toloza, E. H. S., van der Goes, M. S., Lafourcade, M., Barnagian, D., Williams, Z. M., Eskandar, E. N., Frosch, M. P., Cash, S. S., & Harnett, M. T. (2018). Enhanced Dendritic Compartmentalization in Human Cortical Neurons. *Cell*, *175*(3), 643-651.e14.

Belin, P., Zatorre, R. J., Lafallie, P., Ahad, P., & Pike, B. (2000). Voice-selective areas in human auditory cortex. *Nature*, *403*(6767), 309–312.

Benavides-Piccione, R., Ballesteros-Yáñez, I., DeFelipe, J., & Yuste, R. (2002). Cortical area and species differences in dendritic spine morphology. *Journal of Neurocytology*, *31*, 337–346.

Berger, T., Larkum, M. E., & Lüscher, H. R. (2001). High Ih channel density in the distal apical dendrite of layer V pyramidal cells increases bidirectional attenuation of EPSPs. *Journal of Neurophysiology*, *85*(2), 855–868.

Berg, J., Sorensen, S. A., Ting, J. T., Miller, J. A., Chartrand, T., Buchin, A., Bakken, T. E., Budzillo, A., Dee, N., Ding, S.-L., Gouwens, N. W., Hodge, R. D., Kalmbach, B., Lee, C.,

Lee, B. R., Alfiler, L., Baker, K., Barkan, E., Beller, A., … Lein, E. S. (2020). Human cortical expansion involves diversification and specialization of supragranular intratelencephalic-projecting neurons. *BioRxiv*, 2020.03.31.018820.

Bero, A. W., Meng, J., Cho, S., Shen, A. H., Canter, R. G., Ericsson, M., & Tsai, L. H. (2014). Early remodeling of the neocortex upon episodic memory encoding. *Proceedings of the National Academy of Sciences of the United States of America*, *111*(32), 11852–11857.

Bertaso, F., Lill, Y., Airas, J. M., Espeut, J., Blahos, J., Bockaert, J., Fagni, L., Betz, H., & el Far, O. (2006). MacMARCKS interacts with the metabotropic glutamate receptor type 7 and modulates G protein-mediated constitutive inhibition of calcium channels. *Journal of Neurochemistry*, *99*(1), 288–298.

Betts, M. J., O'Neill, M. J., & Duty, S. (2012). Allosteric modulation of the group III mGlu4 receptor provides functional neuroprotection in the 6-hydroxydopamine rat model of Parkinson's disease. *British Journal of Pharmacology*, *166*(8), 2317–2330.

Beurrier, C., Lopez, S., Révy, D., Selvam, C., Goudet, C., Lhérondel, M., Gubellini, P., Kerkerian-LeGoff, L., Acher, F., Pin, J.-P., & Amalric, M. (2009). Electrophysiological and behavioral evidence that modulation of metabotropic glutamate receptor 4 with a new agonist reverses experimental parkinsonism. *The FASEB Journal*, *23*(10), 3619–3628.

Binder, J. R., Frost, J. A., Hammeke, T. A., Cox, R. W., Rao, S. M., & Prieto, T. (1997). Human brain language areas identified by functional magnetic resonance imaging. *Journal of Neuroscience : The official journal of the Society for Neuroscience*, *17*(1), 353–362.

Blasdel, G. G., & Lund, J. S. (1983). Termination of afferent axons in macaque striate cortex. *Journal of Neuroscience : The official journal of the Society for Neuroscience*, *3*(7), 1389–1413.

Blatow, M., Caputi, A., Burnashev, N., Monyer, H., & Rozov, A. (2003). Ca2+ buffer saturation underlies paired pulse facilitation in calbindin-D28k-containing terminals. *Neuron*, *38*(1), 79–88.

Bliss, T. V. P., & Collingridge, G. L. (1993). A synaptic model of memory: Long-term potentiation in the hippocampus. *Nature*, *361*(6407), 31–39.

Bloodgood, B. L., & Sabatini, B. L. (2005). Neuronal activity regulates diffusion across the neck of dendritic spines. *Science*, *310*(5749), 866–869.

Bocchio, M., Lukacs, I. P., Stacey, R., Plaha, P., Apostolopoulos, V., Livermore, L., Sen, A., Ansorge, O., Gillies, M. J., Somogyi, P., & Capogna, M. (2019). Group II metabotropic glutamate receptors mediate presynaptic inhibition of excitatory transmission in pyramidal neurons of the human cerebral cortex. *Frontiers in Cellular Neuroscience*, *12*, 508.

Bock, D. D., Lee, W.-C. A., Kerlin, A. M., Andermann, M. L., Hood, G., Wetzel, A. W., Yurgenson, S., Soucy, E. R., Kim, H. S., & Reid, R. C. (2011). Network anatomy and in vivo physiology of visual cortical neurons. *Nature*, *471*(7337), 177–182.

Boldog, E., Bakken, T. E., Hodge, R. D., Novotny, M., Aevermann, B. D., Baka, J., Bordé, S., Close, J. L., Diez-Fuertes, F., Ding, S. L., Faragó, N., Kocsis, Á. K., Kovács, B., Maltzer, Z., McCorrison, J. M., Miller, J. A., Molnár, G., Oláh, G., Ozsvár, A., … Tamás, G. (2018). Transcriptomic and morphophysiological evidence for a specialized human cortical GABAergic cell type. *Nature Neuroscience*, *21*(9), 1185–1195.

Bonci, A., Grillner, P., Siniscalchi, A., Mercuri, N. B., & Bernardi, G. (1997). Glutamate Metabotropic Receptor Agonists Depress Excitatory and Inhibitory Transmission on Rat Mesencephalic Principal Neurons. *European Journal of Neuroscience*, *9*(11), 2359–2369.

Bopp, R., Maçarico da Costa, N., Kampa, B. M., Martin, K. A. C., & Roth, M. M. (2014). Pyramidal Cells Make Specific Connections onto Smooth (GABAergic) Neurons in Mouse Visual Cortex. *PLoS Biology*, *12*(8), e1001932.

Boss, V., Nutt, K. M., & Conn, P. J. (1994). L-cysteine sulfinic acid as an endogenous agonist of a novel metabotropic receptor coupled to stimulation of phospholipase D activity. *Molecular Pharmacology*, *45*(6), 1177–1182.

Bourgeois, J. P., Goldman-Rakic, P. S., & Rakic, P. (1994). Synaptogenesis in the prefrontal cortex of rhesus monkeys. *Cerebral Cortex*, *4*(1), 78–96.

Bourgeois, J. P., & Rakic, P. (1993). Changes of synaptic density in the primary visual cortex of the macaque monkey from fetal to adult stage. *Journal of Neuroscience : The official journal of the Society for Neuroscience*, *13*(7), 2801–2820.

Bradley, S. R., Levey, A. I., Hersch, S. M., & Conn, P. J. (1996). Immunocytochemical localization of group III metabotropic glutamate receptors in the hippocampus with subtype-specific antibodies. *Journal of Neuroscience : The official journal of the Society for Neuroscience*, *16*(6), 2044–2056.

Bradley, S. R., Rees, H. D., Yi, H., Levey, A. I., & Conn, P. J. (1998). Distribution and developmental regulation of metabotropic glutamate receptor 7a in rat brain. *Journal of Neurochemistry*, *71*(2), 636–645.

Brett, M., Johnsrude, I. S., & Owen, A. M. (2002). The problem of functional localization in the human brain. *Nature Reviews Neuroscience*, *3*(3), 243–249.

Broca, M. P. (1861). Remarques sur le siège de la faculté du langage articulé; suivies d'une observation d'aphemie. *Bulletin de La Société Anatomique*, *6*, 330–357.

Brodmann, K. (1909). *Vergleichende lokalisationslehre der großhirnrinde in ihren prinzipien dargestellt auf grund des zellenbaues*. Barth, Leipzig.

Brown-Séquard, C. É. (1877). Aphasia as an effect of brain-disease. *The Dublin Journal of Medical Science*, *63*(3), 209–225.

Bugbee, N. M., & Goldman-Rakic, P. S. (1983). Columnar organization of corticocortical projections in squirrel and rhesus monkeys: Similarity of column width in species differing in cortical volume. *Journal of Comparative Neurology*, *220*(3), 355–364.

Buxhoeveden, D. P., & Casanova, M. F. (2002). The minicolumn hypothesis in neuroscience. *Brain*, *125*(5), 935–951.

Callaway, E. M., Dong, H.-W., Ecker, J. R., Hawrylycz, M. J., Huang, Z. J., Lein, E. S., Ngai, J., Osten, P., Ren, B., Tolias, A. S., White, O., Zeng, H., Zhuang, X., Ascoli, G. A., Behrens, M. M., Chun, J., Feng, G., Gee, J. C., Ghosh, S. S., … Sunkin, S. (2021). A multimodal cell census and atlas of the mammalian primary motor cortex. *Nature*, *598*(7879), 86–102.

Calò, L., Bruno, V., Spinsanti, P., Molinari, G., Korkhov, V., Esposito, Z., Patanè, M., Melchiorri, D., Freissmuth, M., & Nicoletti, F. (2005). Interactions between ephrin-B and

metabotropic glutamate 1 receptors in brain tissue and cultured neurons. *Journal of Neuroscience*, *25*(9), 2245–2254.

Cano-Astorga, N., DeFelipe, J., & Alonso-Nanclares, L. (2021). Three-Dimensional Synaptic Organization of Layer III of the Human Temporal Neocortex. *Cerebral Cortex*, *31*(10), 4742–4764.

Capogna, M. (2004). Distinct properties of presynaptic group II and III metabotropic glutamate receptor-mediated inhibition of perforant pathway-CA1 EPSCs. *European Journal of Neuroscience*, *19*(10), 2847–2858.

Caputi, A., Rozov, A., Blatow, M., & Monyer, H. (2009). Two calretinin-positive gabaergic cell types in layer 2/3 of the mouse neocortex provide different forms of inhibition. *Cerebral Cortex*, *19*(6), 1345–1359.

Carmichael, S. T., & Price, J. L. (1994). Architectonic subdivision of the orbital and medial prefrontal cortex in the macaque monkey. *Journal of Comparative Neurology*, *346*(3), 366–402.

Carmichael, S. T., & Price, J. L. (1996). Connectional networks within the orbital and medial prefrontal cortex of macaque monkeys. *Journal of Comparative Neurology*, *371*(2), 179–207.

Cartmell, J., & Schoepp, D. D. (2000). Regulation of neurotransmitter release by metabotropic glutamate receptors. *Journal of Neurochemistry*, *75*(3), 889–907.

Casanova, M. F., & Casanova, E. L. (2019). The modular organization of the cerebral cortex: Evolutionary significance and possible links to neurodevelopmental conditions. *Journal of Comparative Neurology*, *527*(10), 1720–1730.

Catani, M., & Ffytche, D. H. (2005). The rises and falls of disconnection syndromes. *Brain*, *128*(10), 2224–2239.

Cauli, B., Audinat, E., Lambolez, B., Angulo, M. C., Ropert, N., Tsuzuki, K., Hestrin, S., & Rossier, J. (1997). Molecular and Physiological Diversity of Cortical Nonpyramidal Cells. *Journal of Neuroscience : The official journal of the Society for Neuroscience*, *17*(10), 3894–3906.

Cauli, B., Porter, J. T., Tsuzuki, K., Lambolez, B., Rossier, J., Quenet, B., & Audinat, E. (2000). Classification of fusiform neocortical interneurons based on unsupervised clustering. *Proceedings of the National Academy of Sciences of the United States of America*, *97*(11), 6144–6149.

Celio, M. R., Baier, W., Schärer, L., De Viragh, P. A., & Gerday, C. (1988). Monoclonal antibodies directed against the calcium binding protein parvalbumin. *Cell Calcium*, *9*(2), 81–86.

Chapman, A. G., Talebi, A., Yip, P. K., & Meldrum, B. S. (2001). Anticonvulsant activity of a mGlu4α receptor selective agonist, (1S,3R,4S)-1-aminocyclopentane-1,2,4-tricarboxylic acid. *European Journal of Pharmacology*, *424*(2), 107–113.

Charvin, D. (2018). mGlu4 allosteric modulation for treating Parkinson's disease. *Neuropharmacology*, *135*, 308–315.

Charvin, D., di Paolo, T., Bezard, E., Gregoire, L., Takano, A., Duvey, G., Pioli, E., Halldin, C., Medori, R., & Conquet, F. (2018). An mGlu4-Positive Allosteric Modulator Alleviates Parkinsonism in Primates. *Movement Disorders*, *33*(10), 1619–1631.

Charvin, D., Pomel, V., Ortiz, M., Frauli, M., Scheffler, S., Steinberg, E., Baron, L., Deshons, L., Rudigier, R., Thiarc, D., Morice, C., Manteau, B., Mayer, S., Graham, D., Giethlen, B., Brugger, N., Hédou, G., Conquet, F., & Schann, S. (2017). Discovery, Structure-Activity Relationship, and Antiparkinsonian Effect of a Potent and Brain-Penetrant Chemical Series of Positive Allosteric Modulators of Metabotropic Glutamate Receptor 4. *Journal of Medicinal Chemistry*, *60*(20), 8515–8537.

Chiu, C. Q., Lur, G., Morse, T. M., Carnevale, N. T., Ellis-Davies, G. C. R., & Higley, M. J. (2013). Compartmentalization of GABAergic inhibition by dendritic spines. *Science*, *340*(6133), 759–762.

Choi, S., & Lovinger, D. M. (1996). Metabotropic glutamate receptor modulation of voltage-gated Ca2+ channels involves multiple receptor subtypes in cortical neurons. *Journal of Neuroscience : The official journal of the Society for Neuroscience*, *16*(1), 36–45.

Chu, Z., & Moenter, S. M. (2005). Endogenous Activation of Metabotropic Glutamate Receptors Modulates GABAergic Transmission to Gonadotropin-Releasing Hormone Neurons and Alters Their Firing Rate: A Possible Local Feedback Circuit. *Journal of Neuroscience : The official journal of the Society for Neuroscience*, *25*(24), 5740–5749.

Clark, D. A., Mitra, P. P., & Wang, S. S. H. (2001). Scalable architecture in mammalian brains. *Nature*, *411*(6834), 189–193.

Cobb, S. R., Buhl, E. H., Halasy, K., Paulsen, O., & Somogyi, P. (1995). Synchronizartion of Neuronal Actrivity in Hippocampus By Individual GABAergic Interneurons. *Nature*, *378*(6552), 75-78.

Cochilla, A. J., & Alford, S. (1998). Metabotropic glutamate receptor-mediated control of neurotransmitter release. *Neuron*, *20*(5), 1007–1016.

Colonnier, M. (1968). Synaptic patterns on different cell types in the different laminae of the cat visual cortex. An electron microscope study. *Brain Research*, *9*(2), 268–287.

Condé, F., Lund, J. S., Jacobowitz, D. M., Baimbridge, K. G., & Lewis, D. A. (1994). Local circuit neurons immunoreactive for calretinin, calbindin D-28k or parvalbumin in monkey prefronatal cortex: Distribution and morphology. *Journal of Comparative Neurology*, *341*(1), 95–116.

Connors, B. W., & Gutnick, M. J. (1990). Intrinsic firing patterns of diverse neocortical neurons. *Trends in Neurosciences*, *13*(3), 99–104.

Conn, P. J., & Pin, J. P. (1997). Pharmacology and functions of metabotropic glutamate receptors. *Annual Review of Pharmacology and Toxicology*, *37*(1), 205–237.

Constantinidis, C., Funahashi, S., Lee, D., Murray, J. D., Qi, X.-L., Wang, M., & Arnsten, A. F. T. (2018). Persistent Spiking Activity Underlies Working Memory. *The Journal of Neuroscience : The official journal of the Society for Neuroscience, 38*(32), 7020–7028.

Corti, C., Aldegheri, L., Somogyi, P., & Ferraguti, F. (2002). Distribution and synaptic localisation of the metabotropic glutamate receptor 4 (mGluR4) in the rodent CNS. *Neuroscience*, *110*(3), 403–420.

Corti, C., Restituito, S., Rimland, J. M., Brabet, I., Corsi, M., Pin, J. P., & Ferraguti, F. (1998). Cloning and characterization of alternative mRNA forms for the rat metabotropic glutamate receptors mGluR7 and mGluR8. *European Journal of Neuroscience*, *10*(12), 3629–3641.

Cossell, L., Iacaruso, M. F., Muir, D. R., Houlton, R., Sader, E. N., Ko, H., Hofer, S. B., & Mrsic-Flogel, T. D. (2015). Functional organization of excitatory synaptic strength in primary visual cortex. *Nature*, *518*(7539), 399–403.

Cryan, J. F., Kelly, P. H., Neijt, H. C., Sansig, G., Flor, P. J., & van der Putten, H. (2003a). Antidepressant and anxiolytic-like effects in mice lacking the group III metabotropic glutamate receptor mGluR7. *European Journal of Neuroscience*, *17*(11), 2409–2417.

Cryan, J. F., Kelly, P. H., Neijt, H. C., Sansig, G., Flor, P. J., & van der Putten, H. (2003b). Antidepressant and anxiolytic-like effects in mice lacking the group III metabotropic glutamate receptor mGluR7. *European Journal of Neuroscience*, *17*(11), 2409–2417.

Cuomo, D., Martella, G., Barabino, E., Platania, P., Vita, D., Madeo, G., Selvam, C., Goudet, C., Oueslati, N., Pin, J.-P., Acher, F., Pisani, A., Beurrier, C., Melon, C., Goff, L. K.-L., & Gubellini, P. (2009). Metabotropic glutamate receptor subtype 4 selectively modulates both glutamate and GABA transmission in the striatum: implications for Parkinson's disease treatment. *Journal of Neurochemistry*, *109*(4), 1096–1105.

Dalezios, Y., Luján, R., Shigemoto, R., Roberts, J. D. B., & Somogyi, P. (2002). Enrichment of mGluR7a in the presynaptic active zones of GABAergic and non-GABAergic terminals on interneurons in the rat somatosensory cortex. *Cerebral Cortex*, *12*(9), 961–974.

Dammann, F., Kirschstein, T., Guli, X., Müller, S., Porath, K., Rohde, M., Tokay, T., & Köhling, R. (2018). Bidirectional shift of group III metabotropic glutamate receptor-mediated synaptic depression in the epileptic hippocampus. *Epilepsy Research*, *139*, 157–163.

Dávid, C., Schleicher, A., Zuschratter, W., & Staiger, J. F. (2007). The innervation of parvalbumin-containing interneurons by VIP-immunopositive interneurons in the primary somatosensory cortex of the adult rat. *European Journal of Neuroscience*, *25*(8), 2329–2340.

Davies, C. A., Mann, D. M. A., Sumpter, P. Q., & Yates, P. O. (1987). A quantitative morphometric analysis of the neuronal and synaptic content of the frontal and temporal cortex in patients with Alzheimer's disease. *Journal of the Neurological Sciences*, *78*(2), 151–164.

de Carlos, J. A., López-Mascaraque, L., Cajal-Agüeras, S. R., & Valverde, F. (1987). Chandelier cells in the auditory cortex of monkey and man: a Golgi study. *Experimental Brain Research*, *66*(2), 295–302.

DeFelipe, J., Marco, P., Busturia, I., Merchán-Pérez, A. (1999). Estimation of the number of synapses in the cerebral cortex: Methodological considerations. *Cerebral Cortex*, *9*(7), 722–732.

DeFelipe, J. (2011). The evolution of the brain, the human nature of cortical circuits, and intellectual creativity. *Frontiers in Neuroanatomy*, *5*, 29.

DeFelipe, J. (2002). Cortical interneurons: From Cajal to 2001. *Progress in Brain Research*, *136*, 215–238.

DeFelipe, J., Alonso-Nanclares, L., & Arellano, J. I. (2002). Microstructure of the neocortex: Comparative aspects. *Journal of Neurocytology*, *31*(3), 299–316.

DeFelipe, J., Ballesteros-Yáñez, I., Inda, M. C., & Muñoz, A. (2006). Double-bouquet cells in the monkey and human cerebral cortex with special reference to areas 17 and 18. *Progress in brain research*, *154*, *15-32*.

DeFelipe, J., & Fairén, A. (1982). A type of basket cell in superficial layers of the cat visual cortex. A Golgi-electron microscope study. *Brain Research*, *244*(1), 9–16.

DeFelipe, J., & Fairén, A. (1988). Synaptic connections of an interneuron with axonal arcades in the cat visual cortex. *Journal of Neurocytology*, *17*(3), 313–323.

DeFelipe, J., González-Albo, M. C., del Río, M. R., & Elston, G. N. (1999). Distribution and patterns of connectivity of interneurons containing calbindin, calretinin, and parvalbumin in visual areas of the occipital and temporal lobes of the macaque monkey. *Journal of Comparative Neurology*, *412*(3), 515–526.

DeFelipe, J., Hendry, S. H. C., Hashikawa, T., Molinari, M., & Jones, E. G. (1990). A microcolumnar structure of monkey cerebral cortex revealed by immunocytochemical studies of double bouquet cell axons. *Neuroscience*, *37*(3), 655–673.

DeFelipe, J., Hendry, S. H. C., & Jones, E. G. (1986). A correlative electron microscopic study of basket cells and large gabaergic neurons in the monkey sensory-motor cortex. *Neuroscience*, *17*(4), 991–1009.

DeFelipe, J., Hendry, S. H. C., & Jones, E. G. (1989a). Synapses of double bouquet cells in monkey cerebral cortex visualized by calbindin immunoreactivity. *Brain Research*, *503*(1), 49–54.

DeFelipe, J., Hendry, S. H., & Jones, E. G. (1989b). Visualization of chandelier cell axons by parvalbumin immunoreactivity in monkey cerebral cortex. *Proceedings of the National Academy of Sciences*, *86*(6), 2093–2097.

DeFelipe, J., & Jones, E. G. (1992). High-Resolution Light and Electron Microscopic Immunocytochemistry of Colocalized GABA and Calbindin D-28k in Somata and Double Bouquet Cell Axons of Monkey Somatosensory Cortex. *European Journal of Neuroscience*, *4*(1), 46–60.

DeFelipe, J., López-Cruz, P. L., Benavides-Piccione, R., Bielza, C., Larrañaga, P., Anderson, S., Burkhalter, A., Cauli, B., Fairén, A., Feldmeyer, D., Fishell, G., Fitzpatrick, D., Freund, T. F., González-Burgos, G., Hestrin, S., Hill, S., Hof, P. R., Huang, J., Jones, E. G., … Ascoli, G. A. (2013). New insights into the classification and nomenclature of cortical GABAergic interneurons. *Nature Reviews Neuroscience*, *14*(3), 202–216.

del Río, M. R., & DeFelipe, J. (1995). A light and electron microscopic study of calbindin D-28k immunoreactive double bouquet cells in the human temporal cortex. *Brain Research*, *690*(1), 133–140.

del Río, M. R., & DeFelipe, J. (1996). Colocalization of calbindin D-28k, calretinin, and GABA immunoreactivities in neurons of the human temporal cortex. *Journal of Comparative Neurology*, *369*(3), 472–482.

del Río, M. R., & DeFelipe, J. (1997a). Colocalization of parvalbumin and calbindin D-28k in neurons including chandelier cells of the human temporal neocortex. *Journal of Chemical Neuroanatomy*, *12*(3), 165–173.

del Río, M. R., & DeFelipe, J. (1997b). Synaptic connections of calretinin-immunoreactive neurons in the human neocortex. *Journal of Neuroscience : The official journal of the Society for Neuroscience*, *17*(13), 5143–5154.

del Río, M. R., & DeFelipe, J. (1997c). Double bouquet cell axons in the human temporal neocortex: Relationship to bundles of myelinated axons and colocalization of calretinin and calbindin D-28k immunoreactivities. *Journal of Chemical Neuroanatomy*, *13*(4), 243–251.

Demeulemeester, H., Arckens, L., Vandesande, F., Orban, G., Heizmann, C., & Pochet, R. (1991). Calcium binding proteins and neuropeptides as molecular markers of GABAergic interneurons in the cat visual cortex. *Experimental Brain Research*, *84*(3), 538–544.

Demeulemeester, H., Vandesande, F., Orban, G., Brandon, C., & Vanderhaeghen, J. (1988). Heterogeneity of GABAergic cells in cat visual cortex. *Journal of Neuroscience : The official journal of the Society for Neuroscience*, *8*(3), 988–1000.

de Sarro, G., Chimirri, A., & Meldrum, B. S. (2002). Group III mGlu receptor agonists potentiate the anticonvulsant effect of AMPA and NMDA receptor block. *European Journal of Pharmacology*, *451*(1), 55–61.

Deutch, A. Y. (2013). Neurotransmitters. In *Fundamental Neuroscience* (4th ed., pp. 117–138). Academic Press.

de Winter, W., & Oxnard, C. E. (2001). Evolutionary radiations and convergences in the structural organization of mammalian brains. *Nature*, *409*(6821), 710–714.

Dickinson, M. E., Bearman, G., Tille, S., Lansford, R., & Fraser, S. E. (2001). Multi-spectral imaging and linear unmixing add a whole new dimension to laser scanning fluorescence microscopy. *BioTechniques*, *31*(6), 1272–1278.

Dietrich, D. (1999). Reduced function of L-AP4-sensitive metabotropic gjutamate receptors in human epileptic sclerotic hippocampus. *European Journal of Neuroscience*, *11*(3), 1109–1113.

Disbrow, E., Roberts, T., & Krubitzer, L. (2000). Somatotopic organization of cortical fields in the lateral sulcus of Homo sapiens: Evidence for SII and PV. *Journal of Comparative Neurology*, *418*(1), 1–21.

Doi, A., Ishibashi, H., Jinno, S., Kosaka, T., & Akaike, N. (2002). Presynaptic inhibition of GABAergic miniature currents by metabotropic glutamate receptor in the rat CNS. *Neuroscience*, *109*(2), 299–311.

Doller, D., Bespalov, A., Miller, R., Pietraszek, M., & Kalinichev, M. (2020). A case study of foliglurax, the first clinical mGluR4 PAM for symptomatic treatment of Parkinson's disease: translational gaps or a failing industry innovation model? *Expert Opinion on Investigational Drugs*, *29*(12), 1323–1338.

Domínguez-Álvaro, M., Montero-Crespo, M., Blazquez-Llorca, L., DeFelipe, J., & Alonso-Nanclares, L. (2019). 3D electron microscopy study of synaptic organization of the normal human transentorhinal cortex and its possible alterations in alzheimer's disease. *ENeuro*, *6*(4), 1–17.

Domínguez-Álvaro, M., Montero-Crespo, M., Blazquez-Llorca, L., DeFelipe, J., & Alonso-Nanclares, L. (2021). 3D Ultrastructural Study of Synapses in the Human Entorhinal Cortex. *Cerebral Cortex*, *31*(1), 410–425.

Domínguez-Álvaro, M., Montero-Crespo, M., Blazquez-Llorca, L., Insausti, R., DeFelipe, J., & Alonso-Nanclares, L. (2018). Three-dimensional analysis of synapses in the transentorhinal cortex of Alzheimer's disease patients. *Acta Neuropathologica Communications*, *6*(1), 20.

Doumazane, E., Scholler, P., Zwier, J. M., Trinquet, E., Rondard, P., & Pin, J. (2011). A new approach to analyze cell surface protein complexes reveals specific heterodimeric metabotropic glutamate receptors. *The FASEB Journal*, *25*(1), 66–77.

Drew, G. M., & Vaughan, C. W. (2004). Multiple metabotropic glutamate receptor subtypes modulate GABAergic neurotransmission in rat periaqueductal grey neurons in vitro. *Neuropharmacology*, *46*(7), 927–934.

Dudok, B., Barna, L., Ledri, M., Szabó, S. I., Szabadits, E., Pintér, B., Woodhams, S. G., Henstridge, C. M., Balla, G. Y., Nyilas, R., Varga, C., Lee, S. H., Matolcsi, M., Cervenak, J., Kacskovics, I., Watanabe, M., Sagheddu, C., Melis, M., Pistis, M., … Katona, I. (2015). Cell-specific STORM super-resolution imaging reveals nanoscale organization of cannabinoid signaling. *Nature Neuroscience*, *18*(1), 75–86.

East, S. J., Hill, M. P., & Brotchie, J. M. (1995). Metabotropic glutamate receptor agonists inhibit endogenous glutamate release from rat striatal synaptosomes. *European Journal of Pharmacology*, *277*(1), 117–121.

Edwards, F. A., Konnerth, A., & Sakmann, B. (1990). Quantal analysis of inhibitory synaptic transmission in the dentate gyrus of rat hippocampal slices: a patch-clamp study. *The Journal of Physiology*, *430*(1), 213–249.

Ekstrand, J. J., Domroese, M. E., Feig, S. L., Illig, K. R., & Haberly, L. B. (2001). Immunocytochemical analysis of basket cells in rat piriform cortex. *The Journal of Comparative Neurology*, *434*(3), 308–328.

Elston, G. N., Benavides-Piccione, R., & DeFelipe, J. (2001). The pyramidal cell in cognition: a comparative study in human and monkey. In *The Journal of neuroscience : The official journal of the Society for Neuroscience*, *21*(17), RC163.

Erdmann, E., Rupprecht, V., Matthews, E., Kukley, M., Schoch, S., & Dietrich, D. (2012). Depression of release by mGluR8 Alters Ca 2+ dependence of release machinery. *Cerebral Cortex*, *22*(7), 1498–1509.

Erisir, A., Lau, D., Rudy, B., & Leonard, C. S. (1999). Function of specific K+ channels in sustained high-frequency firing of fast-spiking neocortical interneurons. *Journal of Neurophysiology*, *82*(5), 2476–2489.

Evans, D. I., Jones, R. S. G., & Woodhall, G. (2000). Activation of presynaptic group III metabotropic receptors enhances glutamate release in rat entorhinal cortex. *Journal of Neurophysiology*, *83*(5), 2519–2525.

Eyal, G., Verhoog, M. B., Testa-Silva, G., Deitcher, Y., Lodder, J. C., Benavides-Piccione, R., Morales, J., DeFelipe, J., de Kock, C. P. J., Mansvelder, H. D., & Segev, I. (2016). Unique membrane properties and enhanced signal processing in human neocortical neurons. *ELife*, *5*, 316553.

Faber, E. S. L., Callister, R. J., & Sah, P. (2001). Morphological and electrophysiological properties of principal neurons in the rat lateral amygdala in vitro. *Journal of Neurophysiology*, *85*(2), 714–723.

Louise Faber, E. S., & Sah, P. (2003). Calcium-activated potassium channels: Multiple contributions to neuronal function. *Neuroscientist*, *9*(3), 181–194.

Fairén, A., & Valverde, F. (1980). A specialized type of neuron in the visual cortex of cat: A Golgi and electron microscope study of chandelier cells. *Journal of Comparative Neurology*, *194*(4), 761–779.

Fallarino, F., Volpi, C., Fazio, F., Notartomaso, S., Vacca, C., Busceti, C., Bicciato, S., Battaglia, G., Bruno, V., Puccetti, P., Fioretti, M. C., Nicoletti, F., Grohmann, U., & di Marco, R. (2010). Metabotropic glutamate receptor-4 modulates adaptive immunity and restrains neuroinflammation. *Nature Medicine*, *16*(8), 897–902.

Far, O. el, Airas, J., Wischmeyer, E., Nehring, R. B., Karschin, A., & Betz, H. (2000). Interaction of the C-terminal tail region of the metabotropic glutamate receptor 7 with the protein kinase C substrate PICK1. *European Journal of Neuroscience*, *12*(12), 4215–4221.

Farrant, M., & Kaila, K. (2007). The cellular, molecular and ionic basis of GABAA receptor signalling. *Progress in Brain Research*, *160*, 59–87.

Farrant, M., & Nusser, Z. (2005). Variations on an inhibitory theme: Phasic and tonic activation of GABA A receptors. *Nature Reviews Neuroscience*, *6*(3), 215–229.

Fayyad, J., Sampson, N. A., Hwang, I., Adamowski, T., Aguilar-Gaxiola, S., Al-Hamzawi, A., Andrade, L. H. S. G., Borges, G., de Girolamo, G., Florescu, S., Gureje, O., Haro, J. M., Hu, C., Karam, E. G., Lee, S., Navarro-Mateu, F., O'Neill, S., Pennell, B. E., Piazza, M., … Wojtyniak, B. (2017). The descriptive epidemiology of DSM-IV Adult ADHD in the World Health Organization World Mental Health Surveys. *ADHD Attention Deficit and Hyperactivity Disorders*, *9*(1), 47–65.

Feldman, M. L., & Peters, A. (1978). The forms of non-pyramidal neurons in the visual cortex of the rat. *Journal of Comparative Neurology*, *179*(4), 761–793.

Fendt, M., Imobersteg, S., Peterlik, D., Chaperon, F., Mattes, C., Wittmann, C., Olpe, H. R., Mosbacher, J., Vranesic, I., van der Putten, H., McAllister, K. H., Flor, P. J., & Gee, C. E. (2013). Differential roles of mGlu7 and mGlu8 in amygdala-dependent behavior and physiology. *Neuropharmacology*, *72*, 215–223.

Férézou, I., Cauli, B., Hill, E. L., Rossier, J., Hamel, E., & Lambolez, B. (2002). 5-HT3 receptors mediate serotonergic fast synaptic excitation of neocortical vasoactive intestinal peptide/cholecystokinin interneurons. *Journal of Neuroscience: The Official Journal of the Society for Neuroscience*, *22*(17), 7389–7397.

Ferraguti, F. (2018). Metabotropic glutamate receptors as targets for novel anxiolytics. *Current Opinion in Pharmacology*, *38*, 37–42.

Ferraguti, F., Klausberger, T., Cobden, P., Baude, A., Roberts, J. D. B., Szucs, P., Kinoshita, A., Shigemoto, R., Somogyi, P., & Dalezios, Y. (2005). Metabotropic glutamate receptor 8-expressing nerve terminals target subsets of GABAergic neurons in the hippocampus. *The Journal of Neuroscience : The Official Journal of the Society for Neuroscience*, *25*(45), 10520–10536.

Ferraguti, F., & Shigemoto, R. (2006). Metabotropic glutamate receptors. *Cell and Tissue Research*, *326*(2), 483–504.

Ferrer, I., Tuñón, T., Soriano, E., del Rio, A., Iraizoz, I., Fonseca, M., & Guionnet, N. (1992). Calbindin immunoreactivity in normal human temporal neocortex. *Brain Research*, *572*(1–2), 33–41.

Ferrier, D., & Yeo, G. (1884). A record of experiments on the effects of lesion of different regions of the cerebral hemispheres. *Philosophical Transactions of the Royal Society of London*, *175*, 479–564.

Ferstl, E. C., & von Cramon, D. Y. (2002). What does the frontomedian cortex contribute to language processing: Coherence or theory of mind? *NeuroImage*, *17*(3), 1599–1612.

Field, M., Lukacs, I. P., Hunter, E., Stacey, R., Plaha, P., Livermore, L., Ansorge, O., & Somogyi, P. (2021). Tonic GABA A receptor mediated currents of human cortical GABAergic interneurons vary amongst cell types. *The Journal of Neuroscience: The Official Journal of the Society for Neuroscience*, *41*(47), 9702-9719.

Finger, S. (1994). *Origins of Neuroscience* . Oxford University Press.

Fink, G. R., Frackowiak, R. S. J., Pietrzyk, U., & Passingham, R. E. (1997). Multiple nonprimary motor areas in the human cortex. *Journal of Neurophysiology*, *77*(4), 2164–2174.

Fishell, G., Mason, C. A., & Hatten, M. E. (1993). Dispersion of neural progenitors within the germinal zones of the forebrain. *Nature*, *362*(6421), 636–638.

Flajolet, M., Rakhilin, S., Wang, H., Starkova, N., Nuangchamnong, N., Nairn, A. C., & Greengard, P. (2003). Protein phosphatase 2C binds selectively to and dephosphorylates metabotropic glutamate receptor 3. *Proceedings of the National Academy of Sciences of the United States of America*, *100*(26), 16006–16011.

Fleischhauer, K., Petsche, H., & Wittkowski, W. (1972). Vertical bundles of dendrites in the neocortex. *Zeitschrift Für Anatomie Und Entwicklungsgeschichte*, *136*(2), 213–223.

Foerster, O. (1936). Motorische felder und bahnen. In O. Bumke & O. Foerster (Eds.), *Handbuch der Neurologie*, *Band VI* (pp. 1–448). Springer.

Folbergrová, J., Druga, R., Haugvicová, R., Mareš, P., & Otáhal, J. (2008). Anticonvulsant and neuroprotective effect of (S)-3,4-dicarboxyphenylglycine against seizures induced in immature rats by homocysteic acid. *Neuropharmacology*, *54*(4), 665–675.

Folbergrová, J., Haugvicová, R., & Mareš, P. (2001). Attenuation of seizures induced by homocysteic acid in immature rats by metabotropic glutamate group II and group III receptor agonists. *Brain Research*, *908*(2), 120–129.

Folbergrová, J., Haugvicová, R., & Mareš, P. (2003). Seizures induced by homocysteic acid in immature rats are prevented by group III metabotropic glutamate receptoragonist (R,S)-4-phosphonophenylglycine. *Experimental Neurology*, *180*(1), 46–54.

Fonseca, M., & Soriano, E. (1995). Calretinin-immunoreactive neurons in the normal human temporal cortex and in Alzheimer's disease. *Brain Research*, *691*(1–2), 83–91.

Freund, T. F., Maglóczky, Z., Soltész, I., & Somogyi, P. (1986). Synaptic connections, axonal and dendritic patterns of neurons immunoreactive for cholecystokinin in the visual cortex of the cat. *Neuroscience*, *19*(4), 1133–1159.

Freund, T. F., Martin, K. A. C., Soltesz, I., Somogyi, P., & Whitteridge, D. (1989). Arborisation pattern and postsynaptic targets of physiologically identified thalamocortical afferents in striate cortex of the macaque monkey. *Journal of Comparative Neurology*, *289*(2), 315–336.

Freund, T. F., Martin, K. A., Smith, A. D., & Somogyi, P. (1983). Glutamate decarboxylase-immunoreactive terminals of Golgi-impregnated axoaxonic cells and of presumed basket cells in synaptic contact with pyramidal neurons of the cat's visual cortex. *The Journal of Comparative Neurology*, *221*(3), 263–278.

Fukudome, Y., Ohno-Shosaku, T., Matsui, M., Omori, Y., Fukaya, M., Tsubokawa, H., Taketo, M. M., Watanabe, M., Manabe, T., & Kano, M. (2004). Two distinct classes of muscarinic action on hippocampal inhibitory synapses: M2-mediated direct suppression and M1/M 3-mediated indirect suppression through endocannabinoid signalling. *European Journal of Neuroscience*, *19*(10), 2682–2692.

Fuster, J. M., & Alexander, G. E. (1971). Neuron activity related to short-term memory. *Science*, *173*(3997), 652–654.

Gabbott, P. L. A., & Bacon, S. J. (1996). Local circuit neurons in the medial prefrontal cortex (areas 24a,b,c, 25 and 32) in the monkey: II. Quantitative areal and laminar distributions. *Journal of Comparative Neurology*, *364*(4), 609–636.

Gabbott, P. L. A., & Bacon, S. J. (1997). Vasoactive intestinal polypeptide containing neurones in monkey medial prefrontal cortex (mPFC): Colocalisation with calretinin. *Brain Research*, *744*(1), 179–184.

Geerling, J. C., Kawata, M., & Loewy, A. D. (2006). Aldosterone-sensitive neurons in the rat central nervous system. *Journal of Comparative Neurology*, *494*(3), 515–527.

Georgopoulos, A. P., Kalaska, J. F., Caminiti, R., & Massey, J. T. (1982). On the relations between the direction of two-dimensional arm movements and cell discharge in primate motor cortex. *Journal of Neuroscience*, *2*(11), 1527–1537.

Gerber, G., Zhong, J., Youn, D. H., & Randic, M. (2000). Group II and group III metabotropic glutamate receptor agonists depress synaptic transmission in the rat spinal cord dorsal horn. *Neuroscience*, *100*(2), 393–406.

Gereau IV, R. W., & Conn, P. J. (1995). Multiple presynaptic metabotropic glutamate receptors modulate excitatory and inhibitory synaptic transmission in hippocampal area CA1. *Journal of Neuroscience*, *15*(10), 6879–6889.

Gerlai, R., Roder, J. C., & Hampson, D. R. (1998). Altered spatial learning and memory in mice lacking the mGluR4 subtype of metabotropic glutamate receptor. *Behavioral Neuroscience*, *112*(3), 525–532.

Geschwind, N. (1965). Disconnexion syndromes in animals and man. *Brain*, *88*(2), 237.

Geyer, S., Matelli, M., Luppino, G., & Zilles, K. (2000). Functional neuroanatomy of the primate isocortical motor system. *Anatomy and Embryology*, *202*(6), 443–474.

Fritsch, G., & Hitzig, E. (1870). Ueber die elektrische Erregbarkeit des Grosshirns. *Archiv Fur Anatomie Und Physiologie Wissenschaftliche Medicin*, *37*, 300–332.

Gidon, A., Zolnik, T. A., Fidzinski, P., Bolduan, F., Papoutsi, A., Poirazi, P., Holtkamp, M., Vida, I., & Larkum, M. E. (2020). Dendritic action potentials and computation in human layer 2/3 cortical neurons. *Science*, *367*(6473), 83–87.

Giustizieri, M., Bernardi, G., Mercuri, N. B., & Berretta, N. (2005). Distinct Mechanisms of Presynaptic Inhibition at GABAergic Synapses of the Rat Substantia Nigra Pars Compacta. *Journal of neurophysiology*, *94*(3), 1992–2003.

Glasser, M. F., Coalson, T. S., Robinson, E. C., Hacker, C. D., Harwell, J., Yacoub, E., Ugurbil, K., Andersson, J., Beckmann, C. F., Jenkinson, M., Smith, S. M., & van Essen, D. C. (2016). A multi-modal parcellation of human cerebral cortex. *Nature*, *536*(7615), 171–178.

Goddyn, H., Callaerts-Vegh, Z., Stroobants, S., Dirikx, T., Vansteenwegen, D., Hermans, D., Putten, H. van der, & D'Hooge, R. (2008). Deficits in acquisition and extinction of conditioned responses in mGluR7 knockout mice. *Neurobiology of Learning and Memory*, *90*(1), 103–111.

Goldman-Rakic, P. S., & Schwartz, M. L. (1982). Interdigitation of contralateral and ipsilateral columnar projections to frontal association cortex in primates. *Science*, *216*(4547), 755–757.

Golowasch, J., Thomas, G., Taylor, A. L., Patel, A., Pineda, A., Khalil, C., & Nadim, F. (2009). Membrane capacitance measurements revisited: Dependence of capacitance value on measurement method in nonisopotential neurons. *Journal of Neurophysiology*, *102*(4), 2161–2175.

Gonchar, Y., & Burkhalter, A. (1997). Three distinct families of GABAergic neurons in rat visual cortex. *Cerebral Cortex*, *7*(4), 347–358.

Gonchar, Y., Wang, Q., & Burkhalter, A. H. (2008). Multiple distinct subtypes of GABAergic neurons in mouse visual cortex identified by triple immunostaining. *Frontiers in Neuroanatomy*, *2*, 3.

González-Albo, M. C., Elston, G. N., & DeFelipe, J. (2001). The human temporal cortex: Characterization of neurons expressing nitric oxide synthase, neuropeptides and calcium-binding proteins, and their glutamate receptor subunit profiles. *Cerebral Cortex*, *11*(12), 1170–1181.

Gouwens, N. W., Sorensen, S. A., Baftizadeh, F., Budzillo, A., Lee, B. R., Jarsky, T., Alfiler, L., Baker, K., Barkan, E., Berry, K., Bertagnolli, D., Bickley, K., Bomben, J., Braun, T., Brouner, K., Casper, T., Crichton, K., Daigle, T. L., Dalley, R., … Zeng, H. (2020). Integrated Morphoelectric and Transcriptomic Classification of Cortical GABAergic Cells. *Cell*, *183*(4), 935-953.e19.

Gouwens, N. W., Sorensen, S. A., Berg, J., Lee, C., Jarsky, T., Ting, J., Sunkin, S. M., Feng, D., Anastassiou, C. A., Barkan, E., Bickley, K., Blesie, N., Braun, T., Brouner, K., Budzillo, A., Caldejon, S., Casper, T., Castelli, D., Chong, P., … Koch, C. (2019). Classification of electrophysiological and morphological neuron types in the mouse visual cortex. *Nature Neuroscience*, *22*(7), 1182–1195.

Gray, E. G. (1959). Axo-somatic and axo-dendritic synapses of the cerebral cortex: an electron microscope study. *Journal of Anatomy*, *93*(4), 420–433.

Graziano, M. S. A., Aflalo, T. N. S., & Cooke, D. F. (2005). Arm movements evoked by electrical stimulation in the motor cortex of monkeys. *Journal of Neurophysiology*, *94*(6), 4209–4223.

Gubellini, P., Melon, C., Dale, E., Doller, D., & Kerkerian-Le Goff, L. (2014). Distinct effects of mGlu4 receptor positive allosteric modulators at corticostriatal vs. striatopallidal synapses may differentially contribute to their antiparkinsonian action. *Neuropharmacology*, *85*, 166–177.

Gulyás, A. I., Tóth, K., Dános, P., & Freund, T. F. (1991). Subpopulations of GABAergic neurons containing parvalbumin, calbindin D28k, and cholecystokinin in the rat hippocampus. *Journal of Comparative Neurology*, *312*(3), 371–378.

Guo, J., & Ikeda, S. R. (2005). Coupling of metabotropic glutamate receptor 8 to N-type Ca2+ channels in rat sympathetic neurons. *Molecular Pharmacology*, *67*(6), 1840–1851.

Haller, M., Case, J., Crone, N. E., Chang, E. F., King-Stephens, D., Laxer, K. D., Weber, P. B., Parvizi, J., Knight, R. T., & Shestyuk, A. Y. (2018). Persistent neuronal activity in human prefrontal cortex links perception and action. *Nature Human Behaviour*, *2*(1), 80–91.

Harlow, J. M. (1868). Recovery from the passage of an iron bar through the head: *Bull Massachusetts Med Soc*, *2*, 3–20.

Hashimoto, K., & Kano, M. (1998). Presynaptic origin of paired-pulse depression at climbing fibre–Purkinje cell synapses in the rat cerebellum. *The Journal of Physiology*, *506*(2), 391.

Haug, H. (1987). Brain sizes, surfaces, and neuronal sizes of the cortex cerebri: A stereological investigation of man and his variability and a comparison with some mammals (primates, whales, marsupials, insectivores, and one elephant). *American Journal of Anatomy*, *180*(2), 126–142.

Hecking, J., Davoudian, P. A., & Wilkinson, S. T. (2021). Emerging Therapeutics Based on the Amino Acid Neurotransmitter System: An Update on the Pharmaceutical Pipeline for Mood Disorders. *Chronic Stress*, *5*, 247054702110204.

Hendry, S. H. C., & Jones, E. G. (1991). GABA neuronal subpopulations in cat primary auditory cortex: co-localization with calcium binding proteins. *Brain Research*, *543*(1), 45–55.

Hendry, S. H., Schwark, H. D., Jones, E. G., & Yan, J. (1987). Numbers and proportions of GABA-immunoreactive neurons in different areas of monkey cerebral cortex. *The Journal of Neuroscience : The Official Journal of the Society for Neuroscience*, *7*(5), 1503–1519.

Henschen, S. E. (1893). On the visual path and centre. *Brain*, *16*(1–2), 170–180.

Hermans, E., & Challiss, R. A. J. (2001). Structural, signalling and regulatory properties of the group I metabotropic glutamate receptors: Prototypic family C G-protein-coupled receptors. *Biochemical Journal*, *359*(3), 465–484.

Herrero, I. (1996). A Decrease in [Ca2+]c but not in cAMP Mediates L-AP4 Inhibition of Glutamate Release: PKC-mediated Suppression of this Inhibitory Pathway. *European Journal of Neuroscience*, *8*(4), 700–709.

Heuss, C., Scanziani, M., Gähwiler, B. H., & Gerber, U. (1999). G-protein-independent signaling mediated by metabotropic glutamate receptors. *Nature Neuroscience*, *2*(12), 1070–1077.

Higo, S., Udaka, N., & Tamamaki, N. (2007). Long-Range GABAergic Projection Neurons in the Cat Neocortex. *The Journal of Comparative Neurology*, *504*(3), 287–297.

Hioki, H., Okamoto, S., Konno, M., Kameda, H., Sohn, J., Kuramoto, E., Fujiyama, F., & Kaneko, T. (2013). Cell Type-Specific Inhibitory Inputs to Dendritic and Somatic Compartments of Parvalbumin-Expressing Neocortical Interneuron. *Journal of Neuroscience*, *33*(2), 544–555.

Hodge, R. D., Bakken, T. E., Miller, J. A., Smith, K. A., Barkan, E. R., Graybuck, L. T., Close, J. L., Long, B., Johansen, N., Penn, O., Yao, Z., Eggermont, J., Höllt, T., Levi, B. P., Shehata, S. I., Aevermann, B., Beller, A., Bertagnolli, D., Brouner, K., … Lein, E. S. (2019). Conserved cell types with divergent features in human versus mouse cortex. *Nature*, *573*(7772), 61–68.

Hodgson, A. J., Penke, B., Erdei, A., Chubb, I. W., & Somogyi, P. (1985). Antisera to γ-aminobutyric acid. 1. Production and characterization using a new model system. *Journal of Histochemistry and Cytochemistry*, *33*(3), 229–239.

Holler, T., Cappel, E., Klein, J., & Löffelholz, K. (1993). Glutamate Activates Phospholipase D in Hippocampal Slices of Newborn and Adult Rats. *Journal of Neurochemistry*, *61*(4), 1569–1572.

Hölscher, C., Schmid, S., Pilz, P. K. D., Sansig, G., van der Putten, H., & Plappert, C. F. (2004). Lack of the metabotropic glutamate receptor subtype 7 selectively impairs short-term working memory but not long-term memory. *Behavioural Brain Research*, *154*(2), 473–481.

Hölscher, C., Schmid, S., Pilz, P. K. D., Sansig, G., van der Putten, H., & Plappert, C. F. (2005). Lack of the metabotropic glutamate receptor subtype 7 selectively modulates Theta rhythm and working memory. *Learning and Memory*, *12*(5), 450–455.

Hubel, D. H., & Wiesel, T. N. (1959). Receptive fields of single neurones in the cat's striate cortex. *The Journal of Physiology*, *148*(3), 574–591.

Hubel, D. H., & Wiesel, T. N. (1962). Receptive fields, binocular interaction and functional architecture in the cat's visual cortex. *The Journal of Physiology*, *160*(1), 106–154.

Hubel, D. H., & Wiesel, T. N. (1968). Receptive fields and functional architecture of monkey striate cortex. *The Journal of Physiology*, *195*(1), 215–243.

Hubel, D. H., & Wiesel, T. N. (1969). Anatomical demonstration of columns in the monkey striate cortex. *Nature*, *221*(5182), 747–750.

Hubel, D. H., & Wiesel, T. N. (1972). Laminar and columnar distribution of geniculo-cortical fibers in the macaque monkey. *Journal of Comparative Neurology*, *146*(4), 421–450.

Hubel, D. H., Wiesel, T. N., & Stryker, M. P. (1978). Anatomical demonstration of orientation columns in macaque monkey. *Journal of Comparative Neurology*, *177*(3), 361–379.

Huttenlocher, P. R., & Dabholkar, A. S. (1997). Regional differences in synaptogenesis in human cerebral cortex. *Journal of Comparative Neurology*, *387*(2), 167–178.

Iacaruso, M. F., Gasler, I. T., & Hofer, S. B. (2017). Synaptic organization of visual space in primary visual cortex. *Nature*, *547*(7664), 449–452.

Insel, N., & Takehara-Nishiuchi, K. (2013). The cortical structure of consolidated memory: A hypothesis on the role of the cingulate-entorhinal cortical connection. *Neurobiology of Learning and Memory*, *106*, 343–350.

Iskhakova, L., & Smith, Y. (2016). MGluR4-Containing Corticostriatal Terminals: Synaptic Interactions with Direct and Indirect Pathway Neurons in Mice. *Brain Structure & Function*, *221*(9), 4589.

Isseroff, A., Schwartz, M. L., Dekker, J. J., & Goldman-Rakic, P. S. (1984). Columnar organization of callosal and associational projections from rat frontal cortex. *Brain Research*, *293*(2), 213–223.

Jakovcevski, I., Mayer, N., & Zecevic, N. (2011). Multiple origins of human neocortical interneurons are supported by distinct expression of transcription factors. *Cerebral Cortex*, *21*(8), 1771–1782.

Jiang, X., Shen, S., Cadwell, C. R., Berens, P., Sinz, F., Ecker, A. S., Patel, S., & Tolias, A. S. (2015). Principles of connectivity among morphologically defined cell types in adult neocortex. *Science*, *350*(6264), 9462–9462.

Jiang, X., Wang, G., Lee, A. J., Stornetta, R. L., & Zhu, J. J. (2013). The organization of two new cortical interneuronal circuits. *Nature Neuroscience*, *16*(2), 210–218.

Jingami, H., Nakanishi, S., & Morikawa, K. (2003). Structure of the metabotropic glutamate receptor. *Current Opinion in Neurobiology*, *13*(3), 271–278.

Johansen, P. A., Chase, L. A., Sinor, A. D., Koerner, J. F., Johnson, R. L., & Robinson, M. B. (1995). Type 4a metabotropic glutamate receptor: Identification of new potent agonists and differentiation from the L-(+)-2-amino-4-phosphonobutanoic acid- sensitive receptor in the lateral perforant pathway in rats. *Molecular Pharmacology*, *48*(1), 140–149.

Jones, C. K., Bubser, M., Thompson, A. D., Dickerson, J. W., Turle-Lorenzo, N., Amalric, M., Blobaum, A. L., Bridges, T. M., Morrison, R. D., Jadhav, S., Engers, D. W., Italiano, K., Bode, J., Daniels, J. S., Lindsley, C. W., Hopkins, C. R., Conn, P. J., & Niswender, C. M. (2012). The metabotropic glutamate receptor 4-positive allosteric modulator VU0364770 produces efficacy alone and in combination with L-DOPA or an adenosine 2A antagonist in preclinical rodent models of Parkinson's disease. *Journal of Pharmacology and Experimental Therapeutics*, *340*(2), 404–421.

Jones, E. G. (1975). Varieties and distribution of non-pyramidal cells in the somatic sensory cortex of the squirrel monkey. *Journal of Comparative Neurology*, *160*(2), 205–267.

Jones, E. G., & Burton, H. (1976). Areal differences in the laminar distribution of thalamic afferents in cortical fields of the insular, parietal and temporal regions of primates. *Journal of Comparative Neurology*, *168*(2), 197–247.

Jones, E. G., Burton, H., & Porter, R. (1975). Commissural and cortico-cortical "columns" in the somatic sensory cortex of primates. *Science*, *190*(4214), 572–574.

Jones, E. G., & Wise, S. P. (1977). Size, laminar and columnar distribution of efferent cells in the sensory-motor cortex of monkeys. *Journal of Comparative Neurology*, *175*(4), 391–437.

Kalinichev, M., le Poul, E., Boléa, C., Girard, F., Campo, B., Fonsi, M., Royer-Urios, I., Browne, S. E., Uslaner, J. M., Davis, M. J., Raber, J., Duvoisin, R., Bate, S. T., Reynolds, I. J., Poli, S., & Celanire, S. (2014). Characterization of the novel positive allosteric

modulator of the metabotropic glutamate receptor 4 ADX88178 in rodent models of neuropsychiatric disorders. *Journal of Pharmacology and Experimental Therapeutics*, *350*(3), 495–505.

Kalmbach, B. E., Buchin, A., Long, B., Close, J., Nandi, A., Miller, J. A., Bakken, T. E., Hodge, R. D., Chong, P., de Frates, R., Dai, K., Maltzer, Z., Nicovich, P. R., Keene, C. D., Silbergeld, D. L., Gwinn, R. P., Cobbs, C., Ko, A. L., Ojemann, J. G., … Ting, J. T. (2018). h-Channels Contribute to Divergent Intrinsic Membrane Properties of Supragranular Pyramidal Neurons in Human versus Mouse Cerebral Cortex. *Neuron*, *100*(5), 1194-1208.e5.

Kammermeier, P. J. (2012). Functional and pharmacological characteristics of metabotropic glutamate receptors 2/4 heterodimers. *Molecular Pharmacology*, *82*(3), 438–447.

Kammermeier, P. J., & Ikeda, S. R. (1999). Expression of RGS2 alters the coupling of metabotropic glutamate receptor 1a to M-type K+ and N-type Ca2+ channels. *Neuron*, *22*(4), 819–829.

Kammermeier, P. J., Xiao, B., Jian Cheng Tu, Worley, P. F., & Ikeda, S. R. (2000). Homer proteins regulate coupling of group I metabotropic glutamate receptors to N-type calcium and M-type potassium channels. *Journal of Neuroscience*, *20*(19), 7238–7245.

Karube, F., Kubota, Y., & Kawaguchi, Y. (2004). Axon Branching and Synaptic Bouton Phenotypes in GABAergic Nonpyramidal Cell Subtypes. *Journal of Neuroscience*, *24*(12), 2853–2865.

Kasthuri, N., Hayworth, K. J., Berger, D. R., Schalek, R. L., Conchello, J. A., Knowles-Barley, S., Lee, D., Vázquez-Reina, A., Kaynig, V., Jones, T. R., Roberts, M., Morgan, J. L., Tapia, J. C., Seung, H. S., Roncal, W. G., Vogelstein, J. T., Burns, R., Sussman, D. L., Priebe, C. E., … Lichtman, J. W. (2015). Saturated Reconstruction of a Volume of Neocortex. *Cell*, *162*(3), 648–661.

Kato, A., Ozawa, F., Saitoh, Y., Fukazawa, Y., Sugiyama, H., & Inokuchi, K. (1998). Novel members of the Vesl/Homer family of PDZ proteins that bind metabotropic glutamate receptors. *Journal of Biological Chemistry*, *273*(37), 23969–23975.

Katona, I., Sperlágh, B., Sík, A., Käfalvi, A., Vizi, E. S., Mackie, K., & Freund, T. F. (1999). Presynaptically located CB1 cannabinoid receptors regulate GABA release from axon terminals of specific hippocampal interneurons. *Journal of Neuroscience*, *19*(11), 4544–4558.

Katona, L., Hartwich, K., Tomioka, R., Somogyi, J., Roberts, J. D. B., Wagner, K., Joshi, A., Klausberger, T., Rockland, K. S., & Somogyi, P. (2020). Synaptic organisation and behaviour-dependent activity of mGluR8a-innervated GABAergic trilaminar cells projecting from the hippocampus to the subiculum. *Brain Structure and Function*, *225*(2), 705–734.

Kavalali, E. T. (2014). The mechanisms and functions of spontaneous neurotransmitter release. *Nature Reviews Neuroscience*, *16*(1), 5–16.

Kawaguchi, Y. (1993). Groupings of nonpyramidal and pyramidal cells with specific physiological and morphological characteristics in rat frontal cortex. *Journal of Neurophysiology*, *69*(2), 416–431.

Kawaguchi, Y. (1995). Physiological subgroups of nonpyramidal cells with specific morphological characteristics in layer II/III of rat frontal cortex. *Journal of Neuroscience*, *15*(4), 2638–2655.

Kawaguchi, Y. (1997). Selective Cholinergic Modulation of Cortical GABAergic Cell Subtypes. *Journal of Neurophysiology*, *78*(3), 1743–1747.

Kawaguchi, Y., & Kondo, S. (2002). Parvalbumin, somatostatin and cholecystokinin as chemical markers for specific GABAergic interneuron types in the rat frontal cortex. *Journal of Neurocytology*, *31*(3–5), 277–287.

Kawaguchi, Y., & Kubota, Y. (1993). Correlation of physiological subgroupings of nonpyramidal cells with parvalbumin- and calbindin(D28k)-immunoreactive neurons in layer V of rat frontal cortex. *Journal of Neurophysiology*, *70*(1), 387–396.

Kawaguchi, Y., & Kubota, Y. (1996). Physiological and morphological identification of somatostatin- or vasoactive intestinal polypeptide-containing cells among GABAergic cell subtypes in rat frontal cortex. *Journal of Neuroscience*, *16*(8), 2701–2715.

Kawaguchi, Y., & Kubota, Y. (1997). GABAergic Cell Subtypes and their Synaptic Connections in Rat Frontal Cortex. *Cerebral Cortex*, *7*(6), 476–486.

Kawaguchi, Y., & Kubota, Y. (1998). Neurochemical features and synaptic connections of large physiologically-identified GABAergic cells in the rat frontal cortex. *Neuroscience*, *85*(3), 677–701.

Kinoshita, A., Ohishi, H., Neki, A., Nomura, S., Shigemoto, R., Takada, M., Nakanishi, S., & Mizuno, N. (1996). Presynaptic localization of a metabotropic glutamate receptor, mGluR8, in the rhinencephalic areas: a light and electron microscope study in the rat. *Neuroscience Letters*, *207*(1), 61–64.

Kinoshita, A., Ohishi, H., Nomura, S., Shigemoto, R., Nakanishi, S., & Mizuno, N. (1996). Presynaptic localization of a metabotropic glutamate receptor, mGluR4a, in the cerebellar cortex: a light and electron microscope study in the rat. *Neuroscience Letters*, *207*(3), 199–202.

Kinoshita, A., Shigemoto, R., Ohishi, H., van der Putten, H., & Mizuno, N. (1998). Immunohistochemical Localization of Metabotropic Glutamate Receptors, mGluR7a and mGluR7b, in the Central Nervous System of the Adult Rat and Mouse: A Light and Electron Microscopic Study. *Journal of Comparative Neurology*, *393*(3), 332–352.

Kinzie, J. M., Saugstad, J. A., Westbrook, G. L., & Segerson, T. P. (1995). Distribution of metabotropic glutamate receptor 7 messenger RNA in the developing and adult rat brain. *Neuroscience*, *69*(1), 167–176.

Kinzie, J. M., Shinohara, M. M., van den Pol, A. N., Westbrook, G. L., & Segerson, T. P. (1997). Immunolocalization of metabotropic glutamate receptor 7 in the rat olfactory bulb. *Journal of Comparative Neurology*, *385*(3), 372–384.

Kisvárday, Z. F., Adams, C. B. T., & Smith, A. D. (1986a). Synaptic connections of axo-axonic (chandelier) cells in human epileptic temporal cortex. *Neuroscience*, *19*(4), 1179–1186.

Kisvárday, Z. F., Beaulieu, C., & Eysel, U. T. (1993). Network of GABAergic large basket cells in cat visual cortex (area 18): Implication for lateral disinhibition. *Journal of Comparative Neurology*, *327*(3), 398–415.

Kisvárday, Z. F., & Eysel, U. T. (1992). Cellular organization of reciprocal patchy networks in layer III of cat visual cortex (area 17). *Neuroscience*, *46*(2), 275–286.

Kisvárday, Z. F., Gulyas, A., Beroukas, D., North, J. B., Chubb, I. W., & Somogyi, P. (1990). Synapses, axonal and dendritic patterns of GABA-immunoreactive neurons in human cerebral cortex. *Brain*, *113*(3), 793–812.

Kisvárday, Z. F., Martin, K. A. C., Freund, T. F., Maglóczky, Z., Whitteridge, D., & Somogyi, P. (1986b). Synaptic targets of HRP-filled layer III pyramidal cells in the cat striate cortex. *Experimental Brain Research*, *64*(3), 541–552.

Kisvárday, Z. F., Martin, K. A. C., Somogyi, P., & Friedlander, M. J. (1987). Evidence for interlaminar inhibitory circuits in the striate cortex of the cat. *Journal of Comparative Neurology*, *260*(1), 1–19.

Kisvárday, Z. F., Martin, K. A. C., Whitteridge, D., & Somogyi, P. (1985). Synaptic connections of intracellularly filled clutch cells: A type of small basket cell in the visual cortex of the cat. *Journal of Comparative Neurology*, *241*(2), 111–137.

Koerner, J. F., & Cotman, C. W. (1981). Micromolar L-2-amino-4-phosphonobutyric acid selectively inhibits perforant path synapses from lateral entorhinal cortex. *Brain Research*, *216*(1), 192–198.

Koester, H. J., & Sakmann, B. (1998). Calcium dynamics in single spines during coincident pre- and postsynaptic activity depend on relative timing of back-propagating action potentials and subthreshold excitatory postsynaptic potentials. *Proceedings of the National Academy of Sciences of the United States of America*, *95*(16), 9596–9601.

Koester, S., & O'Leary, D. (1992). Functional classes of cortical projection neurons develop dendritic distinctions by class-specific sculpting of an early common pattern. *Journal of Neuroscience*, *12*(4), 1382–1393.

Kogo, N., Dalezios, Y., Capogna, M., Ferraguti, F., Shigemoto, R., & Somogyi, P. (2004). Depression of GABAergic input to identified hippocampal neurons by group III metabotropic glutamate receptors in the rat. *The European Journal of Neuroscience*, *19*(10), 2727–2740.

Ko, H., Hofer, S. B., Pichler, B., Buchanan, K. A., Sjöström, P. J., & Mrsic-Flogel, T. D. (2011). Functional specificity of local synaptic connections in neocortical networks. *Nature*, *473*(7345), 87–91.

Krimer, L. S., Zaitsev, A. v., Czanner, G., Kröner, S., González-Burgos, G., Povysheva, N. v., Iyengar, S., Barrionuevo, G., & Lewis, D. A. (2005). Cluster analysis-based physiological classification and morphological properties of inhibitory neurons in layers 2-3 of monkey dorsolateral prefrontal cortex. *Journal of Neurophysiology*, *94*(5), 3009–3022.

Krook-Magnuson, E., Luu, L., Lee, S.-H., Varga, C., & Soltesz, I. (2011). Ivy and Neurogliaform Interneurons Are a Major Target of μ-Opioid Receptor Modulation. *Journal of Neuroscience*, *31*(42), 14861–14870.

Kroon, T., Dawitz, J., Kramvis, I., Anink, J., Obermayer, J., Verhoog, M. B., Wilbers, R., Goriounova, N. A., Idema, S., Baayen, J. C., Aronica, E., Mansvelder, H. D., & Meredith, R. M. (2019). Group I mGluR-Mediated Activation of Martinotti Cells Inhibits Local Cortical Circuitry in Human Cortex. *Frontiers in Cellular Neuroscience*, *13*, 315.

Kubota, K., & Niki, H. (1971). Prefrontal cortical unit activity and delayed alternation performance in monkeys. *Journal of Neurophysiology*, *34*(3), 337–347.

Kubota, Y., Hatada, S., Kondo, S., Karube, F., & Kawaguchi, Y. (2007). Neocortical inhibitory terminals innervate dendritic spines targeted by thalamocortical afferents. *Journal of Neuroscience*, *27*(5), 1139–1150.

Kubota, Y., Hattori, R., & Yui, Y. (1994). Three distinct subpopulations of GABAergic neurons in rat frontal agranular cortex. *Brain Research*, *649*(1–2), 159–173.

Kubota, Y., & Jones, E. G. (1993). Co-localization of two calcium binding proteins in GABA cells of rat piriform cortex. *Brain Research*, *600*(2), 339–344.

Kubota, Y., & Kawaguchi, Y. (1997). Two distinct subgroups of cholecystokinin-immunoreactive cortical interneurons. *Brain Research*, *752*(1–2), 175–183.

Kubota, Y., Kondo, S., Nomura, M., Hatada, S., Yamaguchi, N., Mohamed, A. A., Karube, F., Lübke, J., & Kawaguchi, Y. (2015). Functional effects of distinct innervation styles of pyramidal cells by fast spiking cortical interneurons. *ELife*, *4*, e07919.

Kubota, Y., Shigematsu, N., Karube, F., Sekigawa, A., Kato, S., Yamaguchi, N., Hirai, Y., Morishima, M., & Kawaguchi, Y. (2011). Selective coexpression of multiple chemical markers defines discrete populations of neocortical gabaergic neurons. *Cerebral Cortex*, *21*(8), 1803–1817.

Kuffler, S., & Edwards, C. (1958). Mechanism of gamma aminobutyric acid (GABA) action and its relation to synaptic inhibition. *Journal of Neurophysiology*, *21*(6), 589–610.

Kwan, H. C., MacKay, W. A., Murphy, J. T., & Wong, Y. C. (1978). Spatial organization of precentral cortex in awake primates. II. Motor outputs. *Journal of Neurophysiology*, *41*(5), 1120–1131.

Kwon, T., Merchán-Pérez, A., Rial Verde, E. M., Rodríguez, J. R., DeFelipe, J., & Yuste, R. (2019). Ultrastructural, Molecular and Functional Mapping of GABAergic Synapses on Dendritic Spines and Shafts of Neocortical Pyramidal Neurons. *Cerebral Cortex*, *29*(7), 2771–2781.

Kyuyoung, C. L., & Huguenard, J. R. (2014). Modulation of Short-Term Plasticity in the Corticothalamic Circuit by Group III Metabotropic Glutamate Receptors. *The Journal of Neuroscience*, *34*(2), 675.

Laezza, F., Doherty, J. J., & Dingledine, R. (1999). Long-term depression in hippocampal interneurons: Joint requirement for pre- and postsynaptic events. *Science*, *285*(5432), 1411–1414.

Lafon-Cazal, M., Viennois, G., Kuhn, R., Malitschek, B., Pin, J. P., Shigemoto, R., & Bockaert, J. (1999). mGluR7-like receptor and GABA(B) receptor activation enhance neurotoxic effects of N-methyl-D-aspartate in cultured mouse striatal GABAergic neurones. *Neuropharmacology*, *38*(10), 1631–1640.

Lancaster, B., & Nicoll, R. A. (1987). Properties of two calcium-activated hyperpolarizations in rat hippocampal neurones. *The Journal of Physiology*, *389*(1), 187–203.

Lashley, K. S. (1933). Integrative Functions of the Cerebral Cortex. *Physiological Reviews*, *13*(1), 1–42.

Laurienti, P. J., Wallace, M. T., Maldjian, J. A., Susi, C. M., Stein, B. E., & Burdette, J. H. (2003). Cross-modal sensory processing in the anterior cingulate and medial prefrontal cortices. *Human Brain Mapping*, *19*(4), 213–223.

Lee, W.-C. A., Bonin, V., Reed, M., Graham, B. J., Hood, G., Glattfelder, K., & Reid, R. C. (2016). Anatomy and function of an excitatory network in the visual cortex. *Nature*, *532*(7599), 370–374.

Lefort, S., Tomm, C., Floyd Sarria, J. C., & Petersen, C. C. H. (2009). The Excitatory Neuronal Network of the C2 Barrel Column in Mouse Primary Somatosensory Cortex. *Neuron*, *61*(2), 301–316.

Leonard, C. M. (1969). The prefrontal cortex of the rat. I. cortical projection of the mediodorsal nucleus. II. efferent connections. *Brain Research*, *12*(2), 321–343.

Letinic, K., Zoncu, R., & Rakic, P. (2002). Origin of GABAergic neurons in the human neocortex. *Nature*, *417*(6889), 645–649.

Letzkus, J., Wolff, S., & Lüthi, A. (2015). Disinhibition, a Circuit Mechanism for Associative Learning and Memory. *Neuron*, *88*(2), 264–276.

Leuba, G., & Saini, K. (1997). Colocalization of parvalbumin, calretinin and calbindin D-28k in human cortical and subcortical visual structures. *Journal of Chemical Neuroanatomy*, *13*(1), 41–52.

LeVay, S., Hubel, D. H., & Wiesel, T. N. (1975). The pattern of ocular dominance columns in macaque visual cortex revealed by a reduced silver stain. *Journal of Comparative Neurology*, *159*(4), 559–575.

Levitz, J., Habrian, C., Bharill, S., Fu, Z., Vafabakhsh, R., & Isacoff, E. Y. (2016). Mechanism of Assembly and Cooperativity of Homomeric and Heteromeric Metabotropic Glutamate Receptors. *Neuron*, *92*(1), 143–159.

Lewis, D. A., & Lund, J. S. (1990). Heterogeneity of chandelier neurons in monkey neocortex: Corticotropin-releasing factor-and parvalbumin-immunoreactive populations. *Journal of Comparative Neurology*, *293*(4), 599–615.

Lillicrap, T. P., & Scott, S. H. (2013). Preference Distributions of Primary Motor Cortex Neurons Reflect Control Solutions Optimized for Limb Biomechanics. *Neuron*, *77*(1), 168–179.

Linden, A. M., Johnson, B. G., Peters, S. C., Shannon, H. E., Tian, M., Wang, Y., Yu, J. L., Köster, A., Baez, M., & Schoepp, D. D. (2002). Increased anxiety-related behavior in mice deficient for metabotropic glutamate 8 (mGlu8) receptor. *Neuropharmacology*, *43*(2), 251–259.

Lipovsek, M., Bardy, C., Cadwell, C. R., Hadley, K., Kobak, D., & Tripathy, S. J. (2021). Patch-seq: Past, Present, and Future. *Journal of Neuroscience*, *41*(5), 937–946.

Livingstone, M. S., & Hubel, D. H. (1984). Anatomy and physiology of a color system in the primate visual cortex. *Journal of Neuroscience*, *4*(1), 309–356.

Lopez, S., Jouve, L., Turle-Lorenzo, N., Kerkerian-LeGoff, L., Salin, P., & Amalric, M. (2012). Antiparkinsonian action of a selective group III mGlu receptor agonist is associated with reversal of subthalamonigral overactivity. *Neurobiology of Disease*, *46*(1), 69–77.

Lopez, S., Turle-Lorenzo, N., Acher, F., de Leonibus, E., Mele, A., & Amalric, M. (2007). Targeting group III metabotropic glutamate receptors produces complex behavioral effects in rodent models of Parkinson's disease. *Journal of Neuroscience*, *27*(25), 6701–6711.

Lorente De Nó, R. (1922). La cortaleza cerebral del raton. *Trabajos Del Laboratorio de Investigaciones Biológicas de La Universidad de Madrid*, *20*, 41–78.

Lübke, J., Egger, V., Sakmann, B., & Feldmeyer, D. (2000). Columnar Organization of Dendrites and Axons of Single and Synaptically Coupled Excitatory Spiny Neurons in Layer 4 of the Rat Barrel Cortex. *Journal of Neuroscience*, *20*(14), 5300–5311.

Ludwig, A., Zong, X., Jeglitsch, M., Hofmann, F., & Biel, M. (1998). A family of hyperpolarization-activated mammalian cation channels. *Nature*, *393*(6685), 587–591.

Luján, R., Nusser, Z., Roberts, J. D. B., Shigemoto, R., & Somogyi, P. (1996). Perisynaptic location of metabotropic glutamate receptors mGluR1 and mGluR5 on dendrites and dendritic spines in the rat hippocampus. *European Journal of Neuroscience*, *8*(7), 1488–1500.

Luján, R., Roberts, J. D. B., Shigemoto, R., Ohishi, H., & Somogyi, P. (1997). Differential plasma membrane distribution of metabotropic glutamate receptors mGluR1α, mGluR2 and mGluR5, relative to neurotransmitter release sites. *Journal of Chemical Neuroanatomy*, *13*(4), 219–241.

Lund, J. S. (1973). Organization of neurons in the visual cortex, area 17, of the monkey (Macaca mulatta). *Journal of Comparative Neurology*, *147*(4), 455–495.

Lund, J. S. (1987). Local circuit neurons of macaque monkey striate cortex: I. Neurons of laminae 4C and 5A. *Journal of Comparative Neurology*, *257*(1), 60–92.

Lund, J. S. (1988). Anatomical organization of macaque monkey striate visual cortex. *Annual Review of Neuroscience*, *11*, 253–288.

Lund, J. S., & Lewis, D. A. (1993). Local circuit neurons of developing and mature macaque prefrontal cortex: Golgi and immunocytochemical characteristics. *Journal of Comparative Neurology*, *328*(2), 282–312.

Lund, J. S., & Wu, C. Q. (1997). Local Circuit Neurons of Macaque Monkey Striate Cortex: IV. Neurons of Laminae 1-3A . *The Journal of Comparative Neurology*, *384*(1), 109–126.

Lund, J. S., & Yoshioka, T. (1991). Local circuit neurons of macaque monkey striate cortex: III. Neurons of laminae 4B, 4A, and 3B. *Journal of Comparative Neurology*, *311*(2), 234–258.

Lu, Y. (2007). Endogenous mGluR activity suppresses GABAergic transmission in avian cochlear nucleus magnocellularis neurons. *Journal of Neurophysiology*, *97*(2), 1018–1029.

Maccaferri, G., David, J., Roberts, B., Szucs, P., Cottingham, C. A., & Somogyi, P. (2000). Cell surface domain specific postsynaptic currents evoked by identified GABAergic neurones in rat hippocampus in vitro. *Journal of Physiology*, *524*(1), 91–116.

Maccaferri, G., Mangoni, M., Lazzari, A., & DiFrancesco, D. (1993). Properties of the hyperpolarization-activated current in rat hippocampal CA1 pyramidal cells. *Journal of Neurophysiology*, *69*(6), 2129–2136.

MacInnes, N., & Duty, S. (2008). Group III metabotropic glutamate receptors act as hetero-receptors modulating evoked GABA release in the globus pallidus in vivo. *European Journal of Pharmacology*, *580*(1–2), 95–99.

MacInnes, N., Messenger, M. J., & Duty, S. (2004). Activation of group III metabotropic glutamate receptors in selected regions of the basal ganglia alleviates akinesia in the reserpine-treated rat. *British Journal of Pharmacology*, *141*(1), 15–22.

Magee, J. C. (1998). Dendritic Hyperpolarization-Activated Currents Modify the Integrative Properties of Hippocampal CA1 Pyramidal Neurons. *Journal of Neuroscience*, *18*(19), 7613–7624.

Maksymetz, J., Moran, S. P., & Conn, P. J. (2017). Targeting metabotropic glutamate receptors for novel treatments of schizophrenia. *Molecular Brain*, *10*(1), 15.

Manahan-Vaughan, D., Herrero, I., Reymann, K. G., & Sánchez-Prieto, J. (1999). Presynaptic group 1 metabotropic glutamate receptors may contribute to the expression of long-term potentiation in the hippocampal CA1 region. *Neuroscience*, *94*(1), 71–82.

Marabese, I., de Novellis, V., Palazzo, E., Mariani, L., Siniscalco, D., Rodella, L., Rossi, F., & Maione, S. (2005). Differential roles of mGlu8 receptors in the regulation of glutamate and γ-aminobutyric acid release at periaqueductal grey level. *Neuropharmacology*, *49*, 157–166.

Marie, R. L. S., & Peters, A. (1985). The morphology and synaptic connections of spiny stellate neurons in monkey visual cortex (area 17): A golgi-electron microscopic study. *Journal of Comparative Neurology*, *233*(2), 213–235.

Marino, M. J., Williams, D. L., O'Brien, J. A., Valenti, O., McDonald, T. P., Clements, M. K., Wang, R., DiLella, A. G., Hess, J. F., Kinney, G. G., & Conn, P. J. (2003). Allosteric modulation of group III metabotropic glutamate receptor 4: A potential approach to Parkinson's disease treatment. *Proceedings of the National Academy of Sciences of the United States of America*, *100*(23), 13668–13673.

Marin-Padilla, M. (1987). The chandelier cell of the human visual cortex: A Golgi study. *Journal of Comparative Neurology*, *256*(1), 61–70.

Marin-Padilla, M., & Stibitz, G. R. (1974). Three-dimensional reconstruction of the basket cell of the human motor cortex. *Brain Research*, *70*(3), 511–514.

Markram, H. (2000). Organizing principles for a diversity of GABAergic interneurons and synapses in the neocortex. *Science*, *287*(5451), 273–278.

Markram, H., Toledo-Rodriguez, M., Wang, Y., Gupta, A., Silberberg, G., & Wu, C. (2004). Interneurons of the neocortical inhibitory system. *Nature Reviews Neuroscience*, *5*(10), 793–807.

Martin, K. A. C., Somogyi, P., & Whitteridge, D. (1983). Physiological and morphological properties of identified basket cells in the cat's visual cortex. *Experimental Brain Research 1983 50:2*, *50*(2), 193–200.

Martinotti, C. (1890). Beutrag zum Studium der Hirnrinde und dem Centralursprung der Nerven. *Internationale Monatsschrift Für Anatomie Und Physiologie*, *7*, 69–90.

Martín, R., Torres, M., & Sánchez-Prieto, J. (2007). mGluR7 inhibits glutamate release through a PKC-independent decrease in the activity of P/Q-type Ca2+ channels and by diminishing

cAMP in hippocampal nerve terminals. *European Journal of Neuroscience*, *26*(2), 312–322.

Masugi, M., Yokoi, M., Shigemoto, R., Muguruma, K., Watanabe, Y., Sansig, G., van der Putten, H., & Nakanishi, S. (1999). Metabotropic glutamate receptor subtype 7 ablation causes deficit in fear response and conditioned taste aversion. *Journal of Neuroscience*, *19*(3), 955–963.

Matsubara, J. A., & Boyd, J. D. (1992). Presence of GABA-immunoreactive neurons within intracortical patches in area 18 of the cat. *Brain Research*, *583*(1–2), 161–170.

Matsui, T., & Kita, H. (2003). Activation of group III metabotropic glutamate receptors presynaptically reduces both GABAergic and glutamatergic transmission in the rat globus pallidus. *Neuroscience*, *122*(3), 727–737.

Matsuzaki, M., Ellis-Davies, G. C. R., Nemoto, T., Miyashita, Y., Iino, M., & Kasai, H. (2001). Dendritic spine geometry is critical for AMPA receptor expression in hippocampal CA1 pyramidal neurons. *Nature Neuroscience*, *4*(11), 1086–1092.

Matsuzaki, M., Honkura, N., Ellis-Davies, G. C. R., & Kasai, H. (2004). Structural basis of long-term potentiation in single dendritic spines. *Nature*, *429*(6993), 761–766.

McCaffery, B., Cho, K., Bortolotto, Z. A., Aggleton, J. P., Brown, M. W., Conquet, F., Collingridge, G. L., & Bashir, Z. I. (1999). Synaptic depression induced by pharmacological activation of metabotropic glutamate receptors in the perirhinal cortex in vitro. *Neuroscience*, *93*(3), 977–984.

McCool, B. A., Pin, J. P., Harpold, M. M., Brust, P. F., Stauderman, K. A., & Lovinger, D. M. (1998). Rat group I metabotropic glutamate receptors inhibit neuronal Ca2+ channels via multiple signal transduction pathways in HEK 293 cells. *Journal of Neurophysiology*, *79*(1), 379–391.

McCormick, D. A., Connors, B. W., Lighthall, J. W., & Prince, D. A. (1985). Comparative electrophysiology of pyramidal and sparsely spiny stellate neurons of the neocortex. *Journal of Neurophysiology*, *54*(4), 782–806.

McCormick, D. A., & Pape, H. C. (1990). Properties of a hyperpolarization-activated cation current and its role in rhythmic oscillation in thalamic relay neurones. *The Journal of Physiology*, *431*(1), 291–318.

McDonald, C. T., & Burkhalter, A. (1993). Organization of long-range inhibitory connections within rat visual cortex. *Journal of Neuroscience*, *13*(2), 768–781.

McGarry, L. M., Packer, A. M., Fino, E., Nikolenko, V., Sippy, T., & Yuste, R. (2010). Quantitative classifi cation of somatostatin-positive neocortical interneurons identifies three interneuron subtypes. *Frontiers in Neural Circuits*, *4*, 12.

McGuire, B. A., Gilbert, C. D., Rivlin, P. K., & Wiesel, T. N. (1991). Targets of horizontal connections in macaque primary visual cortex. *Journal of Comparative Neurology*, *305*(3), 370–392.

McGuire, P. K., Bates, J. F., & Goldman-Rakic, P. S. (1991). Interhemispheric integration: I. symmetry and convergence of the corticocortical connections of the left and the right principal sulcus (PS) and the left and the right supplementary motor area (SMA) in the rhesus monkey. *Cerebral Cortex*, *1*(5), 390–407.

McKinstry, R. C., Mathur, A., Miller, J. H., Ozcan, A., Snyder, A. Z., Schefft, G. L., Almli, C. R., Shiran, S. I., Conturo, T. E., & Neil, J. J. (2002). Radial organization of developing preterm human cerebral cortex revealed by non-invasive water diffusion anisotropy MRI. *Cerebral Cortex*, *12*(12), 1237–1243.

McNaughton, B. L. (1982). Long-term synaptic enhancement and short-term potentiation in rat fascia dentata act through different mechanisms. *The Journal of Physiology*, *324*(1), 249–262.

Melchitzky, D. S., González, G., González-Burgos, G., Barrionuevo, G., & Lewis, D. A. (2001). Synaptic Targets of the Intrinsic Axon Collaterals of Supragranular Pyramidal Neurons in Monkey Prefrontal Cortex. *Journal of Comparative Neurology*, *430*(2), 209–221.

Melchitzky, D. S., & Lewis, D. A. (2003). Pyramidal Neuron Local Axon Terminals in Monkey Prefrontal Cortex: Differential Targeting of Subclasses of GABA Neurons. *Cerebral Cortex*, *13*(5), 452–460.

Melchitzky, D. S., Sesack, S. R., Pucak, M. L., & Lewis, D. A. (1998). Synaptic targets of pyramidal neurons providing intrinsic horizontal connections in monkey prefrontal cortex. *Journal of Comparative Neurology*, *390*(2), 211–224.

Menon, V., Mackenzie, K., Rivera, S. M., & Reiss, A. L. (2002). Prefrontal cortex involvement in processing incorrect arithmetic equations: Evidence from event-related fMRI. *Human Brain Mapping*, *16*(2), 119–130.

Merchán-Pérez, A., Rodriguez, J. R., Alonso-Nanclares, L., Schertel, A., & DeFelipe, J. (2009). Counting synapses using FIB/SEM microscopy: A true revolution for ultrastructural volume reconstruction. *Frontiers in Neuroanatomy*, *3*, 18.

Merchán-Pérez, A., Rodríguez, J. R., González, S., Robles, V., DeFelipe, J., Larrañaga, P., & Bielza, C. (2014). Three-dimensional spatial distribution of synapses in the neocortex: A dual-beam electron microscopy study. *Cerebral Cortex*, *24*(6), 1579–1588.

Mercier, M. S., & Lodge, D. (2014). Group III Metabotropic Glutamate Receptors: Pharmacology, Physiology and Therapeutic Potential. *Neurochemical Research*, *39*(10), 1876–1894.

Meskenaite, V. (1997). Calretinin-immunoreactive local circuit neurons in area 17 of the cynomolgus monkey, Macaca fascicularis. *Journal of Comparative Neurology*, *379*(1), 113–132.

Mesulam, M. M. (1998). From sensation to cognition. *Brain*, *121*(6), 1013–1052.

Meyer, G. (1983). Axonal patterns and topography of short-axon neurons in visual areas 17, 18, and 19 of the cat. *Journal of Comparative Neurology*, *220*(4), 405–438.

Meyer, G. (1987). Forms and spatial arrangement of neurons in the primary motor cortex of man. *Journal of Comparative Neurology*, *262*(3), 402–428.

Meyer, G., & Ferres-Torres, R. (1984). Postnatal maturation of nonpyramidal neurons in the visual cortex of the cat. *Journal of Comparative Neurology*, *228*(2), 226–244.

Millán, C., Luján, R., Shigemoto, R., & Sánchez-Prieto, J. (2002). Subtype-specific expression of Group III metabotropic glutamate receptors and Ca2+ channels in single nerve terminals. *Journal of Biological Chemistry*, *277*(49), 47796–47803.

Mills, C. K. (1891). On The Localisation Of The Auditory Centre. *Brain*, *14*(4), 465–472.

Mitchell, S. J., & Silver, R. a. (2000). Glutamate spillover suppresses inhibition by activating presynaptic mGluRs. *Nature*, *404*(6777), 498–502.

Mohan, H., Verhoog, M. B., Doreswamy, K. K., Eyal, G., Aardse, R., Lodder, B. N., Goriounova, N. A., Asamoah, B., B. Brakspear, A. B. C., Groot, C., van der Sluis, S., Testa-Silva, G., Obermayer, J., Boudewijns, Z. S. R. M., Narayanan, R. T., Baayen, J. C., Segev, I., Mansvelder, H. D., & de Kock, C. P. J. (2015). Dendritic and axonal architecture of individual pyramidal neurons across layers of adult human neocortex. *Cerebral Cortex*, *25*(12), 4839–4853.

Molnár, G., Faragó, N., Kocsis, Á. K., Rózsa, M., Lovas, S., Boldog, E., Báldi, R., Csajbók, É., Gardi, J., Puskás, L. G., & Tamás, G. (2014). GABAergic neurogliaform cells represent local sources of insulin in the cerebral cortex. *Journal of Neuroscience*, *34*(4), 1133–1137.

Molnár, G., Oláh, S., Komlósi, G., Füle, M., Szabadics, J., Varga, C., Barzó, P., & Tamás, G. (2008). Complex events initiated by individual spikes in the human cerebral cortex. *PLoS Biology*, *6*(9), 1842–1849.

Molnár, G., Rózsa, M., Baka, J., Holderith, N., Barzó, P., Nusser, Z., & Tamás, G. (2016). Human pyramidal to interneuron synapses are mediated by multi-vesicular release and multiple docked vesicles. *ELife*, *5*, e18167.

Mongillo, G., Barak, O., & Tsodyks, M. (2008). Synaptic Theory of Working Memory. *Science*, *319*(5869), 1543–1546.

Mountcastle, V. B. (1957). Modality and topographic properties of single neurons of cat's somatic sensory cortex. *Journal of Neurophysiology*, *20*(4), 408–434.

Mountcastle, V. B. (1997). The columnar organization of the neocortex. *Brain*, *120*(4), 701–722.

Mountcastle, V. B., Lynch, J. C., Georgopoulos, A., Sakata, H., & Acuna, C. (1975). Posterior parietal association cortex of the monkey: command functions for operations within extrapersonal space. *Journal of Neurophysiology*, *38*(4), 871–908.

Mozrzymas, J. W. (2004). Dynamism of GABAA receptor activation shapes the "personality" of inhibitory synapses. *Neuropharmacology*, *47*(7), 945–960.

Murphy, S. N., & Miller, R. J. (1988). A glutamate receptor regulates Ca2+ mobilization in hippocampal neurons. *Proceedings of the National Academy of Sciences of the United States of America*, *85*(22), 8737–8741.

Nadarajah, B., Alifragis, P., Wong, R. O. L., & Parnavelas, J. G. (2002). Ventricle-directed migration in the developing cerebral cortex. *Nature Neuroscience*, *5*(3), 218–224.

Naie, K., Gundimi, S., Siegmund, H., Heinemann, U., & Manahan-Vaughan, D. (2006). Group III metabotropic glutamate receptor-mediated, chemically induced long-term depression differentially affects cell viability in the hippocampus. *European Journal of Pharmacology*, *535*(1–3), 104–113.

Naie, K., & Manahan-Vaughan, D. (2005). Investigations of the protein synthesis dependency of mGluR-induced long-term depression in the dentate gyrus of freely moving rats. *Neuropharmacology*, *49*, 35–44.

Nakagawa, S., Watanabe, M., Isobe, T., Kondo, H., & Inoue, Y. (1998). Cytological compartmentalization in the staggerer cerebellum, as revealed by calbindin

immunohistochemistry for Purkinje cells. *Journal of Comparative Neurology*, *395*(1), 112–120.

Nakajima, Y., Iwakabe, H., Akazawa, C., Nawa, H., Shigemoto, R., Mizuno, N., & Nakanishi, S. (1993). Molecular characterization of a novel retinal metabotropic glutamate receptor mGluR6 with a high agonist selectivity for L-2-amino-4- phosphonobutyrate. *Journal of Biological Chemistry*, *268*(16), 11868–11873.

Nakanishi, S. (1992). Molecular diversity of glutamate receptors and implications for brain function. *Science*, *258*(5082), 597–603.

Nandi, A., Chartrand, T., Geit, W. van, Buchin, A., Yao, Z., Lee, S. Y., Wei, Y., Kalmbach, B., Lee, B., Lein, E., Berg, J., Sümbül, U., Koch, C., Tasic, B., & Anastassiou, C. A. (2020). Single-neuron models linking electrophysiology, morphology and transcriptomics across cortical cell types. *BioRxiv*, 2020.04.09.030239.

Neki, A., Ohishi, H., Kaneko, T., Shigemoto, R., Nakanishi, S., & Mizuno, N. (1996). Pre- and postsynaptic localization of a metabotropic glutamate receptor, mGluR2, in the rat brain: An immunohistochemical study with a monoclonal antibody. *Neuroscience Letters*, *202*(3), 197–200.

Neu, A., Földy, C., & Soltesz, I. (2007). Postsynaptic origin of CB1-dependent tonic inhibition of GABA release at cholecystokinin-positive basket cell to pyramidal cell synapses in the CA1 region of the rat hippocampus. *Journal of Physiology*, *578*(1), 233–247.

Nicoletti, F., Bockaert, J., Collingridge, G. L., Conn, P. J., Ferraguti, F., Schoepp, D. D., Wroblewski, J. T., & Pin, J. P. (2011). Metabotropic glutamate receptors: From the workbench to the bedside. *Neuropharmacology*, *60*(7–8), 1017–1041.

Nicoletti, F., Iadarola, M. J., Wroblewski, J. T., & Costa, E. (1986). Excitatory amino acid recognition sites coupled with inositol phospholipid metabolism: Developmental changes and interaction with α1-adrenoceptors. *Proceedings of the National Academy of Sciences of the United States of America*, *83*(6), 1931–1935.

Nicoletti, F., Meek, J. L., Iadarola, M. J., Chuang, D. M., Roth, B. L., & Costa, E. (1986). Coupling of Inositol Phospholipid Metabolism with Excitatory Amino Acid Recognition Sites in Rat Hippocampus. *Journal of Neurochemistry*, *46*(1), 40–46.

Nicoletti, F., Wroblewski, J. T., Novelli, A., Alho, H., Guidotti, A., & Costa, E. (1986). The activation of inositol phospholipid metabolism as a signal-transducting system for excitatory amino acids in primary cultures of cerebellar granule cells. *Journal of Neuroscience*, *6*(7), 1905–1911.

Nieman, D. H. (2015). New treatments for psychotic disorders. In *The Lancet Psychiatry*, *2*(4), 282–283.

Nieuwenhuys, R. (1994). The neocortex - An overview of its evolutionary development, structural organization and synaptology. *Anatomy and Embryology*, *190*(4), 307–337.

Nieuwenhuys, R., Voogd, J., & van Huijzen, C. (2008). *The human central nervous system* (4th ed.). Springer, Berlin, Heidelberg.

Niswender, C. M., Johnson, K. A., Luo, Q., Ayala, J. E., Kim, C., Conn, P. J., & Weaver, C. D. (2008). A novel assay of Gi/o-linked G protein-coupled receptor coupling to potassium channels provides new insights into the pharmacology of the group III metabotropic glutamate receptors. *Molecular Pharmacology*, *73*(4), 1213–1224.

Noguchi, J., Matsuzaki, M., Ellis-Davies, G. C. R., & Kasai, H. (2005). Spine-neck geometry determines NMDA receptor-dependent Ca2+ signaling in dendrites. *Neuron*, *46*(4), 609–622.

Nomura, A., Shigemoto, R., Nakamura, Y., Okamoto, N., Mizuno, N., & Nakanishi, S. (1994). Developmentally regulated postsynaptic localization of a metabotropic glutamate receptor in rat rod bipolar cells. *Cell*, *77*(3), 361–369.

Nusser, Z., Cull-Candy, S., & Farrant, M. (1997). Differences in Synaptic GABAA Receptor Number Underlie Variation in GABA Mini Amplitude. *Neuron*, *19*(3), 697–709.

Obermayer, J., Heistek, T. S., Kerkhofs, A., Goriounova, N. A., Kroon, T., Baayen, J. C., Idema, S., Testa-Silva, G., Couey, J. J., & Mansvelder, H. D. (2018). Lateral inhibition by Martinotti interneurons is facilitated by cholinergic inputs in human and mouse neocortex. *Nature Communications*, *9*(1), 1–14.

Ohishi, H., Akazawa, C., Shigemoto, R., Nakanishi, S., & Mizuno, N. (1995). Distributions of the mRNAs for L-2-amino-4-phosphonobutyrate-sensitive metabotropic glutamate receptors, mGluR4 and mGluR7, in the rat brain. *Journal of Comparative Neurology*, *360*(4), 555–570.

Ohning, G. V., Wong, H. C., Lloyd, K. C. K., & Walsh, J. H. (1996). Gastrin mediates the gastric mucosal proliferative response to feeding. *American Journal of Physiology - Gastrointestinal and Liver Physiology*, *271*(3 34-3).

O'Kusky, J., & Colonnier, M. (1982). Postnatal changes in the number of neurons and synapses in the visual cortex (area 17) of the macaque monkey: A stereological analysis in normal and monocularly deprived animals. *Journal of Comparative Neurology*, *210*(3), 291–306.

Oláh, S., Füle, M., Komlósi, G., Varga, C., Báldi, R., Barzó, P., & Tamás, G. (2009). Regulation of cortical microcircuits by unitary GABA-mediated volume transmission. *Nature*, *461*(7268), 1278–1281.

Oláh, S., Komlósi, G., Szabadics, J., Varga, C., Tóth, É., Barzó, P., & Tamás, G. (2007). Output of neurogliaform cells to various neuron types in the human and rat cerebral cortex. *Frontiers in Neural Circuits*, *0*, 4.

Olshausen, B. A., & Field, D. J. (1996). Emergence of simple-cell receptive field properties by learning a sparse code for natural images. *Nature*, *381*(6583), 607–609.

Öngür, D., Ferry, A. T., & Price, J. L. (2003). Architectonic subdivision of the human orbital and medial prefrontal cortex. *Journal of Comparative Neurology*, *460*(3), 425–449.

Osaka, N., Osaka, M., Kondo, H., Morishita, M., Fukuyama, H., & Shibasaki, H. (2004). The neural basis of executive function in working memory: An fMRI study based on individual differences. *NeuroImage*, *21*(2), 623–631.

Ozsvár, A., Komlósi, G., Oláh, G., Baka, J., Molnár, G., & Tamás, G. (2021). Predominantly linear summation of metabotropic postsynaptic potentials follows coactivation of neurogliaform interneurons. *ELife*, *10*.

Packer, A. M., & Yuste, R. (2011). Dense, unspecific connectivity of neocortical parvalbumin-positive interneurons: A canonical microcircuit for inhibition? *Journal of Neuroscience*, *31*(37), 13260–13271.

Padamsey, Z., & Emptage, N. J. (2011). Imaging synaptic plasticity. *Molecular Brain*, *4*(1), 1–10.

Padamsey, Z., Tong, R., & Emptage, N. (2019). Optical Quantal Analysis Using Ca2+ Indicators: A Robust Method for Assessing Transmitter Release Probability at Excitatory Synapses by Imaging Single Glutamate Release Events. *Frontiers in Synaptic Neuroscience*, *11*, 5.

Pałucha, A., Tatarczyńska, E., Brański, P., Szewczyk, B., Wierońska, J. M., Kłak, K., Chojnacka-Wójcik, E., Nowak, G., & Pilc, A. (2004). Group III mGlu receptor agonists produce anxiolytic- and antidepressant-like effects after central administration in rats. *Neuropharmacology*, *46*(2), 151–159.

Panatier, A., Poulain, D. A., & Oliet, S. H. R. (2004). Regulation of transmitter release by high-affinity group III mGluRs in the supraoptic nucleus of the rat hypothalamus. *Neuropharmacology*, *47*(3), 333–341.

Pape, H.-C., & McCormick, D. A. (1989). Noradrenaline and serotonin selectively modulate thalamic burst firing by enhancing a hyperpolarization-activated cation current. *Nature*, *340*(6236), 715–718.

Park, M., Niciu, M. J., & Zarate, C. A. (2015). Novel Glutamatergic Treatments for Severe Mood Disorders. In *Current Behavioral Neuroscience Reports*, *2*(4), 198-208.

Pearce, B., Albrecht, J., Morrow, C., & Murphy, S. (1986). Astrocyte glutamate receptor activation promotes inositol phospholipid turnover and calcium flux. *Neuroscience Letters*, *72*(3), 335–340.

Pekhletski, R., Gerlai, R., Overstreet, L. S., Huang, X. P., Agopyan, N., Slater, N. T., Abramow-Newerly, W., Roder, J. C., & Hampson, D. R. (1996). Impaired cerebellar synaptic plasticity and motor performance in mice lacking the mGluR4 subtype of metabotropic glutamate receptor. *Journal of Neuroscience*, *16*(20), 6364–6373.

Pelkey, K. A., Lavezzari, G., Racca, C., Roche, K. W., & McBain, C. J. (2005). mGluR7 is a metaplastic switch controlling bidirectional plasticity of feedforward inhibition. *Neuron*, *46*(1), 89–102.

Pelkey, K. A., Topolnik, L., Lacaille, J. C., & McBain, C. J. (2006). Compartmentalized Ca2+ Channel Regulation at Divergent Mossy-Fiber Release Sites Underlies Target Cell-Dependent Plasticity. *Neuron*, *52*(3), 497–510.

Penfield, W., & Boldrey, E. (1937). Somatic motor and sensory representation in the cerebral cortex of man as studied by electrical stimulation. *Brain*, *60*(4), 389–443.

Peng, H., Xie, P., Liu, L., Kuang, X., Wang, Y., Qu, L., Gong, H., Jiang, S., Li, A., Ruan, Z., Ding, L., Yao, Z., Chen, C., Chen, M., Daigle, T. L., Dalley, R., Ding, Z., Duan, Y., Feiner, A., … Zeng, H. (2021). Morphological diversity of single neurons in molecularly defined cell types. *Nature*, *598*(7879), 174–181.

Pernice, V., & Silveira, R. A. da. (2018). Interpretation of correlated neural variability from models of feed-forward and recurrent circuits. *PLOS Computational Biology*, *14*(2), e1005979.

Perrett, D. I., Hietanen, J. K., Oram, M. W., & Benson, P. J. (1992). Organization and functions of cells responsive to faces in the temporal cortex. *Philosophical Transactions of the Royal Society of London. Series B, Biological Sciences*, *335*(1273), 23–30.

Pessoa, L., Kastner, S., & Ungerleider, L. G. (2003). Neuroimaging studies of attention: From modulation of sensory processing to top-down control. *Journal of Neuroscience*, *23*(10), 3990–3998.

Peter R., H. (1979). Synaptic density in human frontal cortex - Developmental changes and effects of aging. *Brain Research*, *163*(2), 195–205.

Peters, A., & Sethares, C. (1991). Organization of pyramidal neurons in area 17 of monkey visual cortex. *Journal of Comparative Neurology*, *306*(1), 1–23.

Peters, A., & Sethares, C. (1996). Myelinated axons and the pyramidal cell modules in monkey primary visual cortex. *Journal of Comparative Neurology*, *365*(2), 232–255.

Peters, A., & Sethares, C. (1997). The organization of double bouquet cells in monkey striate cortex. *Journal of Neurocytology*, *26*(12), 779–797.

Peters, A., Sethares, C., & Luebke, J. I. (2008). Synapses are lost during aging in the primate prefrontal cortex. *Neuroscience*, *152*(4), 970–981.

Peters, A., & Walsh, T. M. (1972). A study of the organization of apical dendrites in the somatic sensory cortex of the rat. *Journal of Comparative Neurology*, *144*(3), 253–268.

Peters, A., & Yilmaz, E. (1993). Neuronal organization in area 17 of cat visual cortex. *Cerebral Cortex*, *3*(1), 49–68.

Petersen, S. E., & Posner, M. I. (2012). The attention system of the human brain: 20 years after. *Annual Review of Neuroscience*, *35*, 73–89.

Pi, H.-J., Hangya, B., Kvitsiani, D., Sanders, J. I., Huang, Z. J., & Kepecs, A. (2013). Cortical interneurons that specialize in disinhibitory control. *Nature*, *503*(7477), 521–524.

Pin, J. P., & Duvoisin, R. (1995). The metabotropic glutamate receptors: Structure and functions. *Neuropharmacology*, *34*(1), 1–26.

Pin, J. P., Galvez, T., & Prézeau, L. (2003). Evolution, structure, and activation mechanism of family 3/C G-protein-coupled receptors. *Pharmacology and Therapeutics*, *98*(3), 325–354.

Pisani, A., Calabresi, P., Centonze, D., & Bernardi, G. (1997). Activation of group III metabotropic glutamate receptors depresses glutamatergic transmission at corticostriatal synapse. *Neuropharmacology*, *36*(6), 845–851.

Platt, M. L., & Glimcher, P. W. (1999). Neural correlates of decision variables in parietal cortex. *Nature*, *400*(6741), 233–238.

Porter, J. T., Cauli, B., Staiger, J. F., Lambolez, B., Rossier, J., & Audinat, E. (1998). Properties of bipolar VIPergic interneurons and their excitation by pyramidal neurons in the rat neocortex. *European Journal of Neuroscience*, *10*(12), 3617–3628.

Povysheva, N. v., Zaitsev, A. v., Gonzalez-Burgos, G., & Lewis, D. A. (2013). Electrophysiological Heterogeneity of Fast-Spiking Interneurons: Chandelier versus Basket Cells. *PLoS ONE*, *8*(8), e70553.

Rakic, P. (1974). Neurons in rhesus monkey visual cortex: Systematic relation between time of origin and eventual disposition. *Science*, *183*(4123), 425–427.

Rakic, P. (2008). Intrinsic and Extrinsic Determinants of Neocortical Parcellation: A Radial Unit Model. In M. H. Johnson, Y. Munakata, & R. O. gilmore (Eds.), *Brain Dovelopement and Cognition* (2nd ed., pp. 83–100). John Wiley & Sons, Ltd.

Rakic, P., Bourgeois, J. P., Eckenhoff, M. F., Zecevic, N., & Goldman-Rakic, P. S. (1986). Concurrent overproduction of synapses in diverse regions of the primate cerebral cortex. *Science*, *232*(4747), 232–235.

Ramer, M. S. (2008). Anatomical and functional characterization of neuropil in the gracile fasciculus. *Journal of Comparative Neurology*, *510*(3), 283–296.

Ramón y Cajal, S. (1899a). Estudios sobre la corteza cerebral humana I: Corteza visual. *Revista Trimestral Micrográfica*, *4*, 1–63.

Ramón y Cajal, S. (1899b). Estudios sobre la corteza cerebral humana II: Estructura de la corteza motriz del hombre y mamíferos superiores. *Revista Trimestral Micrográfica*, *4*, 117–200.

Ramón y Cajal, S. (1909). *Histologie du système nerveux de l'homme & des vertébrés*. Maloine.

Ren, W., Palazzo, E., Maione, S., & Neugebauer, V. (2011). Differential effects of mGluR7 and mGluR8 activation on pain-related synaptic activity in the amygdala. *Neuropharmacology*, *61*(8), 1334–1344.

Riedemann, T., Straub, T., & Sutor, B. (2018). Two types of somatostatin-expressing GABAergic interneurons in the superficial layers of the mouse cingulate cortex. *PLoS ONE*, *13*(7), 1–26.

Riley, M. R., & Constantinidis, C. (2016). Role of prefrontal persistent activity in working memory. *Frontiers in Systems Neuroscience*, *9*, 181.

Robbins, M. J., Starr, K. R., Honey, A., Soffin, E. M., Rourke, C., Jones, G. A., Kelly, F. M., Strum, J., Melarange, R. A., Harris, A. J., Rocheville, M., Rupniak, T., Murdock, P. R., Jones, D. N. C., Kew, J. N. C., & Maycox, P. R. (2007). Evaluation of the mGlu8 receptor as a putative therapeutic target in schizophrenia. *Brain Research*, *1152*(1), 215–227.

Rodríguez-Moreno, A., Sistiaga, A., Lerma, J., & Sánchez-Prieto, J. (1998). Switch from facilitation to inhibition of excitatory synaptic transmission by group I mGluR desensitization. *Neuron*, *21*(6), 1477–1486.

Rogers, J. H. (1992). Immunohistochemical markers in rat cortex: co-localization of calretinin and calbindin-D28k with neuropeptides and GABA. *Brain Research*, *587*(1), 147–157.

Rose, J. E., & Woolsey, C. N. (1948). Structure and relations of limbic cortex and anterior thalamic nuclei in rabbit and cat. *Journal of Comparative Neurology*, *89*(3), 279–347.

Rose, J. E., & Woolsey, C. N. (1949). The relations of thalamic connections, cellular structure and evocable electrical activity in the auditory region of the cat. *Journal of Comparative Neurology*, *91*(3), 441–466.

Rose, M., Dütting, E., & Enz, R. (2008). Band 4.1 proteins are expressed in the retina and interact with both isoforms of the metabotropic glutamate receptor type 8. *Journal of Neurochemistry*, *105*(6), 2375–2387.

Rossi, L. F., Harris, K. D., & Carandini, M. (2020). Spatial connectivity matches direction selectivity in visual cortex. *Nature*, *588*(7839), 648–652.

Rozov, A., Burnashev, N., Sakmann, B., & Neher, E. (2001). Transmitter release modulation by intracellular Ca2+ buffers in facilitating and depressing nerve terminals of pyramidal cells in layer 2/3 of the rat neocortex indicates a target cell-specific difference in presynaptic calcium dynamics. *The Journal of Physiology*, *531*(3), 807–826.

Rudy, B., Fishell, G., Lee, S. H., & Hjerling-Leffler, J. (2011). Three groups of interneurons account for nearly 100% of neocortical GABAergic neurons. *Developmental Neurobiology*, *71*(1), 45–61.

Rusakov, D. A., Wuerz, A., & Kullmann, D. M. (2004). Heterogeneity and Specificity of Presynaptic Ca2+ Current Modulation by mGluRs at Individual Hippocampal Synapses. *Cerebral Cortex*, *14*(7), 748–758.

Sah, P., & Faber, E. S. L. (2002). Channels underlying neuronal calcium-activated potassium currents. *Progress in Neurobiology*, *66*(5), 345–353.

Salt, T. E., & Eaton, S. A. (1995). Distinct presynaptic metabotropic receptors for l-AP4 and CCG1 on GABAergic terminals: Pharmacological evidence using novel α-methyl derivative mGluR antagonists, MAP4 and MCCG, in the rat thalamus in vivo. *Neuroscience*, *65*(1), 5–13.

Sanacora, G., Treccani, G., & Popoli, M. (2012). Towards a glutamate hypothesis of depression: An emerging frontier of neuropsychopharmacology for mood disorders. *Neuropharmacology*, *62*(1), 63–77.

Sansig, G., Bushell, T. J., Clarke, V. R. J., Rozov, A., Burnashev, N., Portet, C., Gasparini, F., Schmutz, M., Klebs, K., Shigemoto, R., Flor, P. J., Kuhn, R., Knoepfel, T., Schroeder, M., Hampson, D. R., Collett, V. J., Zhang, C., Duvoisin, R. M., Collingridge, G. L., & van der Putten, H. (2001). Increased seizure susceptibility in mice lacking metabotropic glutamate receptor 7. *Journal of Neuroscience*, *21*(22), 8734–8745.

Sarkissov, S. A., Filimonoff, I. N., Kononowa, E. P., Preobraschenskaja, I. S., & Kukuew, L. A. (1955). *Atlas of the cytoarchitectonics of the human cerebral cortex.* Moscow: Medgiz.

Scanziani, M., Gähwiler, B. H., & Charpak, S. (1998). Target cell-specific modulation of transmitter release at terminals from a single axon. *Proceedings of the National Academy of Sciences of the United States of America*, *95*(20), 12004–12009.

Schaffhauser, H., Knoflach, F., Pink, J. R., Bleuel, Z., Cartmell, J., Goepfert, F., Kemp, J. A., Richards, J. G., Adam, G., & Mutel, V. (1998). Multiple pathways for regulation of the KCl-induced [3H]-GABA release by metabotropic glutamate receptors, in primary rat cortical cultures. *Brain Research*, *782*(1–2), 91–104.

Schiffmann, S. N., Cheron, G., Lohof, A., D'Alcantara, P., Meyer, M., Parmentier, M., & Schurmans, S. (1999). Impaired motor coordination and Purkinje cell excitability in mice lacking calretinin. *Proceedings of the National Academy of Sciences of the United States of America*, *96*(9), 5257–5262.

Schmid, S., & Fendt, M. (2006). Effects of the mGluR8 agonist (S)-3,4-DCPG in the lateral amygdala on acquisition/expression of fear-potentiated startle, synaptic transmission, and plasticity. *Neuropharmacology*, *50*(2), 154–164.

Schoepp, D. D., Jane, D. E., & Monn, J. A. (1999). Pharmacological agents acting at subtypes of metabotropic glutamate receptors. *Neuropharmacology*, *38*(10), 1431–1476.

Schoppa, N. E., & Westbrook, G. L. (1997). Modulation of mEPSCs in olfactory bulb mitral cells by metabotropic glutamate receptors. *Journal of Neurophysiology*, *78*(3), 1468–1475.

Schrader, L. A., & Tasker, J. G. (1997). Presynaptic Modulation by Metabotropic Glutamate Receptors of Excitatory and Inhibitory Synaptic Inputs to Hypothalamic Magnocellular Neurons. *Journal of Neurophysiology*, *77*(2), 527–536.

Schuman, B., Machold, R. P., Hashikawa, Y., Fuzik, J., Fishell, G. J., & Rudy, B. (2019). Four unique interneuron populations reside in neocortical layer 1. *Journal of Neuroscience*, *39*(1), 125–139.

Schwaller, B., Dick, J., Dhoot, G., Carroll, S., Vrbova, G., Nicotera, P., Pette, D., Wyss, A., Bluethmann, H., Hunziker, W., & Celio, M. R. (1999). Prolonged contraction-relaxation cycle of fast-twitch muscles in parvalbumin knockout mice. *American Journal of Physiology - Cell Physiology*, *276*(2 45-2), 395–403.

Seebahn, A., Rose, M., & Enz, R. (2008). RanBPM is expressed in synaptic layers of the mammalian retina and binds to metabotropic glutamate receptors. *FEBS Letters*, *582*(16), 2453–2457.

Selemon, L. D., & Goldman-Rakic, P. S. (1988). Common cortical and subcortical targets of the dorsolateral prefrontal and posterior parietal cortices in the rhesus monkey: evidence for a distributed neural network subserving spatially guided behavior. *Journal of Neuroscience*, *8*(11), 4049–4068.

Selvam, C., Goudet, C., Oueslati, N., Pin, J. P., & Acher, F. C. (2007). L-(+)-2-amino-4-thiophosphonobutyric acid (L-thioAP4), a new potent agonist of group III metabotropic glutamate receptors: Increased distal acidity affords enhanced potency. *Journal of Medicinal Chemistry*, *50*(19), 4656–4664.

Semyanov, A., & Kullmann, D. M. (2000). Modulation of GABAergic signaling among interneurons by metabotropic glutamate receptors. *Neuron*, *25*(3), 663–672.

Shigemoto, R., Kinoshita, A., Wada, E., Nomura, S., Ohishi, H., Takada, M., Flor, P. J., Neki, A., Abe, T., Nakanishi, S., & Mizuno, N. (1997). Differential Presynaptic Localization of Metabotropic Glutamate Receptor Subtypes in the Rat Hippocampus. *Journal of Neuroscience*, *17*(19), 7503–7522.

Shigemoto, R., Kulik, A., Roberts, J. D. B., Ohishi, H., Nusser, Z., Kaneko, T., & Somogyi, P. (1996). Target-cell-specific concentration of a metabotropic glutamate receptor in the presynaptic active zone. *Nature*, *381*(6582), 523–525.

Sibille, P., Lopez, S., Brabet, I., Valenti, O., Oueslati, N., Gaven, F., Goudet, C., Bertrand, H. O., Neyton, J., Marino, M. J., Amalric, M., Pin, J. P., & Acher, F. C. (2007). Synthesis and biological evaluation of 1-amino-2- phosphonomethylcyclopropanecarboxylic acids, new group III metabotropic glutamate receptor agonists. *Journal of Medicinal Chemistry*, *50*(15), 3585–3595.

Simon, A., Oláh, S., Molnár, G., Szabadics, J., & Tamás, G. (2005). Gap-junctional coupling between neurogliaform cells and various interneuron types in the neocortex. *Journal of Neuroscience*, *25*(27), 6278–6285.

Simon, O., Kherif, F., Flandin, G., Poline, J., Rivière, D., Mangin, J., le Bihan, D., & Dehaene, S. (2004). Automatized clustering and functional geometry of human parietofrontal networks for language, space, and number. *NeuroImage*, *23*(3), 1192–1202.

Sistiaga, A., & Sánchez-Prieto, J. (2000). Protein phosphatase 1 and 2A inhibitors prolong the switch in the control of glutamate release by group I metabotropic glutamate receptors: Characterization of the inhibitory pathway. *Journal of Neurochemistry*, *75*(4), 1566–1574.

Sladeczek, F., Pin, J. P., Récasens, M., Bockaert, J., & Weiss, S. (1985). Glutamate stimulates inositol phosphate formation in striatal neurones. *Nature*, *317*(6039), 717–719.

Snead, O. C., Banerjee, P. K., Burnham, M., & Hampson, D. (2000). Modulation of Absence Seizures by the GABAA Receptor: A Critical Role for Metabotropic Glutamate Receptor 4 (mGluR4). *Journal of Neuroscience*, *20*(16), 6218–6224.

Somogyi, J., Baude, A., Omori, Y., Shimizu, H., Mestikawy, S. el, Fukaya, M., Shigemoto, R., Watanabe, M., & Somogyi, P. (2004). GABAergic basket cells expressing cholecystokinin contain vesicular glutamate transporter type 3 (VGLUT3) in their synaptic terminals in hippocampus and isocortex of the rat. *European Journal of Neuroscience*, *19*(3), 552–569.

Somogyi, P. (1977). A specific "axo-axonal" interneuron in the visual cortex of the rat. *Brain Research*, *136*(2), 345–350.

Somogyi, P., & Cowey, A. (1981). Combined golgi and electron microscopic study on the synapses formed by double bouquet cells in the visual cortex of the cat and monkey. *Journal of Comparative Neurology*, *195*(4), 547–566.

Somogyi, P., Cowey, A., Halász, N., & Freund, T. F. (1981). Vertical organization of neurones accumulating 3H-GABA in visual cortex of rhesus monkey. *Nature*, *294*(5843), 761–763.

Somogyi, P., Dalezios, Y., Luján, R., Roberts, J. D. B., Watanabe, M., & Shigemoto, R. (2003). High level of mGluR7 in the presynaptic active zones of select populations of GABAergic terminals innervating interneurons in the rat hippocampus. *European Journal of Neuroscience*, *17*(12), 2503–2520.

Somogyi, P., Freund, T. F., & Cowey, A. (1982). The axo-axonic interneuron in the cerebral cortex of the rat, cat and monkey. *Neuroscience*, *7*(11), 2577–2607.

Somogyi, P., & Hodgson, A. J. (1985). Antisera to γ-aminobutyric acid. III. Demonstration of GABA in Golgi-impregnated neurons and in conventional electron microscopic sections of cat striate cortex. *Journal of Histochemistry and Cytochemistry*, *33*(3), 249–257.

Somogyi, P., Kisvárday, Z. F., Martin, K. A. C., & Whitteridge, D. (1983). Synaptic connections of morphologically identified and physiologically characterized large basket cells in the striate cortex of cat. *Neuroscience*, *10*(2), 261–294.

Somogyi, P., & Soltész, I. (1986). Immunogold demonstration of GABA in synaptic terminals of intracellularly recorded, horseradish peroxidase-filled basket cells and clutch cells in the cat's visual cortex. *Neuroscience*, *19*(4), 1051–1065.

Somogyi, P., Tamás, G., Lujan, R., & Buhl, E. H. (1998). Salient features of synaptic organisation in the cerebral cortex. *Brain Research Reviews*, *26*(2–3), 113–135.

Song, S., Sjöström, P. J., Reigl, M., Nelson, S., & Chklovskii, D. B. (2005). Highly Nonrandom Features of Synaptic Connectivity in Local Cortical Circuits. *PLOS Biology*, *3*(3), e68.

Stachniak, T. J., Sylwestrak, E. L., Scheiffele, P., Hall, B. J., & Ghosh, A. (2019). Elfn1-induced constitutive activation of mglur7 determines frequency-dependent recruitment of somatostatin interneurons. *Journal of Neuroscience*, *39*(23), 4461–4474.

Stachowicz, K., Brañski, P., Kłak, K., van der Putten, H., Cryan, J. F., Flor, P. J., & Pilc, A. (2008). Selective activation of metabotropic G-protein-coupled glutamate 7 receptor elicits anxiolytic-like effects in mice by modulating GABAergic neurotransmission. *Behavioural Pharmacology*, *19*(5–6), 597–603.

Stachowicz, K., Chojnacka-Wójcik, E., Kłak, K., & Pilc, A. (2007). Anxiolytic-like effect of group III mGlu receptor antagonist is serotonin-dependent. *Neuropharmacology*, *52*(2), 306–312.

Stachowicz, K., Kłodzińska, A., Palucha-Poniewiera, A., Schann, S., Neuville, P., & Pilc, A. (2009). The group III mGlu receptor agonist ACPT-I exerts anxiolytic-like but not antidepressant-like effects, mediated by the serotonergic and GABA-ergic systems. *Neuropharmacology*, *57*(3), 227–234.

Staiger, J. F., Flagmeyer, I., Schubert, D., Zilles, K., Kötter, R., & Luhmann, H. J. (2004). Functional diversity of layer IV spiny neurons in rat somatosensory cortex: Quantitative morphology of electrophysiologically characterized and biocytin labeled cells. *Cerebral Cortex*, *14*(6), 690–701.

Starr, M. A. (1884). Cortical Lesions of the Brain. A Collection and Analysis of the American Cases of Localized Cerebral Disease. *The American Journal of the Medical Sciences*, *87*(174), 366–391.

Steriade, M., Jones, E. G., & McCormick, D. A. (1997). *Thalamus, vol I: Organisation and function.* Elsevier.

Sterio, D. C. (1984). The unbiased estimation of number and sizes of arbitrary particles using the disector. *Journal of Microscopy*, *134*(2), 127–136.

Summa, M., di Prisco, S., Grilli, M., Usai, C., Marchi, M., & Pittaluga, A. (2013). Presynaptic mGlu7 receptors control GABA release in mouse hippocampus. *Neuropharmacology*, *66*, 215–224.

Suzuki, K., Mori, N., Kittaka, H., Iwata, Y., Yamada, Y., Osonoe, K., & Niwa, S. I. (1996). Anticonvulsant action of metabotropic glutamate receptor agonists in kindled amygdala of rats. *Neuroscience Letters*, *204*(1–2), 41–44.

Szegedi, V., Molnár, G., Paizs, M., Csakvari, E., Barzó, P., Tamás, G., & Lamsa, K. (2017). High-precision fast-spiking basket cell discharges during complex events in the human neocortex. *ENeuro*, *4*(5), ENEURO.0260-17.2017.

Szegedi, V., Paizs, M., Csakvari, E., Molnar, G., Barzo, P., Tamas, G., & Lamsa, K. (2016). Plasticity in Single Axon Glutamatergic Connection to GABAergic Interneurons Regulates Complex Events in the Human Neocortex. *PLoS Biology*, *14*(11), e2000237.

Szentágothai, J. (1973). *Synaptology of the Visual Cortex* (pp. 269–324). Springer, Berlin, Heidelberg.

Szentágothai, J. (1975). The "module-concept" in cerebral cortex architecture. *Brain Research*, *95*(2–3), 475–496.

Szentágothai, J. (1978). The neuron network of the cerebral cortex: a functional interpretation. *Proceedings of the Royal Society of London - Biological Sciences*, *201*(1144), 219–248.

Szentágothai, J., & Arbib, M. A. (1974). Conceptual models of neural organization. *Neurosciences Research Program Bulletin*, *12*(3), 305–510.

Takahashi, T., Forsythe, L. D., Tsujimoto, T., Barnes-Davies, M., & Onodera, K. (1996). Presynaptic calcium current modulation by a metabotropic glutamate receptor. *Science*, *274*(5287), 594–597.

Tamás, G., Buhl, E. H., Lörincz, A., & Somogyi, P. (2000). Proximally targeted GABAergic synapses and gap junctions synchronize cortical interneurons. *Nature Neuroscience*, *3*(4), 366–371.

Tamás, G., Buhl, E. H., & Somogyi, P. (1997a). Fast IPSPs elicited via multiple synaptic release sites by different types of GABAergic neurone in the cat visual cortex. *Journal of Physiology*, *500*(3), 715–738.

Tamás, G., Buhl, E. H., & Somogyi, P. (1997b). Massive autaptic self-innervation of GABAergic neurons in cat visual cortex. *Journal of Neuroscience*, *17*(16), 6352–6364.

Tamás, G., Lörincz, A., Simon, A., & Szabadics, J. (2003). Identified sources and targets of slow inhibition in the neocortex. *Science*, *299*(5614), 1902–1905.

Tamás, G., Somogyi, P., & Buhl, E. H. (1998). Differentially interconnected networks of GABAergic interneurons in the visual cortex of the cat. *Journal of Neuroscience*, *18*(11), 4255–4270.

Tamás, G., Szabadics, J., Lörincz, A., & Somogyi, P. (2004). Input and frequency-specific entrainment of postsynaptic firing by IPSPs of perisomatic or dendritic origin. *European Journal of Neuroscience*, *20*(10), 2681–2690.

Tamás, G., Szabadics, J., & Somogyi, P. (2002). Cell type- and subcellular position-dependent summation of unitary postsynaptic potentials in neocortical neurons. *Journal of Neuroscience*, *22*(3), 740–747.

Tang, Y., Nyengaard, J. R., de Groot, D. M. G., & Gundersen, H. J. G. (2001). Total regional and global number of synapses in the human brain neocortex. *Synapse*, *41*(3), 258–273.

Tasic, B., Yao, Z., Graybuck, L. T., Smith, K. A., Nguyen, T. N., Bertagnolli, D., Goldy, J., Garren, E., Economo, M. N., Viswanathan, S., Penn, O., Bakken, T., Menon, V., Miller, J., Fong, O., Hirokawa, K. E., Lathia, K., Rimorin, C., Tieu, M., … Zeng, H. (2018). Shared and distinct transcriptomic cell types across neocortical areas. *Nature*, *563*(7729), 72–78.

Taylor, H. B. C., Tong, R., Jeans, A. F., & Emptage, N. J. (2020). A Novel Optical Quantal Analysis of Miniature Events Reveals Enhanced Frequency Following Amyloid β Exposure. *Frontiers in Cellular Neuroscience*, *0*, 349.

Testa-Silva, G., Verhoog, M. B., Linaro, D., de Kock, C. P. J., Baayen, J. C., Meredith, R. M., de Zeeuw, C. I., Giugliano, M., & Mansvelder, H. D. (2014). High Bandwidth Synaptic Communication and Frequency Tracking in Human Neocortex. *PLoS Biology*, *12*(11), e1002007.

The Petilla Interneuron Nomenclature Group. (2008). Petilla terminology: nomenclature of features of GABAergic interneurons of the cerebral cortex. *Nature Reviews. Neuroscience*, *9*(7), 557.

Thomas, N. K., Wright, R. A., Howson, P. A., Kingston, A. E., Schoepp, D. D., & Jane, D. E. (2001). (S)-3,4-DCPG, a potent and selective mGlu8a receptor agonist, activates metabotropic glutamate receptors on primary afferent terminals in the neonatal rat spinal cord. *Neuropharmacology*, *40*(3), 311–318.

Ting, J. T., Kalmbach, B., Chong, P., de Frates, R., Keene, C. Di., Gwinn, R. P., Cobbs, C., Ko, A. L., Ojemann, J. G., Ellenbogen, R. G., Koch, C., & Lein, E. (2018). A robust ex vivo experimental platform for molecular-genetic dissection of adult human neocortical cell types and circuits. *Scientific Reports*, *8*(1), 8407.

Tippett, L. J., Waldvogel, H. J., Thomas, S. J., Hogg, V. M., Roon-Mom, W. Van, Synek, B. J., Graybiel, A. M., & Faull, R. L. M. (2007). Striosomes and mood dysfunction in Huntington's disease. *Brain*, *130*(1), 206–221.

Tomioka, R., Okamoto, K., Furuta, T., Fujiyama, F., Iwasato, T., Yanagawa, Y., Obata, K., Kaneko, T., & Tamamaki, N. (2005). Demonstration of long-range GABAergic connections distributed throughout the mouse neocortex. *European Journal of Neuroscience*, *21*(6), 1587–1600.

Tootell, R. B. H., & Hamilton, S. L. (1989). Functional anatomy of the second visual area (V2) in the macaque. *Journal of Neuroscience*, *9*(8), 2620–2644.

Tootell, R. B. H., Mendola, J. D., Hadjikhani, N. K., Ledden, P. J., Liu, A. K., Reppas, J. B., Sereno, M. I., & Dale, A. M. (1997). Functional analysis of V3A and related areas in human visual cortex. *Journal of Neuroscience*, *17*(18), 7060–7078.

Tootell, R. B. H., Nelissen, K., Vanduffel, W., & Orban, G. A. (2004). Search for Color "Center(s)" in Macaque Visual Cortex. *Cerebral Cortex*, *14*(4), 353–363.

Tootell, R. B. H., Tsao, D., & Vanduffel, W. (2003). Neuroimaging weighs in: Humans meet macaques in "primate" visual cortex. *Journal of Neuroscience*, *23*(10), 3981–3989.

Trachtenberg, J. T., Chen, B. E., Knott, G. W., Feng, G., Sanes, J. R., Welker, E., & Svoboda, K. (2002). Long-term in vivo imaging of experience-dependent synaptic plasticity in adult cortex. *Nature*, *420*(6917), 788–794.

Tsai, G., & Coyle, J. T. (2002). Glutamatergic mechanisms in schizophrenia. *Annual Review of Pharmacology and Toxicology*, *42*(1), 165-179.

Tu, J. C., Xiao, B., Naisbitt, S., Yuan, J. P., Petralia, R. S., Brakeman, P., Doan, A., Aakalu, V. K., Lanahan, A. A., Sheng, M., & Worley, P. F. (1999). Coupling of mGluR/Homer and PSD-95 complexes by the Shank family of postsynaptic density proteins. *Neuron*, *23*(3), 583–592.

Tu, J. C., Xiao, B., Yuan, J. P., Lanahan, A. A., Leoffert, K., Li, M., Linden, D. J., & Worley, P. F. (1998). Homer binds a novel proline-rich motif and links group I metabotropic glutamate receptors with IP3 receptors. *Neuron*, *21*(4), 717–726.

Turner, J. P., & Salt, T. E. (1999). Group III metabotropic glutamate receptors control corticothalamic synaptic transmission in the rat thalamus in vitro. *Journal of Physiology*, *519*(2), 481–491.

Turner, J. P., & Salt, T. E. (2003). Group II and III metabotropic glutamate receptors and the control of the nucleus reticularis thalami input to rat thalamocortical neurones in vitro. *Neuroscience*, *122*(2), 459–469.

Turrigiano, G. G., Leslie, K. R., Desai, N. S., Rutherford, L. C., & Nelson, S. B. (1998). Activity-dependent scaling of quantal amplitude in neocortical neurons. *Nature*, *391*(6670), 892–896.

Uylings, H. B. M., Zilles, K., & Rajkowska, G. (1999). Optimal Staining Methods for Delineation of Cortical Areas and Neuron Counts in Human Brains. *NeuroImage*, *9*(4), 439–445.

Valenti, O., Marino, M. J., Wittmann, M., Lis, E., DiLella, A. G., Kinney, G. G., & Conn, P. J. (2003). Group III Metabotropic Glutamate Receptor-Mediated Modulation of the Striatopallidal Synapse. *Journal of Neuroscience*, *23*(18), 7218–7226.

Valverde, F. (1971). Short Axon Neuronal Subsystems In The Visual Cortex of The Monkey. *International Journal of Neuroscience*, *1*(3), 181–197.

Valverde, F. (1976). Aspects of cortical organization related to the geometry of neurons with intra-cortical axons. *Journal of Neurocytology*, *5*(5), 509–529.

Valverde, F. (1978). The organization of area 18 in the monkey. A Golgi study. *Anatomy and Embryology*, *154*(3), 305–334.

Valverde, F. (1986). Intrinsic neocortical organization: Some comparative aspects. *Neuroscience*, *18*(1), 1–23.

van Brederode, J. F. M., Helliesen, M. K., & Hendrickson, A. E. (1991). Distribution of the calcium-binding proteins parvalbumin and calbindin-D28k in the sensorimotor cortex of the rat. *Neuroscience*, *44*(1), 157–171.

van Brederode, J. F. M. van, Mulligan, K. A., & Hendrickson, A. E. (1990). Calcium-binding proteins as markers for subpopulations of GABAergic neurons in monkey striate cortex. *Journal of Comparative Neurology*, *298*(1), 1–22.

van der Loos, H., & Woolsey, T. (1973). Somatosensory cortex: structural alterations following early injury to sense organs. *Science*, *179*(2), 395–398.

Vardi, N., Duvoisin, R., Wu, G., & Sterling, P. (2000). Localization of mGluR6 to dendrites of ON bipolar cells in primate retina. *Journal of Comparative Neurology*, *423*(3), 402–412.

Varga, C., Tamas, G., Barzo, P., Olah, S., & Somogyi, P. (2015). Molecular and electrophysiological characterization of GABAergic interneurons expressing the transcription factor COUP-TFII in the adult human temporal cortex. *Cerebral Cortex*, *25*(11), 4430–4449.

Vázquez, E., & Sánchez-Prieto, J. (1997). Presynaptic modulation of glutamate release targets different calcium channels in rat cerebrocortical nerve terminals. *European Journal of Neuroscience*, *9*(10), 2009–2018.

Vera, G., & Tapia, R. (2012). Activation of group III metabotropic glutamate receptors by endogenous glutamate protects against glutamate-mediated excitotoxicity in the hippocampus in vivo. *Journal of Neuroscience Research*, *90*(5), 1055–1066.

Vogt, C., & Vogt, O. (1926). Die vergleichend-architektonische und die vergleichend-reizphysiologische Felderung der Großhirnrinde unter besonderer Berücksichtigung der menschlichen. *Die Naturwissenschaften*, *14*(50–51), 1190–1194.

Vogt, C., & Vogt, O. (1954). Gestaltung der topistischen hirnforschung und ihre forderung durch den hirnbau und seine anomalien. *J. Hirnforsch*, *1*, 1–46.

Vogt, O. (1910). Die myeloarchitektonische Felderung des menschlichen Stirnhirns. *Journal Für Psychologie Und Neurologie*, *15*, 221-232.

Vogt, O., & Vogt, C. (1919). Ergebnisse unserer Hirnforschung. *J Psychol Neurol*, *25*(25), 277–462.

von Economo, C. F., & Koskinas, G. N. (1925). Die Cytoarchitektonik der Hirnrinde des erwachsenen Menschen. In *Journal of Anatomy*, *61*.

von Monakow, C. (1914). Die Lokalisation im Grosshirn und der Abbau der Funktion durch Kortikale Herde. In *Journal of the American Medical Association*, *63*(9).

Wallis, J. D., Anderson, K. C., & Miller, E. K. (2001). Single neurons in prefrontal cortex encode abstract roles. *Nature*, *411*(6840), 953–956.

Wang, X., Ai, J., Hampson, D. R., & Snead, O. C. (2005). Altered glutamate and GABA release within thalamocortical circuitry in metabotropic glutamate receptor 4 knockout mice. *Neuroscience*, *134*(4), 1195–1203.

Wang, Y., Toledo-Rodriguez, M., Gupta, A., Wu, C., Silberberg, G., Luo, J., & Markram, H. (2004). Anatomical, physiological and molecular properties of Martinotti cells in the somatosensory cortex of the juvenile rat. *The Journal of Physiology*, *561*(1), 65–90.

Wernicke, C. (1874). Der aphasische Symptomenkomplex. In *Der aphasische Symptomenkomplex*. Cohen und Weigert.

West, M. J. (1999). Stereological methods for estimating the total number of neurons and synapses: Issues of precision and bias. In *Trends in Neurosciences*, *22*(2), 51–61.

Wheeler, D. B., Randall, A., & Tsien, R. W. (1994). Roles of N-type and Q-type Ca2+ channels in supporting hippocampal synaptic transmission. *Science*, *264*(5155), 107–111.

White, E. L., & Rock, M. P. (1980). Three-dimensional aspects and synaptic relationships of a Golgi-impregnated spiny stellate cell reconstructed from serial thin sections. *Journal of Neurocytology*, *9*(5), 615–636.

White, W. F., Nadler, J. v., & Cotman, C. W. (1979). The effect of acidic amino acid antagonists on synaptic transmission in the hippocampal formation in vitro. *Brain Research*, *164*(1–2), 177–194.

Wijeratne, C., & Sachdev, P. (2008). Treatment-resistant depression: Critique of current approaches. *Australian and New Zealand Journal of Psychiatry*, *42*(9), 751–762.

Winfield, D. A., Brooke, R. N. L., Sloper, J. J., & Powell, T. P. S. (1981). A combined golgi-electron microscopic study of the synapses made by the proximal axon and recurrent collaterals of a pyramidal cell in the somatic sensory cortex of the monkey. *Neuroscience*, *6*(7), 1217–1230.

Winfield, D. A., Gatter, K. C., & Powell, T. P. S. (1980). An electron microscopic study of the types and proportions of neurons in the cortex of the motor and visual areas of the cat and rat. *Brain*, *103*(2), 245–258.

Wittchen, H. U., Jacobi, F., Rehm, J., Gustavsson, A., Svensson, M., Jönsson, B., Olesen, J., Allgulander, C., Alonso, J., Faravelli, C., Fratiglioni, L., Jennum, P., Lieb, R., Maercker, A., van Os, J., Preisig, M., Salvador-Carulla, L., Simon, R., & Steinhausen, H. C. (2011). The size and burden of mental disorders and other disorders of the brain in Europe 2010. *European Neuropsychopharmacology*, *21*(9), 655–679.

Wittmann, M., Marino, M. J., Bradley, S. R., & Conn, P. J. (2001). Activation of Group III mGluRs Inhibits GABAergic and Glutamatergic Transmission in the Substantia Nigra Pars Reticulata. *Journal of Neurophysiology*, *85*(5), 1960–1968.

Wong, H. C., Sternini, C., Lloyd, K., De Giorgio, R., & Walsh, J. H. (1996). Monoclonal antibody to VIP: Production, characterization, immunoneutralizing activity, and usefulness in cytochemical staining. *Hybridoma*, *15*(2), 133–139.

Woodhall, G. L., Ayman, G., & Jones, R. S. G. (2007). Differential control of two forms of glutamate release by group III metabotropic glutamate receptors at rat entorhinal synapses. *Neuroscience*, *148*(1), 7–21.

Woolsey, C. N., Marshall, W. H., & Bard, P. (1943). Note on the Organization of the Tactile Sensory Area of the Cerebral Cortex of the Chimpanzee. *Journal of Neurophysiology*, *6*(4), 287–291.

Woolsey, T. A., & van der Loos, H. (1970). The structural organization of layer IV in the somatosensory region (S I) of mouse cerebral cortex. The description of a cortical field composed of discrete cytoarchitectonic units. *Brain Research*, *17*(2), 205–242.

Wright, R. A., & Schoepp, D. D. (1996). Differentiation of group 2 and group 3 metabotropic glutamate receptor cAMP responses in the rat hippocampus. *European Journal of Pharmacology*, *297*(3), 275–282.

Wu, L., & Saggau, P. (1994). Presynaptic calcium is increased during normal synaptic transmission and paired-pulse facilitation, but not in long-term potentiation in area CA1 of hippocampus. *Journal of Neuroscience*, *14*(2), 645–654.

Xiang, Z., Lv, X., Lin, X., Brien, D. E. O., Altman, M. K., Lindsley, C. W., Javitch, J. A., Niswender, C. M., & Conn, P. J. (2021). Input-specific regulation of glutamatergic synaptic transmission in the medial prefrontal cortex by mGlu2/mGlu4 receptor heterodimers. *Science Signaling*, *14*(677), eabd2319.

Xi, Z. X., Shen, H., Baker, D. A., & Kalivas, P. W. (2003). Inhibition of non-vesicular glutamate release by group III metabotropic glutamate receptors in the nucleus accumbens. *Journal of Neurochemistry*, *87*(5), 1204–1212.

Xu, H., Jeong, H. Y., Tremblay, R., & Rudy, B. (2013). Neocortical Somatostatin-Expressing GABAergic Interneurons Disinhibit the Thalamorecipient Layer 4. *Neuron*, *77*(1), 155–167.

Yang, X., Fang, Y., Chen, H., Zhang, T., Yin, X., Man, J., Yang, L., & Lu, M. (2021). Global, regional and national burden of anxiety disorders from 1990 to 2019: Results from the Global Burden of Disease Study 2019. *Epidemiology and Psychiatric Sciences*, *30*, e36.

Yin, S., Noetzel, M. J., Johnson, K. A., Zamorano, R., Jalan-Sakrikar, N., Gregory, K. J., Jeffrey Conn, P., & Niswender, C. M. (2014). Selective actions of novel allosteric modulators reveal functional heteromers of Metabotropic glutamate receptors in the CNS. *Journal of Neuroscience*, *34*(1), 79–94.

Yuste, R. (2011). Dendritic spines and distributed circuits. *Neuron*, *71*(5), 772–781.

Yuste, R., & Denk, W. (1995). Dendritic spines as basic functional units of neuronal integration. *Nature*, *375*(6533), 682–684.

Yuste, R., Hawrylycz, M., Aalling, N., Aguilar-Valles, A., Arendt, D., Armañanzas, R., Ascoli, G. A., Bielza, C., Bokharaie, V., Bergmann, T. B., Bystron, I., Capogna, M., Chang, Y., Clemens, A., de Kock, C. P. J., DeFelipe, J., dos Santos, S. E., Dunville, K., Feldmeyer, D., … Lein, E. (2020). A community-based transcriptomics classification and nomenclature of neocortical cell types. *Nature Neuroscience*, *23*(12), 1456–1468.

Zaitsev, A. v., Gonzalez-Burgos, G., Povysheva, N. v., Kröner, S., Lewis, D. A., & Krimer, L. S. (2005). Localization of calcium-binding proteins in physiologically and morphologically characterized interneurons of monkey dorsolateral prefrontal cortex. *Cerebral Cortex*, *15*(8), 1178–1186.

Zeng, H., Shen, E. H., Hohmann, J. G., Oh, S. W., Bernard, A., Royall, J. J., Glattfelder, K. J., Sunkin, S. M., Morris, J. A., Guillozet-Bongaarts, A. L., Smith, K. A., Ebbert, A. J., Swanson, B., Kuan, L., Page, D. T., Overly, C. C., Lein, E. S., Hawrylycz, M. J., Hof, P. R., … Jones, A. R. (2012). Large-scale cellular-resolution gene profiling in human neocortex reveals species-specific molecular signatures. *Cell*, *149*(2), 483–496.

Zhang, S., Xu, M., Kamigaki, T., Hoang Do, J. P., Chang, W., Jenvay, S., Miyamichi, K., Luo, L., & Dan, Y. (2014). Selective attention. Long-range and local circuits for top-down modulation of visual cortex processing. *Science*, *345*(6197), 660–665.

Zhou, F., Hongmin, B., Xiang, Z., & Enyu, L. (2003). Changes of mGluR4 and the effects of its specific agonist L-AP4 in a rodent model of diffuse brain injury. *Journal of Clinical Neuroscience*, *10*(6), 684–688.

Zucker, R. S. (1989). Short-term synaptic plasticity. *Annual Review of Neuroscience*, *12*, 13–31.